

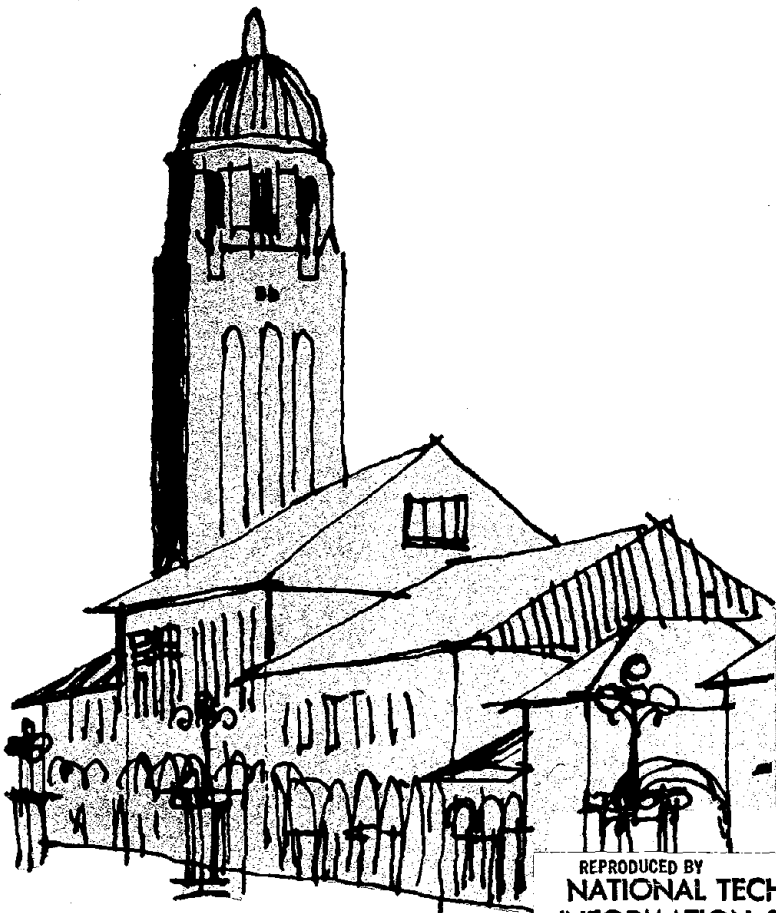
The John A. Blume Earthquake Engineering Center

Department of Civil Engineering
Stanford University

EXPERIMENTAL STUDY ON THE SEISMIC BEHAVIOR OF INDUSTRIAL STORAGE RACKS

by

**Helmut Krawinkler
Nathaniel G. Cofie
Miguel A. Astiz
Charles A. Kircher**



This work was supported by the
National Science Foundation Grant
ENV75-16931 and the
Rack Manufacturers Institute and
was carried out under a subcontract
with URS/John A. Blume &
Associates, San Francisco

REPRODUCED BY
NATIONAL TECHNICAL
INFORMATION SERVICE
U. S. DEPARTMENT OF COMMERCE
SPRINGFIELD, VA. 22161

Report No. 41
November 1979

The John A. Blume Earthquake Engineering Center was established to promote research and education in earthquake engineering. Through its activities our understanding of earthquakes and their effects on mankind's facilities and structures is improving. The Center conducts research, provides instruction, publishes reports and articles, conducts seminars and conferences, and provides financial support for students. The Center is named for Dr. John A. Blume, a well-known consulting engineer and Stanford alumnus.

Address

The John A. Blume Earthquake Engineering Center
Department of Civil Engineering
Stanford University
Stanford, California 94305

REPORT DOCUMENTATION PAGE	1. REPORT NO. NSF/RA-790340	2.	3. Recipient's Accession No. PB00 150899
4. Title and Subtitle Experimental Study on the Seismic Behavior of Industrial Storage Racks		5. Report Date November 1979	
7. Author(s) H. Krawinkler, N. G. Cofie, M. A. Astiz, C. A. Kircher		6.	
9. Performing Organization Name and Address Stanford University The John A. Blume Earthquake Engineering Center Department of Civil Engineering Stanford, California 94305		8. Performing Organization Rept. No. No. 41	
12. Sponsoring Organization Name and Address Engineering and Applied Science (EAS) National Science Foundation 1800 G Street, N.W. Washington, D.C. 20550		10. Project/Task/Work Unit No.	
15. Supplementary Notes		11. Contract(C) or Grant(G) No. (C) (G) ENV7516931	
16. Abstract (Limit: 200 words) <p>This report addresses the development of seismic design criteria for industrial storage racks. The development of loading criteria, the testing and interpretation of test results of a series of experiments on full size rack assemblies, subassemblies, and rack components are described. Forced vibration tests are needed to obtain information on natural frequencies, mode shapes, and damping characteristics, while the behavior of connections and members as well as the stability of the frame-type racks are studied from cyclic loading tests. Objectives of the study include the following: (1) determination of the load-deformation response of cold formed steel members and their connections under cyclic loading similar to that expected under severe seismic excitations; (2) development of mathematical models of response characteristics as needed for subsequent analytical studies; and (3) development of standard seismic testing procedures which can be utilized by the rack manufacturing industry for seismic qualification testing. Types of tests include cantilever, portal, full-size rack (including longitudinal and transverse tests), and dynamic tests.</p>		13. Type of Report & Period Covered	
17. Document Analysis a. Descriptors Earthquake resistant structures Forced vibration Mathematical models b. Identifiers/Open-Ended Terms Storage racks Seismic testing procedures Rack assemblies c. COSATI Field/Group		14.	
18. Availability Statement NTIS		19. Security Class (This Report)	21. No. of Pages
		20. Security Class (This Page)	22. Price

EXPERIMENTAL STUDY
ON THE SEISMIC BEHAVIOR OF INDUSTRIAL STORAGE RACKS

by

Helmut Krawinkler
Nathaniel G. Cofie
Miguel A. Astiz
Charles A. Kircher

Any opinions, findings, conclusions
or recommendations expressed in this
publication are those of the author(s)
and do not necessarily reflect the views
of the National Science Foundation.

The John A. Blume Earthquake Engineering Center
Department of Civil Engineering
Stanford University
Stanford, California 94305

This work was supported by the National Science
Foundation Grant ENV75-16931 and the Rack
Manufacturers Institute and was carried out under
a subcontract with URS/John A. Blume & Associates,
San Francisco.

Report No. 41

November 1979

i. a

ABSTRACT

This report discusses the development of loading criteria, the testing and the interpretation of test results of a series of experiments on full size rack assemblies, subassemblies and rack components. Forced vibration tests as well as quasi-static monotonic and cyclic loading tests to failure were carried out. The forced vibration tests are needed to obtain information on natural frequencies, modes shapes and damping characteristics, while the behavior of connections and members as well as the stability of the frame-type racks are studied from cyclic loading tests.

The objectives of the study summarized in this report are:

1. The determination of the load-deformation response of cold formed steel members and their connections under cyclic loading similar to that expected under severe seismic excitations.
2. The development of mathematical models of response characteristics as needed for subsequent analytical studies.
3. The development of standardized seismic testing procedures which can be utilized by the rack manufacturing industry for seismic qualification testing.

ACKNOWLEDGEMENTS

This experimental study was part of a project on the development of seismic design criteria for industrial storage racks, sponsored jointly by the National Science Foundation and the Rack Manufacturers Institute, with J. A. Blume as principal investigator and R. E. Scholl as project manager.

The assistance of Dr. Roger E. Scholl and Dr. C. K. Chen, both with URS/John A. Blume & Associates, in developing the testing program and providing analytical data is gratefully acknowledged. The NSF Seismic Rack Study Advisory Committee under the chairmanship of Dr. John A. Blume was most helpful and contributed many valuable suggestions.

The experimental work was carried out at the John A. Blume Earthquake Engineering Center at Stanford University. The graduate student Bahman Lashkari-Irvani assisted skillfully in preparing and performing the experiments.

TABLE OF CONTENTS

	<u>Page</u>
1. INTRODUCTION	1
1.1 Scope and Objectives	1
1.2 Response Parameters	3
1.3 Experimental Set-Up and Test Procedures	6
2. TYPES OF RACKS	10
3. CANTILEVER TESTS	11
3.1 Test Procedure.	11
3.2 Moment - Rotation Relationships	12
3.3 Experimental Results and Observations	13
4. PORTAL TESTS	15
4.1 Test Procedure.	15
4.2 Moment - Rotation Relationships	16
4.3 Experimental Results and Observations	18
5. FULL-SIZE RACK TESTS	21
5.1 Longitudinal Tests (A-R-1 and B-R-1).	21
5.1.1 Experimental Set-Up.	21
5.1.2 Loading Histories.	23
5.1.3 Experimental Results and Observations.	24
5.2 Transverse Tests (A-R-2 and B-R-2).	28
5.2.1 Experimental Set-Up.	28
5.2.2 Loading Histories.	29
5.2.3 Experimental Results and Observations.	30
6. DYNAMIC TESTS	33
6.1 Forced Vibration Studies.	33
6.2 Free Vibration Studies.	35
7. SUMMARY AND CONCLUSIONS.	37
REFERENCES	39
TABLES	40
FIGURES.	56

1. INTRODUCTION

1.1 Scope and Objectives

At any given time a large percentage of the movable goods in the United States is stored on industrial storage racks which usually consist of prefabricated cold formed steel elements assembled on site into various frame-type configurations. In the event of earthquakes these racks will be subjected to ground motions similar to those expected in building structures. Although it is debatable whether generally accepted seismic design criteria for building structures should be directly applied to storage racks, there is an evident need for a rational seismic design approach based on the same parameters that govern the response of building structures.

Until recently, very little was known about the structural response parameters governing the seismic behavior of industrial storage racks, such as lateral resistance and stiffness, as well as energy dissipation through damping and inelastic deformations. A thorough study of these parameters is needed to evaluate the dynamic response of storage racks from which a simplified design methodology can be developed. It appears rational that this simplified design method be based on equivalent static lateral forces derived from a base shear equation of the UBC type

$$V = ZKCW \quad (1-1)$$

where K and C need not necessarily be identical to presently used values for building structures. In particular, the value of K should be based on a rational evaluation of ductility and energy dissipation capacity of

rack configurations.

Discussed in this report is an experimental study on the seismic behavior of industrial storage racks which has the following specific objectives:

1. Investigation of the strength and stiffness characteristics of frame-type racks and their components under lateral loads.
2. Development of mathematical models for the load-deformational response of rack components.
3. Determination of the dynamic characteristics of racks (frequencies, mode shapes, and damping).
4. Study of energy dissipation characteristics which should aid in the determination of design shear forces.

One specific rack configuration was selected for this study, namely, the standard pallet rack. These racks consist of semi-rigid moment resisting frames in the longitudinal direction and braced frames in the transverse direction. Two types of racks (types A and B) were studied in detail, both of similar geometric configuration (two bays long, one bay deep, and three levels high, see Fig. 1.1), but built with different structural shapes and beam-to-post connections. Cantilever and portal tests were also performed on two additional types of racks (types C and D).

The purpose of this report is to identify the response parameters of importance in the seismic response of these racks, to discuss the types of experiments and the experimental procedures recommended for the evaluation of these response parameters, to present experimental data useful for further evaluation, and to present conclusions that can be drawn from experimental results on the behavior of industrial storage

racks under various levels of seismic excitations.

1.2 Response Parameters

To achieve a correlation between analytical response prediction and the true dynamic response of structures, experimental research needs to be directed towards defining each term in the discretized equation of motion

$$[M]\{\ddot{u}\} + [C]\{\dot{u}\} + [K]\{u\} = [M]\{\ddot{u}_g\} \quad (1.2)$$

where, assuming that the motion $\{\ddot{u}_g\}$ at the base of the structure is known, $[M]$ ideally should represent the proper mass distribution throughout the structure; $[C]$ ideally should represent all damping contributions which cannot be included with confidence in the formulation of the $[K]$ matrix; and $[K]$ ideally should represent all stiffness characteristics of the structure, including geometry and material nonlinearities, stiffness degradations, and time dependent effects.

To apply these considerations to industrial storage racks, several characteristics of such cold-formed steel structures need to be pointed out.

The pallet beams which usually consist of stiff sections with high moment capacity are connected to perforations of the upright posts by means of grip-type mechanical connectors. The beam-to-post connections do not behave as rigid connections since distortions can occur in the walls of the posts at the joints and in the connectors themselves. Consequently, relative rotation takes place between posts and beams which can be modeled closely by rotational springs at the joints. In most practical cases these springs are nonlinear and rather flexible

and have an ultimate moment capacity which is less than the flexural capacity of the beam sections. Hence, strength and stiffness of pallet beams under lateral loads are usually controlled by the response characteristics of the beam-to-post connections.

Thus, the strength parameters which need to be studied experimentally are the ultimate moment capacities at the beam-to-post connections for positive and negative bending as well as moments for an "allowable stress" or "service load" level. The latter moments are needed for a rational allowable stress or service load analysis and design which needs to be based on elastic behavior of the structure.

The upright posts usually consist of C-shaped thin-walled sections subjected to axial loads and bending moments. Under axial loads these posts may fail in either flexural or torsional-flexural buckling, while the interaction between axial loads and bending moments can be treated by means of M-P interaction diagrams.

Stability considerations will play a significant part in the seismic response of industrial storage racks. In the transverse direction the posts and the bracing members will be subjected to high axial forces and buckling can occur in the bracing members due to excessive horizontal story shears and in the posts due to overturning effects. However, these high shears and overturning moments will develop only in lagged racks (bolted to the floor) where the base plates can transmit the necessary uplift forces to the posts. In the longitudinal direction, overturning moments will be relatively small and possible buckling in the posts will depend primarily on the amount of vertical load on the racks. However, in this direction the semi-rigid frames may be subjected to large lateral drifts and $P-\delta$ effects may greatly amplify the

moments attracted by beams and posts and may also lead to dynamic instability problems.

Member stiffnesses are needed for the computation of internal force distribution as well as period and drift calculations. The elastic stiffnesses of pallet beams, posts, and transverse bracing systems can confidently be predicted analytically, but the stiffness of the beam-to-post connections can only be obtained from experiments. Also, the degree of fixity that can be achieved by bolting the post base plates to the floor needs to be studied experimentally.

Horizontal diaphragm action will affect the dynamic response and force distribution in the racks. Only few racks have horizontal bracing systems, but partial diaphragm action will be developed through pallets and pay load.

Like most other structures, industrial storage racks must rely on energy dissipation through inelastic deformations in the event of severe earthquakes. Measures of this energy dissipation capacity are member ductility as well as size, shape and stability of the hysteresis loops obtained under cyclic loading.

The level of forces attracted in structures during seismic excitations will also depend on the damping in the structure and the pay load. Although the damping from the pay load can be significant, this parameter was not included in the scope of the reported study. The structural damping which will come primarily from the beam-to-post connections will be strongly amplitude dependent and will be affected by the looseness of the connections.

The parameters discussed in this section were investigated in the experimental study reported herein. Monotonic as well as quasi-static

cyclic loading tests were carried out on structural elements, subassemblies and full-size rack assemblies. All tests were carried to failure or, where failure did not take place, to deformation levels which are larger than those expected in severe earthquakes. The configurations selected for element and subassembly tests were essentially the same as those used by Pekoz in previous studies at Cornell University (1,2). Four full-size racks were tested to study the interactions taking place between the individual elements under loading conditions similar to those expected in severe earthquakes.

In addition to these quasi-static tests, two of the full-size racks were also subjected to forced vibrations induced by means of an electromagnetic vibration generator. These tests resulted in information on damping properties, natural frequencies and mode shapes for longitudinal, transverse and torsional vibrations.

1.3 Experimental Set-up and Test Procedures

Selection of Test Specimens. The choice of feasible test specimens will largely determine the outcome of any experimental study. Boundary conditions and load application for components and subassemblies must be selected properly to simulate actual internal force distribution and interactions between the individual components. In the response of industrial storage racks the critical elements were found to be the beam-to-post connections and the posts themselves. The cantilever and portal tests described in the next two sections were utilized for a study of beam-to-post connections. The simple cantilever tests gave reliable results for moment-rotation behavior at the joints for only one specific value of moment to shear ratio in the beams. The actual

moment to shear ratio in pallet beams under combined vertical and lateral loads will be different from that used in the cantilevers. Since it is expected that this ratio will have an effect on the moment-rotation relationship at the joints, it was decided to test simple portal frames which will properly simulate the field conditions.

The behavior of posts under lateral loads in the longitudinal direction will strongly depend on the joint restraints provided by the pallet beams which will determine the effective column length. It was impossible to design a subassembly test which permitted proper simulation of boundary and loading conditions for posts. This together with the need for an investigation of $P-\delta$ effects made it necessary to test full size frame assemblies with lateral loads applied in the longitudinal direction. Tests on full size rack assemblies with lateral loads in the transverse direction were also needed to study the response of the braced transverse frames.

Load Application and Loading Histories. In all subassemblies and full-size racks the pay-loads were simulated by 1000 lb. concrete blocks placed on standard wood pallets. Lateral loads were applied by means of a hydraulic actuator attached to the structures in a manner which closely simulates the effects of inertia forces from horizontally accelerated pay-loads. The loads were applied quasi-statically to permit accurate force and displacement control and the recording of visual observations. Since the natural frequencies of storage racks are low, the strain rate effects due to dynamic excitations are small and quasi-static load application will not significantly distort strength and ductility characteristics.

Rather subjective decisions had to be made regarding the choice of representative loading histories for cyclic loading tests. Basically, two types of loading histories had to be considered, one leading to low cycle fatigue failure (symmetric displacement cycles) and one leading to incremental collapse (displacements predominantly in one direction). Because of the importance of the P- δ effect in longitudinal excitations of storage racks, it is anticipated that lateral displacements will increase in the direction of the first large acceleration pulse leading to incremental collapse type problems. Nevertheless, it was decided to apply loading histories with symmetric cycles of step-wise increasing displacement amplitudes. Three cycles of equal displacement amplitude were carried out at each step. It is believed that such loading histories are critical for steel structures, since cyclic stress reversal will accentuate local instability problems and initiation as well as propagation of cracks in weldments and base materials.

Instrumentation, Recording, and Data Reduction. Since the load-deformational response at the beam-to-post connections is nonlinear and affected by the looseness of the connections, it was decided to obtain continuous analog records of all important response parameters by means of X-Y recorders and strip-chart recorders. The analog records were then digitized electronically on a digitization table for data manipulation on a mini-computer. The final results of the experimentally obtained and analytically derived response parameters were stored on magnetic tape and graphically displayed on a Cal-Comp Plotter.

In the dynamic tests the analog acceleration signals were digitized instantaneously in an A to D converter and data analysis was carried out by means of an on-line Fourier Analyzer system.

The instrumentation system consisted of electronic sensors for the measurement of loads (load transducers), displacements (LVDT's and Linear Potentiometers), rotations (RVDT's), accelerations (accelerometers), and strains (resistance strain gages). The evaluation of the experimental data showed that all pre-calibrated sensors gave consistent and reliable results. However, strain gage arrangements which were not calibrated against known moments and axial forces could only be used for qualitative evaluations. Due to the small thickness of the structural elements and the presence of perforations in the posts it was not possible to establish a reliable relationship between strains and internal forces based on simple elastic beam theory.

2. TYPES OF RACKS

Only standard pallet racks were investigated in this study. A typical rack configuration, which applies to rack types A and B, is shown in Fig. 1.1. Four types of racks, produced by different manufacturers, were tested. Cantilever, portal and full size rack tests were performed on Types A and B, while only cantilever and portal tests were carried out on Types C and D.

Basic section properties, as supplied by the manufacturers, for pallet beams, posts and bracing elements are listed in Table 2.1. The cross-sectional shapes of the rack elements as well as the base plate arrangements are shown in Fig. 2.1. Figure 2.2 shows the upright frames for Types A and B with the dimensions measured in the laboratory.

The pallet beams of all four types of racks were welded to connector angles which in turn permitted connection to perforations of the posts through either hooks (Types A and C) or button grips (Type B). In Type D additional connectors were used to join the connector angles to the posts.

3. CANTILEVER TESTS

3.1 Test Procedure

The distortions at the beam-to-post connections will lead to relative rotations between beams and posts which can be represented by rotational springs. The moment-rotation ($M-\theta$) relationship for these springs was determined from standard cantilever tests (3).

The set-up for the cantilever test is shown in Figure 3.1. The ends of the post were bolted to rigid sections at top and bottom to prevent translation and rotation at those points. RVDTs were used to measure the rotations of the beam (θ_b) close to the connector angle and the rotation of the column (θ_c) at the column centerline. The load was applied by means of a hydraulic jack and its magnitude was measured by a load transducer attached to the end of the hydraulic jack. The deflection at the point of application of the load was measured by means of a linear potentiometer. Strain gages were located at a fixed distance from the point of application of the load as shown in Fig. 3.2 so that a calibration of moment against strain could be obtained for the pallet beam. This calibration permitted the measurement of beam moments in the portal and full size rack tests where strain gages were placed at identical locations.

Twenty cantilevers were tested, two each for positive and negative moment application for five types of racks (A, B, C1, C2, and D). The moment is considered positive when causing tension at the bottom fiber of the pallet beam in a realistic rack configuration. For convenience, a test that causes negative beam moment at the column face was designated with a number 1, i.e., the designation B-C-1 implies a cantilever

test on rack type B with a load causing a negative moment.

Continuous analog records were obtained on X-Y recorders for (a) load-deflection, (b) load-rotation of beam near joint, and (c) load-rotation of column center line. All the records were then digitized and reduced as discussed in Chapter 1.

3.2 Moment - Rotation Relationships

Two methods were employed to determine the spring rotation at the center of the joint. Experimentally, θ was obtained as the difference between rotation measurements taken at the center of the joint and the centerline of the beam adjacent to the connectors. Alternatively, θ can be obtained from the measured value of the tip deflection δ and computations of the elastic beam deflections δ_b and the column rotation θ_c , i.e.

$$\theta = \frac{\delta - \delta_b}{l_b + \frac{d_c}{2}} - \theta_c \quad (3)$$

where

$$\delta_b = \frac{P(l_b + \frac{d_c}{2})^3}{3EI_b} \quad (3a)$$

$$\theta_c = \frac{P(l_b + \frac{d_c}{2})l_c}{16EI_c} \quad (3b)$$

The dimensions used in these equations are shown in Fig. 3.1, I_b and I_c are moments of inertia of beam and column, respectively, and P is the applied load.

The rotations obtained from these equations are not exact since centerline dimensions are used. However, since it is expected that

centerline dimensions will be used in analytical studies, it is consistent that the mathematical model for the artificial rotational spring at the joint also be based on centerline dimensions. The moment M associated with the rotation θ is therefore the beam moment at the column centerline rather than the column face. Thus, M is calculated as $P/(24 + d_c/2)$.

3.3 Experimental Results and Observations

The basic load-tip deflection ($P-\delta$) curves are shown in Figs. 3.3 to 3.7. Figures 3.8 and 3.9 illustrate the experimentally recorded $M-\theta$ relationships for Types A and B, where θ was obtained as the difference of the rotations θ_b and θ_c measured by means of RVDTs. The $M-\theta$ relationships derived from the analytical model (Eq. 3) are presented in Figs. 3.10 to 3.13. Reasonable good agreement (within about 10%) was obtained between the experimentally measured rotations and those computed from Eqs. (3). This shows that the analytical model for computing rotations is adequate and rotation measurements may not be necessary in future experimental studies.

From the presented data it can be seen that strength and stiffness vary significantly for positive and negative bending and from specimen to specimen. The looseness of the connections often led to very small initial stiffnesses which suggests the application of a small pre-load in experiments where continuous records cannot be obtained. In some cases it will be difficult to define a suitable linear range for elastic analysis and design. This indicates that service load design will have to be based on allowable moments (as a percentage of the ultimate moment capacity) and an average stiffness which should not vary substan-

tially within the allowable range of moments.

Certain doubts exist in regard to generalization of the obtained $M-\theta$ relationships. These curves were obtained from a test with a constant and very low shear-to-moment ratio at the column face which is not representative for realistically loaded pallets. The high shears introduced by pay loads on the pallet beams may alter significantly the initial stiffness of the connection, as was observed in the portal tests. Auxiliary displacement measurements in the cantilever tests have shown that the beam translated with respect to the column, a phenomenon which was not observed in the portal tests.

In all tests, the strength of the assembly was governed by the connection rather than the beam itself. Deformations in the connection angles, the connectors and the posts did cause much of the decrease in stiffness of the connection. In the Type A assembly the strength was limited by the capacity of the hook-type grips which started to pull out of the post perforations. In the Type B assemblies fracture of the beam-to-connection angle weld was observed which limited the moment capacity. Early weld fracture was evident particularly in specimens of Types C1 and C2. In Type D assemblies severe distortions of the connectors and at the post perforations was the main cause for the decrease in stiffness and the limited moment capacity.

4. PORTAL TESTS

4.1 Test Procedure

The cantilever tests resulted in accurate data on joint behavior for a particular shear to moment ratio in the pallet beams. In realistic situations this ratio varies under the simultaneous application of vertical and lateral loads and may be quite different from that used in the cantilevers. The portal tests described in this chapter were performed to obtain information on the behavior of the connections when subjected simultaneously to vertical and lateral loads and to compare the results with those obtained from the cantilever tests. One test was carried out under cyclic loading to obtain information on the hysteretic behavior of the load-deformation response of beam-to-post connections.

A sketch of the set-up for the portal test is shown in Figure 4.1. The assembly was mounted on hinges created on T-sections which were tightened to the floor by means of channel sections running in the transverse direction of the frames. Vertical loads (service live loads) were simulated with concrete blocks resting on standard wood pallets as indicated in Fig. 4.2.

A distribution plate bolted to the two frames was used to distribute the lateral loads equally to the two frames. The load was applied by a hydraulic jack attached to a very rigid W-section and also connected to the center of the distribution plate. Strain gages were placed on pallet beams at locations similar to those of the cantilever tests. The strain readings obtained at the strain-gage locations were linearly extrapolated to the centers of the adjacent posts. Using the strain-

moment relationships obtained from the cantilever tests, the moments at the centers of posts can then be readily computed. RVDTs were used to measure the relative rotation between beams and posts close to the joints. Potentiometers attached to the front face of the posts at the intersection of the center-line of the pallet beams were used to measure the lateral deflection of the two frames. Continuous analog records were obtained on X-Y recorder for:

- 1.) Load-lateral deflection of frames
- 2.) Load-rotation of beam close to joint
- 3.) Load-rotation of column close to joint

Strip chart records were obtained for:

- 1.) Load
- 2.) Strains at strain-gage locations.

All readings were digitized and manipulated on a minicomputer as discussed in Chapter 1.

Six portal tests were performed, two each on rack types A and B and one each on rack types C1 and D. These tests are summarized in Table 4.1.

4.2 Moment - Rotation Relationships

The moment-rotation relationships of the individual joint springs can be extracted from experimental data provided that the shear forces in the individual posts can be determined. Since strength and stiffness of the connections may differ significantly for positive and negative bending, the two posts in general will not attract equal shears. The shear forces in the posts were obtained from $V = M/h$ where M is the moment at the center of the beam-post joint as calculated from the

strain gage readings in the pallet beam.

The relative rotation θ between beam and post was measured with rotation gauges and also calculated based on elastic behavior of beams and posts. Very good correlation was obtained between measured and calculated values. Based on elastic behavior of beams and posts, the rotation θ can be computed from

$$\theta = \frac{\delta - \delta_c}{h} - \theta_b \quad (4.1)$$

where

$$\delta_c = \frac{Mh^2}{3EI_c} \quad (4.1a)$$

$$\theta_b = \frac{l}{6EI_b (M + \bar{M})^2} (2M^3 - \bar{M}^3 + 2M^2\bar{M}) \quad (4.1b)$$

The dimensions used in these equations are shown in Fig. 4.1, δ is the lateral deflection at the beam centerline, M is the moment due to lateral load plus the $P-\delta$ effect at the joint where rotations are computed, and \bar{M} is the moment at the opposite joint.

The accuracy of the $M-\theta$ relationships for individual joints obtained from portal tests depends strongly on a precise measurement of beam moments which is difficult to achieve. For industrial testing, the simple cantilever test which requires only load and displacement measurements may give sufficiently accurate results for strength and stiffness of individual joints. The portal test could be utilized to obtain average values for moment-rotation characteristics considering both joints in the portal. These average values characterize the overall lateral resistance and stiffness of pallet beams in frame configurations, which are parameters that should prove useful for the development of seismic

design criteria. The average moment at the two joints can be expressed as

$$M_{av} = \frac{H}{2} h + P\delta \quad (4.2)$$

and the average rotation, assuming that the moments due to a lateral load are equal at the two joints, is given by

$$\theta_{av} = \frac{\delta}{h} - \frac{M_{av} h}{3EI_c} - \frac{M_{av} \ell}{6EI_b} \quad (4.3)$$

where H is the lateral load applied to one portal frame, and P is the axial force in the post due to vertical loads.

4.3 Experimental Results and Observations

The experimentally recorded relationships between lateral load H (per frame) and horizontal displacement δ are shown in Figs. 4.3 to 4.6. Figures 4.7 and 4.8 illustrate the measured M- θ relationships (one in the direction of positive moment, M_2 , and the other in the direction of negative moment, M_1 , for the two joints of specimens A-P-2 and B-P-1, respectively. The moments at the center of posts were obtained as discussed earlier in Section 4.1 and the relative rotations were obtained from the recorded values of the rotations of the beam close to the joints (θ_b) and the rotations of the posts at the joint centers (θ_c). The $M_{av} - \theta_{av}$ relationships derived from Eqs. (4.2) and (4.3) are presented in Figs. 4.9 to 4.12.

It can be noticed in Fig. 4.3 that the H- δ diagrams for specimens A-P-1 and A-P-2 are rather similar although one specimen (A-P-1) was tested with half live load and the other with full live load. This is characteristic for frames with flexible connections where the end

moments due to vertical loads are small compared to moments caused by lateral loads. The magnitude of the end moments due to vertical loads can be read from Figs. 4.7 and 4.8 as the differences between the points of zero moment and the origin of the graphs. These moments could not be determined experimentally and were obtained from a computer analysis based on the stiffnesses measured in the cantilever tests.

The origins in Figs. 4.7 and 4.8 correspond to zero lateral load, i.e., to moments caused by vertical loads alone. When the $M-\theta$ diagrams of the individual joints are compared with those obtained from cantilever tests (Figs. 3.8 and 3.9), it can be seen that the diagrams are similar in shape and moment capacity, however, the diagrams from the portal tests exhibit a significantly higher initial stiffness. This proves that the stiffness depends on the shear to moment ratio in the beams which is significantly higher in the portals due to the presence of vertical loads. Thus, it should be noted that the portal tests are more appropriate than cantilever tests for an experimental determination of the joint spring characteristics under realistic vertical and lateral load applications.

In Figure 4.13 the individually measured $M-\theta$ relationships for the two joints of specimen B-P-1 are compared with the $M_{av} - \theta_{av}$ relationships obtained from Eqs. (4.2) and (4.3). The discrete load points marked on the diagrams illustrate the difference in moments at the joints caused by lateral loads. It is evident that the moments attracted at the two joints depend strongly on the relative joint stiffnesses and differ by a large amount. It can also be seen in this figure that the M_{av} and θ_{av} values are indeed reliable average values for joint moments and rotations.

Figures 4.4 and 4.10 show the $H-\delta$ and $M_{av} - \theta_{av}$ relationships of the cyclic loadings test performed on specimen B-P-2. Loading histories were applied with symmetric cycles of step-wise increasing displacement amplitudes and three cycles of equal displacement amplitude were carried out in each step. It is interesting to note that the hysteresis loops are similar in shape to those obtained in reinforced concrete flexural members with high shear. The looseness of the connections and localized yielding at the connections caused by previous loading led to a pinching of the hysteresis loops similar to that caused by shear transfer in reinforced concrete. It was observed that for constant displacement amplitudes the second load cycle led to a decrease in the area enclosed by the hysteresis loop while the third load cycle was practically identical to the second one.

At the displacement amplitude where failure initiated (in this case cracking at the welds between the beams and the connector angles at a displacement amplitude of 1.5 in.), subsequent load cycling led to a pronounced decrease in strength and hysteresis area. It should be emphasized that the cracking at the welds in the cyclically loaded specimen occurred at smaller displacements than in the monotonically loaded specimen. This indicates that the strength and ductility obtained from monotonic loading tests may not be fully representative for the load-deformation response characteristics under seismic excitations.

5. FULL-SIZE RACK TESTS

Three-level rack assemblies were tested to study the interaction between pallet beams, posts and connections under gravity loads and seismic effects simulated by quasi-static cyclic load application at the level of the pallet beams on the third story. Four rack assemblies were tested, two in the longitudinal direction and two in the transverse direction. In the longitudinal direction the assemblies act as moment resisting frames with semi-rigid connections while in the transverse direction the lateral load resisting units are braced frames. The types of rack tests are summarized in Table 5.1.

5.1 Longitudinal Tests (A-R-1 and B-R-1)

5.1.1 Experimental Set-Up

The experimental set-up for the longitudinal tests is shown in Fig. 5.1. The base plates welded to the ends of the posts are provided with single holes through which the racks were bolted to the floor. Each rack has two frames which are labeled as L1 and L2 in Fig. 5.1. These frames are parallel to each other and are essentially identical. Frame L1 was fully instrumented while frame L2 was only partially instrumented, primarily to verify the degree of symmetry attained in the response.



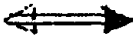
Strain gages similar to those used in the cantilever and portal tests were mounted on the beams of the first level to measure the strains in the beams close to the connections, as shown in Figs. 5.4 to 5.7. The position of the strain gages in the beams relative to the adjacent joints were the same as in the cantilever tests which

permitted a direct measurement of beam moments. Strain gages were also mounted on the center posts and one of the exterior posts of frame L1 to obtain qualitative measurements of the flexural strains in the posts. The strain gage locations are indicated in the details of Fig. 5.8. Since a calibration of strains vs. moments and axial loads was not established, the strain measurements in the posts resulted only in qualitative information.

The lateral displacement measurements for frames L1 and L2 were made at all the three levels by a combination of LVDTs and linear potentiometers attached to the exterior column faces at the center line of the beams. Continuous readings were obtained for the lateral load-deflection curves for the third level and first level, while intermittent readings were obtained for the deflection at the second level. Tables 5.2 and 5.3 summarize the displacement and strain measurements made in test A-R-1 and B-R-1, respectively.

The vertical pay loads were simulated with 1000 lb concrete blocks resting on standard pallets. The vertical loading arrangement for the tests A-R-1 and B-R-1 are shown in Figs. 5.2 and 5.3. Test A-R-1 was loaded with half pay load while B-R-1 was loaded with full pay load. The lateral load was applied to the rack assembly at the third level by means of a hydraulic jack which was connected to a rigid W-section at one end and at the other end to a distribution plate bolted to the two frames at the third level. The lateral load arrangement was similar to that of the portal test. The loading summary and instrumentation for the two frames of Test A-R-1 are shown in Figs. 5.4 and 5.5, while those of test B-R-1 are shown in Figs. 5.6 and 5.7. Photos of the test frames are shown in Fig. 5.9.

Symbols Used in Figures 5.4 to 5.7

	deflection measurement made by a linear potentiometer or an LVDT
	flexural strain measurement made by two strain gages
	lateral load applied by a hydraulic jack in a cyclic manner

5.1.2 Loading Histories

After the application of the vertical loads, all the strain gages, LVDTs and potentiometer readings were zeroed. The lateral load was applied quasi-statically to permit accurate force and displacement control and recording of visual observations. Because storage racks are relatively flexible, their fundamental frequencies are low and hence the application of a quasi-static load is justified since strain rate effects will not be significant at these low frequencies. The racks were subjected to cyclic loading with increasing displacement amplitudes up to 6 inches. Three symmetric cycles were carried out at each displacement amplitude. The loading arrangement did not permit cyclic loading beyond a displacement of 6 in. but loading was continued monotonically until either failure was imminent or the displacement limit of the loading arrangement was reached.

The deflection histories at the third level for tests A-R-1 and B-R-1 are presented in Figs. 5.10 and 5.11, respectively.

5.1.3 Experimental Results and Observations

Tables 5.4 and 5.5 show numerical results at peak displacements (see Figs. 5.10 and 5.11) for tests A-R-1 and B-R-1, respectively. The instrumentation for A-R-1 and B-R-1 was quite similar, hence, these two tables appear in the same form. Where no value has been indicated, a reliable experimental value was not obtained.

Explanation of Symbols Used in Tables 5.4 and 5.5

LP	= Load point
H	= Horizontal load per frame applied at third level
δ_1	= Horizontal deflection of first level
δ_2	= Horizontal deflection of second level
δ_3	= Horizontal deflection of third level
P_1	= Sum of axial forces in the three posts below first level
h_1	= Height of first level
$H_{P\delta}$	= Horizontal force replacing the effect of $P-\delta$ on the posts below first level
M_{grav}	= Moments in beams due to gravity
M_{lat}	= Moments in beams due to the lateral load H
M_{21}, M_{23}, M_{32}	--Beam moments at points defined in Fig. 5.8
$\Delta\epsilon_A, \Delta\epsilon_B, \Delta\epsilon_C, \Delta\epsilon_D$	--Column strains as defined in Tables 5.2 and 5.3 and Fig. 5.8.

The horizontal load-deflection curves at the third level for test A-R-1 are shown in Figs. 5.12 and 5.13. The graph was separated into two to avoid congestion of the hysteresis loops; hysteresis loops with deflection amplitudes of four inches or smaller were plotted on a different scale from those exceeding four inches. The same approach was

used when plotting the hysteresis loops for test B-R-1 at the third level, resulting in the diagrams shown in Figs. 5.14 and 5.15. The horizontal load-deflection hysteresis loops at the first level are presented in Figs. 5.16 and 5.17 for tests A-R-1 and B-R-1, respectively.

On these graphs the first cycle at each displacement amplitude is always shown in a solid line while the second and the third cycles are shown dashed. The shapes of the loops are similar to those obtained in the portal tests. The second cycle showed a decrease of hysteresis area from the first cycle while the third cycle remained practically the same as the second one. The characteristic pinching of the hysteresis loops, caused by the looseness of the connections and localized yielding in previous cycles, is again evident.

Strength and Stiffness: Both rack assemblies, A-R-1 and B-R-1, exhibited only a rather small linear range. Nonlinearity was caused at small loads by the nonlinear behavior of the beam-to-post connections and at a much later stage by inelastic response in the center posts. The nonlinear behavior of the connections led to a considerable deterioration of the loading stiffness and, to a smaller degree, of the unloading stiffness as is illustrated in Fig. 5.18 for assembly A-R-1.

In assembly A-R-1 no sign of imminent failure was evident at the maximum displacement of 17.3 in. although failure of the center post was expected at a much smaller displacement amplitude due to combined action of axial load and bending moment. However, in this case the axial load was too small to affect significantly the capacity of the post. Consequently, flexural plastic hinges developed in the center post above and below the beam-to-post connection, leading to a very

ductile response of the rack assembly. After formation of the plastic hinges in the center posts, moment redistribution to the exterior posts accounted for the additional increase in lateral resistance. The large rotations at the plastic hinges in the center post can be seen in the photo shown in Fig. 5.19. The only element that did exhibit significant distress was the exterior beam-to-post connection which attracted the highest bending moment (M_{32} in Table 5.4) in the pallet beams.

In assembly B-R-1 buckling of the center posts was imminent at the lateral displacement of 9.0 in. at which the test was terminated. In this assembly the axial load on the center posts was too high to permit the development of flexural plastic hinges and consequent redistribution of moments. All beam-to-post connections exhibited little distress and would have been capable of resisting higher moments.

P- δ Effect: Because of the low lateral stiffness of the semi-rigid frames, the P- δ effect did contribute significantly to the moments at each joint. In an approximate manner, this secondary effect can be represented by equivalent story shears of magnitudes $H_{p\delta} = P_i \delta_i / h_i$, where P_i , δ_i and h_i are total axial forces, story drift and height of story i , respectively. Thus, it can be postulated that the internal forces in the frames due to H and the P- δ effect are close to those caused by a story shear $\bar{V} = H + H_{p\delta}$. The ratio of \bar{V}/H represents therefore the amplification of story shears due to the P- δ effect. Values of $H_{p\delta}$ and \bar{V}/H are tabulated in Tables 5.4 and 5.5. It is quite evident from these tables that the P- δ effect will greatly affect the response of the racks in the longitudinal direction.

Beam Moments: The flexural strains, measured at the strain gage locations, due to the lateral loads in tests A-R-1 and B-R-1 were

extrapolated to the post center lines, and using the moment-strain relationships already established in the cantilever tests, the moments M_{21} , M_{23} , and M_{32} , shown in Figs. 5.20 and 5.20 were calculated. These moments due to the lateral loads were added to the moments due to the gravity loads which resulted in the total beam moments presented in Tables 5.4 and 5.5 for A-R-1 and B-R-1, respectively. An equilibrium check of the moments due to the lateral load was made assuming reasonable points of inflection in the posts. The measured moments in Test A-R-1 were found to be in equilibrium with story shears while those of Test B-R-1 were found to be low. The low values of moments in Test B-R-1 may in part be explained by the high fixity achieved at the post-to-floor connections, but may also be caused by instrumentation or calibration errors and thus cannot be considered to be reliable.

The moments due to lateral load are plotted against the total equivalent base shear $\bar{V} = H + P_1 \delta_1 / h_1$ in Figs. 5.20 and 5.21. These graphs illustrate the rate at which each beam-to-post connection attracts moments with an increase in base shear.

Moments in Posts: Actual values of moments in the posts could not be obtained since a reliable calibration of flexural strains vs moments was impossible due to the geometric configuration of the post sections (open sections) and the presence of perforations. Nevertheless, qualitative information on relative moment values can be obtained from the flexural strain measurements ($\Delta\epsilon_B$, $\Delta\epsilon_C$ and $\Delta\epsilon_D$) tabulated in Tables 5.4 and 5.5.

The strain gage locations are indicated in Tables 5.2 and 5.3 and Figures 5.4 to 5.8. The values of $\Delta\epsilon_A$ were found to be consistently low and unreliable and are not included in the tabulated results.

It can be observed from the presented results that the moment at the center column base ($\Delta\epsilon_B$) is always a significant portion of the column moment at the first floor level ($\Delta\epsilon_D$). Thus, the column bases provide a significant restraint against rotation which in turn reduces the column moments at the first floor level. The high level of strains close to the column base ($\Delta\epsilon_B$) in test A-R-1 indicates that the column base was approaching flexural yielding in this test.

If the strains in the positive direction of loading are separated from those in the opposite direction of loading, it is seen that in both directions the flexural strains increase consistently as the lateral load is increased. The strains at the interior post below the first level, $\Delta\epsilon_D$, increase most rapidly. In test A-R-1 clearly visible flexural hinges developed in the interior posts above and below the beam-to-post connection while no inelastic behavior was evident in the exterior posts. This can also be seen from the strain measurements $\Delta\epsilon_C$ and $\Delta\epsilon_D$ which were taken below the first level in the exterior and interior post, respectively.

5.2 Transverse Tests (A-R-2 and B-R-2)

5.2.1 Experimental Set-Up

A plan view of the experimental set-up for the transverse tests is shown in Fig. 5.22. Only single-bay assemblies were tested to assure an equal distribution of lateral load to the two upright frames. Gravity loads between the upright frames were simulated with four 1000 lbs concrete blocks per level, which corresponds to two-thirds pay-load (see Fig. 4.23).

It was intended to test the behavior of interior bays with zero moments in the posts in the longitudinal direction, so 1000 lbs concrete blocks were suspended from cantilever beams as shown in Fig. 5.23 to equilibrate the beam moments at the joints. In this manner the loading condition of interior bays with two-thirds pay-load was simulated. Knee braces were added to prevent displacement in the more flexible longitudinal direction. The lateral load was applied by a hydraulic jack attached to the middle of a distribution beam at the third level so that the load will be distributed equally between the two frames (see Fig. 5.24). A photograph of a rack assembly loaded with concrete blocks is shown in Fig. 5.25.

The instrumentation consisted of LVDTs and linear potentiometers to measure the horizontal deflection at the three levels of the two frames designated at T1 and T2. Strain gages were attached to the columns below the first level and also to the braces which join the posts below the first level. Strain gages were applied in pairs to obtain average readings of axial strains in posts and braces. The parameters measured in tests A-R-2 and B-R-2 are summarized in Tables 5.6 and 5.7. Figures 5.26 and 5.27 show sketches of loading and instrumentation for the two rack assemblies.

5.2.2 Loading Histories

The lateral load was again applied quasi-statically. Load control was used for most of the test to control the loading history except at amplitudes causing severe strength and stiffness degradation where displacement control was applied. The racks were subjected to cyclic loadings with increasing amplitude of load or displacement. Again, three cycles were carried out at each amplitude. The history of lateral deflection at the third level is shown in Figs. 5.28 and 5.29 for tests

A-R-2 and B-R-2, respectively.

5.2.3. Experimental Results and Observations

Tables 5.8 and 5.9 show numerical results for several of the load points indicated in Figs. 5.28 and 5.29. The symbols used in these two tables are similar to those used in Tables 5.4 and 5.5 for the longitudinal tests. The few additional symbols used are defined below.

$$h = h_1 + h_2 + h_3 \text{ (see Fig. 1.1)}$$

P_{lat} = calculated axial force in posts below first level
due to the lateral load

P_{grav} = calculated axial force in posts below first level
due to pay loads

P = calculated total axial force in posts below first
level

The horizontal load-deflection relationships at the third level are shown in Figs. 5.30 (A-R-2) and 5.31 (B-R-2). Again, the first cycle at each amplitude is shown in a solid line while the second and third cycles are shown dashed.

Strength and Stiffness: Both rack assemblies did exhibit nonlinear response characteristics at relatively low lateral loads. As can be seen from Figs 5.26 and 5.27, the diagonal braces were connected eccentrically to the posts causing significant weak axis bending in the posts. This bending in combination with high axial forces accounted for some of the inelastic behavior evident from Figs. 5.30 and 5.31. However, most of the inelastic action must be attributed to other sources which differ between assemblies A-R-2 and B-R-2.

In assembly A-R-2 the nonlinear behavior was caused primarily

by local bending of the 1/4 in. thick base plates at the post-to-floor connections. Because of the large height to width ratio of the upright frames, uplift forces developed in one of the posts when the lateral load on the frame exceeded approximately 1000 lbs. These uplift forces had to be transferred from the post to the anchor bolt through flexural action of the base plate. This flexural action limited the lateral force transfer in this rack assembly, since rather brittle fracture occurred at the weld connecting the post to the base plate before the buckling loads in posts or braces were attained. The magnitude of the uplift force at which weld fracture occurred was approximately 7,000 lbs as can be read from Table 5.8. The corresponding compression force in the opposite post was approximately 16,000 lbs which was significantly higher than the analytically predicted force capacity.

In assembly B-R-2 weld fracture at the base plates did not take place. However, early nonlinear behavior was observed at the connections between the open-section bracing elements and the open-section posts. Localized plastic bending in the lips of the posts was evident at low loads which was followed at higher loads by local buckling of the open-section bracing elements. Distinct local buckling was also visible between perforations in the posts. The strong local buckling in the bracing elements and the plastic bending in the lips of the posts did limit the strength of the upright frames and were the cause of significant stiffness deterioration. However, they were also a source of considerable and unexpected energy dissipation as is evident from the sizeable hysteresis loops shown in Fig. 5.31. Thus, these localized inelastic deformations may not necessarily be disadvantageous when the upright frames are called upon to absorb and dissipate a large energy input from

severe ground motions.

Axial Forces: Since reliable measurement of axial forces in posts and braces was not possible, the tabulated values of axial forces in the posts (Tables 5.8 and 5.9) were calculated from statics and are approximate. A qualitative evaluation of actual force distribution can be obtained from the strain measurements tabulated in Tables 5.8 and 5.9 and plotted in Figs. 5.32 and 5.33.

Deflection Patterns: The deflected shapes of the rack assemblies at various loading stages are shown in Figs. 5.34 and 5.35. The solid lines are for loading in the positive direction and the dashed lines for loading in the negative direction. The deflection patterns clearly illustrate the difference in the behavior of assemblies A-R-2 and B-R-2. While assembly A-R-2 responds primarily in a flexural cantilever mode (rate of deflection increases with height), assembly B-R-2 responds in a shear type mode (largest relative deflection in first story) once inelastic deformations at the brace-to-post connections dominate the response.

6. DYNAMIC TESTS

The two rack assemblies A-R-1 and B-R-1, loaded with pay-loads as summarized in Table 5.1, were subjected to forced and free vibration tests to obtain information on natural frequencies, mode shapes and damping characteristics in the longitudinal and transverse direction.

6.1 Forced Vibration Studies

Forced vibrations were generated by means of an electromagnetic vibration generator mounted on top of the concrete weights at the third level as shown in Fig. 6-1. The vibration generator was located symmetrically with respect to the longitudinal axis but unsymmetrically with respect to the transverse axis. Band-width limited white noise was used as input excitation for the investigation of frequencies and mode shapes.

Two accelerometers were used for response measurements. One accelerometer was mounted at a reference point (point 1 in Figs. 6.2 to 6.5) while the other was placed at various predetermined locations for mode shape determination. Two time histories were recorded simultaneously and the Fourier transform as well as the auto- and crosspower spectral density functions were calculated. All computations were done on-line with a Fourier Analyzer System. To minimize random and recording errors, the white noise excitation was repeated fifty times for each recording station and average values for auto- and crosspower spectra were obtained. The transfer function for the two time histories was then calculated as the ratio of the average crosspower spectral density function over the average autopower spectral density function at the reference

point. The values of the transfer function at the spectral peaks determine the relative modal accelerations and displacements.

The results of the forced vibration tests are summarized in Tables 6.1 to 6.4 and Figures 6.2 to 6.5. While the three longitudinal frequencies and mode shapes were easy to identify through the aforementioned system identification techniques, a large number of modes of usually unsymmetric nature were obtained from excitation in the transverse direction. This unsymmetry was caused in part by the eccentric location of the vibration generator, but was also attributable to unavoidable minor unsymmetry in stiffness and mass distribution and to the excitation of individual floor modes. Nevertheless, principal transverse modes and torsional modes can clearly be identified from the sketches of mode shapes shown in Figs. 6.3 and 6.5.

Assembly A-R-1: Detailed information from which the results for mode shapes and frequencies (Tables 6.1 and 6.2 and Figs. 6.2 and 6.4) were derived are presented in Figs. 6.6 to 6.29. Figures 6.6 to 6.17 represent a complete set of data for identification of the three principal modes in the longitudinal direction. The autopower spectral density functions at Nodes 1, 2 and 3 (Figs. 6.7, 6.9 and 6.14) identify three well defined natural modes whose properties at Nodes 2 and 3, relative to Node 1, are summarized in the tables accompanying Figs. 6.10 and 6.15.

Figures 6.18 to 6.29 illustrate some of the data used to identify modal properties due to transverse excitations. It is important to note that transverse excitation did cause also considerable longitudinal and torsional motion. The properties of the longitudinal motion at Node 1 are illustrated in Figs. 6.25 to 6.29. The autopower spectral density

functions for transverse response at Nodes 1 and 2 (Figs 6-19 and 6.21) contain a large number of spectral peaks whose modal properties (up to 10.8 Hz) are summarized in Table 6.2 and Fig. 6.4. Modes 1 and 4 can be identified as basic transverse modes, modes 2, 3 and 8 are torsional modes, and modes 6 and 7 are horizontal modes with the center frame moving opposite to the exterior frames. From the high frequencies of these modes, it can be concluded that significant diaphragm action was provided by the wooden pallets loaded with concrete blocks.

Assembly B-R-1: Results similar to those for A-R-1 are presented for B-R-1 in Figs. 6.30 to 6.53. Again, the three longitudinal modes were well defined although a transversely placed accelerometer recorded considerable transverse response (Figs. 6.42 to 6.46) under longitudinal excitation.

Under transverse excitation a large number of spectral peaks are again evident in the autopower spectral density functions (Figs. 6.48 and 6.50). The modal properties of these peaks (up to 6.45 Hz) are summarized in Table 6.4 and Fig. 6.5. Modes 1 and 3 can be identified as basic transverse modes, mode 2 is a torsional mode and mode 6 is a horizontal mode with the center frame moving opposite to the exterior frames. The other modes appear to be generated by out-of-phase motion of individual floor masses.

6.2 Free Vibration Studies

Damping properties in the longitudinal and transverse direction were obtained from the decay of free vibrations. Samples of test results are shown in Figs. 6.54 to 6.69. The damping was strongly dependent on the amplitude of motion due to the nonlinear characteristics of the

beam-to-post connections. This dependence on amplitude is illustrated in Figs. 6.56, 6.60, 6.64 and 6.88 and in the subsequent figures which show the increase in frequency with a decrease in damping.

Of some interest is the vibration decay shown in Fig. 6.59 which is a textbook example of Coulomb friction effect. At large amplitudes the grip-type connectors were moving with respect to the perforations in the posts causing significant damping. Once the connectors locked at smaller amplitudes, the damping dropped drastically to a very small value (see Fig. 6.60).

7. SUMMARY AND CONCLUSIONS

The objective of the experimental study reported herein was to acquire basic information on the response characteristics that govern the seismic behavior of industrial storage racks. Although the study was limited to specific types of standard pallet racks, it is expected that much of what has been learned can be applied to other rack configurations. The purpose of the study was to acquire information which, together with results from shaking table tests carried out at the University of California, Berkeley, can serve as a basis for the development of seismic design criteria for storage racks.

The conclusions drawn from this study, which should only be applied to racks of similar configurations, are as follows:

1. The elements which control the seismic response of storage racks are the beam-to-post connections, the upright frames consisting of posts and bracing members, and the frame-to-floor connections.

2. The behavior of the beam-to-post connections can be represented by rotational springs whose characteristics should be determined experimentally. Ideally, strength, stiffness and ductility of these springs should be determined by means of subassembly (portal) tests using cyclic loading. The cantilever test, which is much simpler to carry out and results in more reliable measurements of moments, could be used as an alternative.

3. The determination of the response characteristics of posts and upright frames will require tests of rack assemblies which permit proper simulation of boundary and loading conditions.

4. The $P-\delta$ effect greatly affects the lateral strength and stiff-

ness in the longitudinal unbraced frame direction and should be included in response predictions.

5. Because of local deformations at the beam-to-post connections, hysteresis loops have a pinched shape similar to that obtained in reinforced concrete elements with high shear.

6. Low cycle fatigue phenomena (in particular, early fracture at welds or points of stress concentrations, caused by strain reversals) may affect the strength and ductility of beam-to-post and post-to-floor connections.

7. The ductility and energy dissipation capacity of racks is much larger in the longitudinal (moment resisting frame) direction than in the transverse (braced frame) direction.

8. The ductility of the longitudinal frames depends strongly on the ratio P/P_{cr} (P = axial load, P_{cr} = buckling load) in the individual posts. For small P/P_{cr} ratios, column buckling will not take place and ductile plastic hinges will develop in the posts.

REFERENCES

1. Pekoz, T., "Interpretation of Pallet Rack Test Results", Report to the Rack Manufacturers Institute; Ithaca, Feb. 1978.
2. Pekoz, T., "Pallet Rack Design Criteria", Report to the Rack Manufacturers Institute; Ithaca, Feb. 1978.
3. Rack Manufacturers Institute, "Specification for the Design, Testing, and Utilization of Industrial Steel Storage Racks", March 1977.

Table 2.1

Section Properties of Rack Elements

		A	I_x	I_y	S_x	S_y	r_x	r_y
		in. ²	in. ⁴	in. ⁴	in. ³	in. ³	in.	in.
Type A	Beam	1.010	2.664	1.104	1.109	0.746	1.624	1.045
	Post	0.672	1.037	0.318	0.691	0.277	1.228	0.688
	Brace							
Type B	Beam	1.288	3.265	1.195	1.496	0.760	1.630	0.986
	Post	0.688	1.144	0.879	0.756	0.586	1.288	1.130
	Brace	0.318	0.125	0.075	0.131	0.100	0.628	0.4087
Type C1	Beam	1.094	1.175	0.722	0.940	0.501	1.024	0.803
	Post	0.753	2.206	0.942	1.103	0.543	1.711	1.118
Type C2	Beam							
	Post	0.753	2.206	0.942	1.103	0.543	1.711	1.118
Type D	Beam		2.319	1.071	1.123	0.686		
	Post	0.620	0.671	0.317	0.447	0.317	1.040	0.644

Table 4.1

Types of Portal Tests

		Designation	Type of Test	Vertical Load Per Frame
Type A	1st Test	A-P-1	Monotonic	1500 lbs.
	2nd Test	A-P-2	Monotonic	3000 lbs.
Type B	1st Test	B-P-1	Monotonic	3000 lbs.
	2nd Test	B-P-2	Cyclic	3000 lbs.
Type C1		C1-P	Monotonic	1500 lbs.
Type D		D-P	Monotonic	2000 lbs.

Table 5.1

Types of Full Rack Tests

	Rack Type	Designation	Configuration	Type of Test	Vertical load per frame per level per bay
Longitudinal Tests	A	A-R-1	3 levels, 2 bays	Cyclic	1500 lb.
	B	B-R-1	3 levels, 2 bays	Cyclic	3000 lb.
Transverse Tests	A	A-R-2	3 levels, 1 bay	Cyclic	2000 lb.
	B	B-R-2	3 levels, 1 bay	Cyclic	2000 lb.

Table 5.2
 Test A-R-1, Displacement and Strain Measurements
 of Frames L1 and L2

	Frame L1	Frame L2
Displacement	First Level (δ_1) Second Level (δ_2) Third Level (δ_3)	First Level (δ_1) Second Level (δ_2) Third Level (δ_3)
Flexural Strains and Moments	M_{21} M_{23} refer to Fig. 5.8 M_{32} Top of first level central post $\Delta\epsilon_A$ Bottom of first level central post $\Delta\epsilon_B$ Top of first level exterior post $\Delta\epsilon_C$	Top of first level central post $\Delta\epsilon_D$

Table 5.3
 Test B-R-1, Displacement and Strain Measurements
 of Frames L1 and L2

	Frame L1	Frame L2
Displacement	First Level (δ_1) Second Level (δ_2) Third Level (δ_3)	First Level (δ_1)
Flexural Strains and Moments	M_{21} M_{23} refer fo Fig. 5.8 M_{32} Top of first level central post $\Delta\epsilon_A$ Bottom of first level ex- terior post $\Delta\epsilon_B$ Top of first level exterior post $\Delta\epsilon_C$	Top of first level central post $\Delta\epsilon_D$

Table 5.4 RESULTS OF TEST A-R-1

Calculated axial force in posts due to gravity loads (below first floor): $C_1 = C_3 = 2250$ lbs
 $C_2 = 4500$ lbs

L.P.	Frame L1						
	Horizontal Load	Deflections			$H = P_1 \delta_1 / h_1$	$\bar{V} = H + H_{P\delta}$	\bar{V}/H
	H	δ_1	δ_2	δ_3	$P\delta$		
	lbs.	ins.	ins.	ins.	lbs.	lbs.	
0	0	0	0	0	0	0	
1	160	0.19	0.37	0.50	28	188.5	1.18
2	-160	-0.18	0.39	-0.50	-27	-187	1.17
3	500	0.73	1.47	2.05	110	610	1.22
4	-500	-0.70	-1.41	-2.00	-105	-605	1.21
5	-500	-0.72	-1.44	-1.96	-108	-608	1.22
7	775	1.30	2.71	3.75	195	970	1.25
8	-810	-1.30	-2.84	-3.95	-195	-1005	1.24
9	-800	-1.30	-2.86	-3.95	-195	-995	1.24
12	1080	2.30	4.45	6.18	345	1425	1.32
15	-1010	-2.24	-4.30	-5.40	333	-1343	1.33
20	-1000	-2.24	-4.57	-5.40	336	-1336	1.34
22	1150	2.83	5.57	8.15	425	1575	1.37
24	1350	4.62		12.30	693	2043	1.51
26	1380	5.21		14.10	782	2162	1.57
28	1300	6.92		17.30	1038	2338	1.80

Note

$$P_1 = C_1 + C_2 + C_3$$

Table 5.4 (Continued)

Calculated gravity moments in beams at post center lines: $M_{21} = M_{23} = -3800$ lb-in.
 $M_{32} = -3400$ lb-in.

L.P.	H	Frame L1							
		Beam Moments						Column Flexural Strains Due to H	
		M_{lat} due to H			Total = $M_{lat} + M_{grav}$			$\Delta\epsilon_B$	$\Delta\epsilon_C$
		M_{21}	M_{23}	M_{32}	M_{21}	M_{23}	M_{32}		
lbs.	lb.-in.	lb.-in.	lb.-in.	lb.-in.	lb.-in.	lb.-in.	in./in. x 10^{-6}	in./in. x 10^{-6}	
0	0	0	0	0	-3800	-3800	-3400	0	0
1	160	-3400	1500	-3900	-7200	-2300	-7300	118	75
2	-160	3100	-1400	3200	-700	-5200	-200	132	106
3	500	-8200	7300	-9100	-12000	3500	-12500	468	265
4	-500	8200	-7300	10500	4400	-11100	7100	363	332
5	-500	8500	-7400	10700	4700	-11200	7300	355	329
7	775	-11200	12800	-11600	-15000	9000	-15000	1160	385
8	-810	16900	-13200	20400	13100	-17000	17000	540	664
9	-800	17200	-13000	20700	13400	16800	17300	530	673
12	1080	-13700	18200	-14400	-17500	14400	-17800	1540	1058
15	-1010	24200	-16100	29400	20400	-19900	26000	680	1009
20	-1000	24400	-16000	29000	20600	-19800	25600	670	1000
22	1150	-14700	20300	-14900	-18500	16500	-18300	1600	982
24	1350	-16900	24000	-18900	-20700	20200	-22300	1750	1267
26	1380	-17500	25200	-20700	-21300	21400	-24100	1810	1417
28	1300	-17800	27000	-20800	-21600	23200	-24200	1860	1493

Notes:

- (1) Beam moments obtained at location of strain gages were extrapolated to the center line of column.
- (2) The above column strain gage readings are the values recorded at the strain gage locations.

Table 5.4 (Continued)

L.P.	H	Frame L2						Column Strain $\Delta \epsilon_D$ in./in. $\times 10^{-6}$	Remarks
		Deflections		$H_P \delta = P_1 \delta_1 / h_1$	$\bar{V} = H + H_P \delta$	\bar{V}/H			
		δ_1	δ_2						
lbs.	ins.	ins.	lbs.	lbs.					
0	0	0	0	0	0		0	All readings zeroed after application of vertical load	
1	160	0.18	0.37	27	187	1.17	230	Non-linear behavior in H- δ diagram	
2	-160	-0.18	-0.36	-27	-187	1.17	171		
3	500	0.72	1.44	108	608	1.22	635		
4	-500	-0.72	-1.61	-108	-608	1.22	590		
5	-500	-0.70	-1.66	-105	-605	1.21	685		
7	775	1.34	2.65	201	976	1.26	1190		
8	-810	-1.52	-2.83	-228	-1038	1.28	1390		
9	-800	-1.53	-2.85	-230	-1030	1.29	1360		
12	1080	2.32	4.57	348	1428	1.32	1950		Test discontinued overnight
15	-1010	-2.30	-4.02	-345	-1355	1.34	1910		Test discontinued the next day
20	-1000	-2.31	-4.04	-347	-1347	1.35	1880		
22	1150	2.96	6.04	445	1575	1.39	2490		
24	1350	4.73		714	2064	1.53	3260		
26	1380	5.40		811	2191	1.59	3460		
28	1280	7.12		1070	2350	1.84	4150		Plastic hinges clearly visible in the interior post below first floor level. Strong cracking of welds of base plate.

Table 5.5 - RESULTS OF TEST B-R-1

Calculated axial forces in posts due to gravity loads (below first floor): $C_1 = C_3 \approx 4500$ lbs
 $C_2 \approx 9000$ lbs

L.P.	H	Frame L1					
		Deflections			$H_{p\delta} = P_1 \delta_1 / h_1$	$\bar{V} = H + H_{p\delta}$	\bar{V}/H
		δ_1	δ_2	δ_3			
lbs.	ins.	ins.	ins.	lbs.			
0	0	0	0	0	0	0	
1	400	0.325	0.70	1.05	97.5	497.5	1.24
3	575	0.700	1.40	2.10	210.0	785.0	1.36
4	-590	-0.740	-1.40	-2.10	-222.0	-812.0	1.38
5	600	0.700	1.41	2.10	210.0	810.0	1.35
6	-590	-0.730	-1.42	-2.10	-219.0	809.0	1.37
7	750	1.125	2.14	3.15	337.5	1087.5	1.45
8	-750	-1.175	-2.15	-3.15	-352.5	-1102.5	1.47
9	850	1.425	2.64	3.89	427.5	1277.5	1.50
11	-850	-1.500	-2.66	-3.93	-450.0	-1300.0	1.53
14	1000	2.500		6.30	750.0	1750.0	1.75
15	-1000	-2.200		-5.46	-660.0	-1660.0	1.66
17	960	2.750		6.40	825.0	1785.0	1.86
18	-960	-2.050		-5.35	-615.0	-1575.0	1.64
20	990	3.100		6.93	930.0	1920.0	1.94
21	1010	4.200		9.03	1260.0	2270.0	2.25

Notes

$$P_1 = C_1 + C_2 + C_3$$

Table 5.5 (continued)

Calculated gravity moments in beams at post center lines: $M_{21} = M_{23} = -7600$ lb-in.
 $M_{32} = -6700$ lg-in.

L.P	H.	Frame L1							
		Beam Moments						Column flexural strains due to H	
		M_{lat} due to H (measured)			Total = $M_{lat} + M_{grav}$			$\Delta\epsilon_B$	$\Delta\epsilon_C$
		M_{21}	M_{23}	M_{32}	M_{21}	M_{23}	M_{32}	in/in $\times 10^{-6}$	in/in $\times 10^{-6}$
lb-in	lb-in	lb-in	lb-in	lb-in	lb-in				
0	0	0	0	0	-7600	-7600	-6700	0	0
1	400	-4700	3600	-6000	-12300	-4000	-12700	530	
3	575	-7800	5400	-9100	-15400	-2200	-15800	850	238
4	-590	7300	-6200	9300	-300	-13800	2600	700	305
5	600	-7000	6800	-8500	-14600	-800	-15200	870	240
6	-590	7200	-5200	9600	-400	-12800	2900	720	317
7	750	-9100	9100	-11400	-16700	1500	-18100	1010	397
8	-750	9500	-7500	15800	1900	-15100	9100	830	540
9	850	-9700	11900	-13000	-17300	4300	-19700	1090	442
11	-850	11100	-8200	20800	3500	-15800	14100	840	727
14	1000	-10300	16100	-15900	-17900	8500	-22600	1150	716
15	-1000	15600	-9100		8000	-16700		930	1056
17	960	-9600	16300	-14400	-17200	8700	-21100	1060	690
18	-960	16400	-10700	33200	8800	-18300	26500	970	1008
20	990	-9700	17400	-15700	-17300	9800	-22400	1070	812
21	1010	-9000	22700	-16400	-16600	-15100	-23100	1110	1057

Notes

- 1 Beam moments obtained at the location of strain gages were extrapolated to the center line of column.
- 2 The above column strain gages readings were the values recorded at the strain gage locations.

Table 5.5 (continued)

L.P.	H	Frame L2				Column Strain $\Delta\epsilon_D$	Remarks	
		Deflection δ_1	$H_{P\delta} = P_1 \delta_1 / h_1$	$\bar{V} = H + H_{P\delta}$	\bar{V}/H			
	lbs.	inS.	lbs	lbs				
0						0	All readings zeroed after application of vertical loads	
1	400					380	Nonlinear behavior in load deflection diagram	
3	575	0.67	201	776	1.35	570		
4	-590	-0.71	-213	-803	1.36	690		
5	600	0.68	204	804	1.34	610		
6	-590	-0.72	-216	-806	1.37	740		
7	750	1.12	336	1086	1.45	760		
8	-750	-1.12	-339	-1089	1.45	1020		
9	850	1.41	423	1273	1.50	970		
11	-850	-1.44	-432	-1282	1.51	1210		
14	1000					1290		
15	-1000					1600		Test was discontinued overnight
17	960					1320		Test continued the next day
18	-960					1600		
20	990					1300		
21	1010					1760		Buckling of interior post evident

Table 5.6

Instrumentation for Test A-R-2

	Frame T1	Frame T2
Deflections	Deflection at First Level (δ_1) Deflection at Second Level (δ_2) Deflection at Third Level (δ_3)	Deflection at First Level (δ_1) Deflection at Third Level (δ_3)
Axial Strain Measurements	Post C ₂ Brace	Post C ₃ Post C ₄

Table 5.7

Instrumentation for Test B-R-2

	Frame T1	Frame T2
Deflections	Deflection at First Level (δ_1) Deflection at Second Level (δ_2) Deflection at Third Level (δ_3)	Deflection at First Level (δ_1) Deflection at Second Level (δ_2) Deflection at Third Level (δ_3)
Axial Strain Measurements	Brace	Brace Post C ₃

Table 5.8 RESULTS OF TEST A-R-2

Calculated axial forces due to gravity loads (below first level) in all posts: $P_{grav.} = -4500$ lbs

LP	H	Frame T1					Frame T2			
		Deflections			Average Axial Strains Due to H		Deflections		Average Axial Strains Due to H	
		δ_1	δ_2	δ_3	Post C ₂	Brace	δ_1	δ_2	Post C ₃	Post C ₄
lbs.	ins.	ins.	ins.	in./in. x 10 ⁻⁶	in./in. x 10 ⁻⁶	ins	ins	in./in. x 10 ⁻⁶	in./in. x 10 ⁻⁶	
0	0	0	0	0	0	0	0	0	0	0
1	500	0.075	0.147	0.250	110.4	- 104.0	0.077	0.250	- 88.5	85.5
2	- 512	- 0.087	- 0.138	- 0.225	- 89.5	88.0	- 0.092	- 0.250	66.0	- 100.0
3	775	0.107	0.222	0.375	158.8	- 145.5	0.109	0.375	- 123.5	141.5
4	- 750	- 0.119	- 0.214	- 0.350	- 137.1	137.0	- 0.147	- 0.425	105.0	- 145.0
5	1037	0.154	0.310	0.500	214.9	- 185.0	0.157	0.525	- 157.5	197.5
6	- 1000		0.306	- 0.500	- 188.1	193.0	- 0.212	- 0.600	145.0	- 182.5
7	1537	0.249	0.498	0.800	312.7	- 277.5	0.266	0.850	- 237.5	282.5
8	- 1500	- 0.300	- 0.542	- 0.875	- 286.7	285.0	- 0.356	- 1.025	227.5	- 227.5
10	2050	0.367	0.718	1.175	415.5	- 372.5	0.399	1.250	- 312.5	380.0
11	- 1975	- 0.436	- 0.785	- 1.275	- 367.0	370.0	- 0.527	- 1.475	295.0	- 357.5
12	2575	0.521	1.037	1.675	521.7	- 467.5	0.583	1.825	- 407.5	492.5
13	- 2250		- 1.209	- 1.975		487.5		- 2.225	392.5	- 442.5
15	2250			2.200		- 420.0		2.900	- 322.5	372.5

Note: Sign Convention for Axial Forces: + = Tension
 - = Compression

Table 5.8 (Continued)

LP	H	$P_{lat} = \frac{Hh}{b}$	Posts C_1 and C_3 $P = (P_{grav} - P_{lat})$	Posts C_2 and C_4 $P = (P_{grav} + P_{lat})$	Remarks
	lbs.	lbs.	lbs.	lbs.	
0	0	0	-4500	-4500	All readings zeroed after vertical load applications
1	500	2200	-6700	-2300	Frame behaves elastically on loading and unloading
2	-512	-2253	-2247	-6753	
3	775	3410	-7910	-1090	
4	-750	-3300	-1200	-7800	
5	1037	4563	9063	63	
6	-1000	-4400	-100	-8900	
7	1537	6763	-11263	2263	Inelastic behavior detected from H- δ diagram
8	-1500	-6600	2100	-11100	
10	2050	9020	-13520	4520	
11	-1975	-8690	4190	-13190	
12	2575	11330	-15830	6830	
13	-2550	-11220	6720	-15720	
15	2250	9900	-14400	5400	With a load crack, the weld at the base plate fractured in post C_4 . No buckling in posts or braces.

Table 5.9 RESULTS OF TEST B-R-2

Calculated axial forces due to gravity loads (below first level) in all posts: $P_{grav.} = -4500$ lbs

LP	H	Frame T1				Frame T2				
		Deflections			Average Axial Strain	Deflections			Average Axial Strains	
		δ_1	δ_2	δ_3	Brace	δ_1	δ_2	δ_3	Post C ₃	Brace
lbs.	ins.	ins.	ins.	in./in. x 10 ⁻⁶	ins.	ins.	ins.	in./in. x 10 ⁻⁶	in./in. x 10 ⁻⁶	
0	0	0	0	0	0	0	0	0	0	0
1	1012	0.144	0.304	0.500	- 133	0.164	0.337	0.550	- 130	- 135
2	- 975	- 0.108	- 0.256	- 0.375	153	- 0.136	- 0.297	- 0.475	145	152
3	1575	0.267	0.551	0.875	- 213	0.305	0.605	0.975	- 200	- 215
4	- 1475	- 0.217	- 0.464	- 0.750	218	- 0.259	- 0.529	- 0.900	230	231
5	2025	0.417	0.842	1.325	- 308	0.492	0.911	1.450	- 237.5	- 280
6	- 2000	- 0.486	- 0.889	- 1.400	338	- 0.548	- 0.993	- 1.575	360	335
7	2400	0.708	1.334	2.000	- 347	0.846	1.487	2.250	317.5	- 321
8	- 2400	- 0.884	- 1.488	- 2.125	432	- 0.920	- 1.570	- 2.375	450	434
9	2425		1.858	2.600	- 320	1.208	2.022		305	- 282
10	- 2525		- 1.898	- 2.700	468	- 1.222	- 1.969		452.5	479
11	2200			2.600	- 257	1.224			- 282.5	- 280

Note

Sign Convention for Axial Forces: + = Tension
 - = Compression.

Table 5.9 (Continued)

LP	H	$P_{lat} = \frac{H}{b}$	Posts C_1 & C_3	Posts C_2 & C_4	Remarks
	lbs.	lbs.	$P = P_{grav} - P_{lat}$	$P = P_{grav} + P_{lat}$	
0	0	0	- 9500	- 4500	All readings zeroed after application of vertical loads Inelastic behaviour detected on the H- δ diagram Local Buckling started to occur in all posts close to the base. Severe distortions in diagonal braces and posts at the junction with diagonal braces. No failure at base plate weld.
1	1012	4567	- 9067	67	
2	- 975	- 4400	- 100	- 8900	
3	1575	7108	- 11608	2608	
4	- 1475	- 6656	2156	- 11156	
5	2025	9128	- 13638	4638	
6	- 2000	- 9026	4526	- 13526	
7	2400	10831	- 15331	6331	
8	- 2400	- 10831	6331	- 15331	
9	2425	10944	- 15444	6444	
10	- 2525	- 11395	6895	- 15895	
11	2200	9928	- 14428	5428	

Table 6.1

Mode Shapes and Frequencies
A-R-1 Longitudinal Direction

Mode	1	2	3
Frequency (Hertz)	0.74	2.77	5.10
Node			
1	1.00	-0.80	-0.47
2	0.74	0.49	1.00
3	0.52	1.00	-0.80

Table 6.2

Mode Shapes and Frequencies
A-R-1 Transverse Direction

Mode	1	2	3	4	5	6	7	8
Frequency (Hertz)	2.25	2.83	3.22	5.27	6.25	7.32	8.98	10.84
Node								
1	0.66	-0.43	1.00	1.00	1.00	1.00	1.00	-0.89
2	0.46	-0.30	0.72	0.20	0.24	0.53	0.70	-0.64
3	0.25	-0.16	0.38	-0.35	(0.03)	0.24	0.35	-0.29
4	1.00	0.36	0.06	0.73	0.10	-0.47	-0.68	-0.28
5	0.69	0.27	0.06	-0.55	-0.10	-0.32	-0.55	-0.20
6	0.40	0.15	0.04	-0.95	(-0.02)	-0.16	-0.32	-0.11
7	0.99	1.00	-1.00	0.08	-0.09	0.41	0.77	1.00
8	0.68	0.70	-0.61	-0.57	0.24	0.31	0.54	0.73
9	0.41	0.41	-0.36	-0.65	0.30	0.19	0.33	0.42

Table 6.3

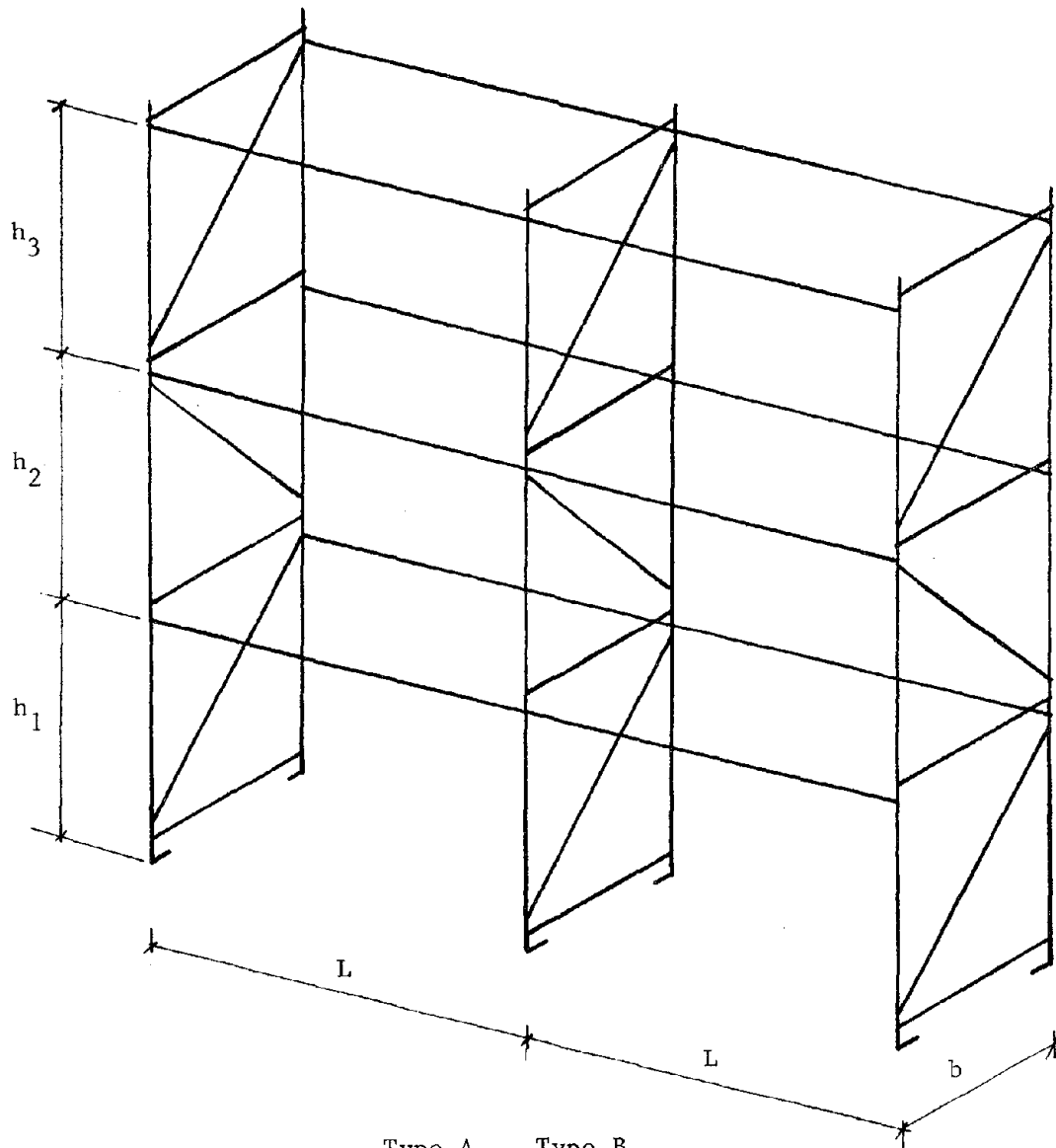
Mode Shapes and Frequencies
B-R-1 Longitudinal Direction

Mode	1	2	3
Frequency (Hertz)	0.63	2.19	3.87
Node			
1	1.00	-0.68	-0.43
2	0.77	0.58	1.00
3	0.44	1.00	-0.86

Table 6.4

Mode Shapes and Frequencies
B-R-1 Transverse Direction

Mode	1	2	3	4	5	6	7
Frequency (Hertz)	1.66	2.25	3.42	3.71	4.10	5.47	6.45
Node							
1	0.77	-0.94	-0.59	0.78	0.70	1.00	-0.64
2	0.59	-0.75	0.12	0.31	-0.51	0.73	-0.52
3	0.30	-0.39	0.29	0.44	-0.87	(0.28)	(0.17)
4	1.00	-0.02	-0.78	0.52	0.18	-0.62	-0.30
5	0.74	-0.04	0.61	-0.67	0.28	-0.47	-0.32
6	0.41	-0.03	1.00	1.00	-0.58	-0.27	-0.12
7	0.93	1.00	-0.25	-0.36	-0.47	0.55	1.00
8	0.66	0.72	0.45	-0.50	1.00	0.41	0.66
9	0.33	0.28	0.65	-0.19	0.84	0.22	0.36



	Type A	Type B
L	99 in.	99 in.
b	40 in.	39 in.
h ₁	58 in.	58 in.
h ₂	58 in.	58 in.
h ₃	58 in.	58 in.

Figure 1.1 Rack Configuration

	Type A	Type B
Post		
Beam		
Base Plate		
Brace		

	Type C1	Type C2	Type D
Post			
Beam			

Figure 2.1 Shapes of Rack Elements

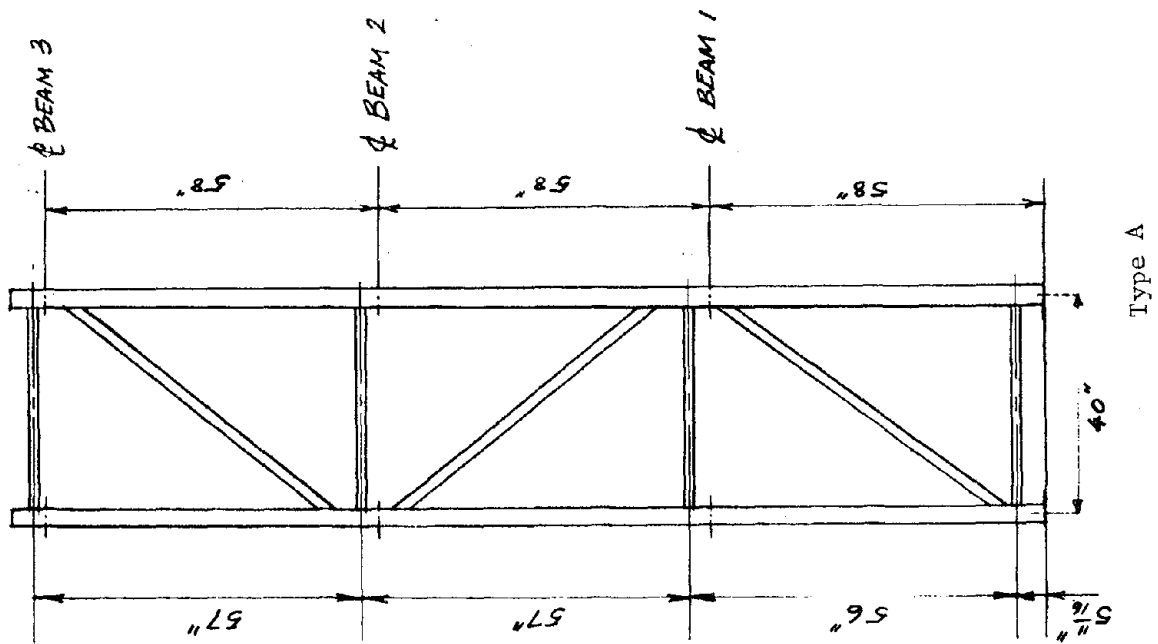
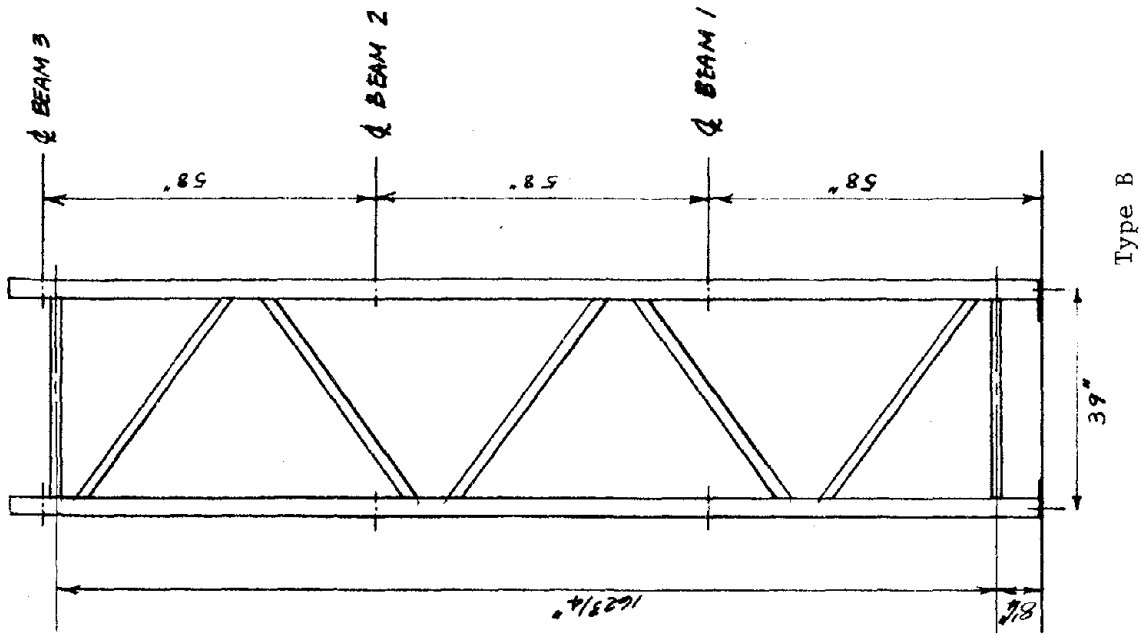


Figure 2.2 Upright Frames

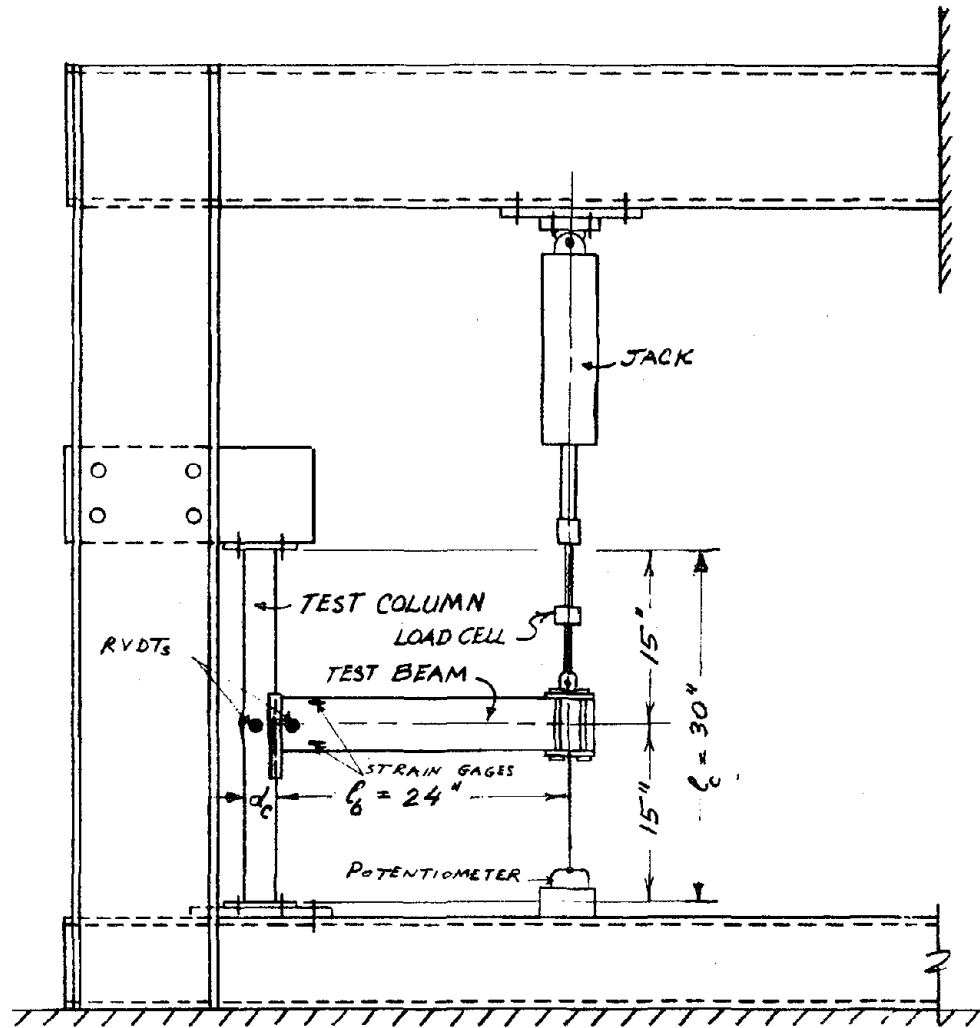


Figure 3.1 Cantilever Test Set-Up

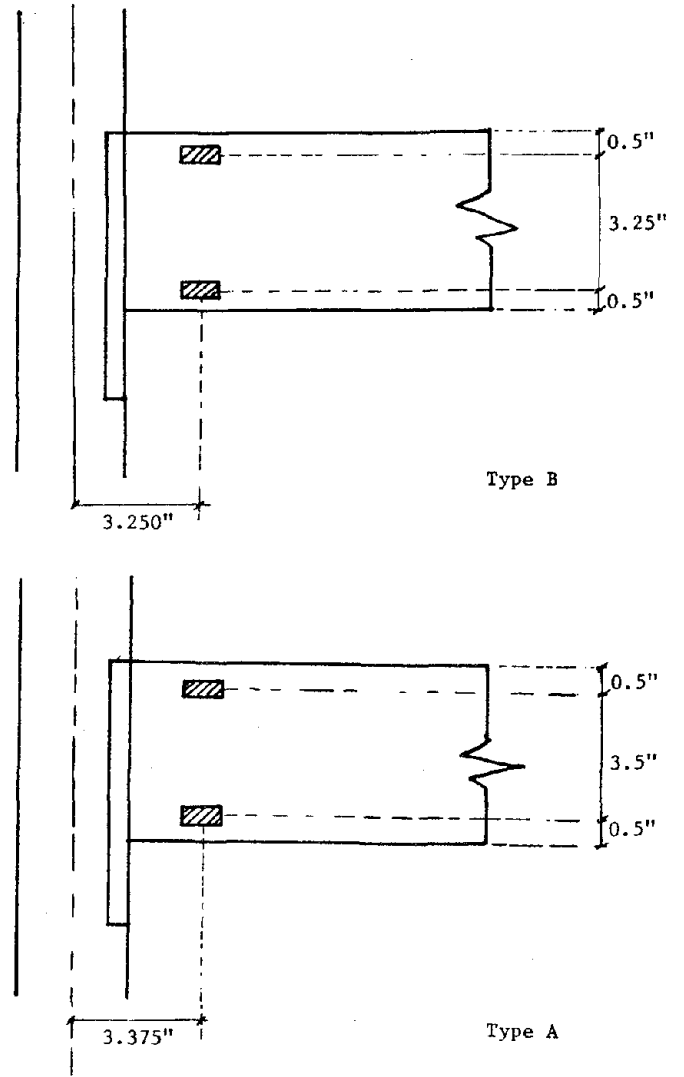
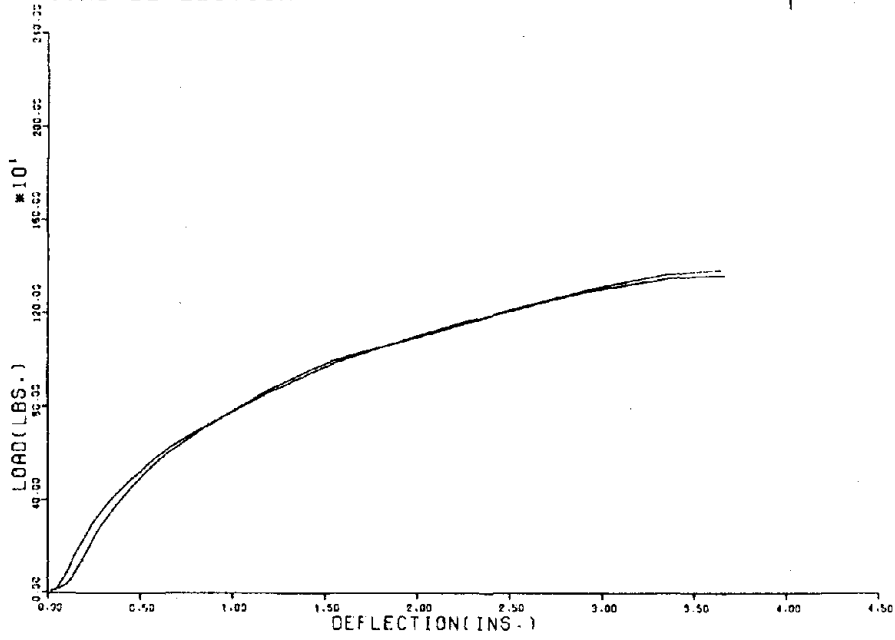


Figure 3.2 Strain Gage Locations

TEST A-C-1
LOAD-DEFLECTION



TEST A-C-2
LOAD-DEFLECTION

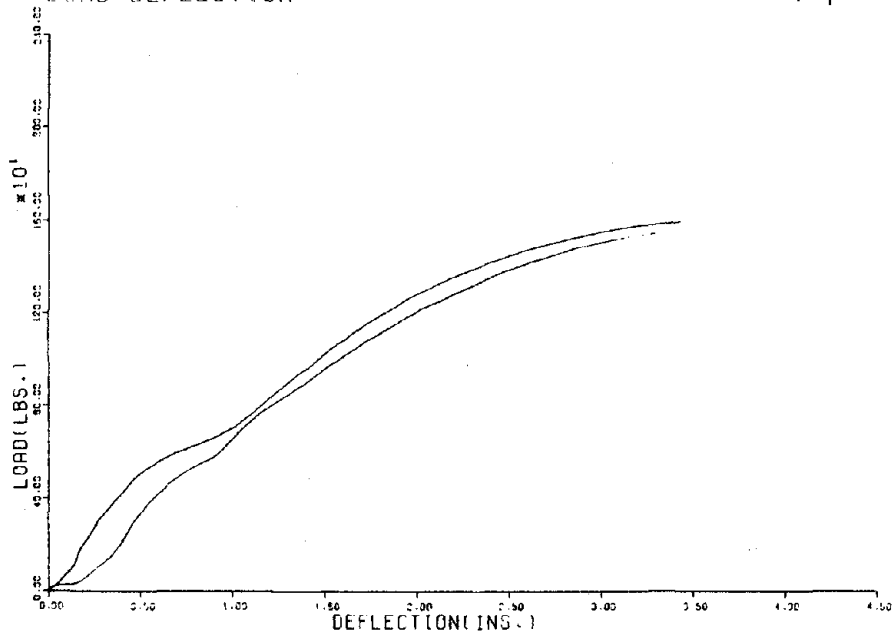


Figure 3.3 Cantilever Tests -- P- δ for Rack Type A

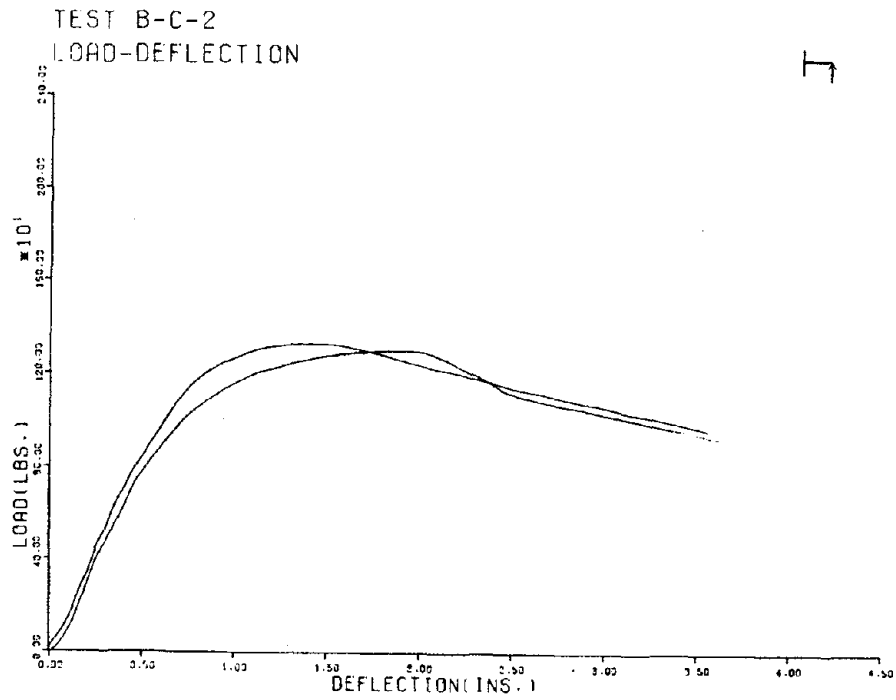
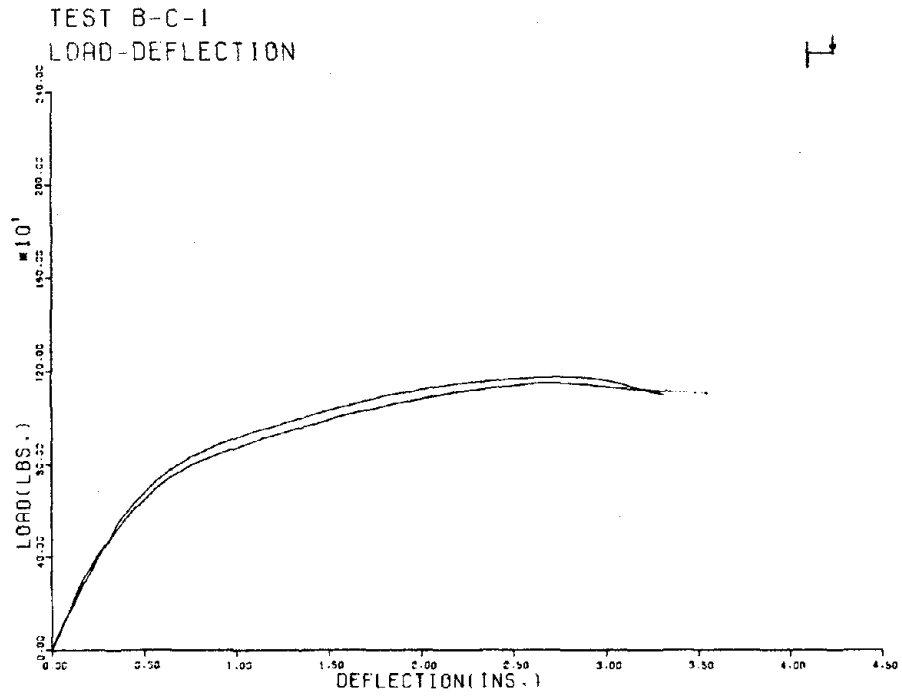
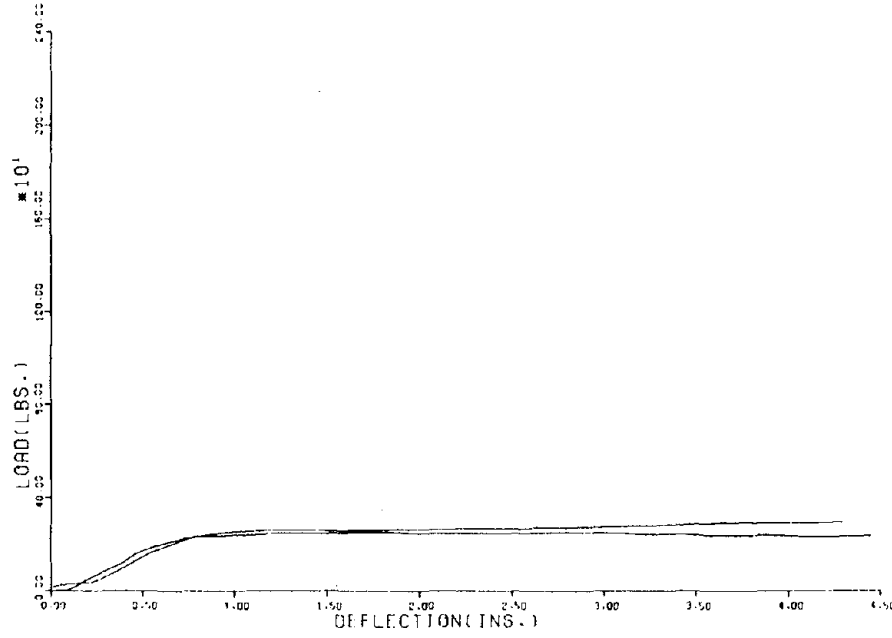


Figure 3.4 Cantilever Tests -- $P-\delta$ for Rack Type B

TEST C1-C-1
LOAD-DEFLECTION



TEST C1-C-2
LOAD-DEFLECTION

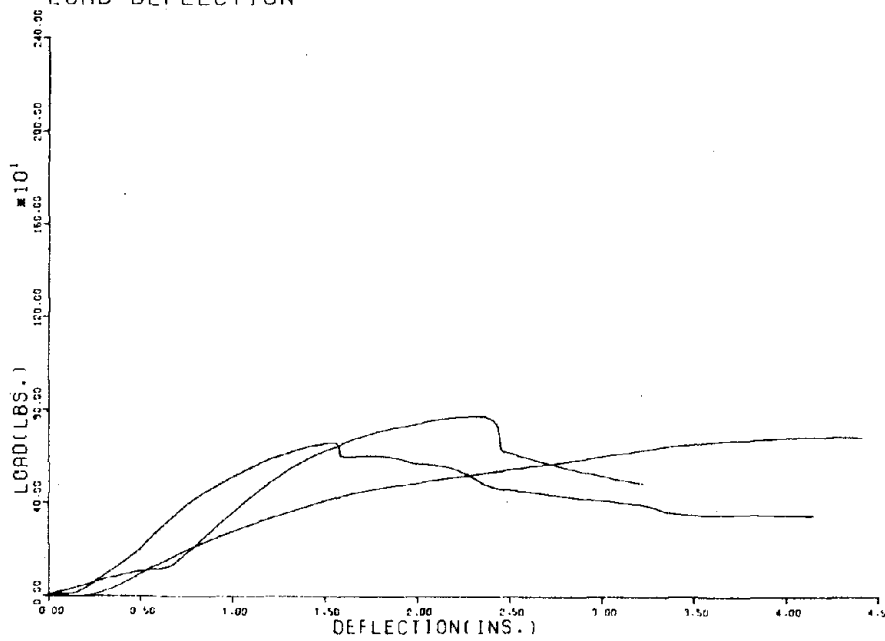


Figure 3.5 Cantilever Tests -- P- δ for Rack Type C1

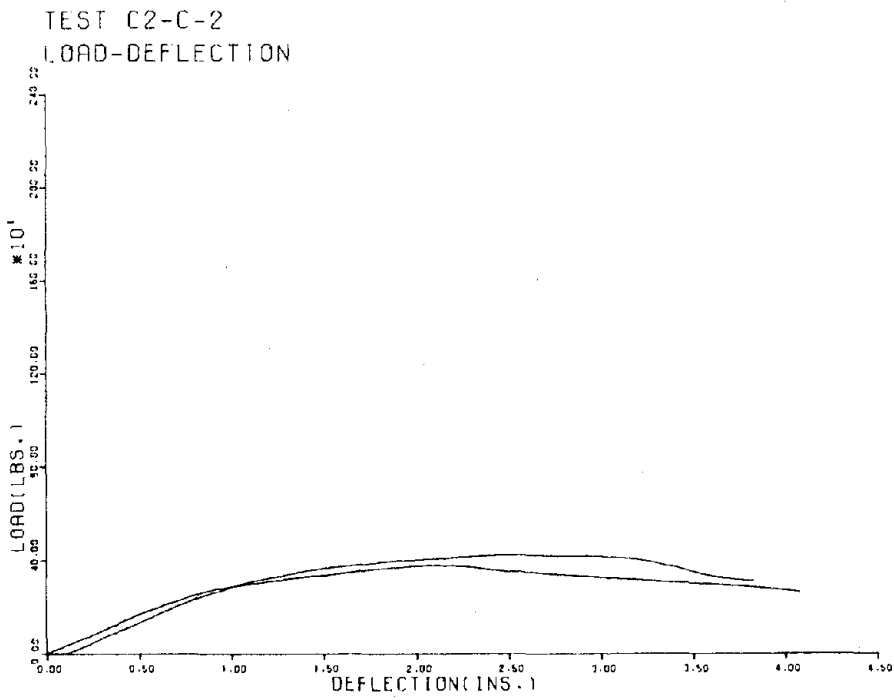
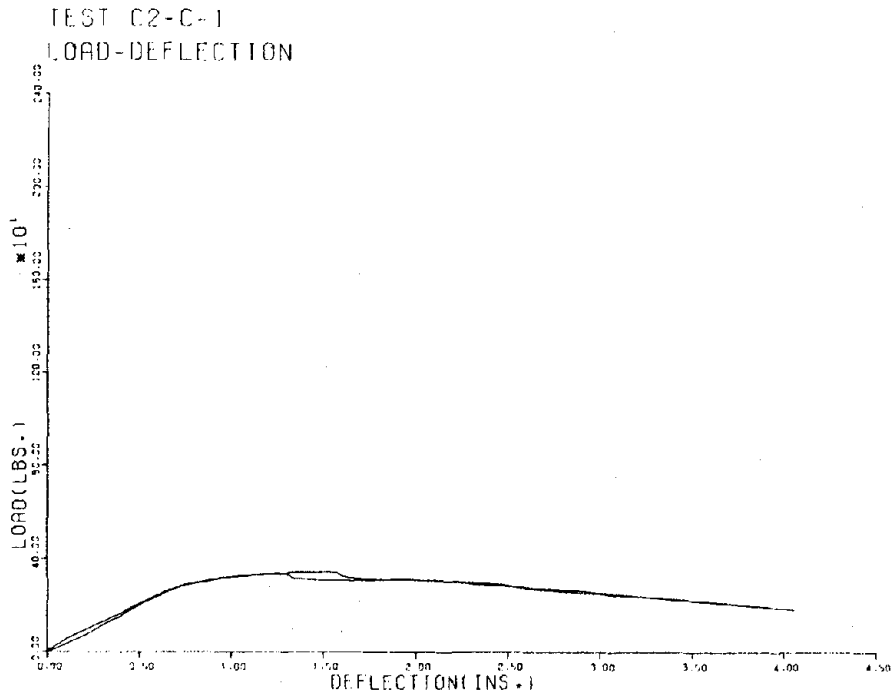
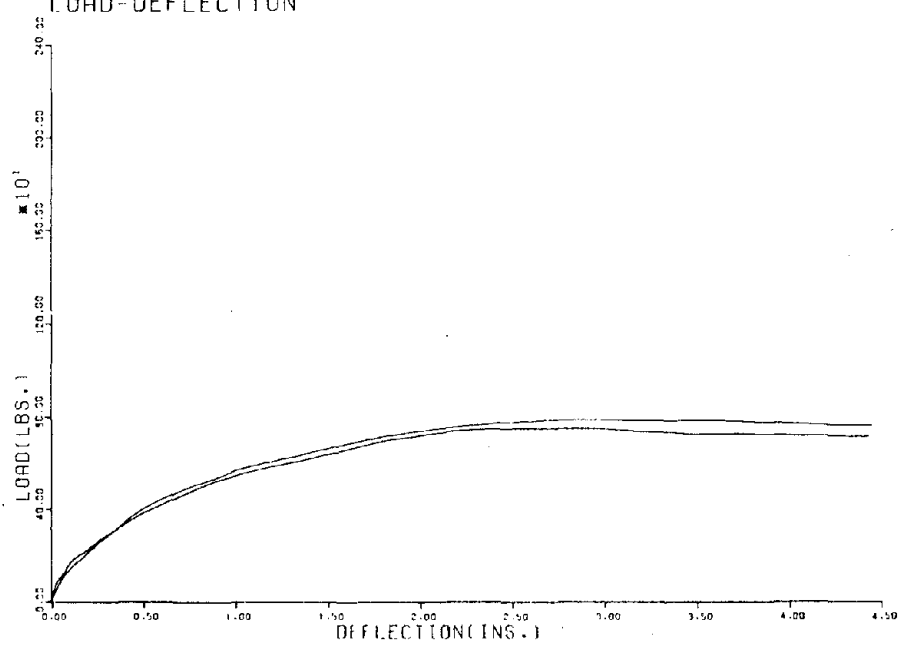


Figure 3.6 Cantilever Tests -- P- δ for Rack Type C2

TEST D-C-1
LOAD-DEFLECTION



TEST D-C-2
LOAD-DEFLECTION

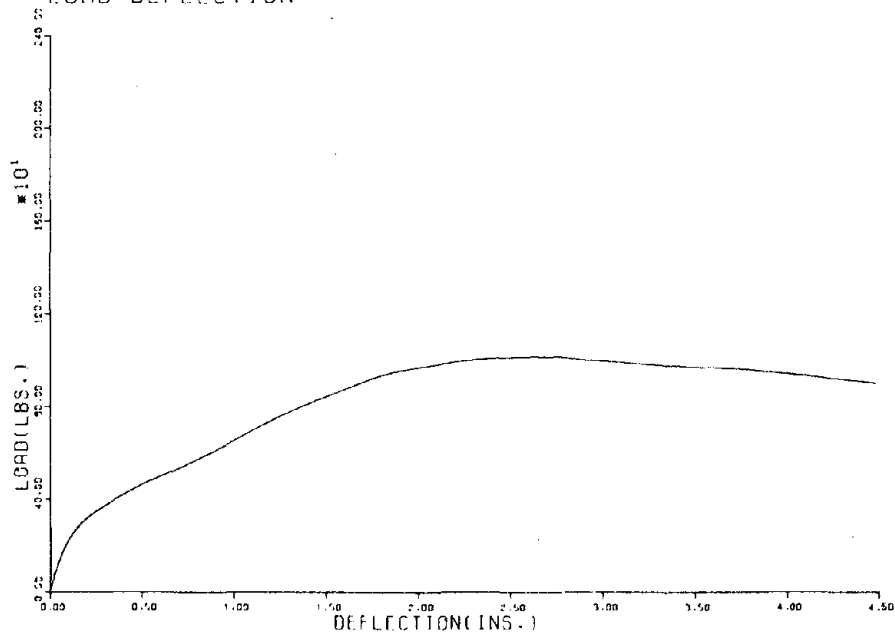
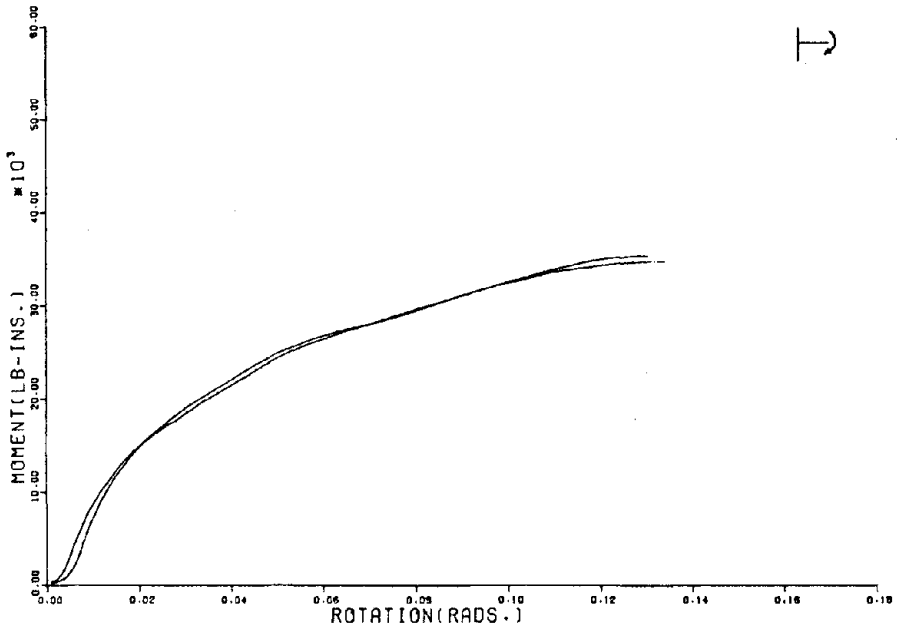


Figure 3.7 Cantilever Test -- P- δ for Rack Type D

TEST A-C-1

MOMENT-RELATIVE ROTATION(FROM ROTATION GAGES)



TEST A-C-2

MOMENT-RELATIVE ROTATION(FROM ROTATION GAGES)

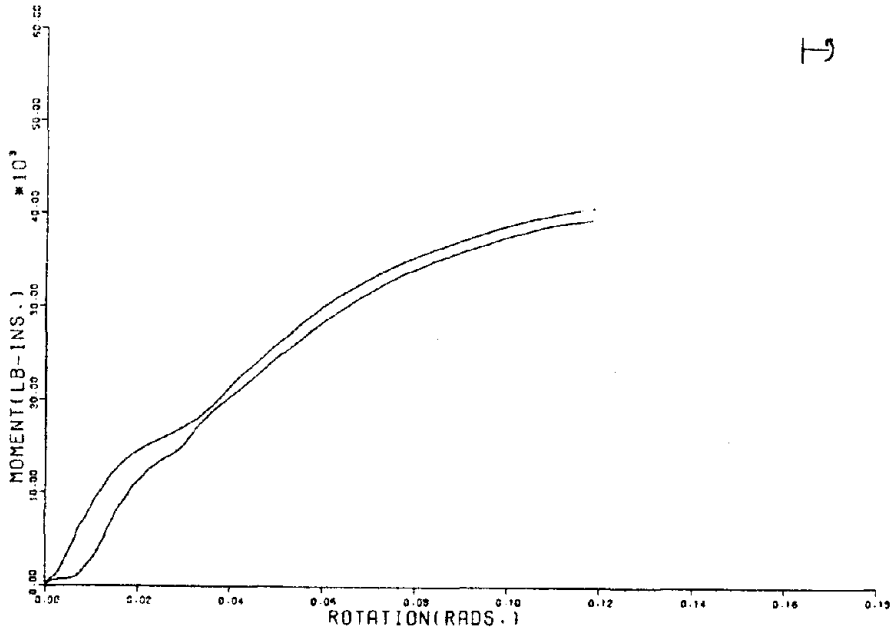
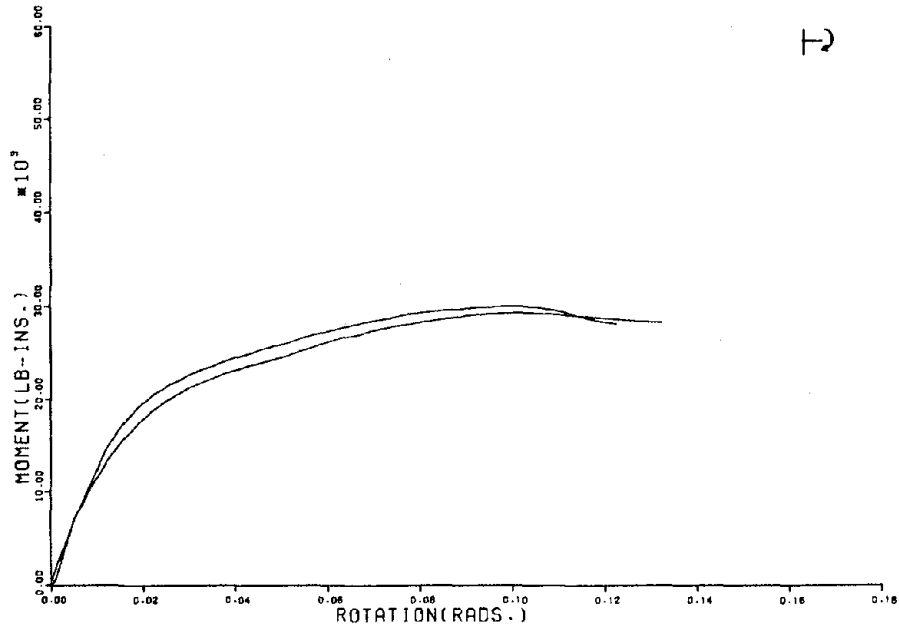


Figure 3.8 Cantilever Test -- M- θ (θ from Rotation Gages)

Rack Type A

TEST B-C-1
 MOMENT-RELATIVE ROTATION(FROM ROTATION GAGES)



TEST B-C-2
 MOMENT-RELATIVE ROTATION(FROM ROTATION GAGES)

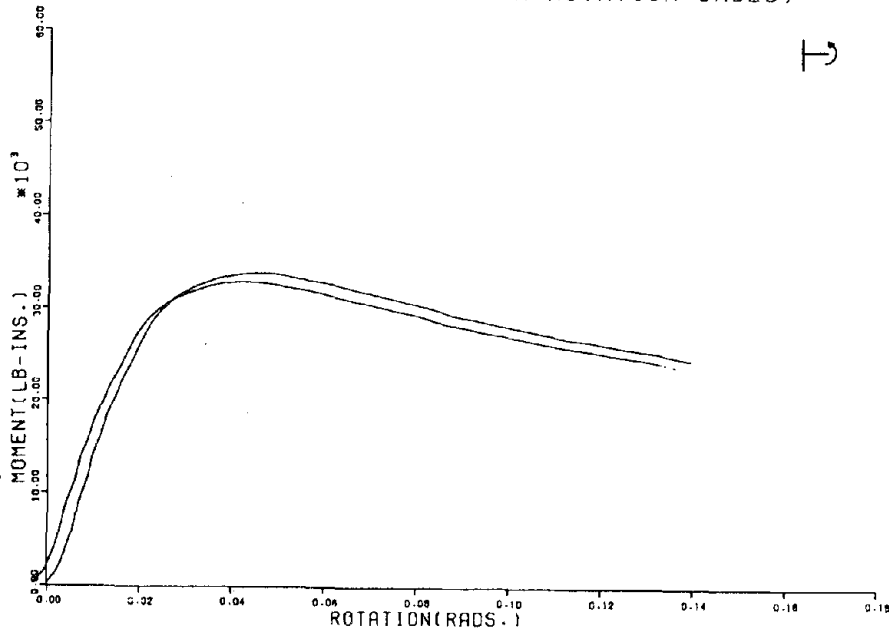
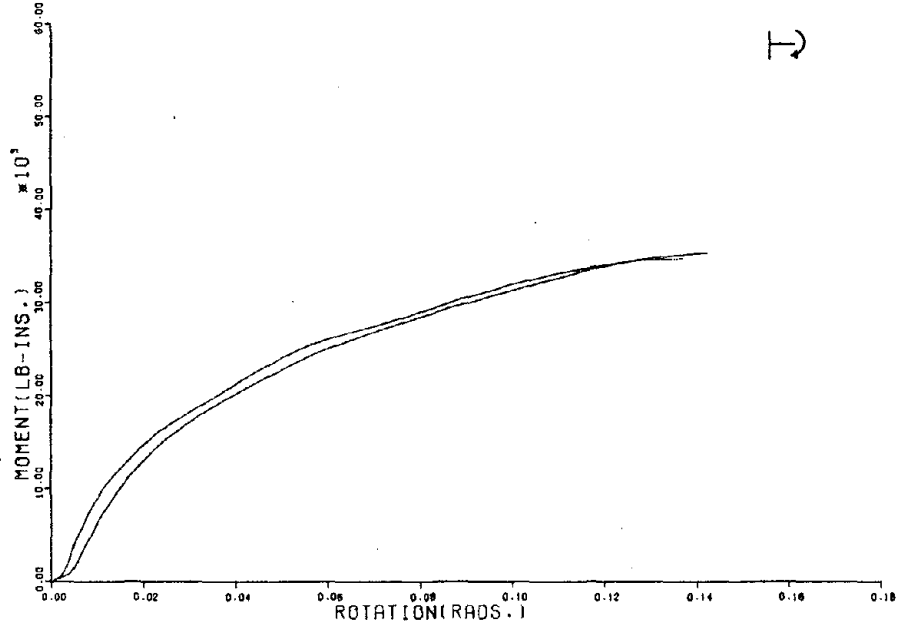


Figure 3.9 Cantilever Test -- M-θ (θ from Rotation Gages)

Rack Type B

TEST A-C-1
 MOMENT-SPRING ROTATION(ANALYTICAL MODEL)



TEST A-C-2
 MOMENT-SPRING ROTATION(ANALYTICAL MODEL)

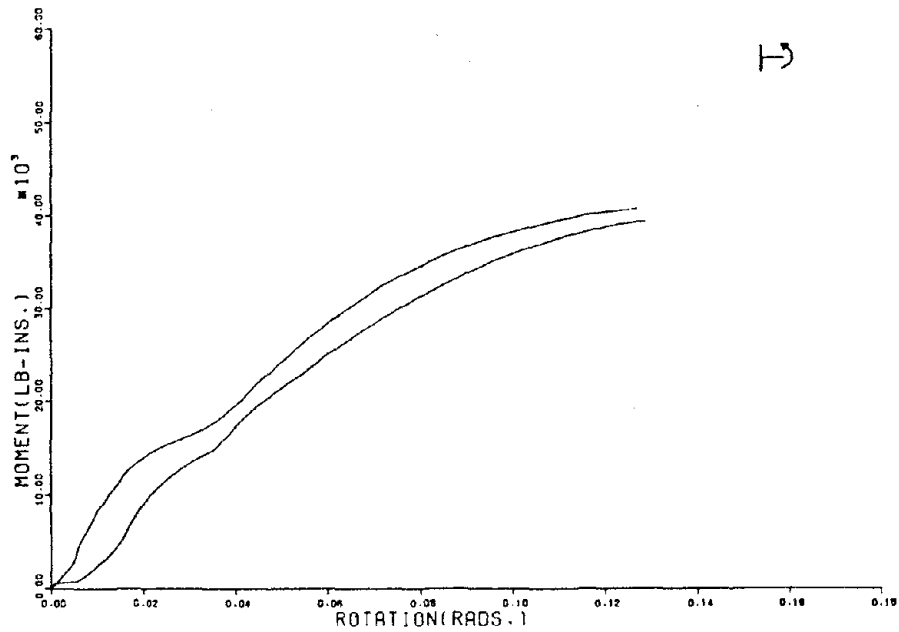
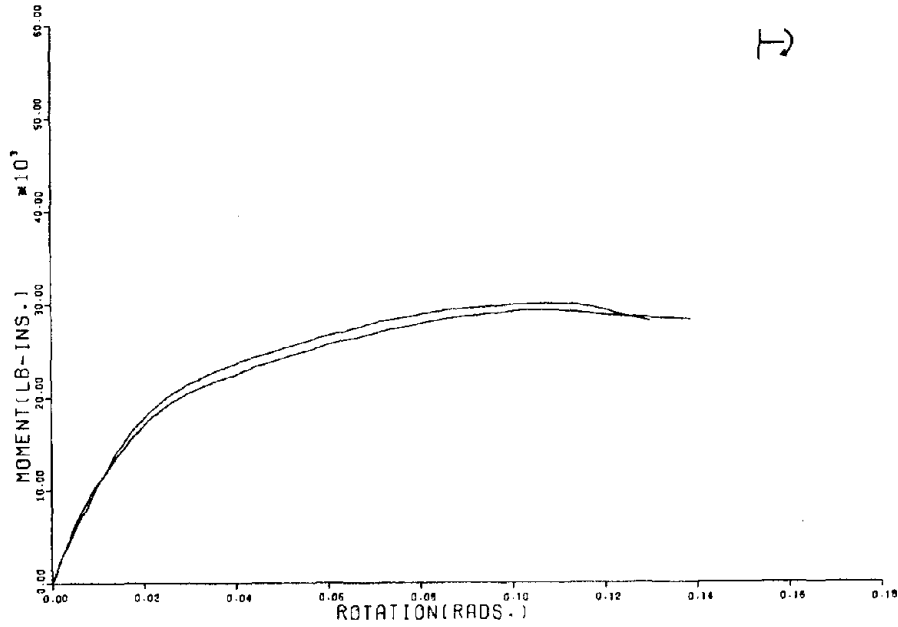


Figure 3.10 Cantilever Tests -- M- θ (θ from Eq. 3)
 for Rack Type A

TEST B-C-1
 MOMENT-SPRING ROTATION(ANALYTICAL MODEL)



TEST B-C-2
 MOMENT-SPRING ROTATION(ANALYTICAL MODEL)

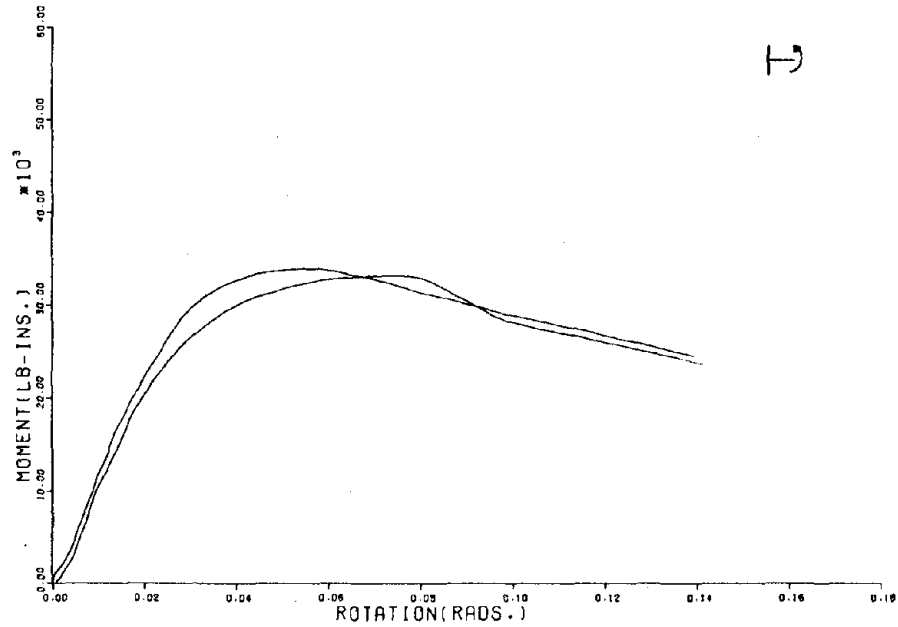
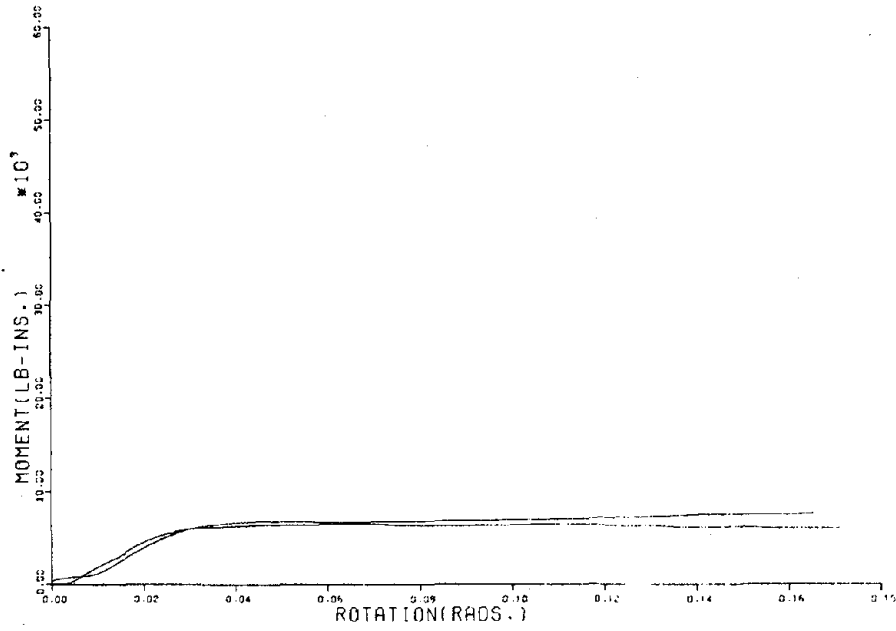


Figure 3.11 Cantilever Tests -- M-0 (θ from Eq. 3)
 for Rack Type B

TEST C1-C-1
MOMENT-SPRING ROTATION(ANALYTICAL MODEL)



TEST C1-C-2
MOMENT-SPRING ROTATION(ANALYTICAL MODEL)

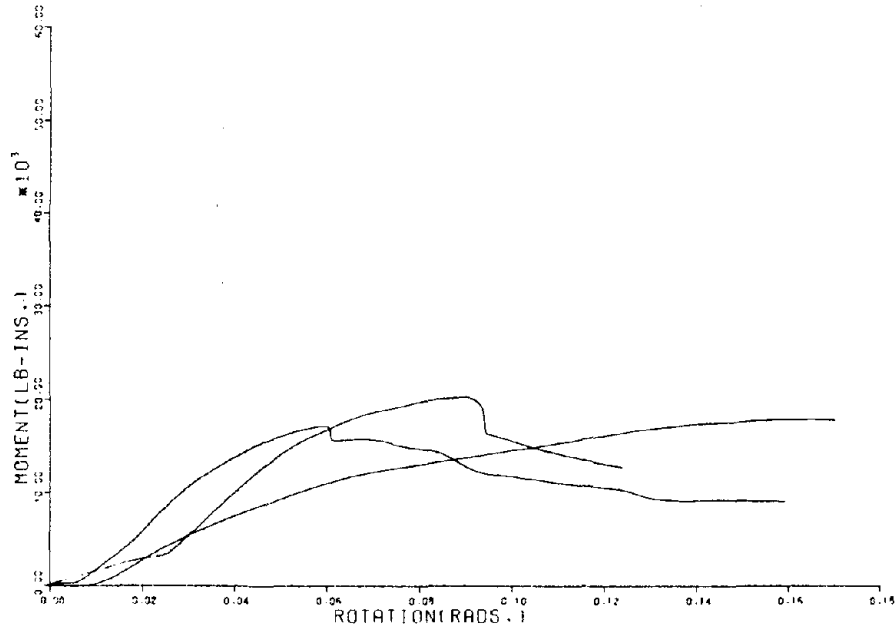
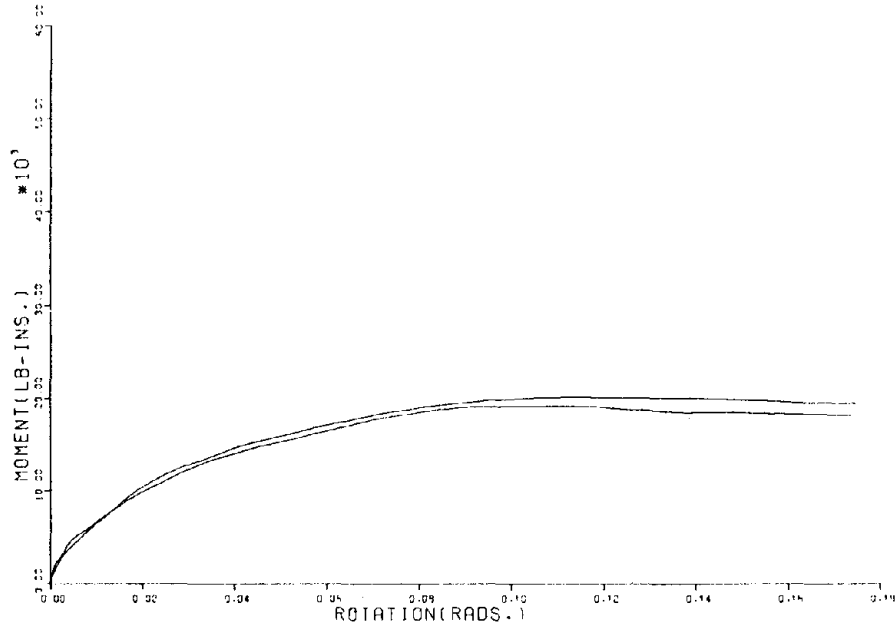


Figure 3.12 Cantilever Tests -- M- θ (θ from Eq. 3)
for Rack Type C1

TEST D-C-1
 MOMENT-SPRING ROTATION (ANALYTICAL MODEL)



TEST D-C-2
 MOMENT-SPRING ROTATION (ANALYTICAL MODEL)

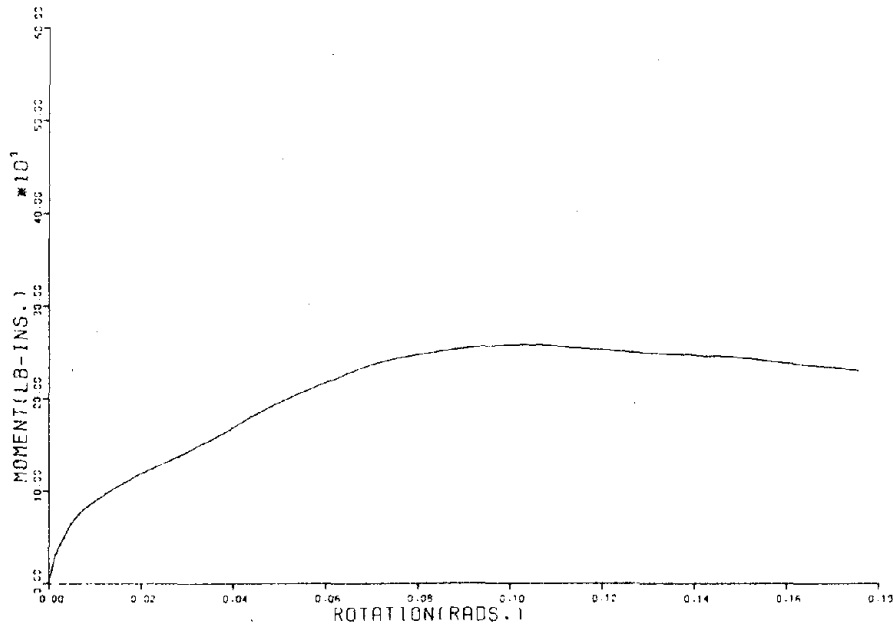


Figure 3.13 Cantilever Tests -- M- θ (θ from Eq. 3)
 for Rack Type D

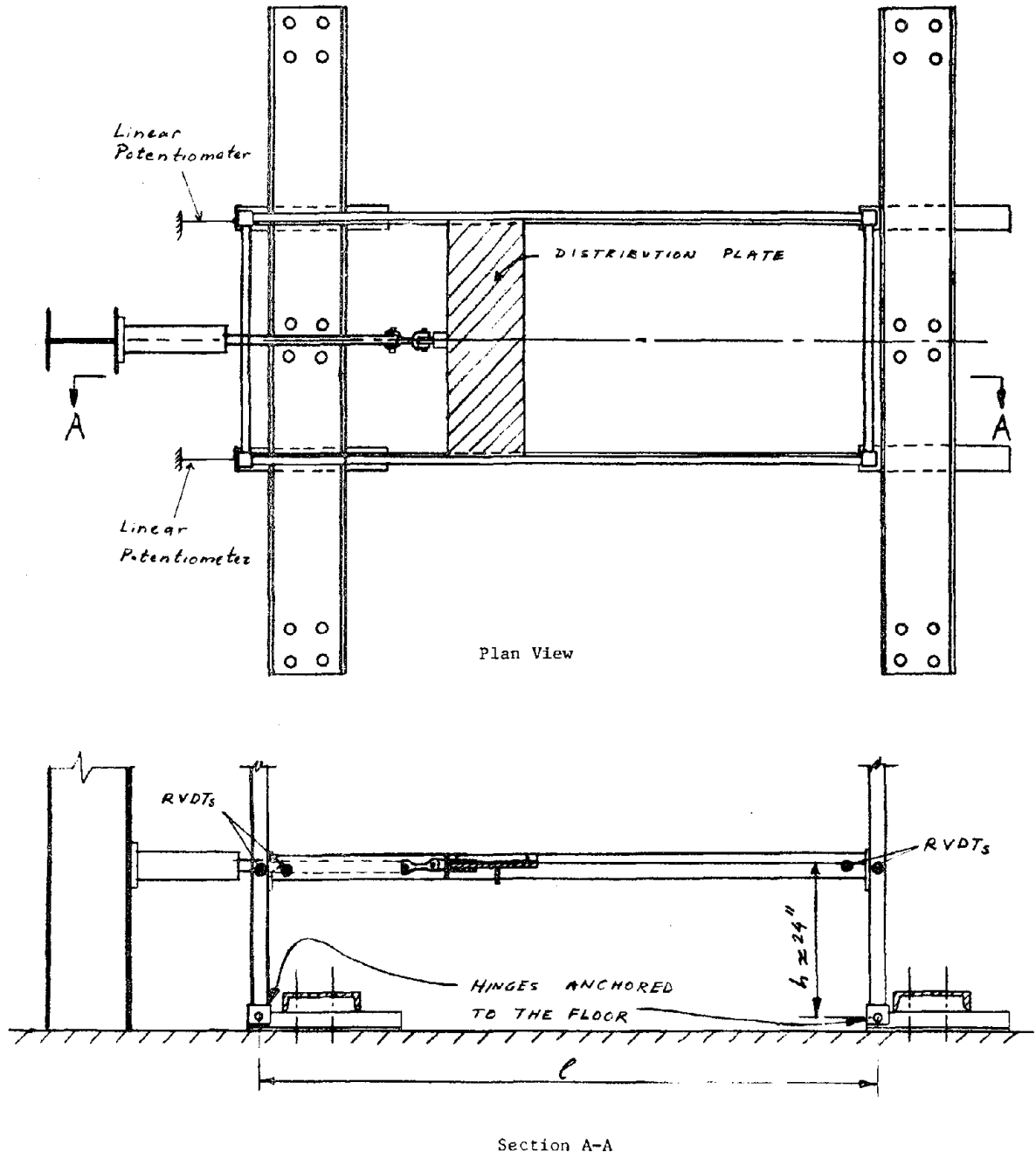


Figure 4.1 Portal Test Set-Up

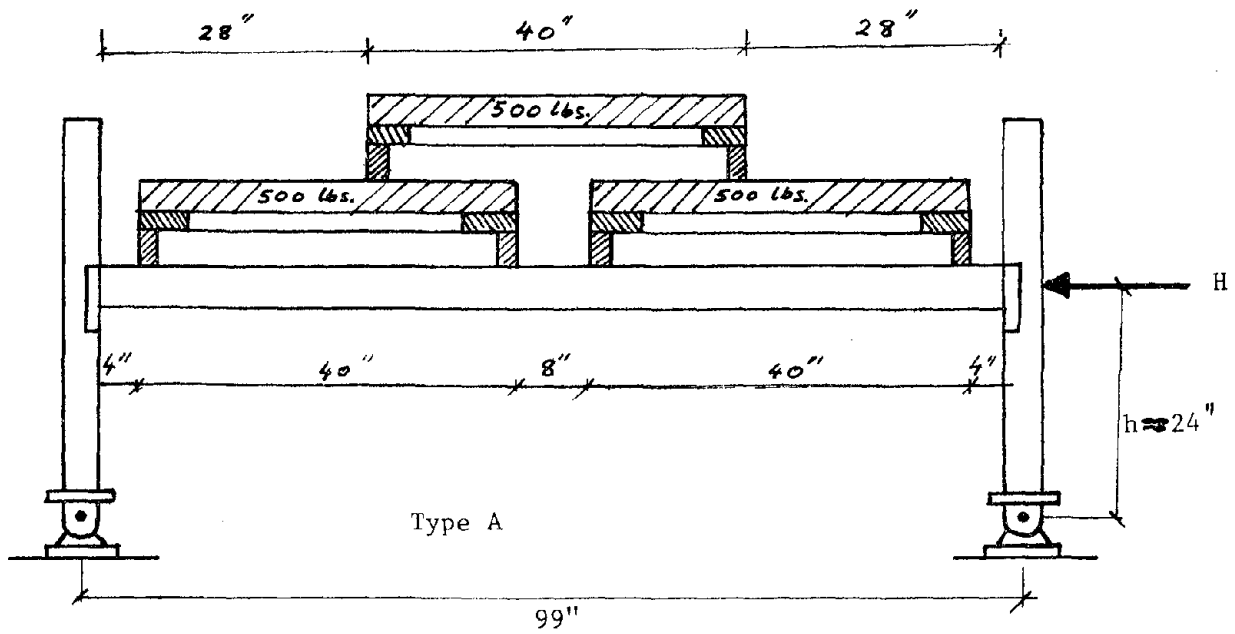
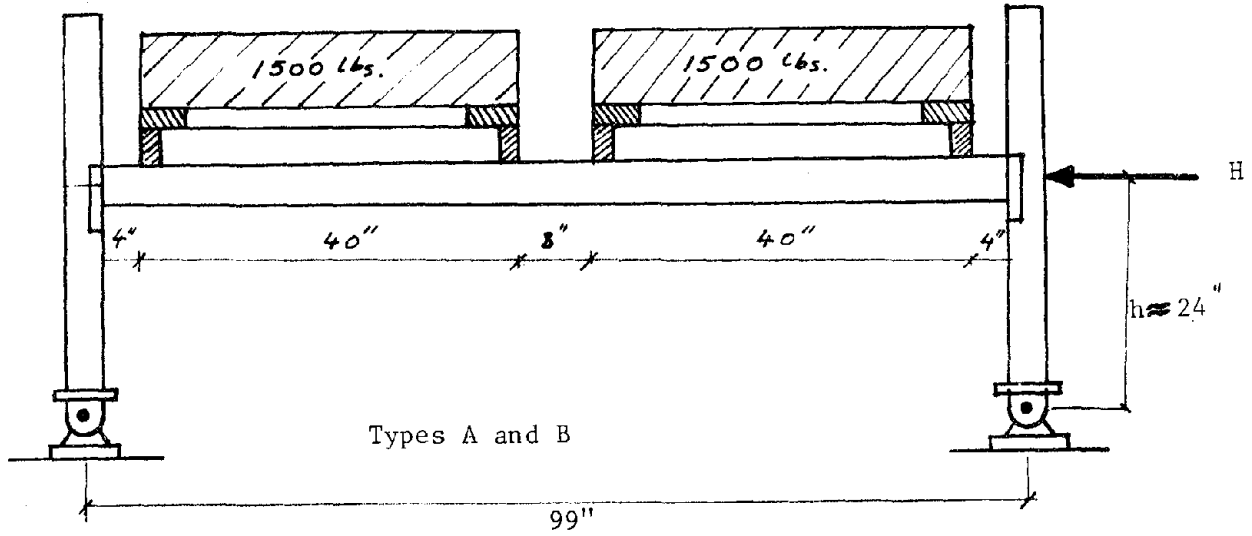


Figure 4.2 Portal Tests -- Loading Arrangements

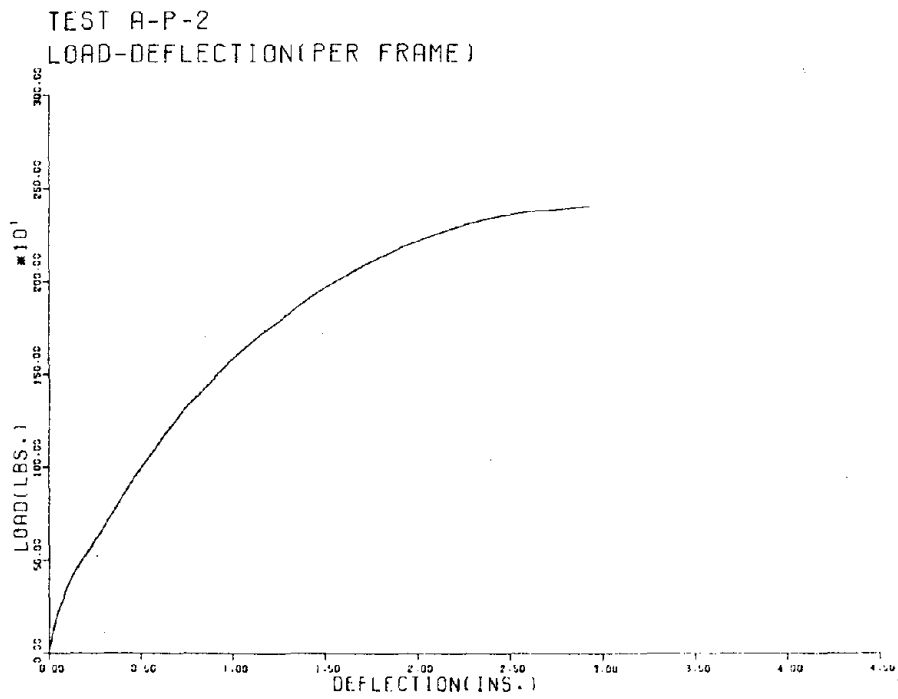
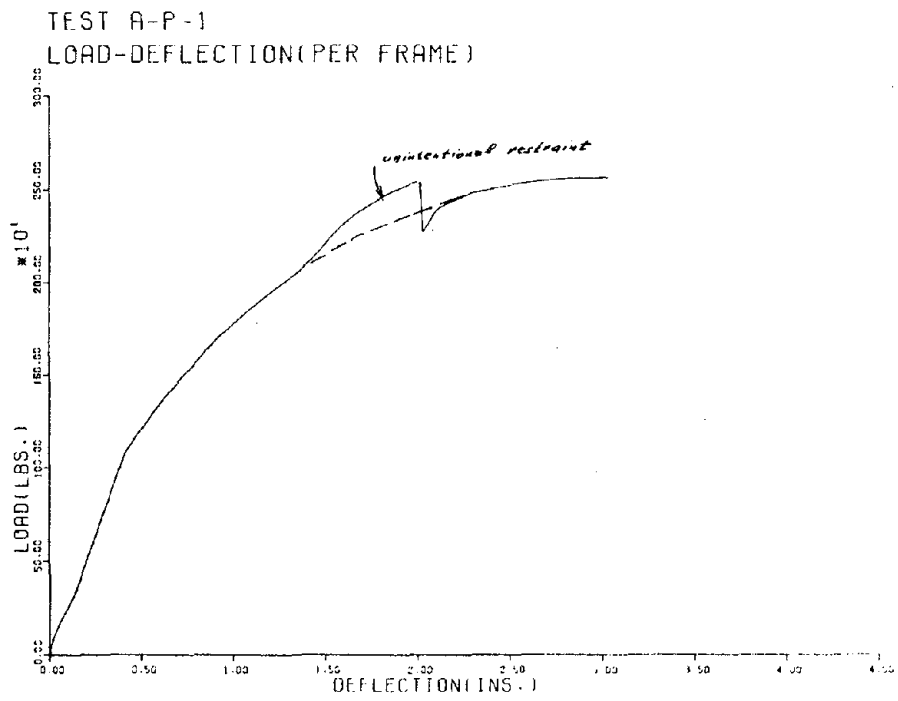


Figure 4.3 Portal Tests -- $H-\delta$ for Rack Type A

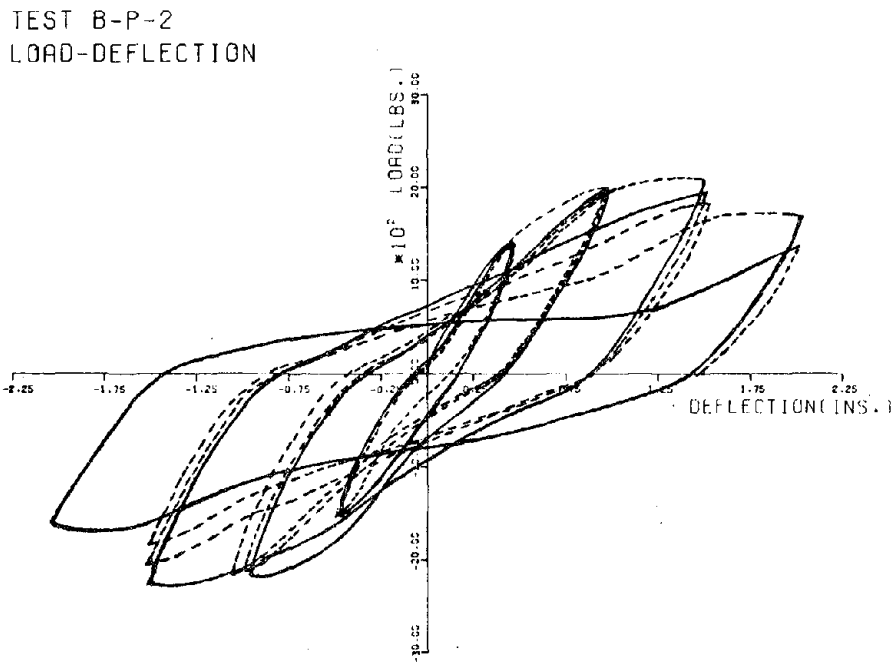
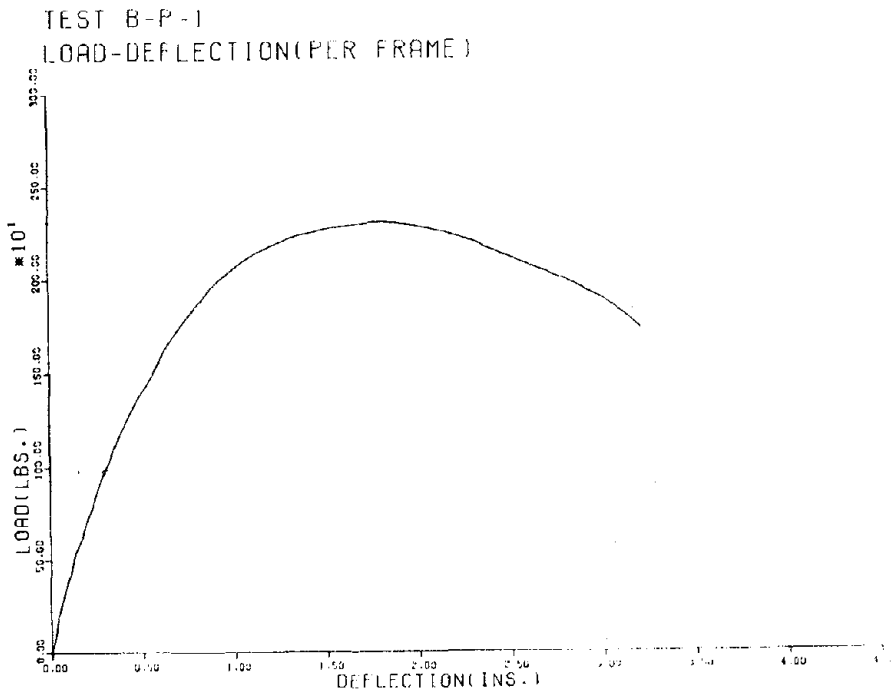


Figure 4.4 Portal Test -- H- δ for Rack Type B

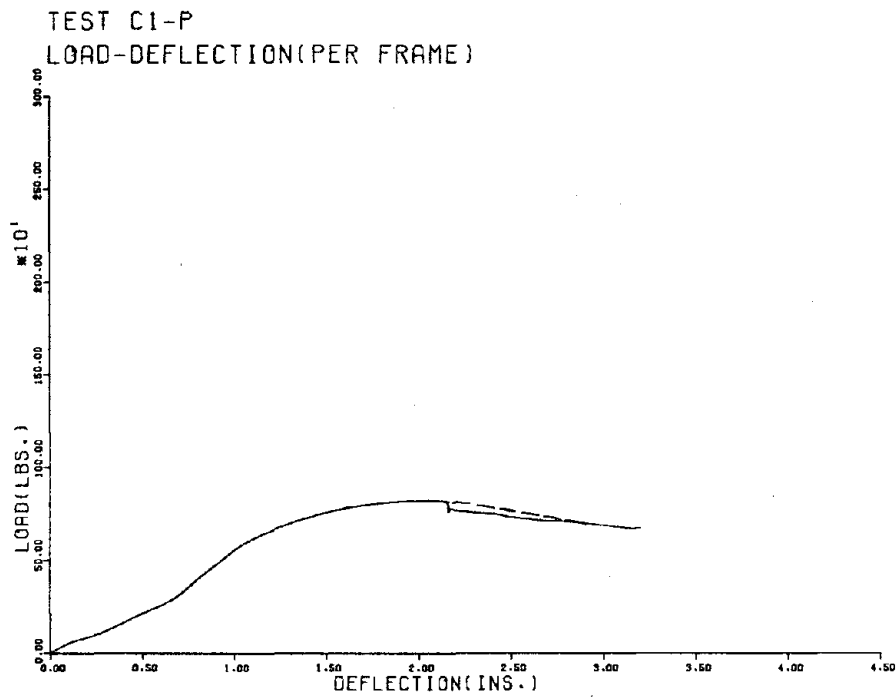


Figure 4.5 Portal Test -- H- δ for Rack Type C1

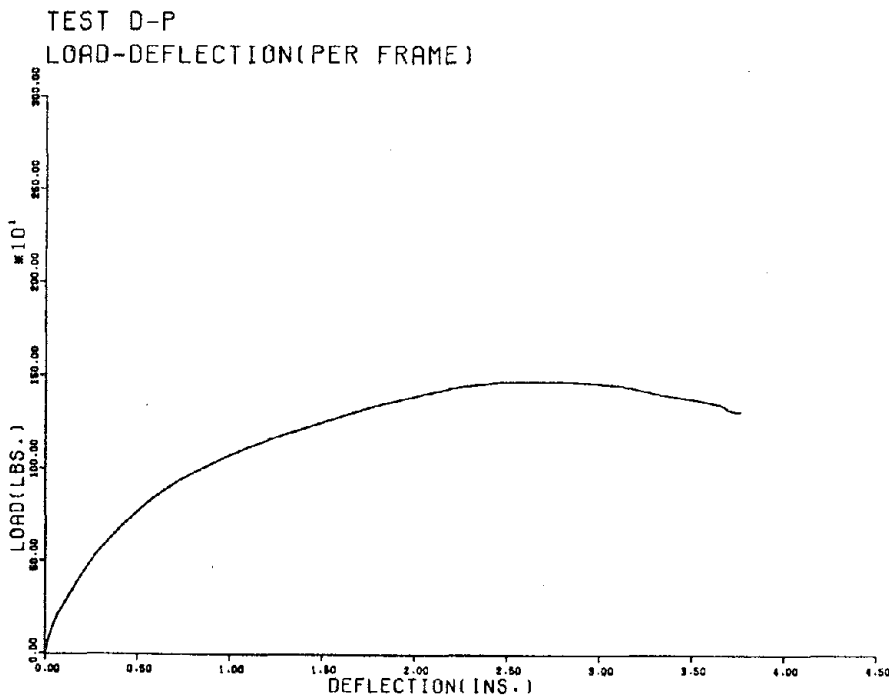


Figure 4.6 Portal Test -- H- δ for Rack Type D

TEST A-P-2
MOMENT-RELATIVE ROTATION(FROM ROTATION GAGES)

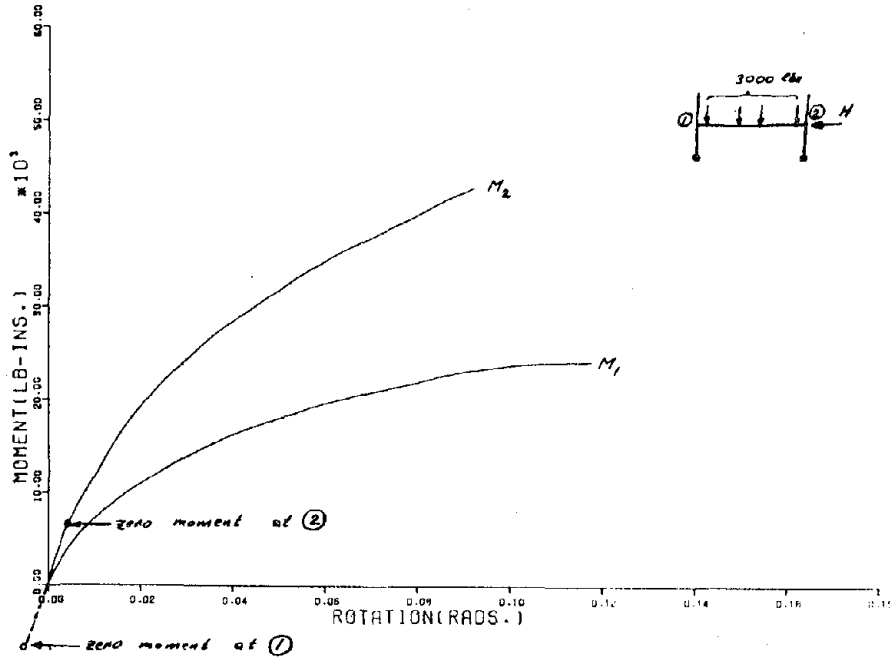


Figure 4.7 Portal Test -- M- θ for Joints 1 (Negative Moment) and 2 (Positive Moment), Rack Type A

TEST B-P-1
MOMENT-RELATIVE ROTATION(FROM ROTATION GAGES)

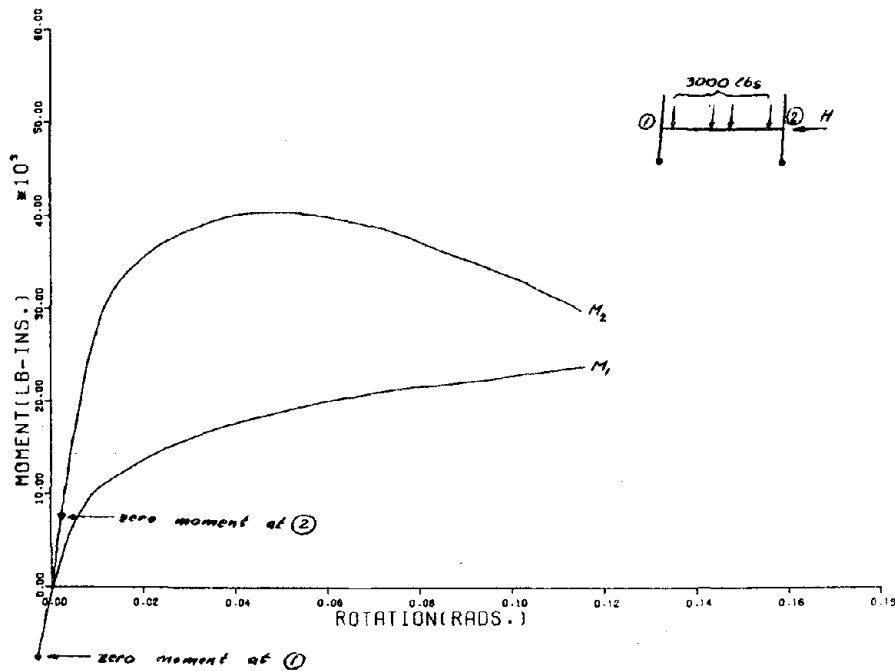
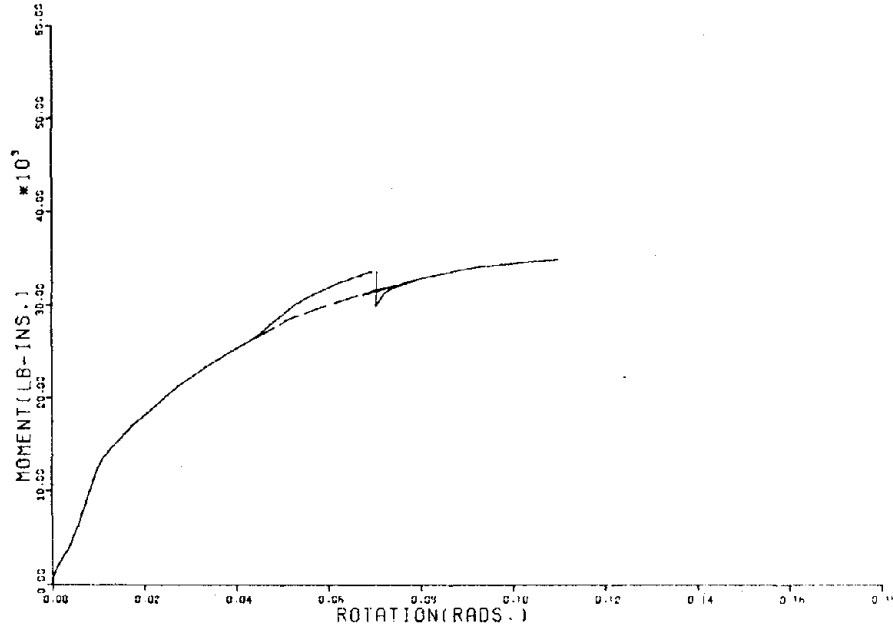


Figure 4.8 Portal Test -- M- θ for Joints 1 (Negative Moment) and 2 (Positive Moment), Rack Type B

TEST A-P-1
 AVERAGE MOMENT-SPRING ROT.(ANALYTICAL MODEL #1)



TEST A-P-2
 AVERAGE MOMENT-SPRING ROT.(ANALYTICAL MODEL #1)

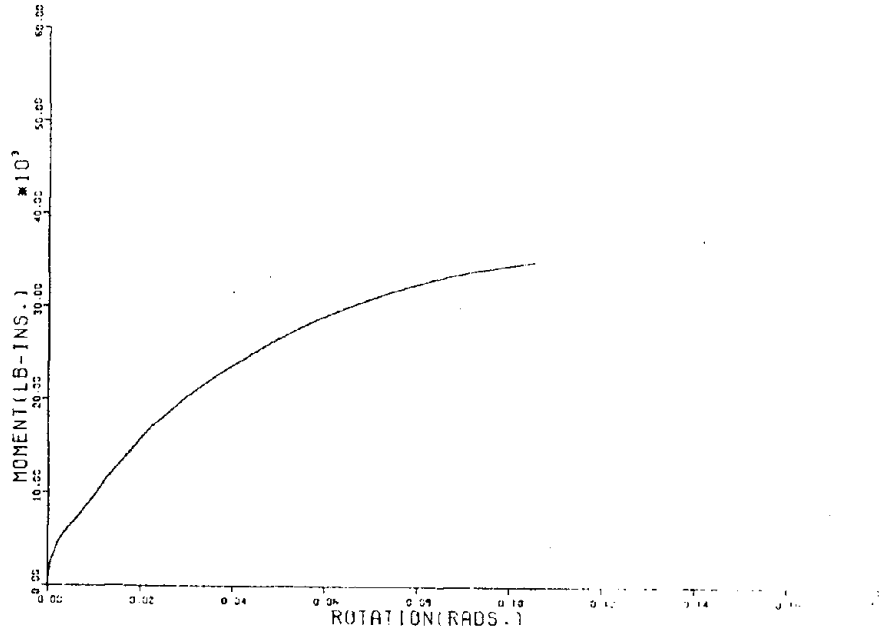
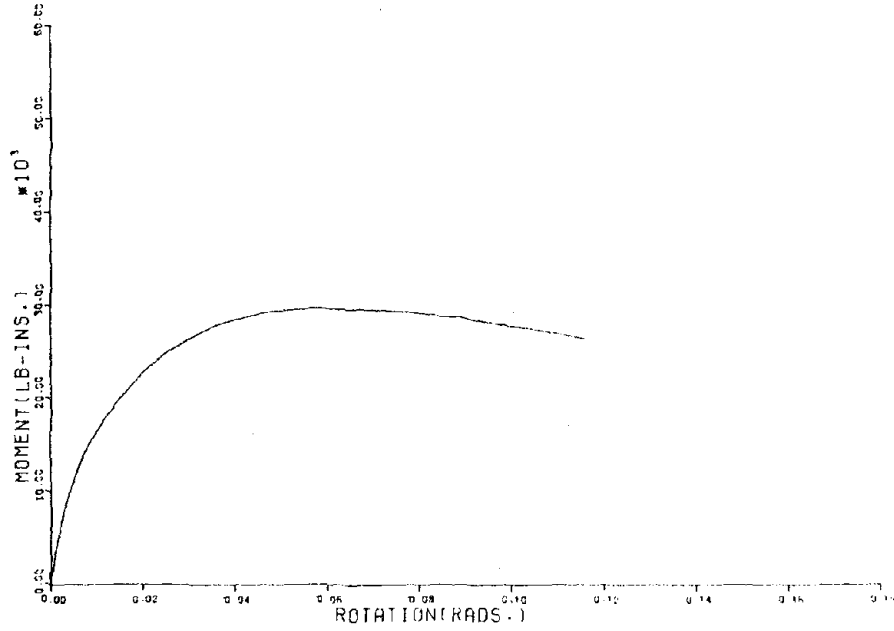


Figure 4.9 Portal Test -- $M_{av} - \theta_{av}$ from Eqs. (4.2) and (4.3)
 for Rack Type A

TEST B-P-1
 AVERAGE MOMENT-SPRING ROT. (ANALYTICAL MODEL #1)



TEST B-P-2
 AVERAGE MOMENT-SPRING ROT. (ANALYTICAL MODEL #1)

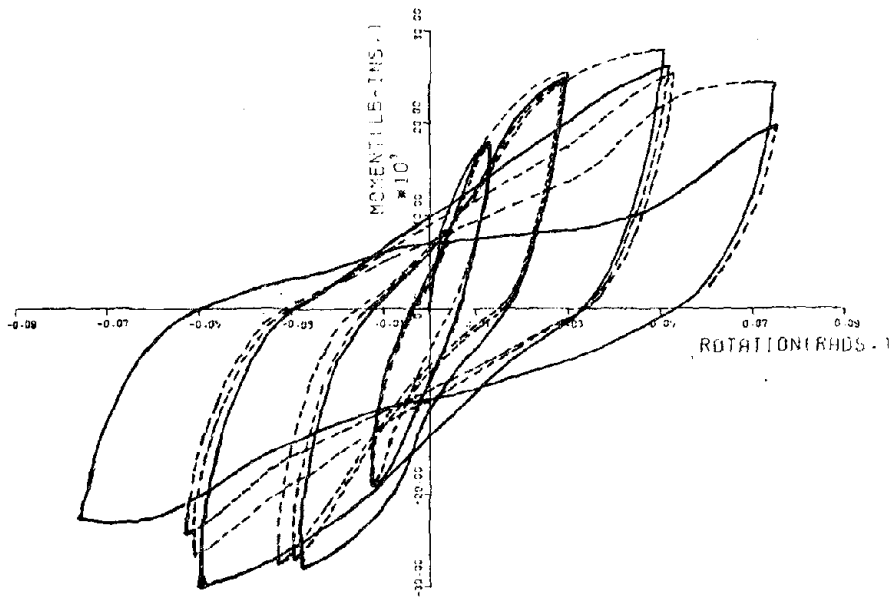


Figure 4.10 Portal Test -- $M_{av} - \theta_{av}$ from Eqs. (4.2) and (4.3)
 Rack Type B

TEST C1-P
AVERAGE MOMENT-SPRING ROT.(ANALYTICAL MODEL)

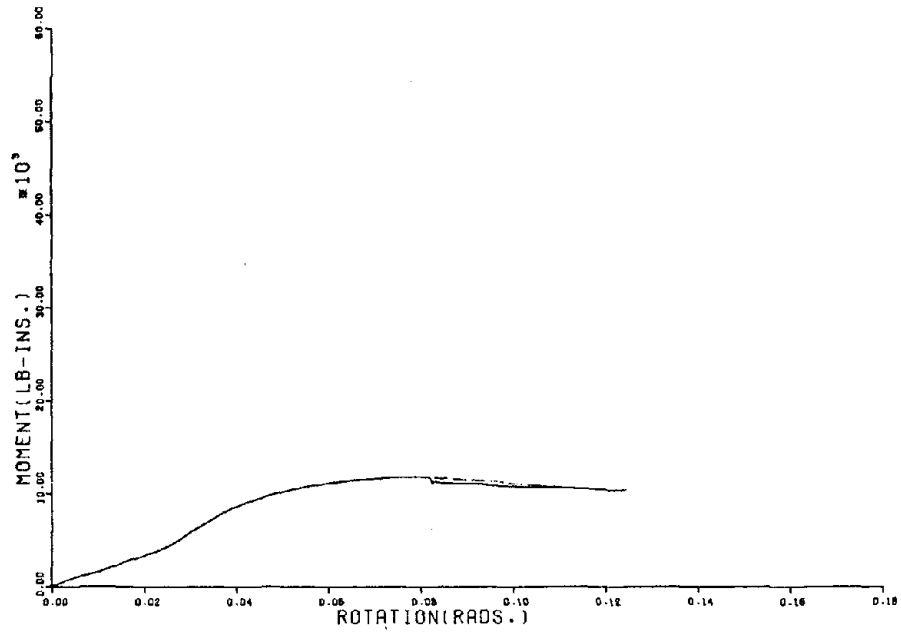


Figure 4.11 Portal Test -- $M_{av} - \theta_{av}$ from Eqs. (4.2) and (4.3)
Rack Type C_1

TEST D-P
AVERAGE MOMENT-SPRING ROT.(ANALYTICAL MODEL)

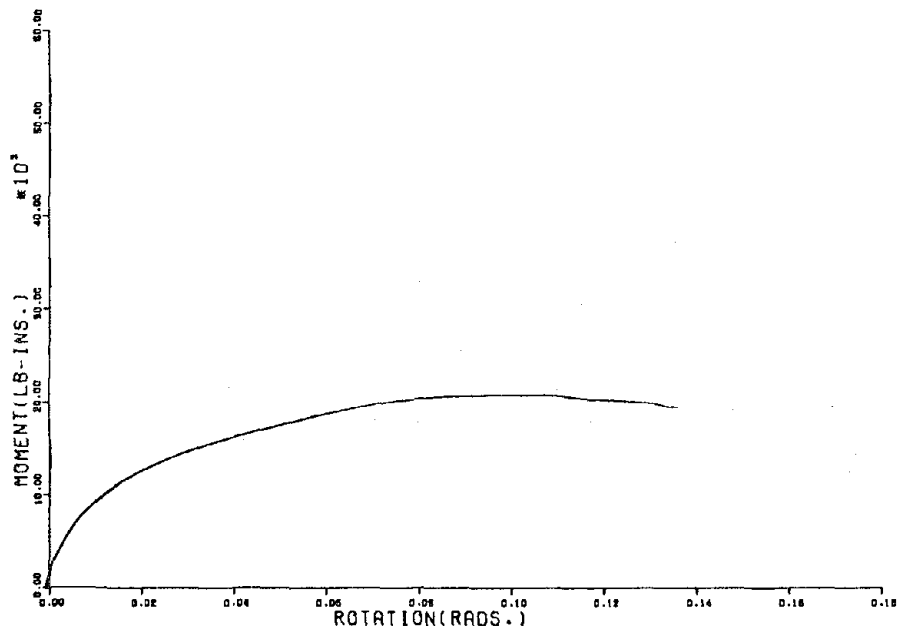


Figure 4.12 Portal Test -- $M_{av} - \theta_{av}$ from Eqs. (4.2) and (4.3)
Rack Type D

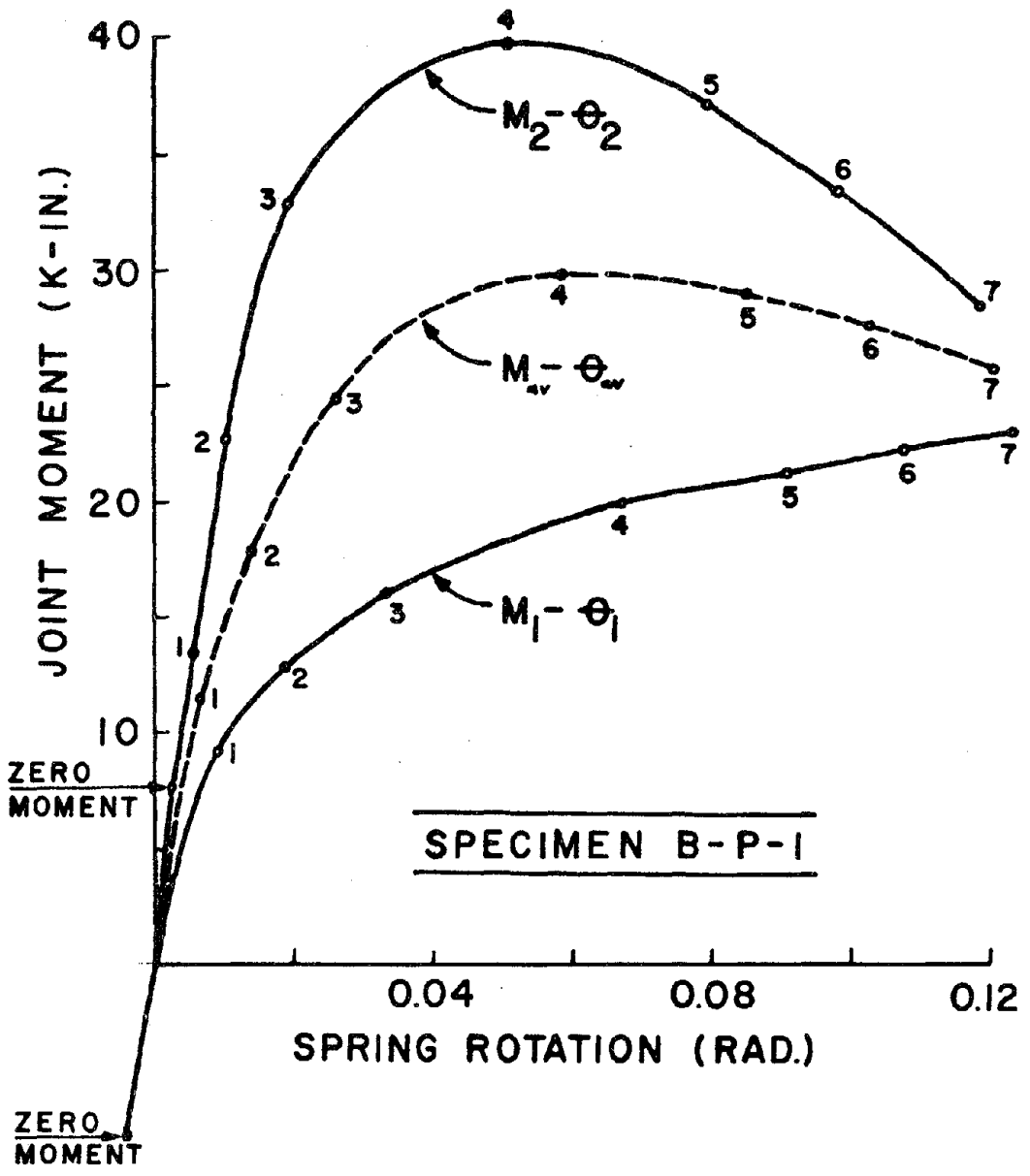


Figure 4.13 Comparison of $M-\theta$ with $M_{av} - \theta_{av}$, Rack Type B

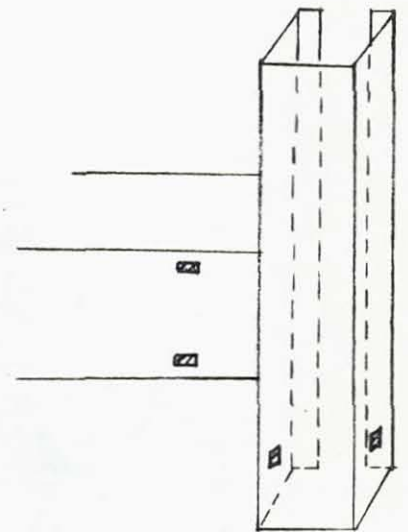
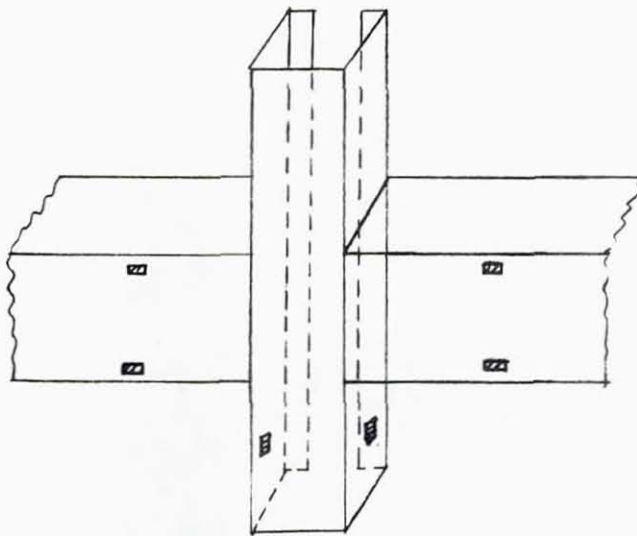
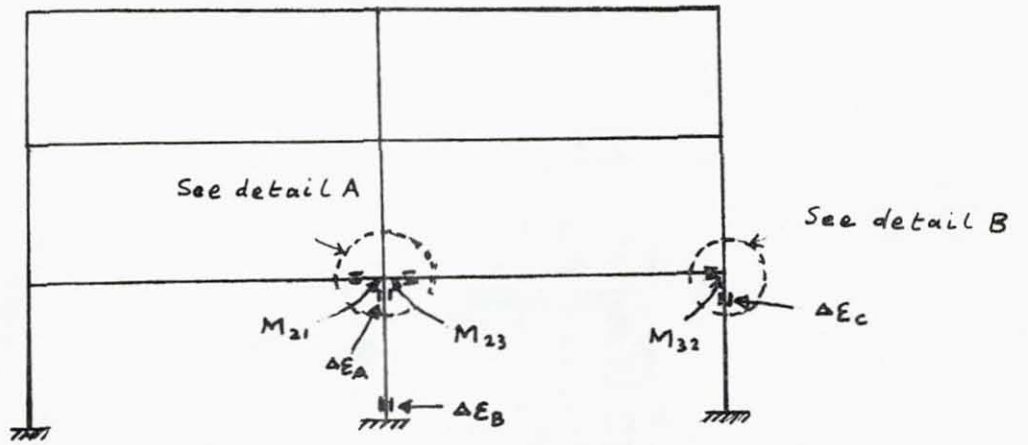
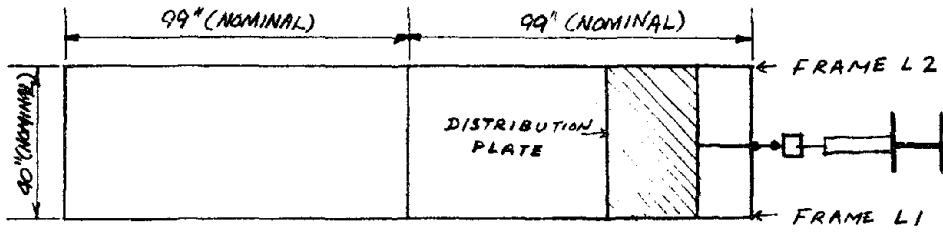
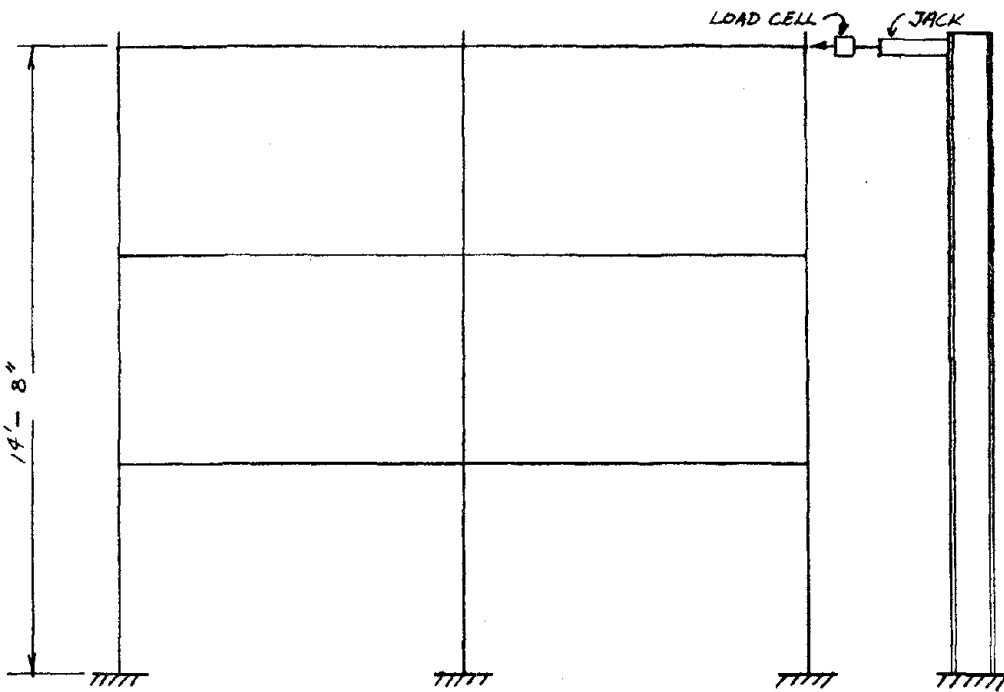


Figure 5.8 Details of Strain Gage Locations--Longitudinal Tests

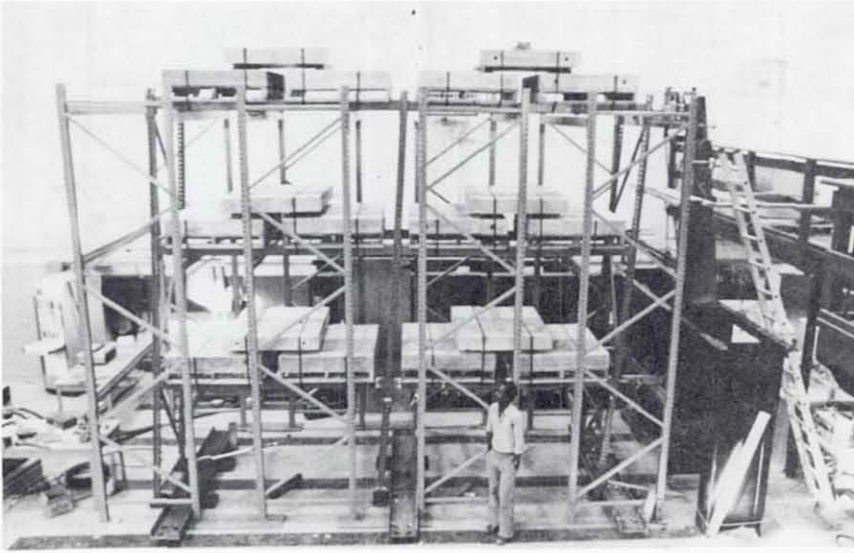


Plan

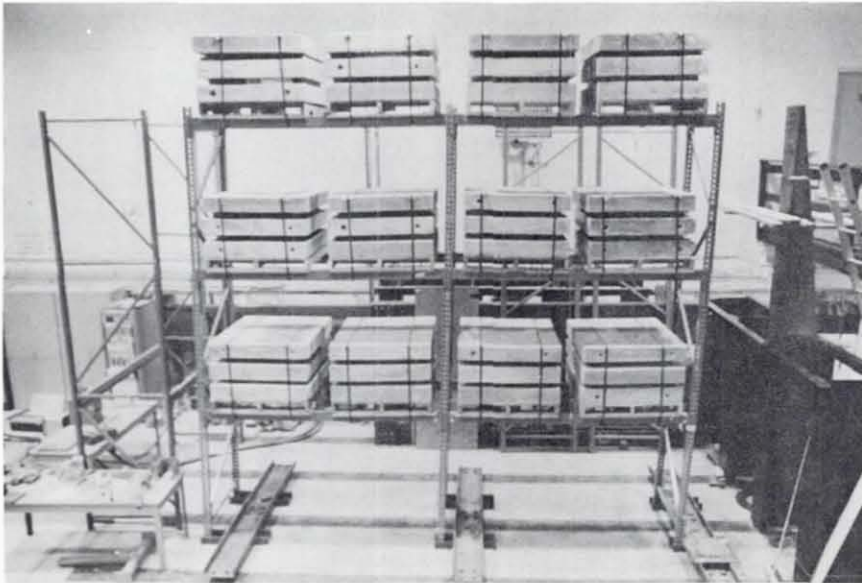


Elevation

Figure 5.1 Experimental Set-Up -- Longitudinal Tests



Assembly A-R-1



Assembly B-R-1

Figure 5.9 Rack Assemblies for Longitudinal Tests

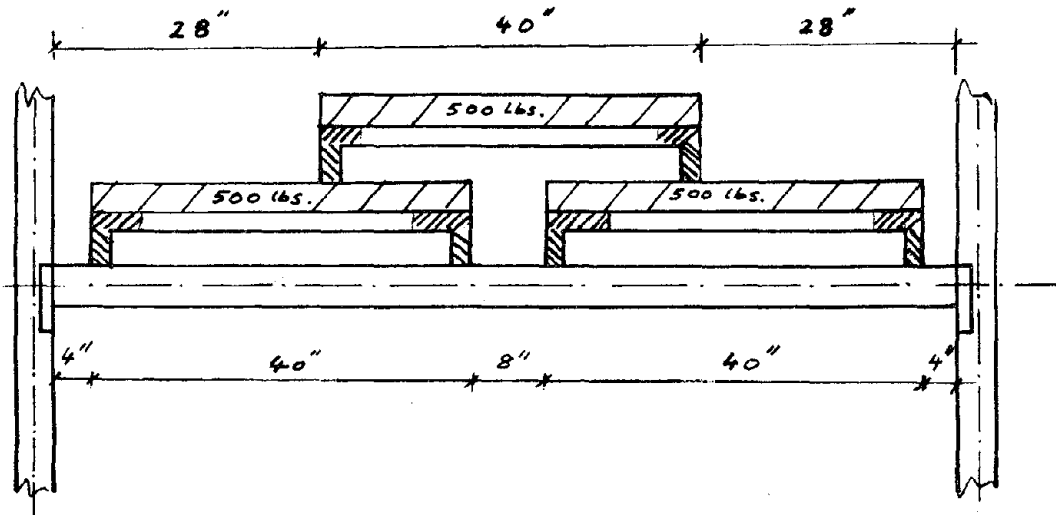


Figure 5.2 Loading Arrangement per Level per Bay per Frame -- Test A-R-1

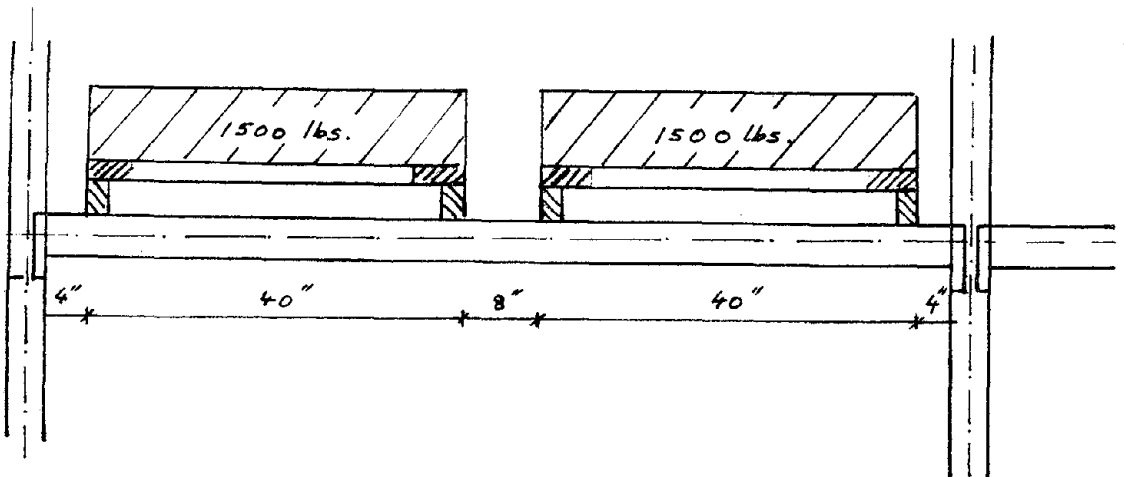


Figure 5.3 Loading Arrangement per Level per Bay per Frame -- Test B-R-1

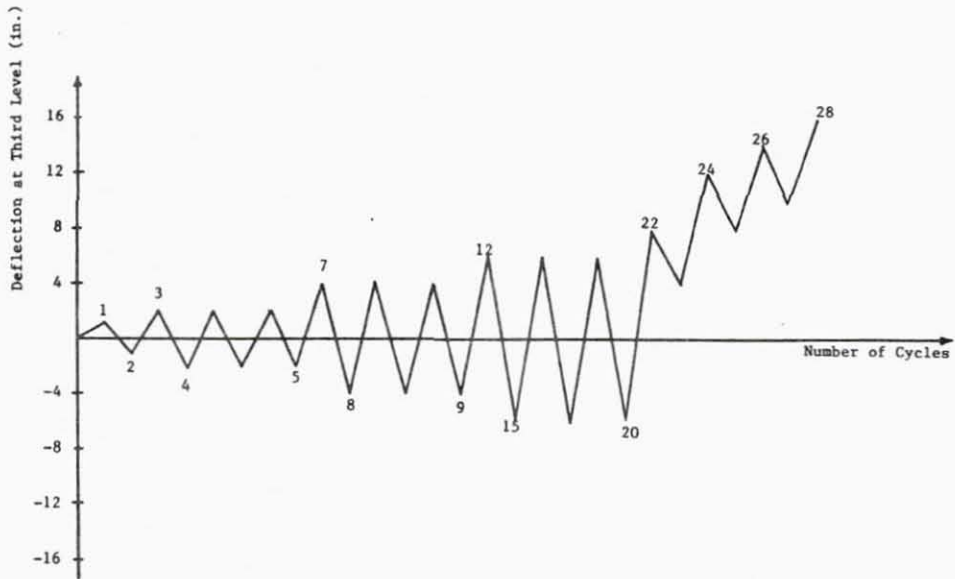


Figure 5.10 Deflection History at Third Level -- Test A-R-1

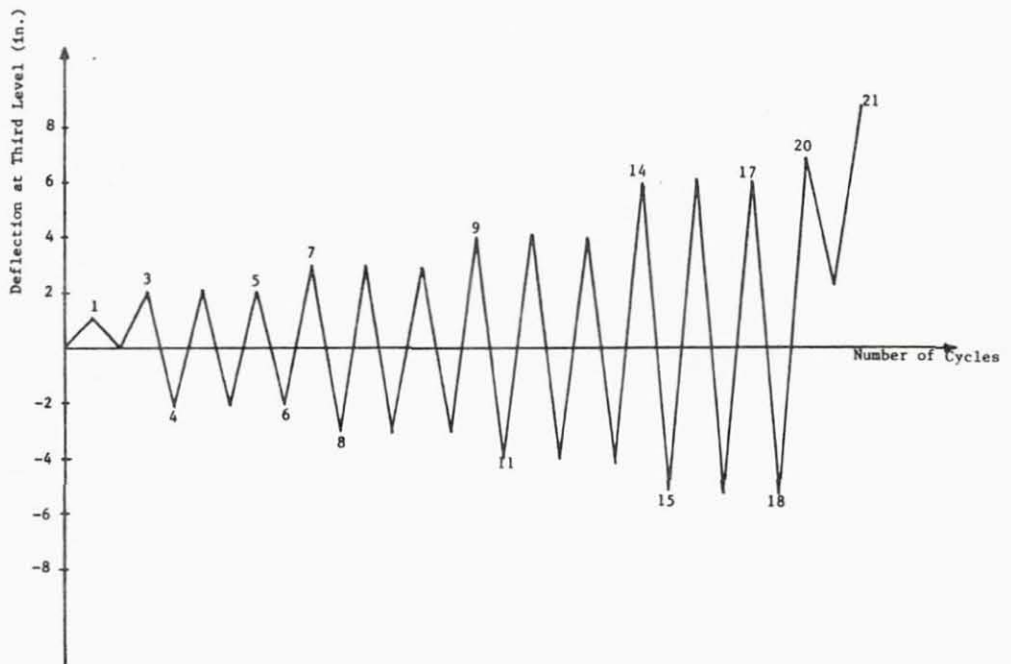


Figure 5.11 Deflection History at Third Level -- Test B-R-1

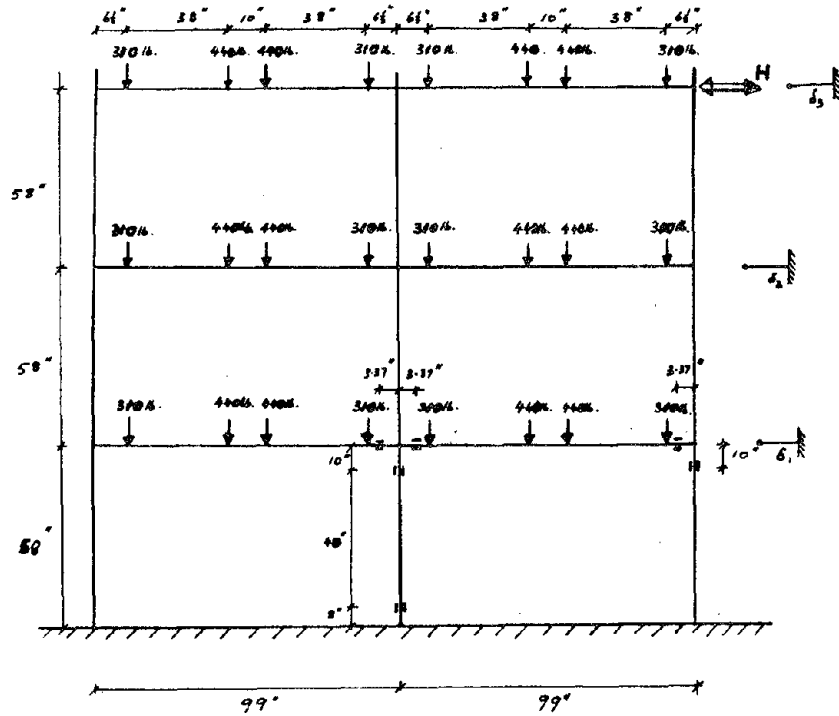


Figure 5.4 Loading Summary and Instrumentation
Frame L1 -- Test A-R-1

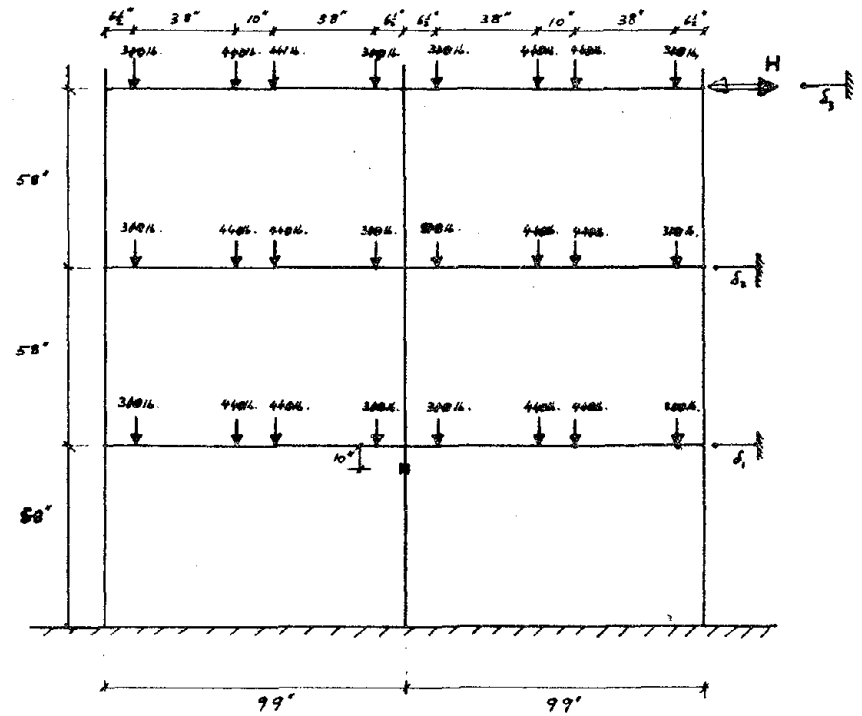


Figure 5.5 Loading Summary and Instrumentation
Frame L2 -- Test A-R-1

TEST A-R-1
LOAD-DEFLECTION AT THIRD LEVEL (PER FRAME)

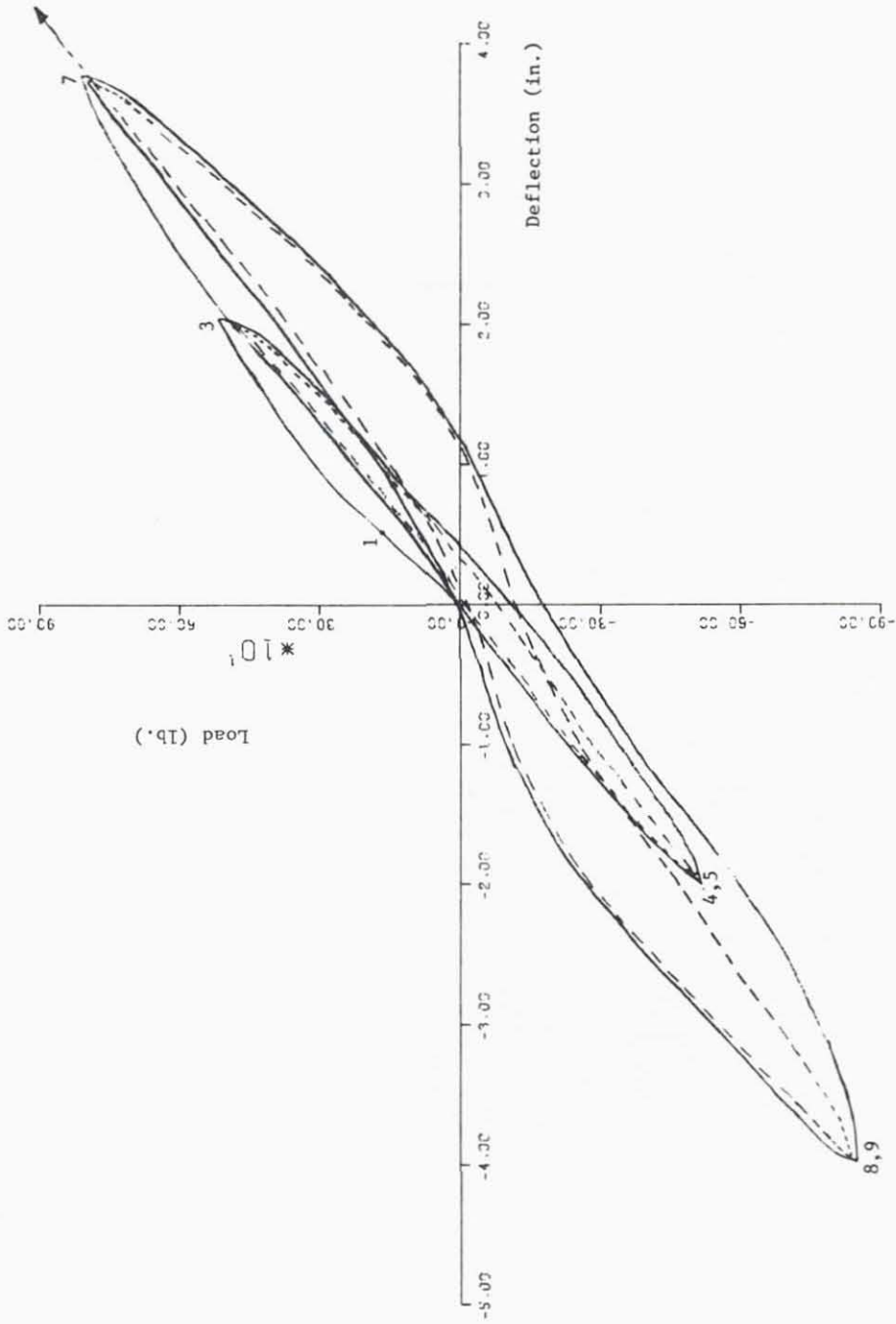


Figure 5.12

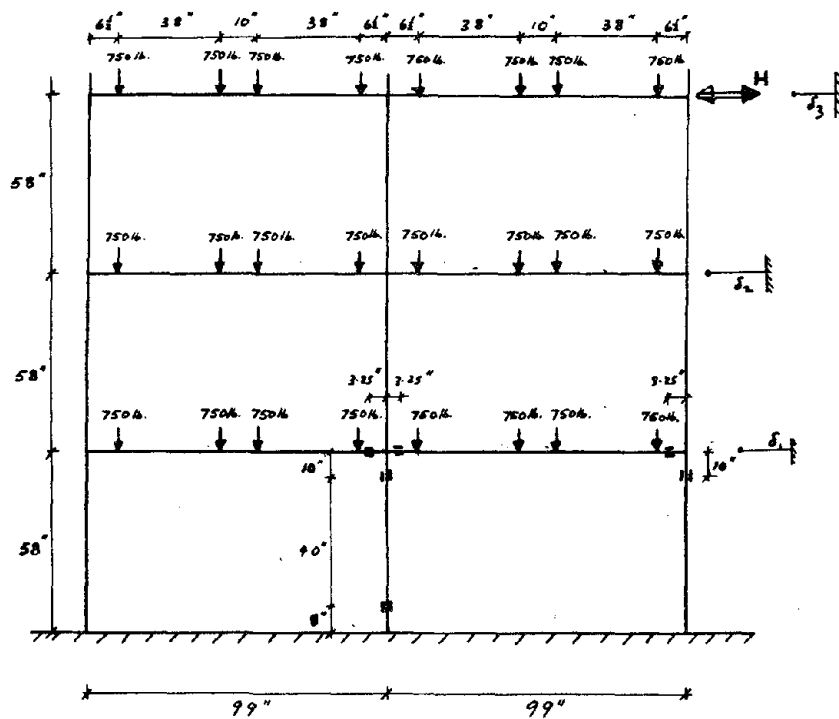


Figure 5.6 Loading Summary and Instrumentation
Frame L1 -- Test B-R-1

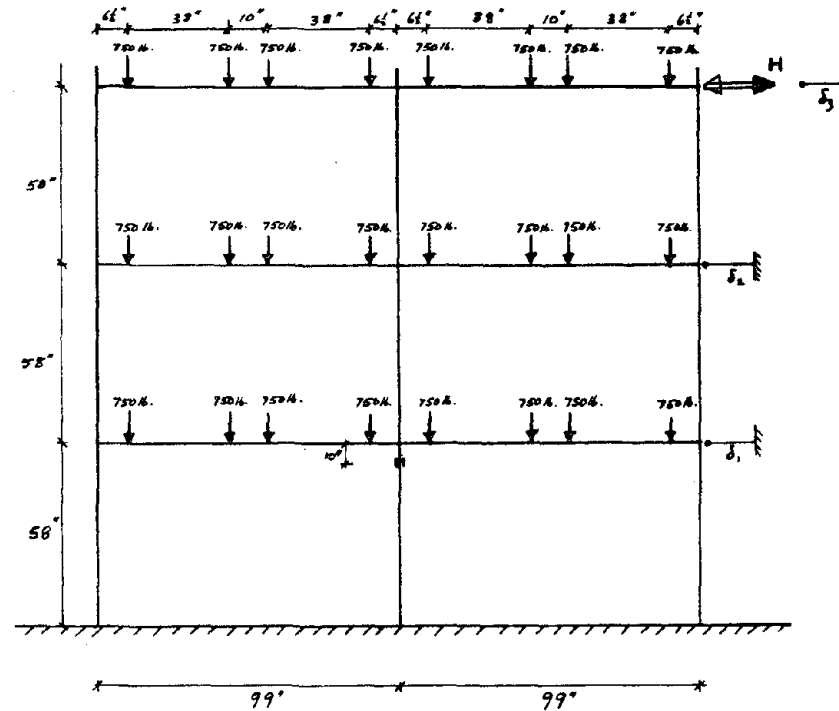


Figure 5.7 Loading Summary and Instrumentation
Frame L2 -- Test B-R-1

TEST A-R-1

LOAD-DEFLECTION AT THIRD LEVEL. (PER FRAME)

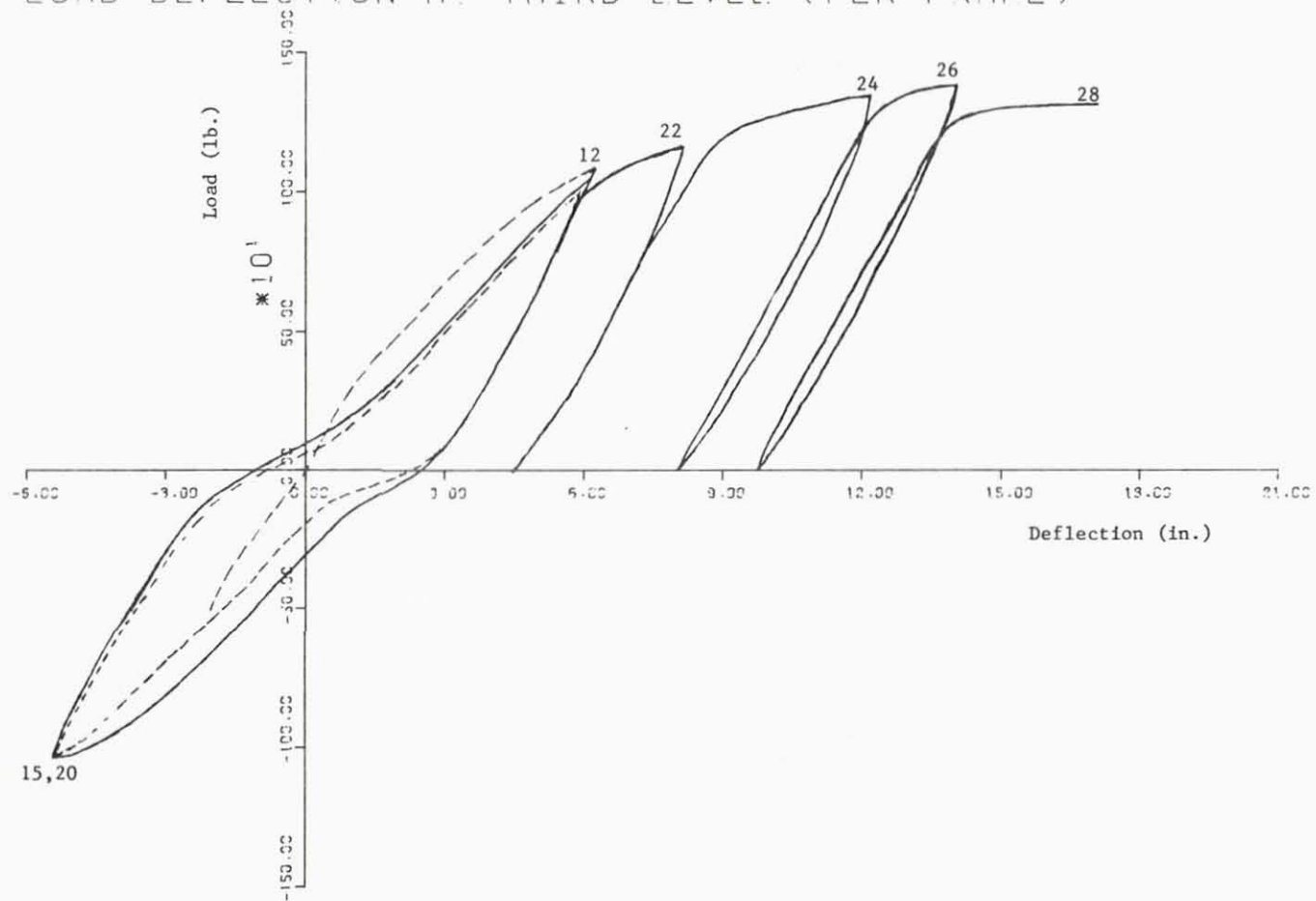


Figure 5.13

TEST B-R-1
LOAD-DEFLECTION AT THIRD LEVEL. (PER FRAME)

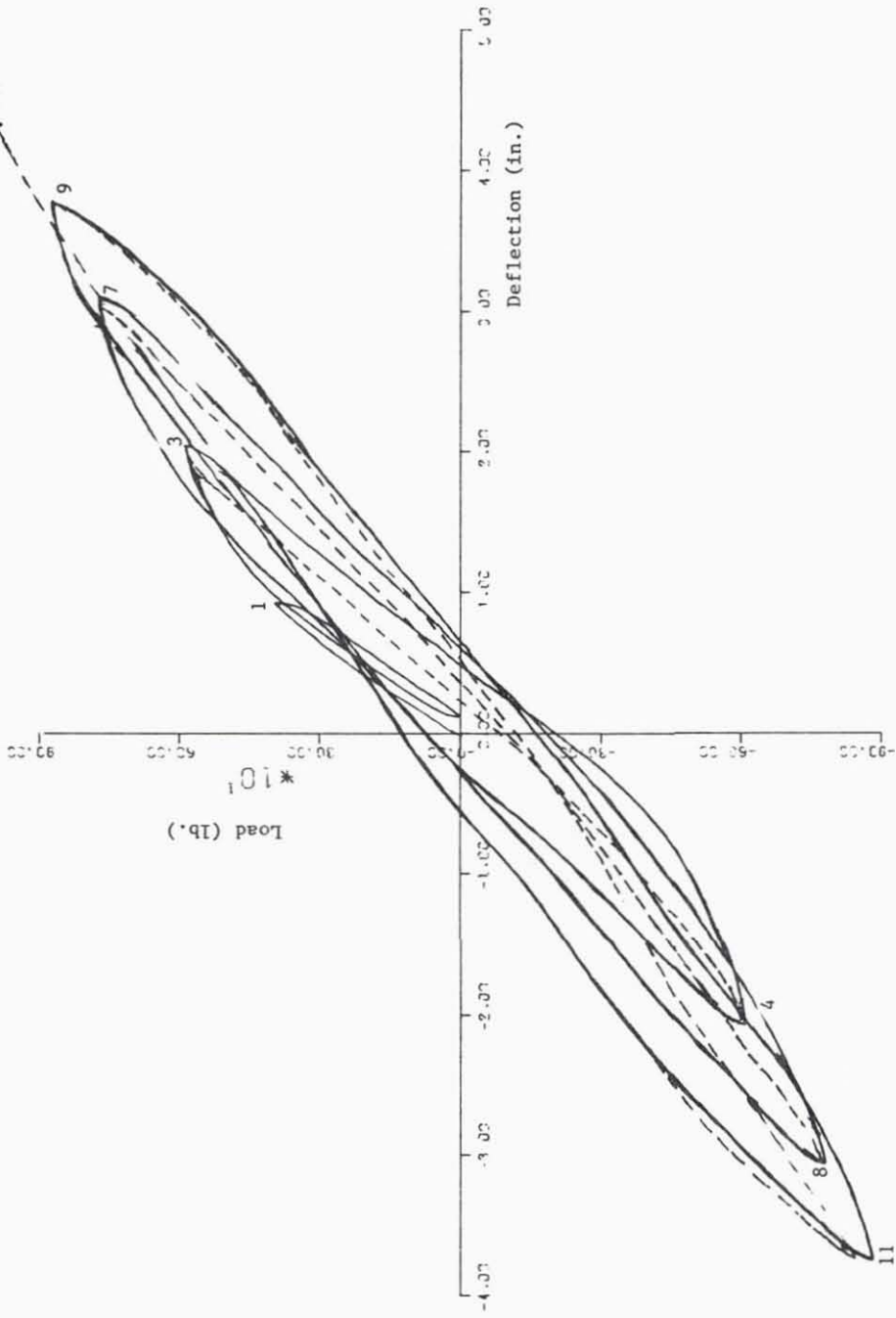


Figure 5.14

TEST B-R-1
 LOAD-DEFLECTION AT THIRD LEVEL (PER FRAME)

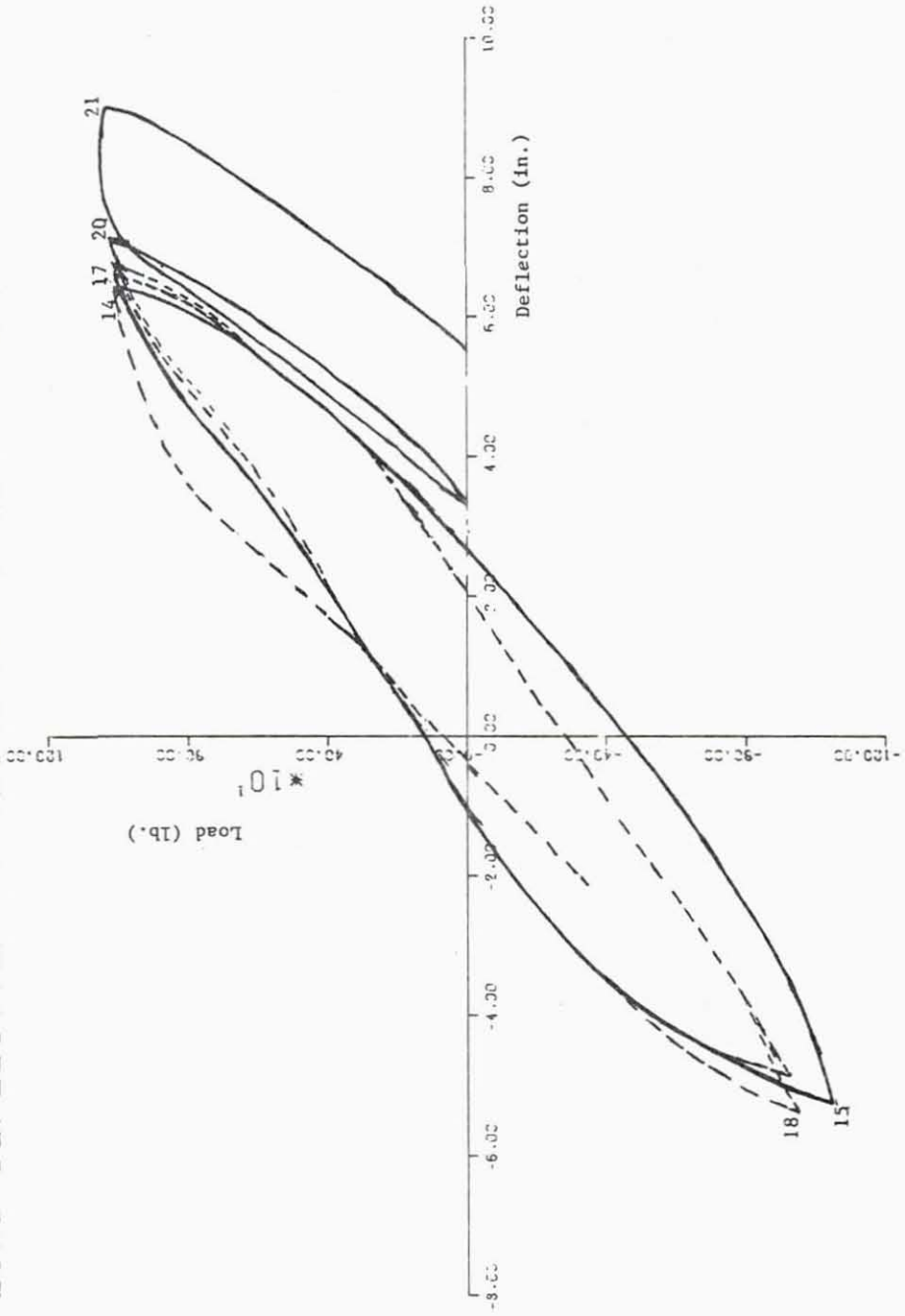


Figure 5.15

TEST A-R-1
LOAD-DEFLECTION AT FIRST LEVEL. (PER FRAME)

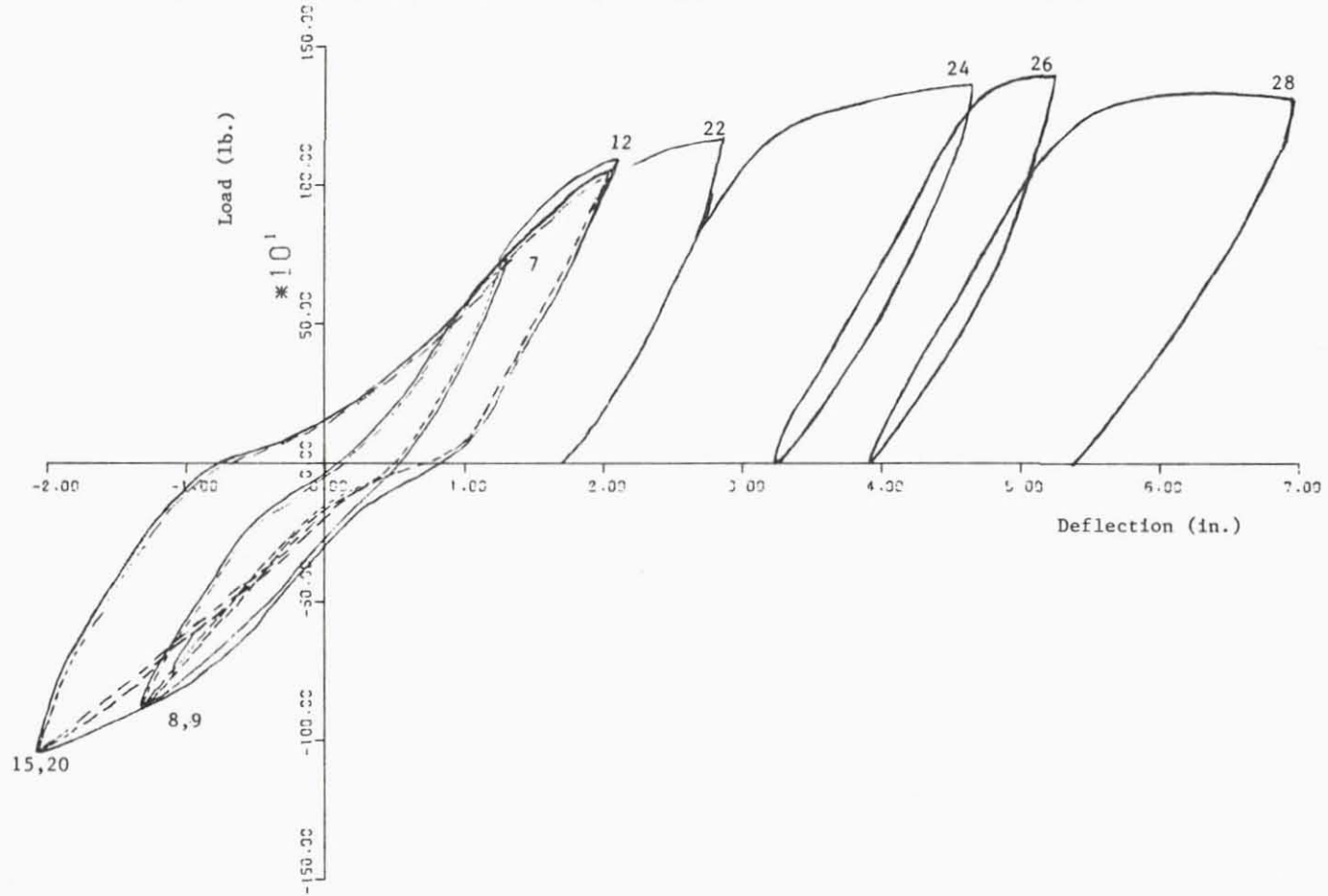


Figure 5.16

TEST B-R-1

LOAD-DEFLECTION AT FIRST LEVEL (PER FRAME)

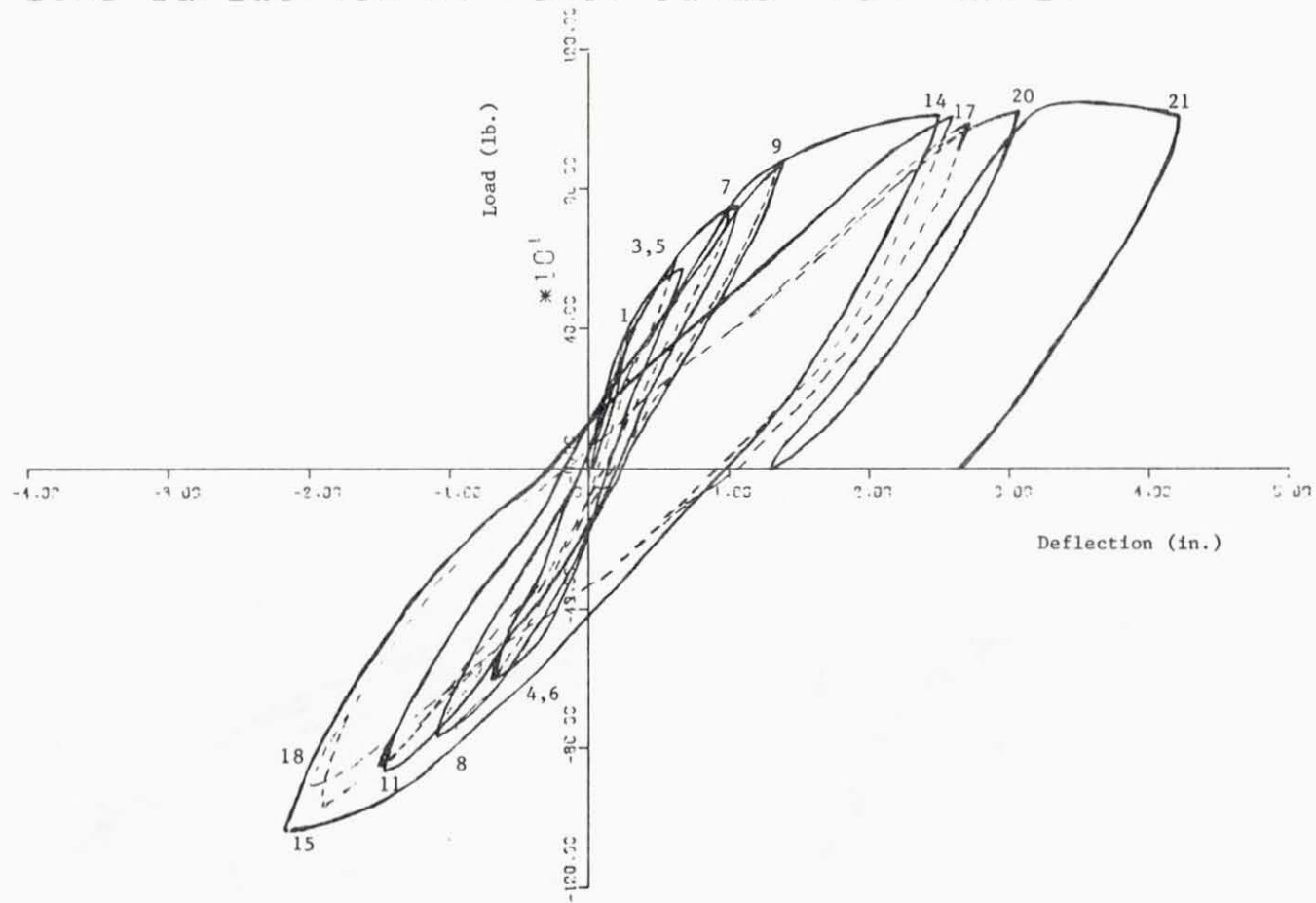


Figure 5.17

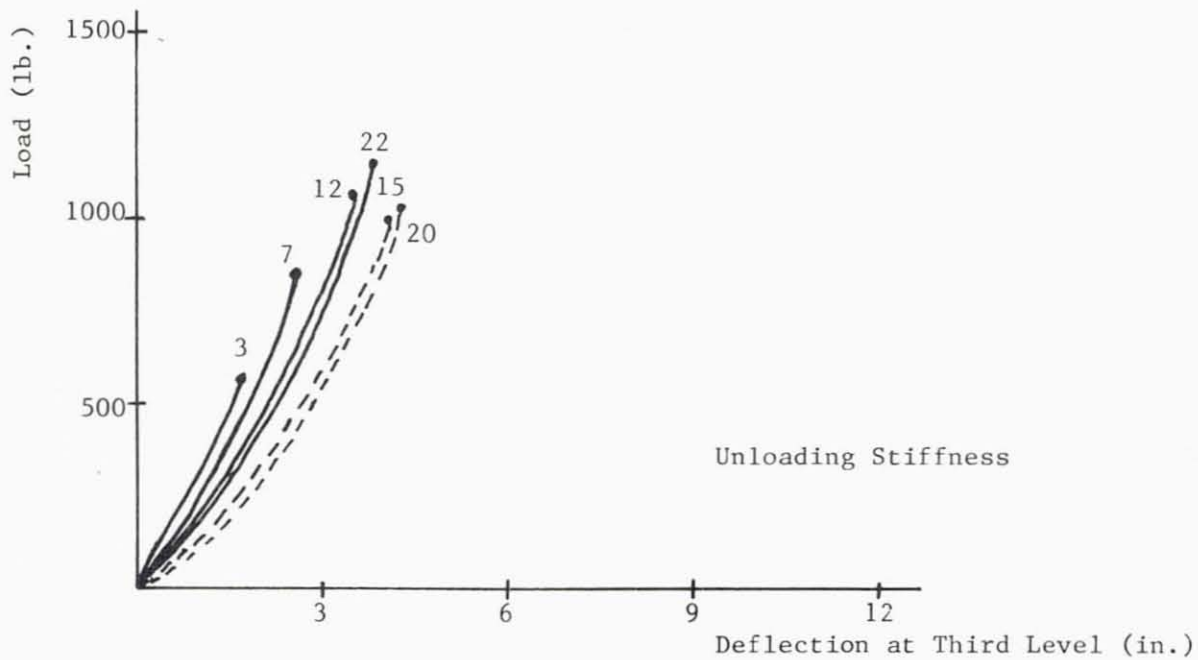
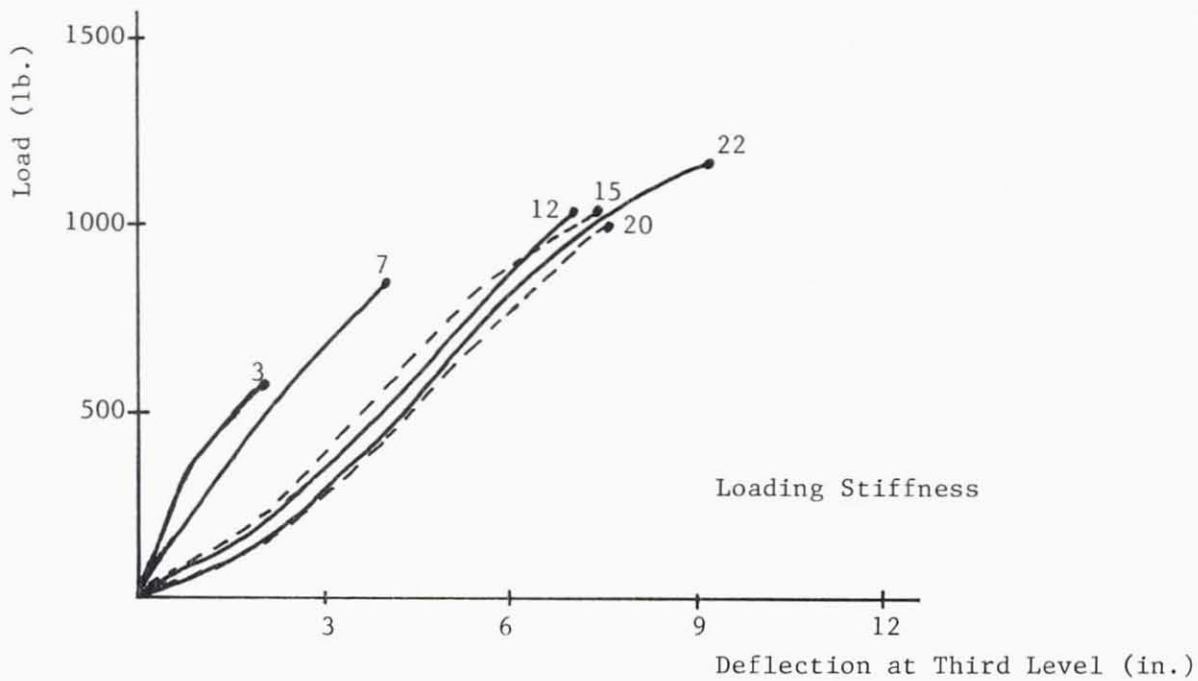


Figure 5.18 Deterioration of Stiffness -- Test A-R-1

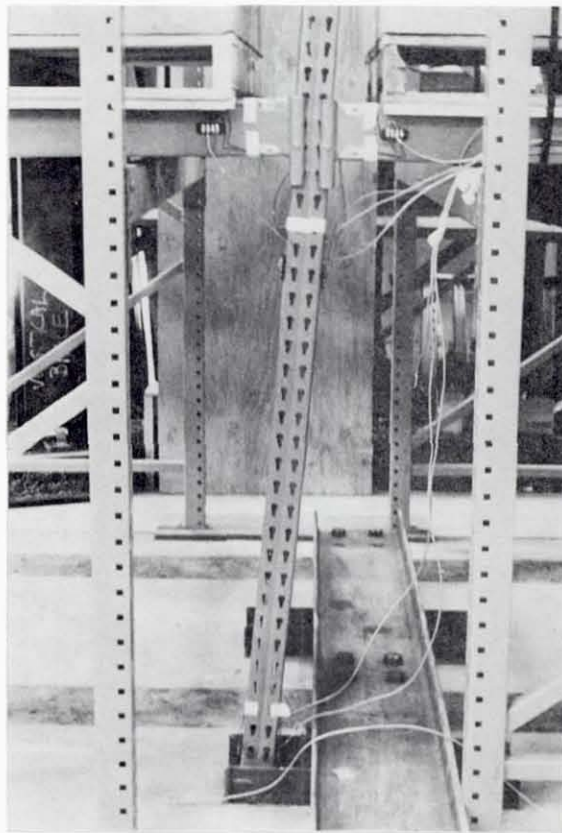


Figure 5.19 Plastic Hinges in Interior Post -- Assembly A-R-1

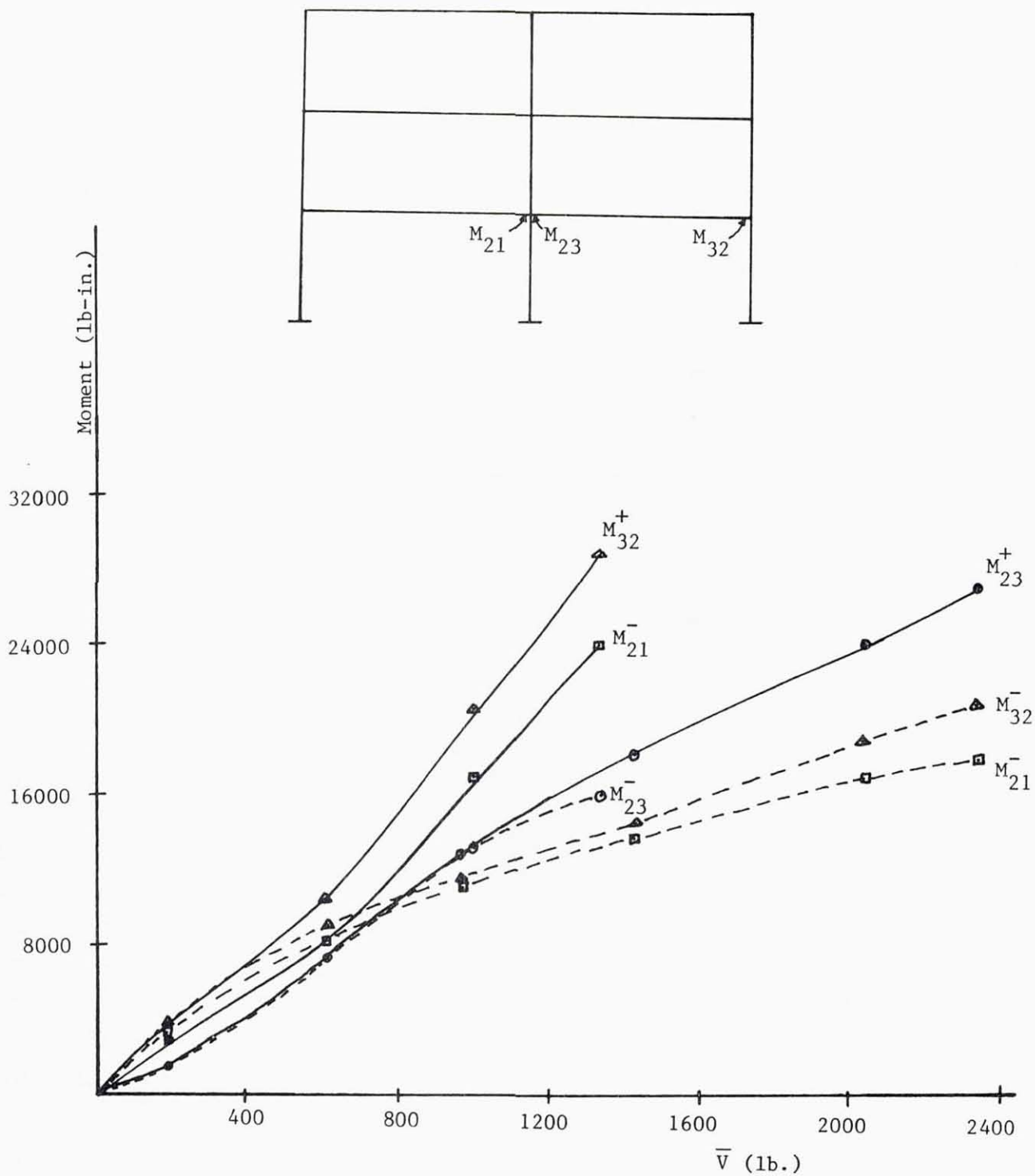


Figure 5.20 Beam Moments Due to Lateral Loads vs Equivalent Story Shear Below First Floor Level -- Test A-R-1

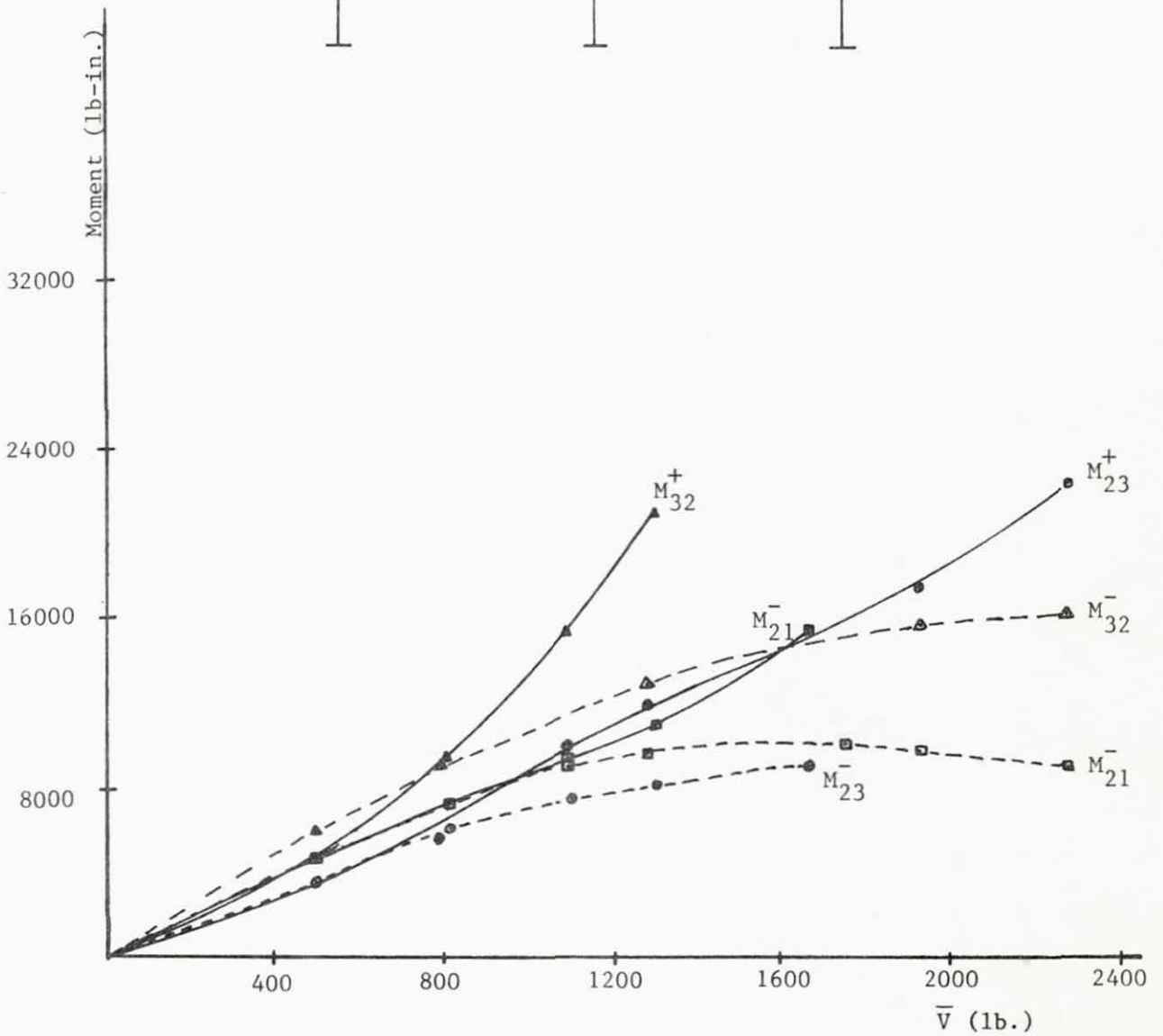
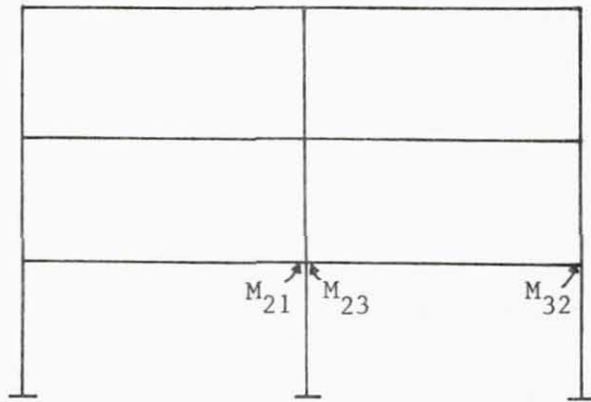


Figure 5.21 Beam Moments Due to Lateral Loads vs Equivalent Story Shear Below First Floor Level -- Test B-R-1

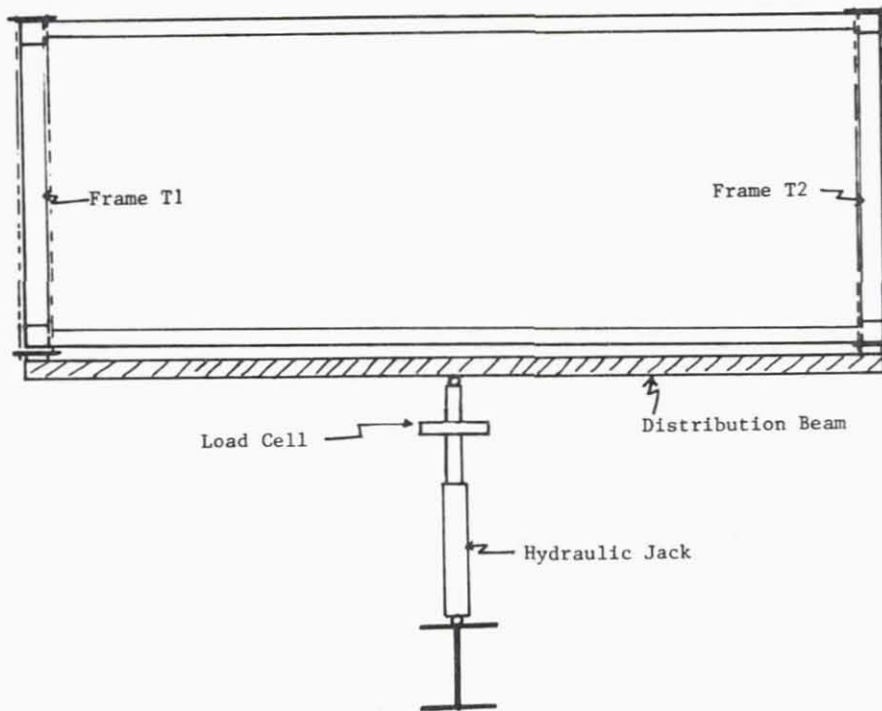


Figure 5.22 Experimental Set-Up -- Transverse Tests

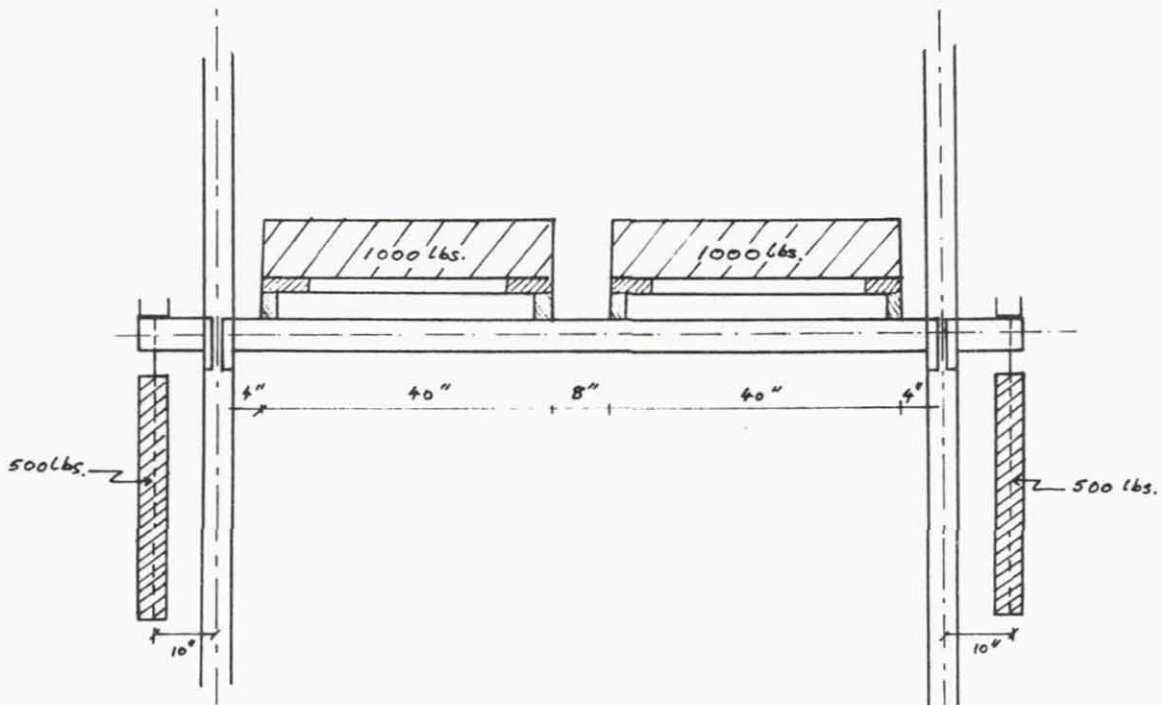


Figure 5.23 Loading Arrangement per Level per Frame -- Tests A-R-2 and B-R-2

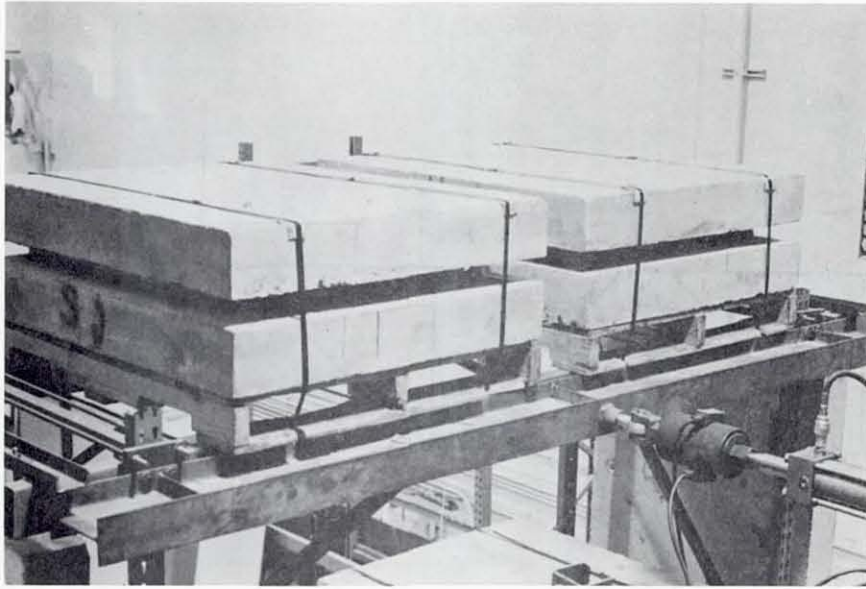


Figure 5.24 Horizontal Loading Arrangement -- Transverse Tests

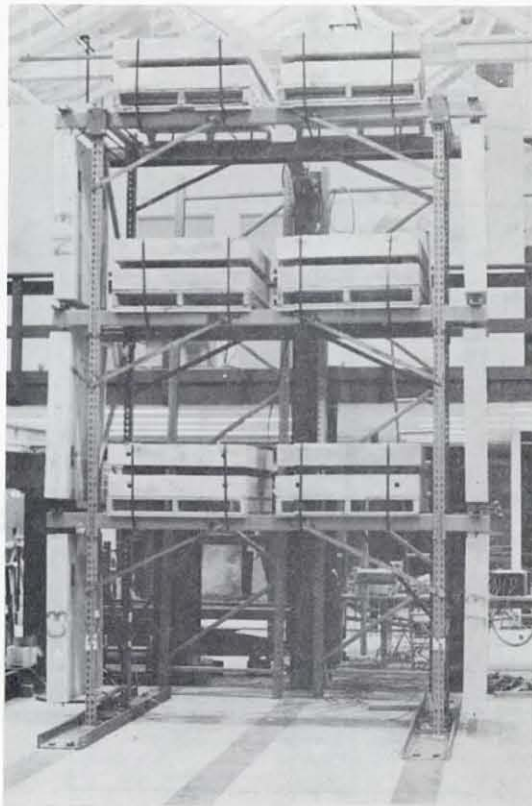


Figure 5.25 Rack Assembly for Transverse Test -- A-R-1

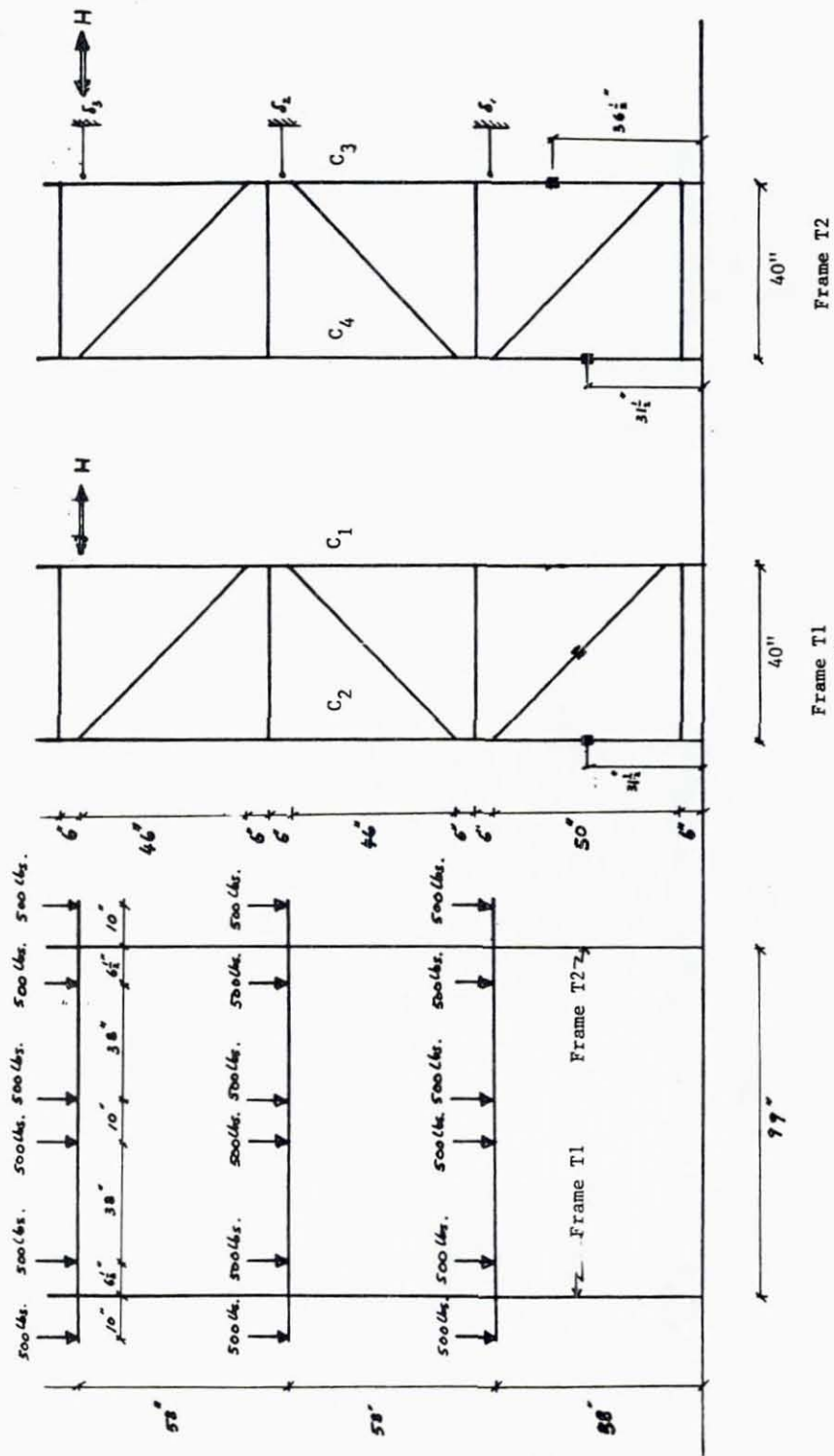


Figure 5.26 Loading Summary and Instrumentation -- Test A-R-2

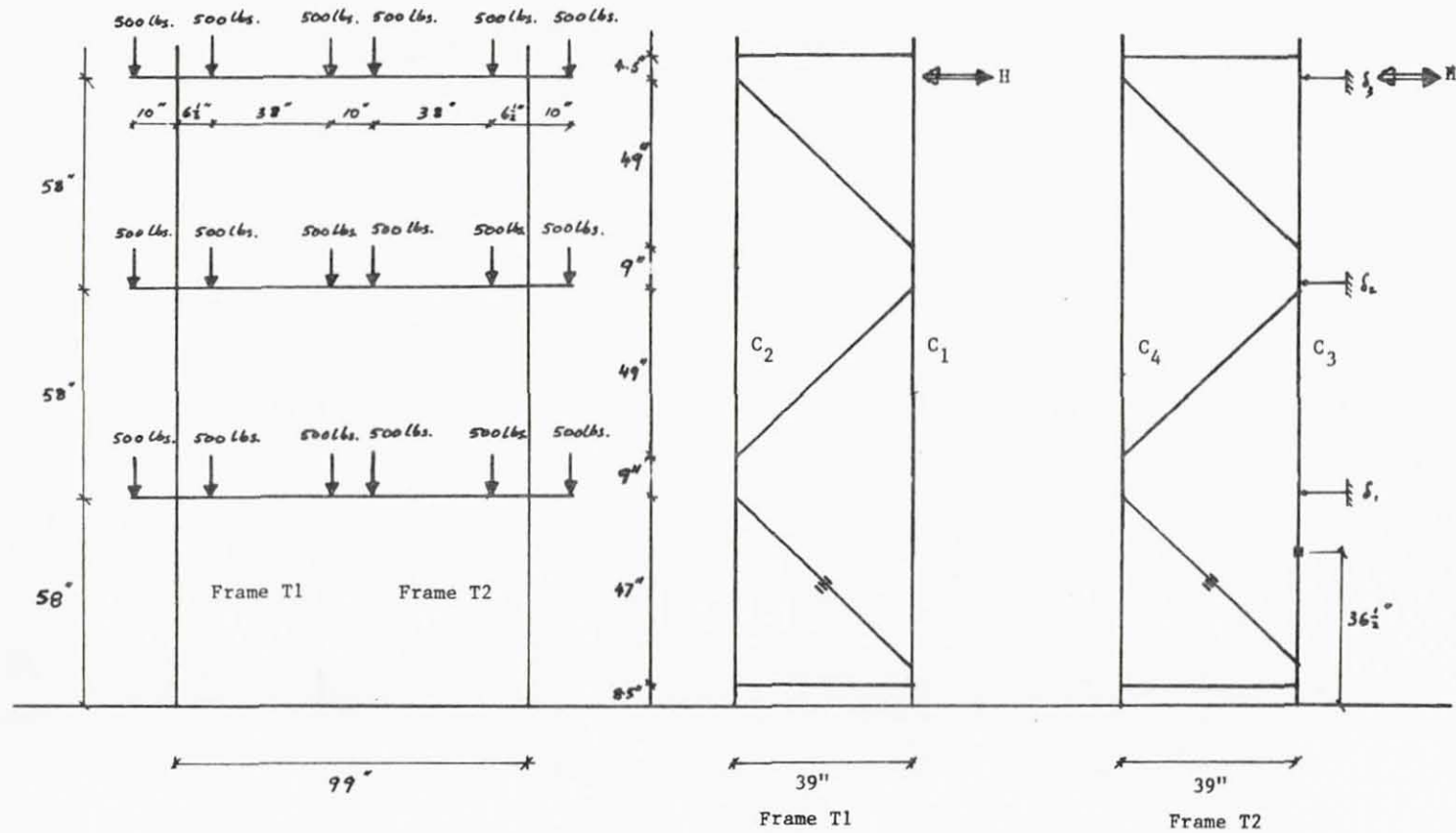


Figure 5.27 Loading Summary and Instrumentation -- Test B-R-2

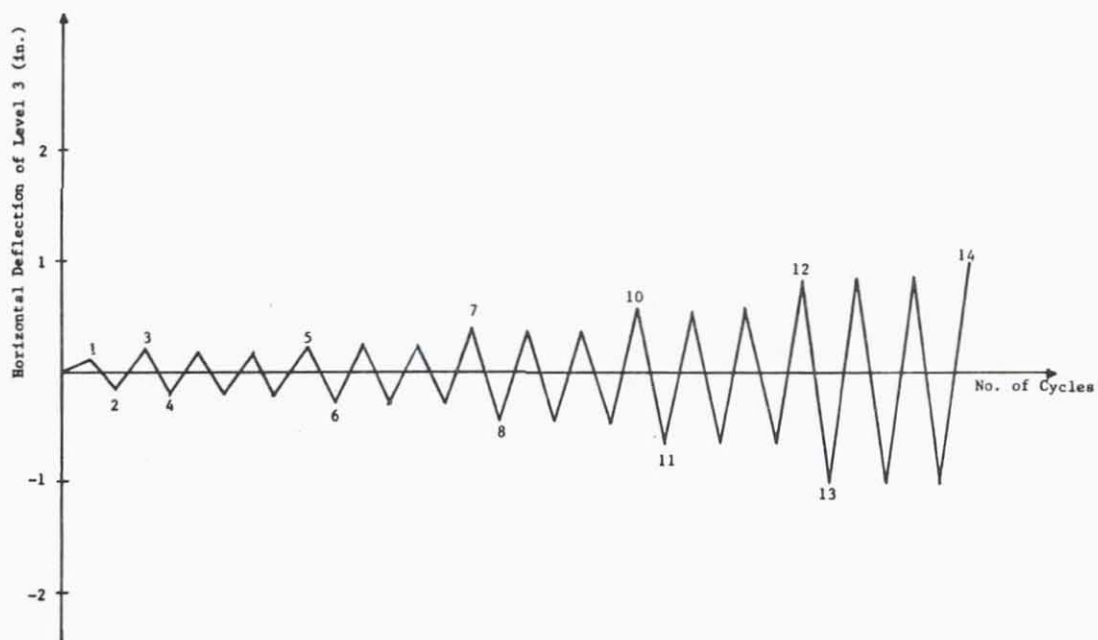


Figure 5.28 Deflection History at Third Level -- Test A-R-2

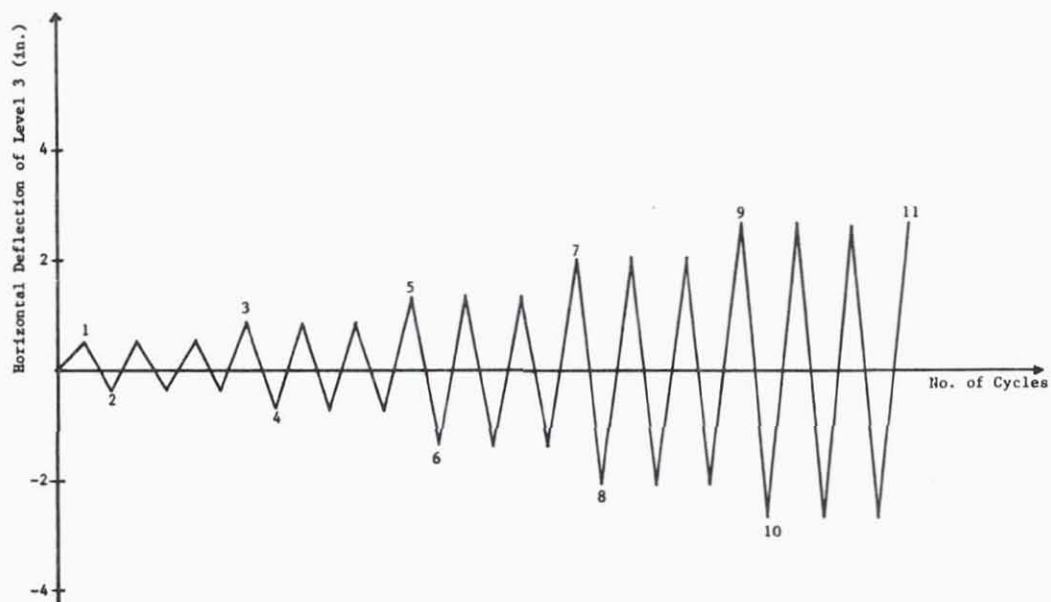


Figure 5.29 Deflection History at Third Level -- Test B-R-2

TEST A-R-2 (TRANSVERSE LOADING)
LOAD-DEFLECTION AT THIRD LEVEL (PER FRAME)

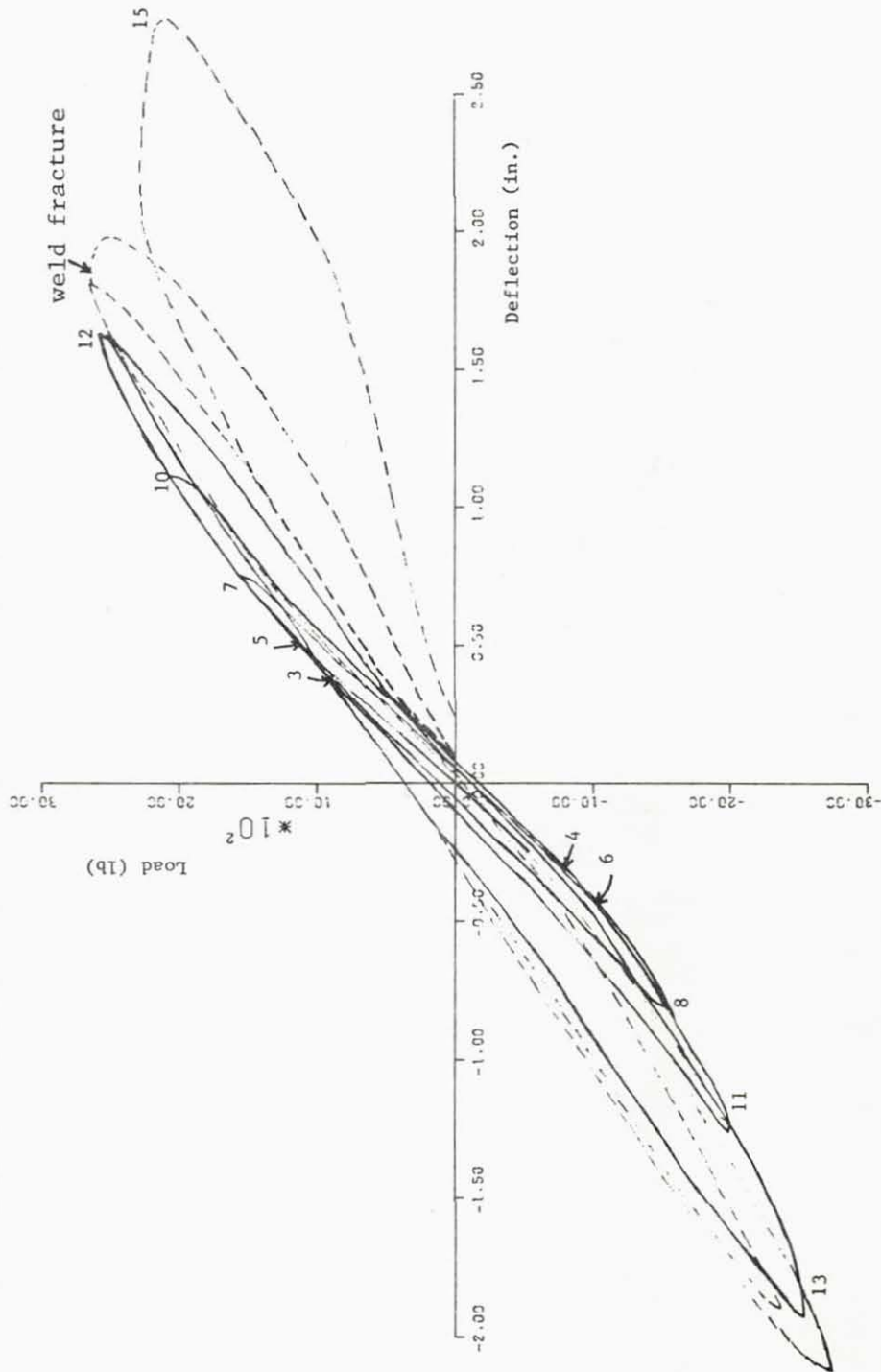


Figure 5.30

TEST B-R-2 (TRANSVERSE LOADING)
LOAD-DEFLECTION AT THIRD LEVEL (PER FRAME)

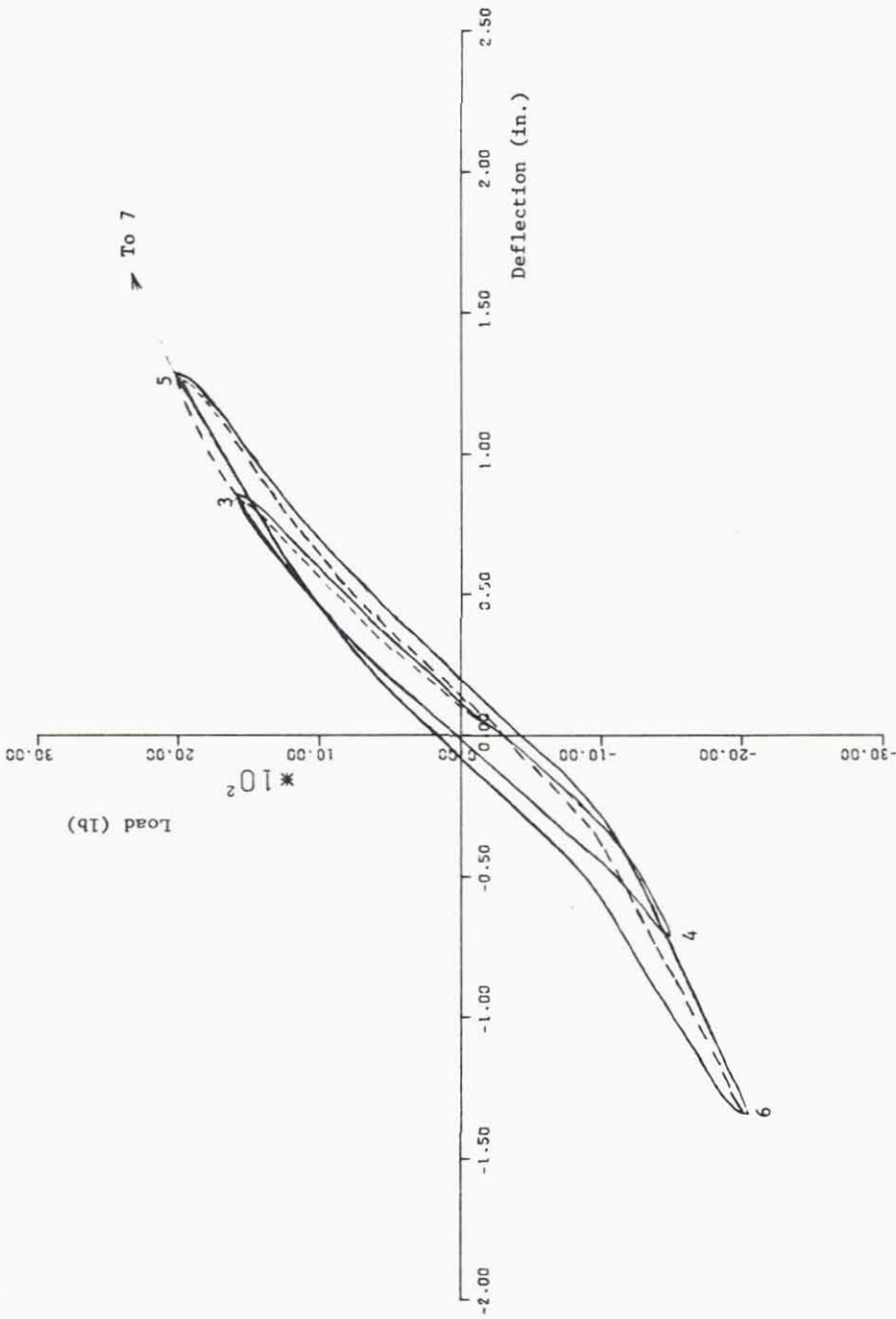


Figure 5.31

TEST B-R-2 (TRANSVERSE LOADING)
LOAD-DEFLECTION AT THIRD LEVEL (PER FRAME)

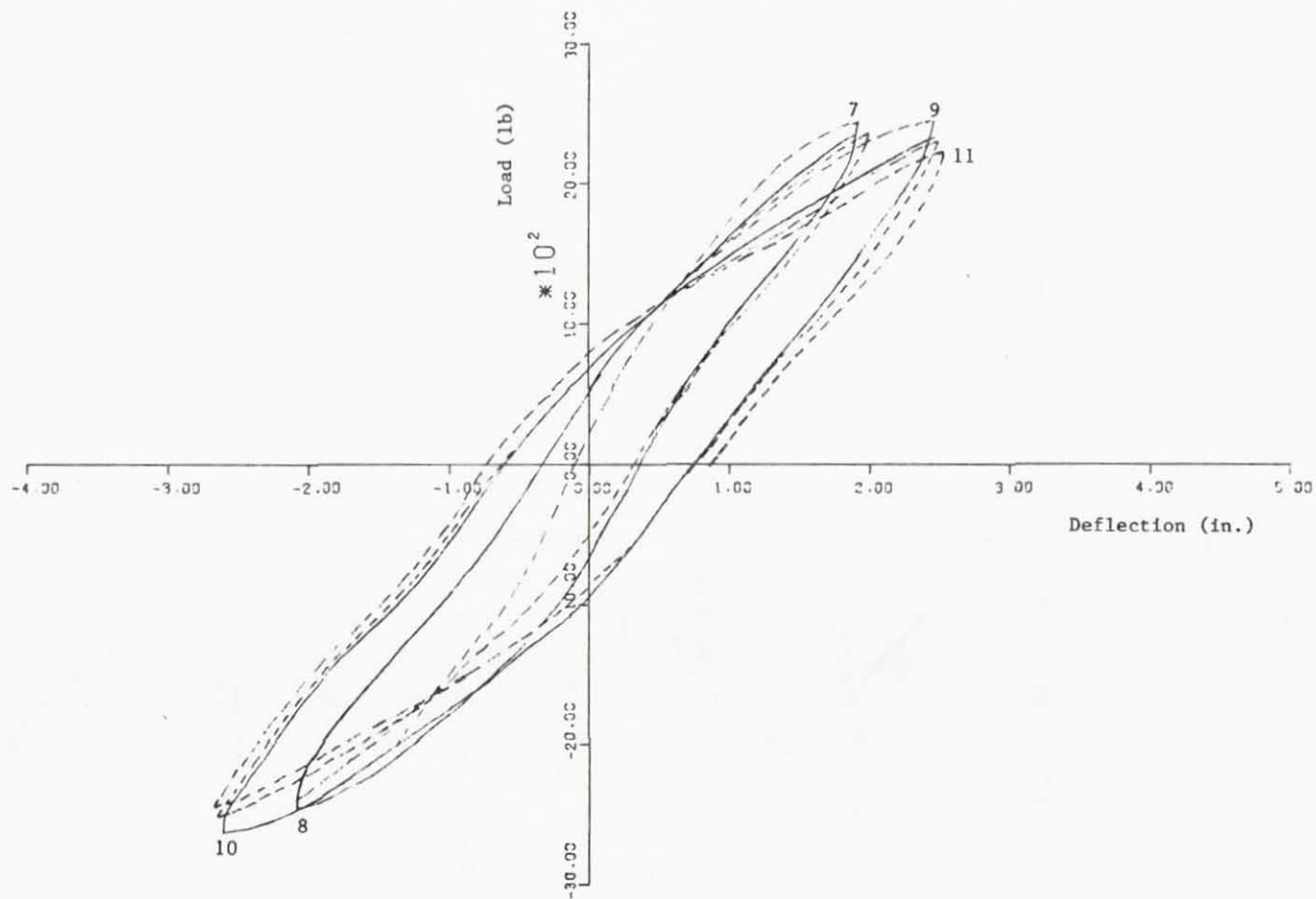


Figure 5.31 (continued)

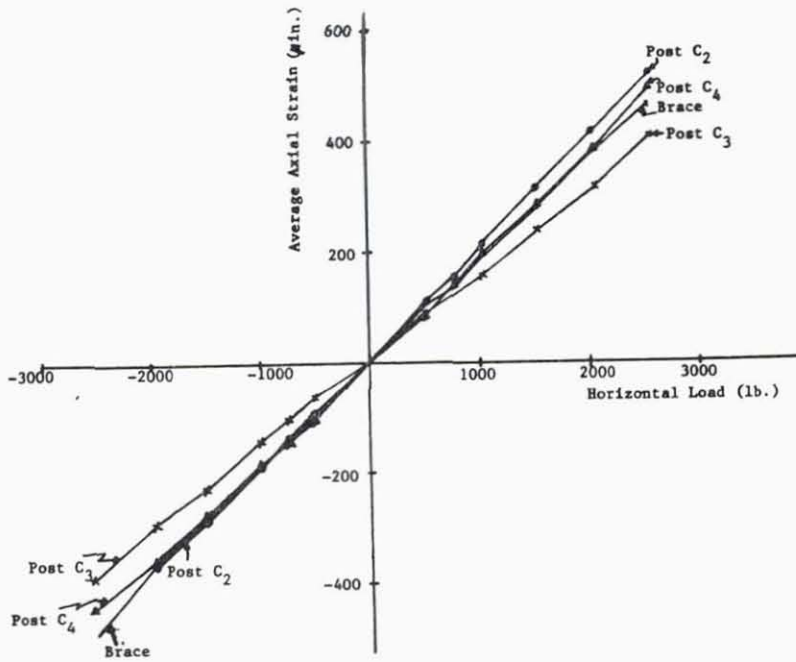


Figure 5.32 Horizontal Load vs Average Axial Strains in Posts and Braces -- Test A-R-2

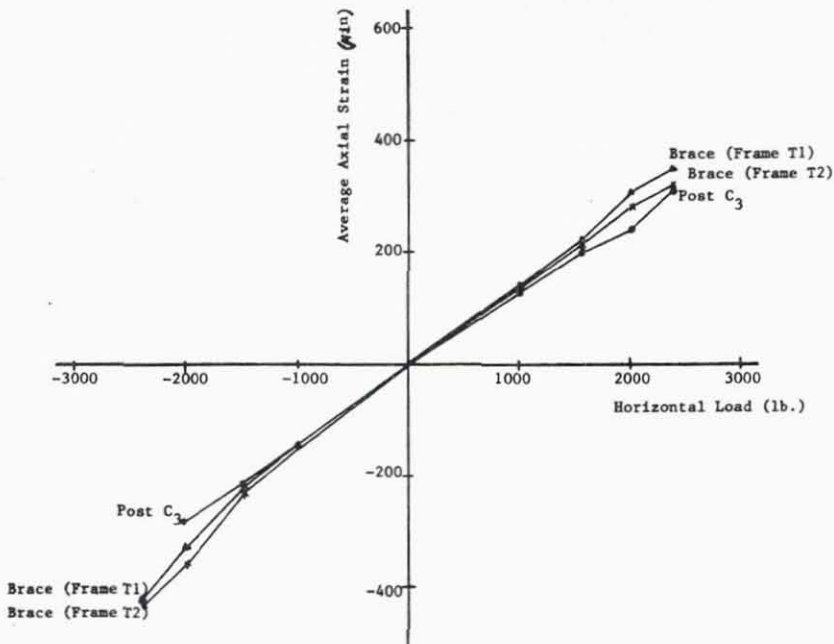


Figure 5.33 Horizontal Load vs Average Axial Strains in Posts and Braces -- Test B-R-2

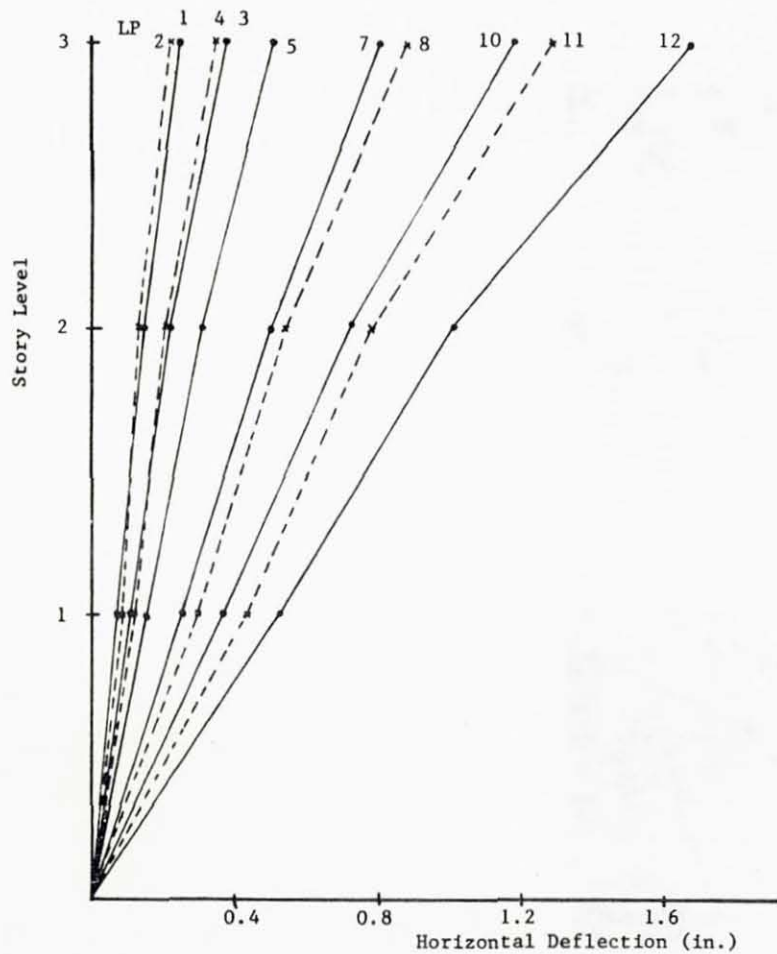


Figure 5.34 Horizontal Deflection of Frame T1
at Various Loading Stages--Test A-R-1

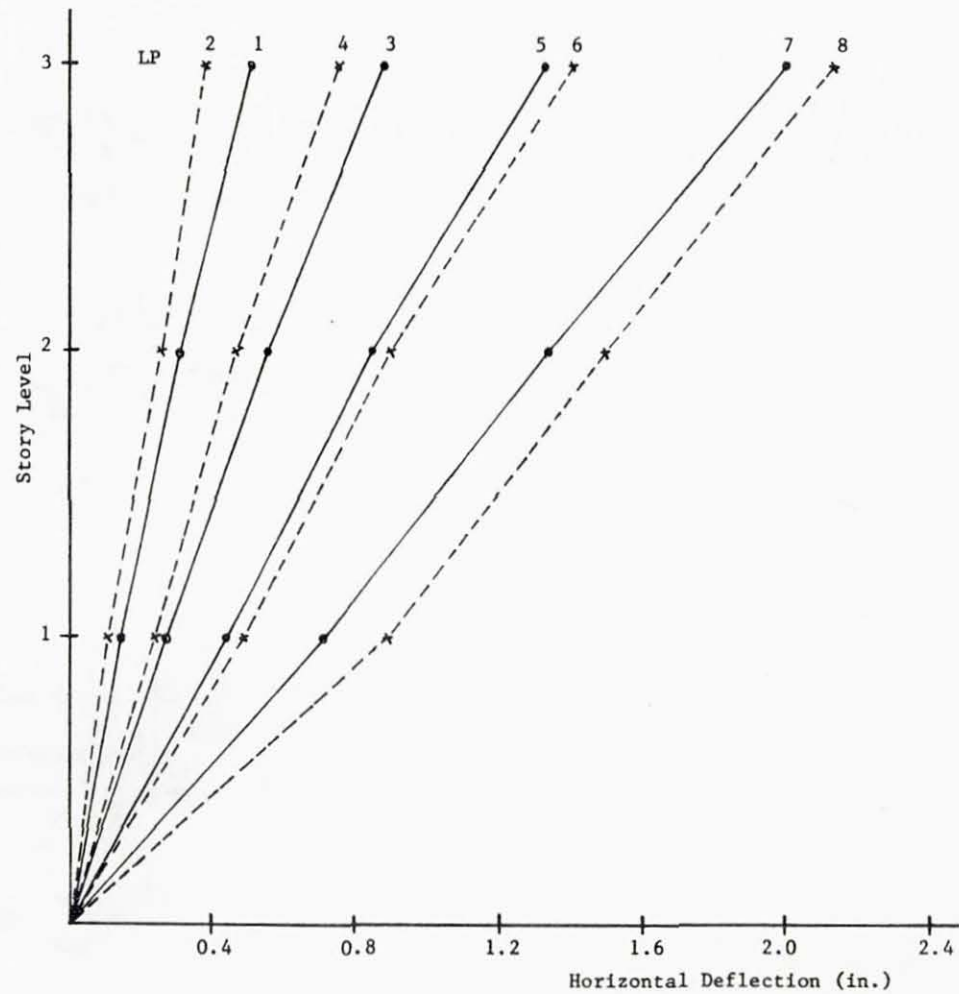


Figure 5.35 Horizontal Deflection of Frame T1
at Various Loading Stages--Test B-R-1

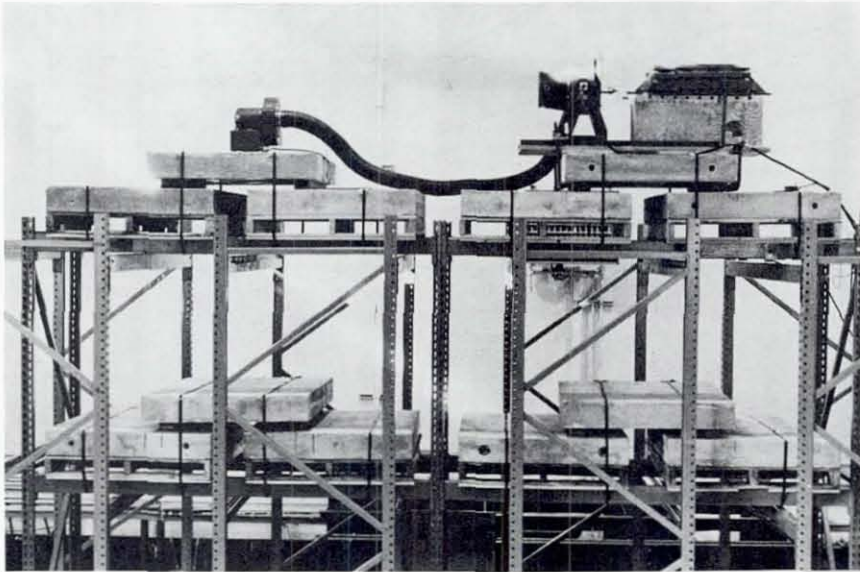


Figure 6.1 Vibration Generator on Rack Assembly A-R-1

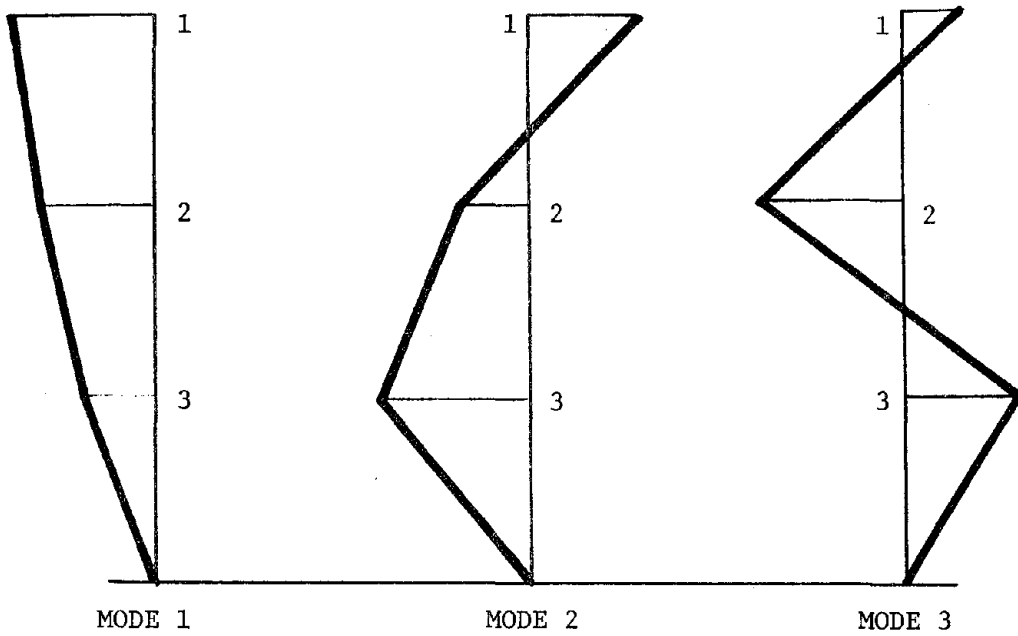


Figure 6.2 Mode Shapes -- A-R-1 -- Longitudinal Direction

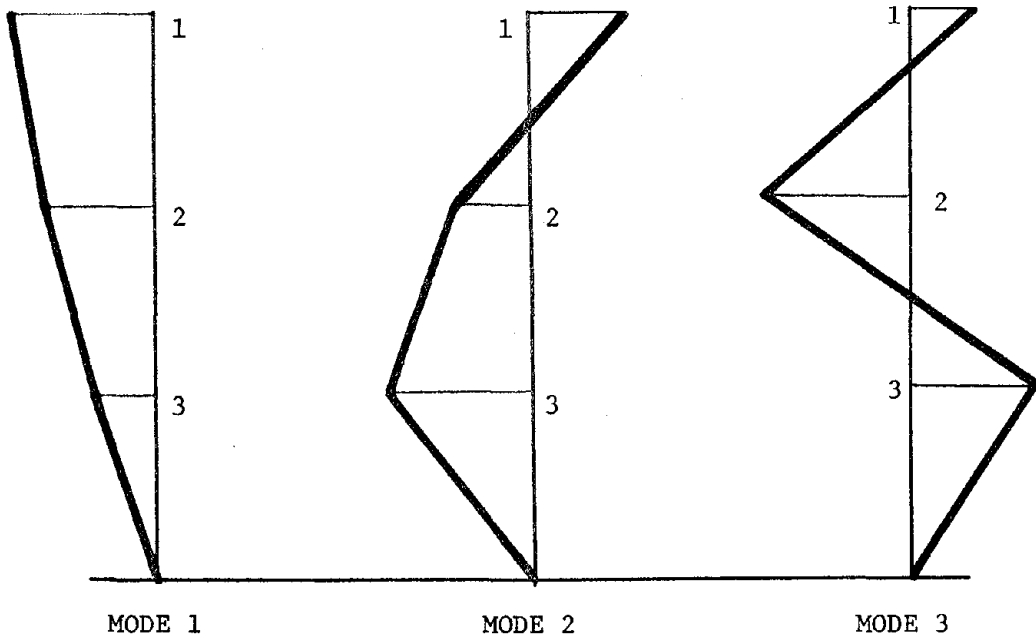


Figure 6.3 Mode Shapes -- B-R-1 -- Longitudinal Direction

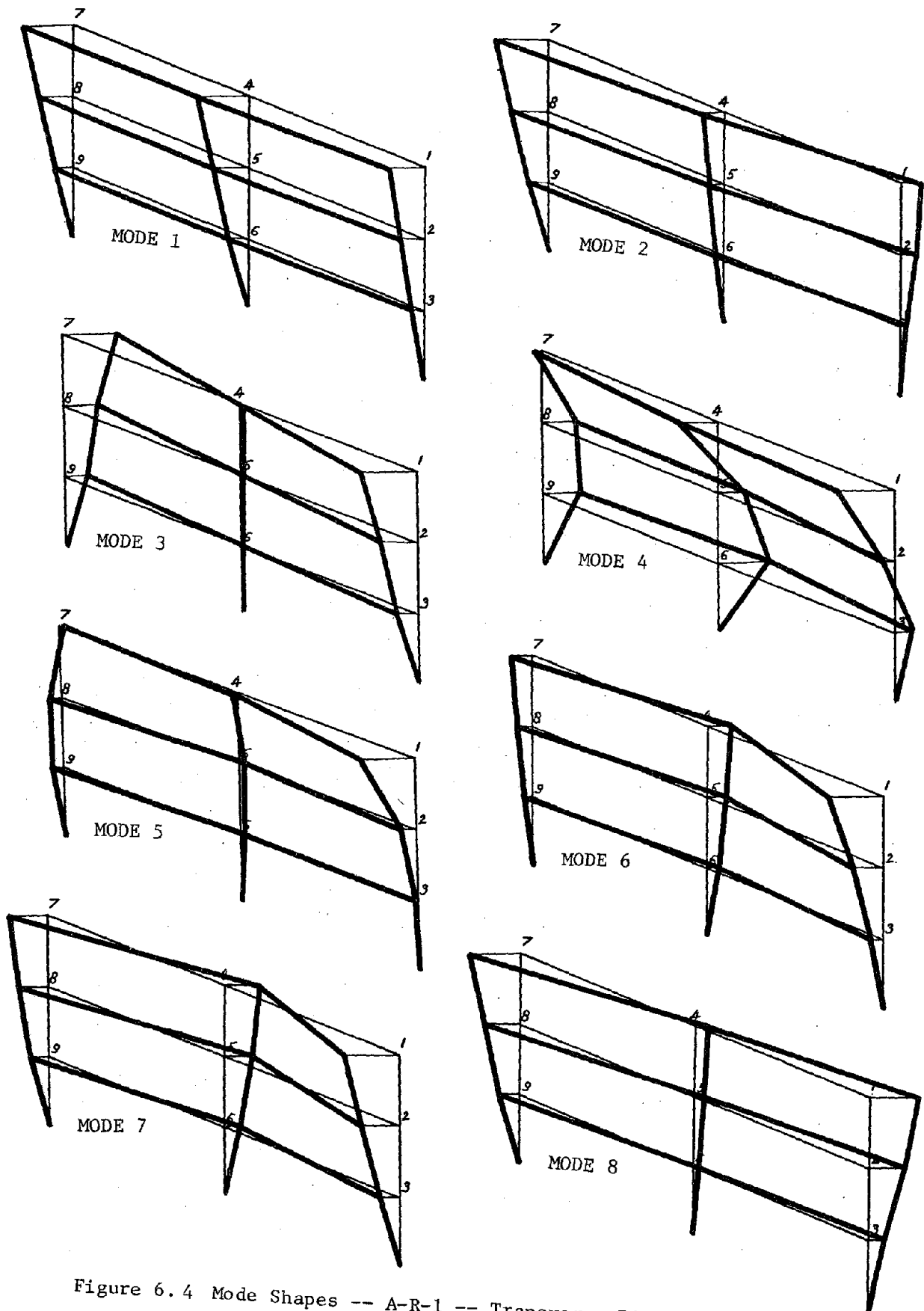


Figure 6.4 Mode Shapes -- A-R-1 -- Transverse Direction

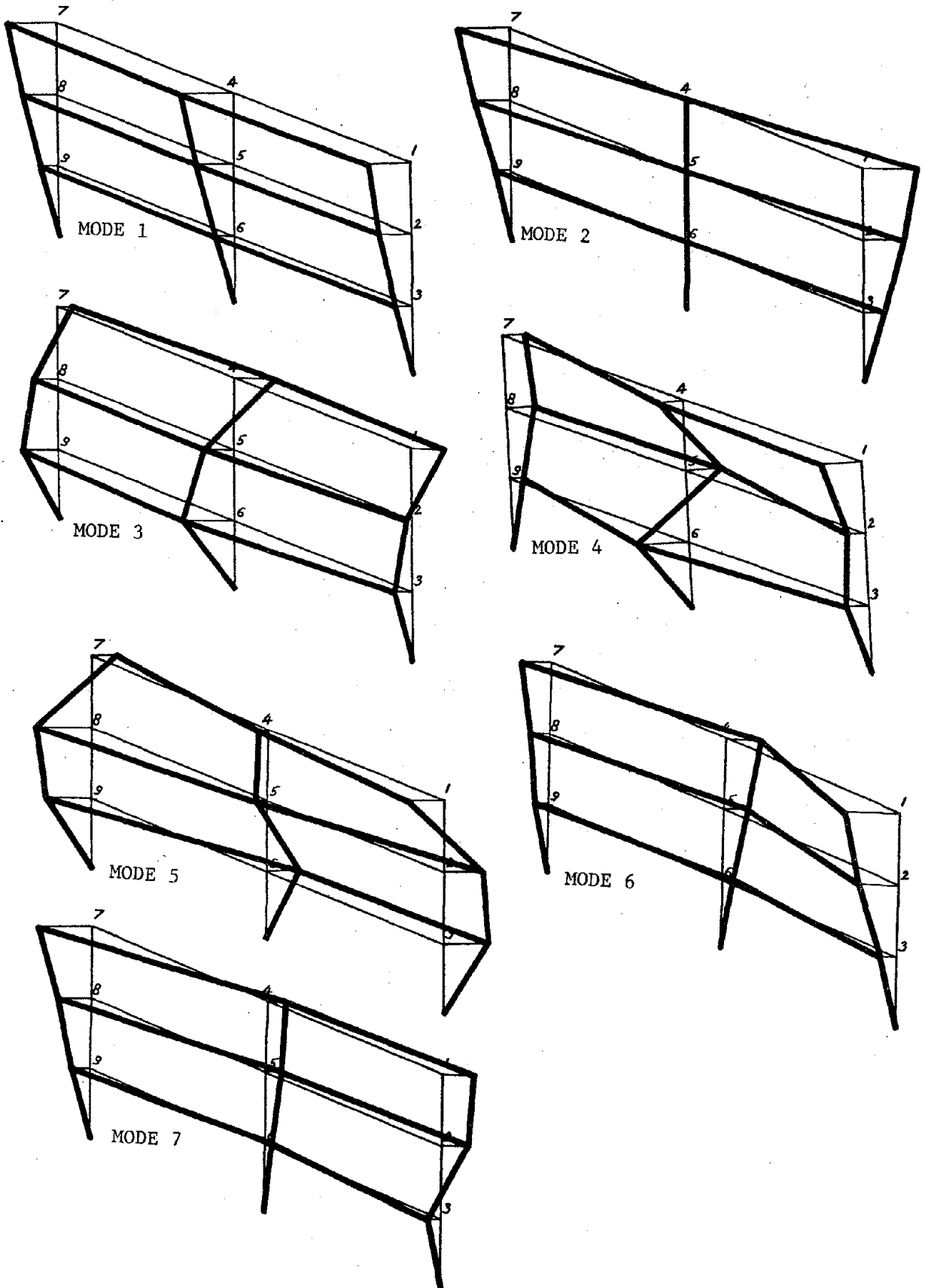


Figure 6.5 Mode Shapes -- B-R-1 -- Transverse Direction

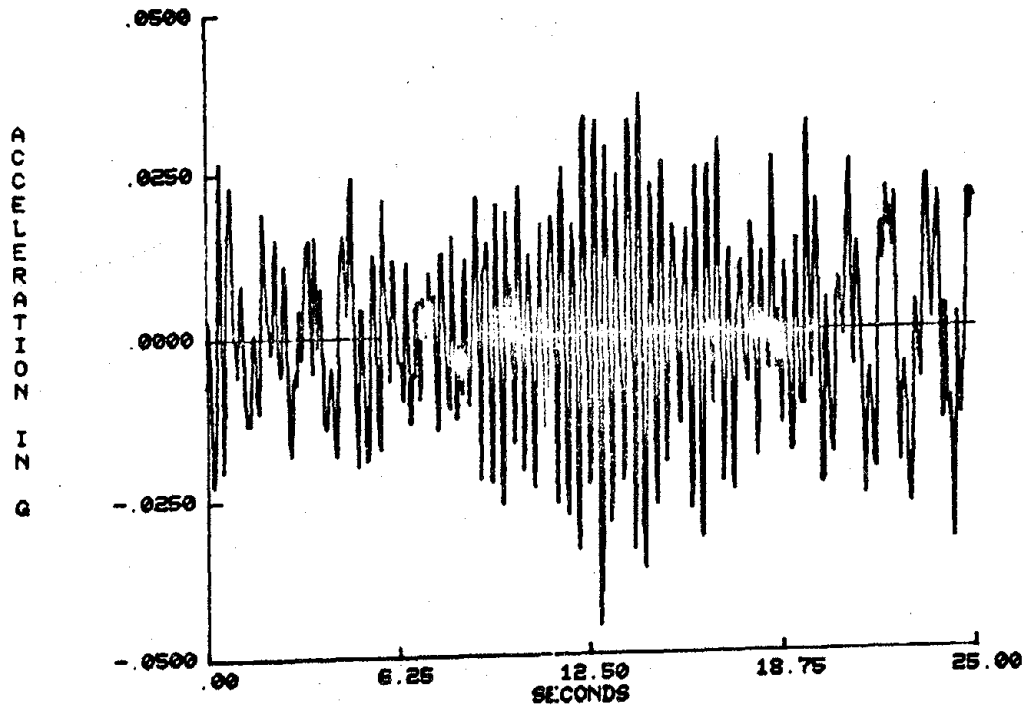


Figure 6.6 ACCELERATION TIME HISTORY, NODE 1, LONGITUDINAL RESPONSE
A-R-1

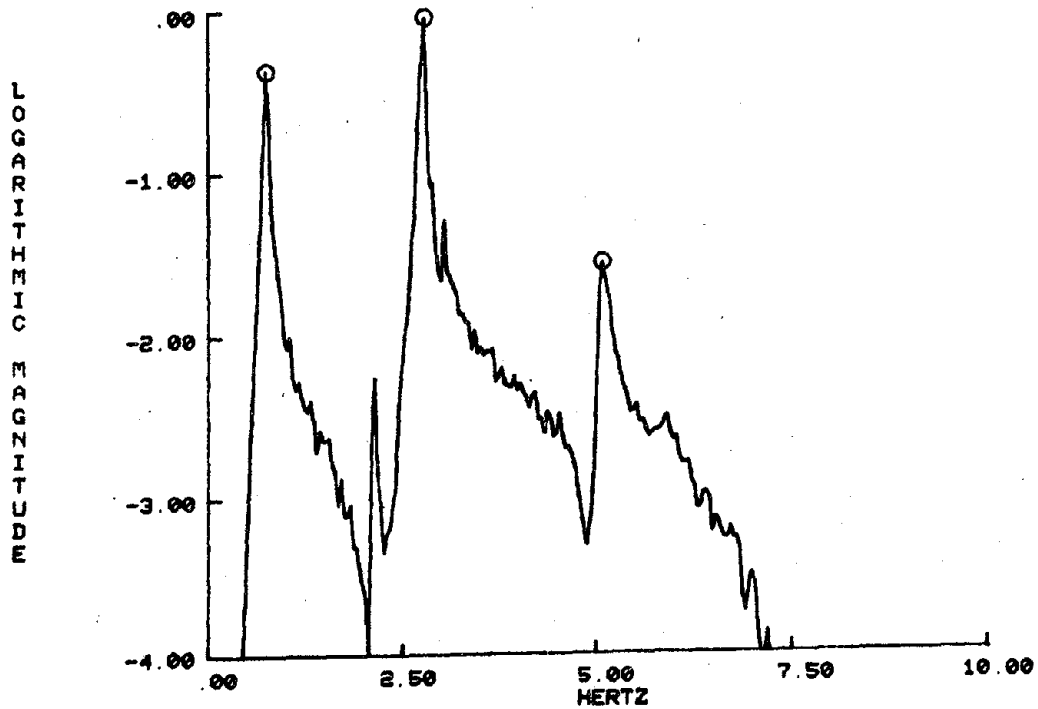


Figure 6.7 AVERAGE AUTOPOWER SPECTRAL DENSITY FUNCTION, 100 SUMS,
NODE 1, LONGITUDINAL RESPONSE

A-R-1

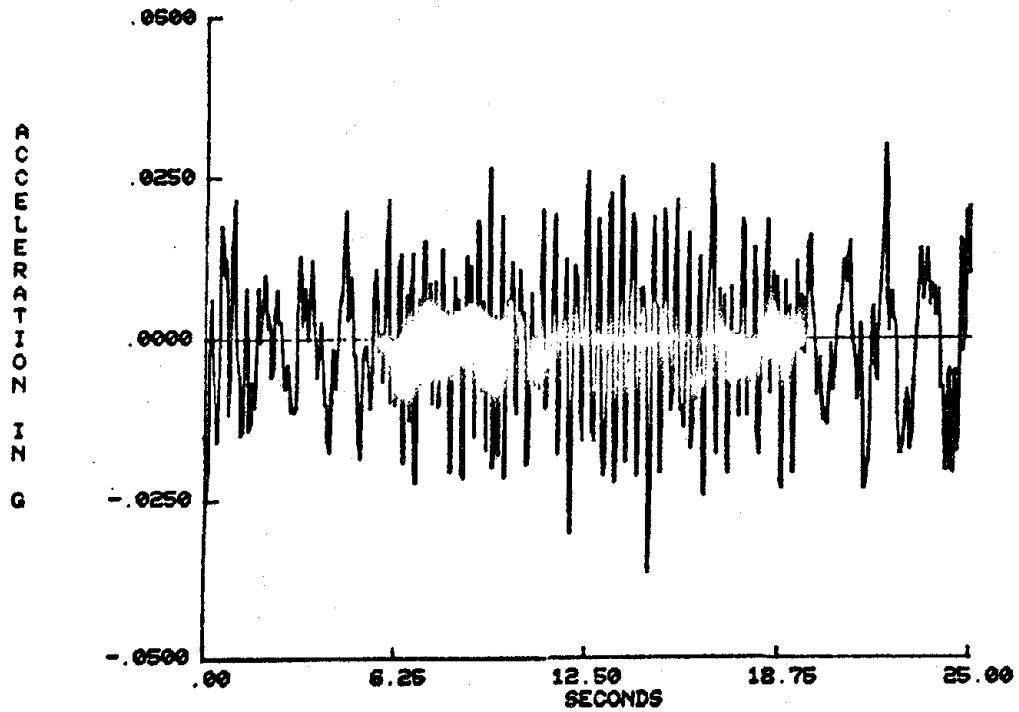


Figure 6.8 ACCELERATION TIME HISTORY, NODE 2, LONGITUDINAL RESPONSE

A-R-1

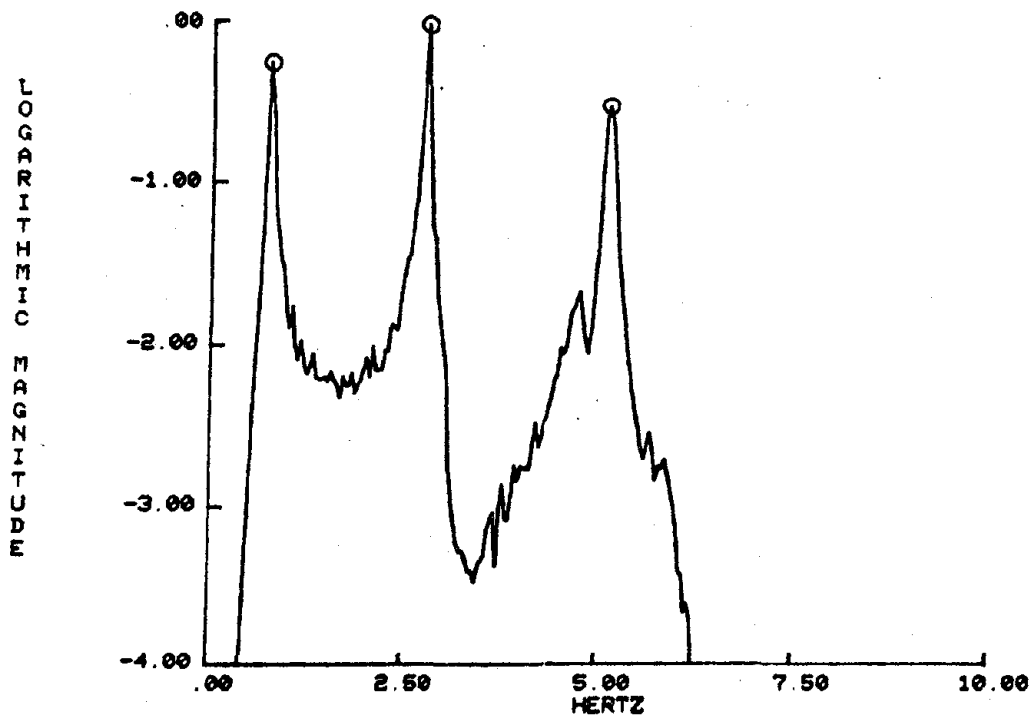


Figure 6.9 AVERAGE AUTOPOWER SPECTRAL DENSITY FUNCTION, 100 SUMS, NODE 2, LONGITUDINAL RESPONSE

A-R-1

MODE	FREQUENCY (HERTZ)	RELATIVE MAGNITUDE	RELATIVE PHASE (DEGREES)	COHERENCE
1	0.74	0.74	0	0.999
2	2.77	0.616	177	0.999
3	5.10	2.13	169	0.979

SUMMARY OF PRINCIPLE MODES, LONGITUDINAL RESPONSE
 NODE 2 RELATIVE TO LONGITUDINAL RESPONSE NODE 1

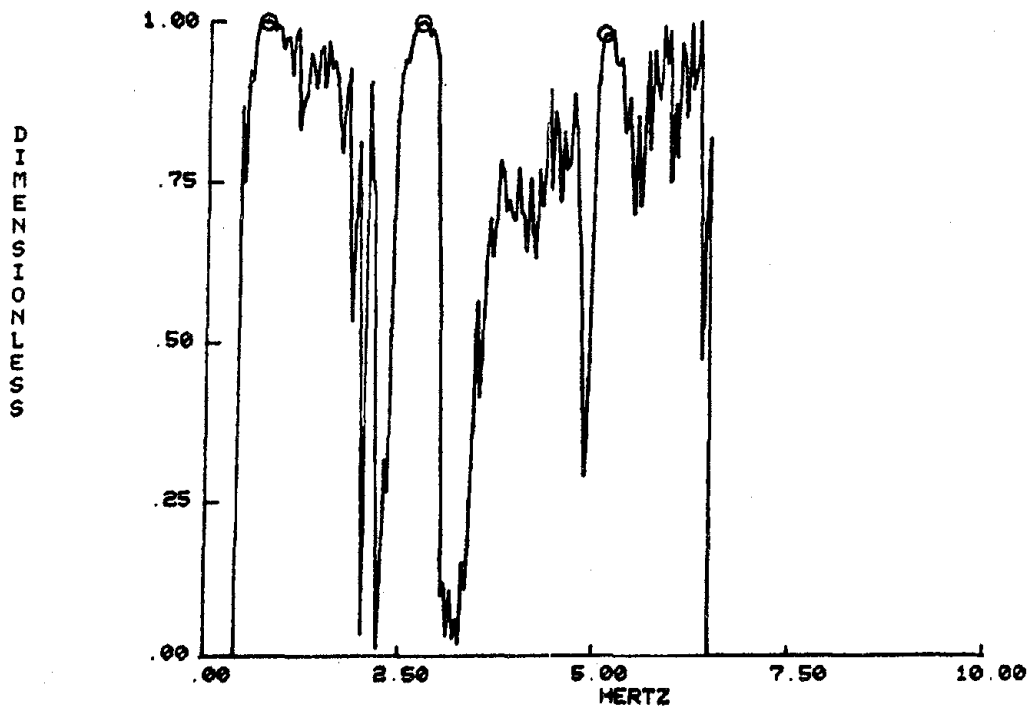


Figure 6.10 COHERENCE FUNCTION, LONGITUDINAL RESPONSE NODE 2
 AND LONGITUDINAL RESPONSE NODE 1

A-R-1

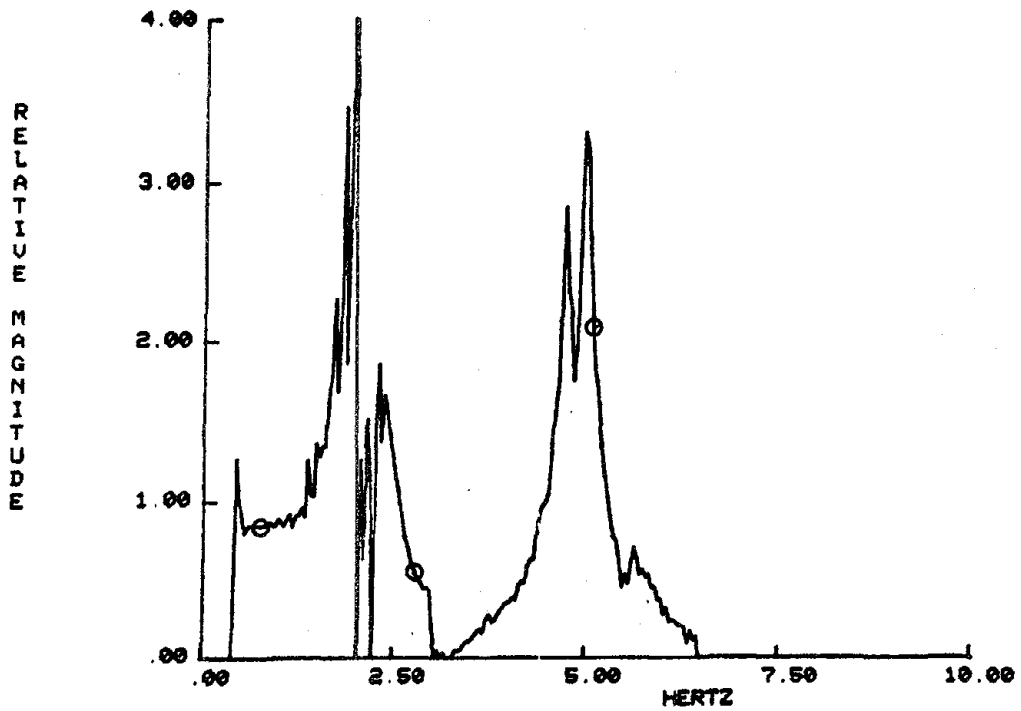


Figure 6.11 TRANSFER FUNCTION MAGNITUDE, LONGITUDINAL RESPONSE
 NODE 2 RELATIVE TO LONGITUDINAL RESPONSE NODE 1
 A-R-1

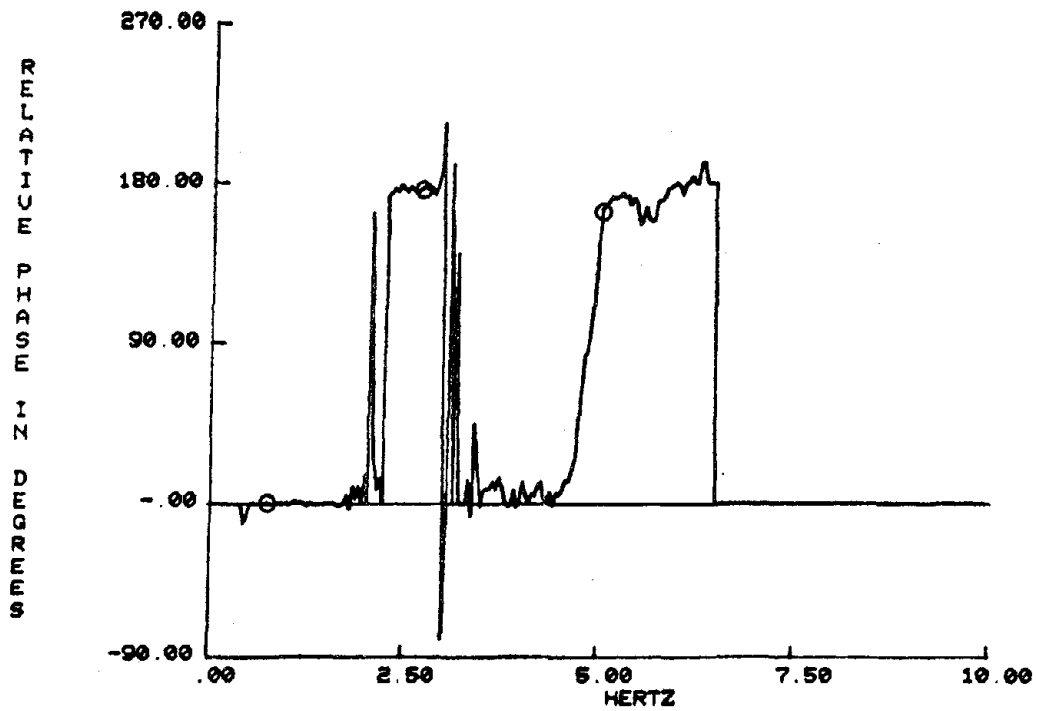


Figure 6.12 TRANSFER FUNCTION PHASE, LONGITUDINAL RESPONSE
 NODE 2 RELATIVE TO LONGITUDINAL RESPONSE NODE 1
 A-R-1

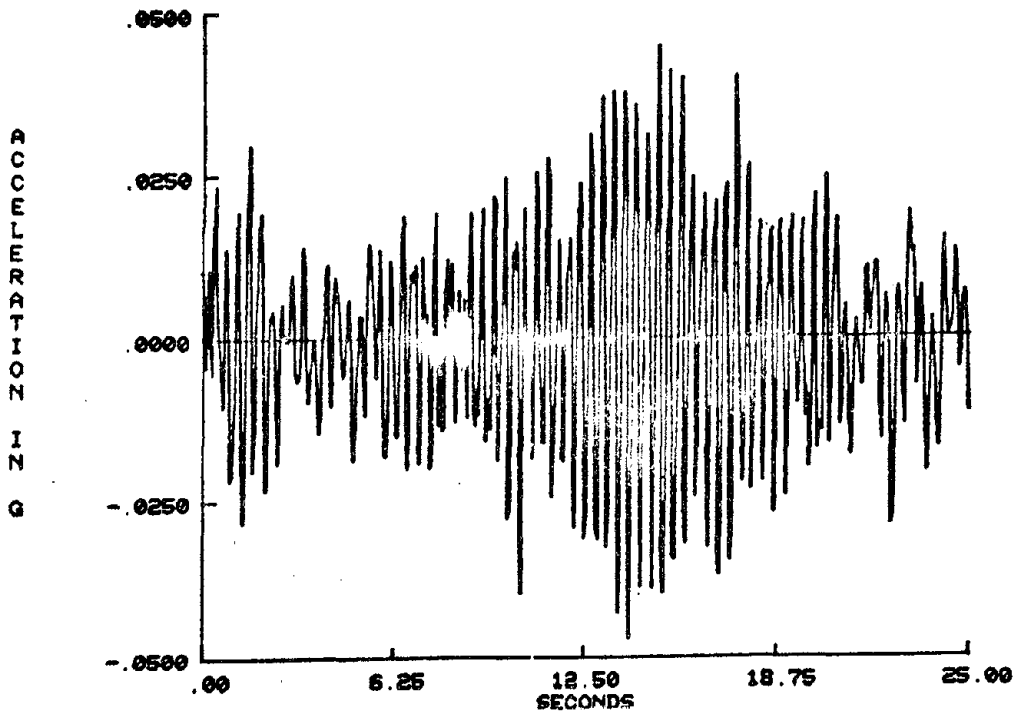


Figure 6.13 ACCELERATION TIME HISTORY, NODE 3, LONGITUDINAL RESPONSE
A-R-1

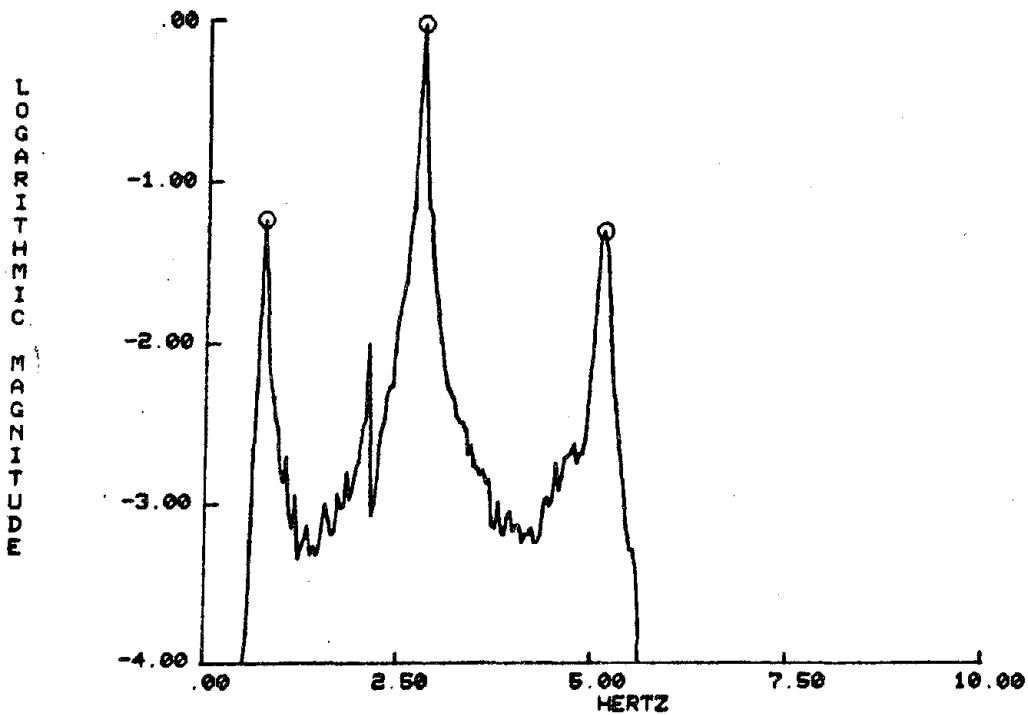


Figure 6.14 AVERAGE AUTOPOWER SPECTRAL DENSITY FUNCTION, 100 SUMS, NODE 3, LONGITUDINAL RESPONSE
A-R-1

MODE	FREQUENCY (HERTZ)	RELATIVE MAGNITUDE	RELATIVE PHASE (DEGREES)	COHERENCE
1	0.74	0.52	0	0.999
2	2.77	1.25	179	1.000
3	5.10	1.71	-14	0.969

SUMMARY OF PRINCIPLE MODES, LONGITUDINAL
RESPONSE NODE 3 RELATIVE TO LONGITUDINAL
RESPONSE NODE 1

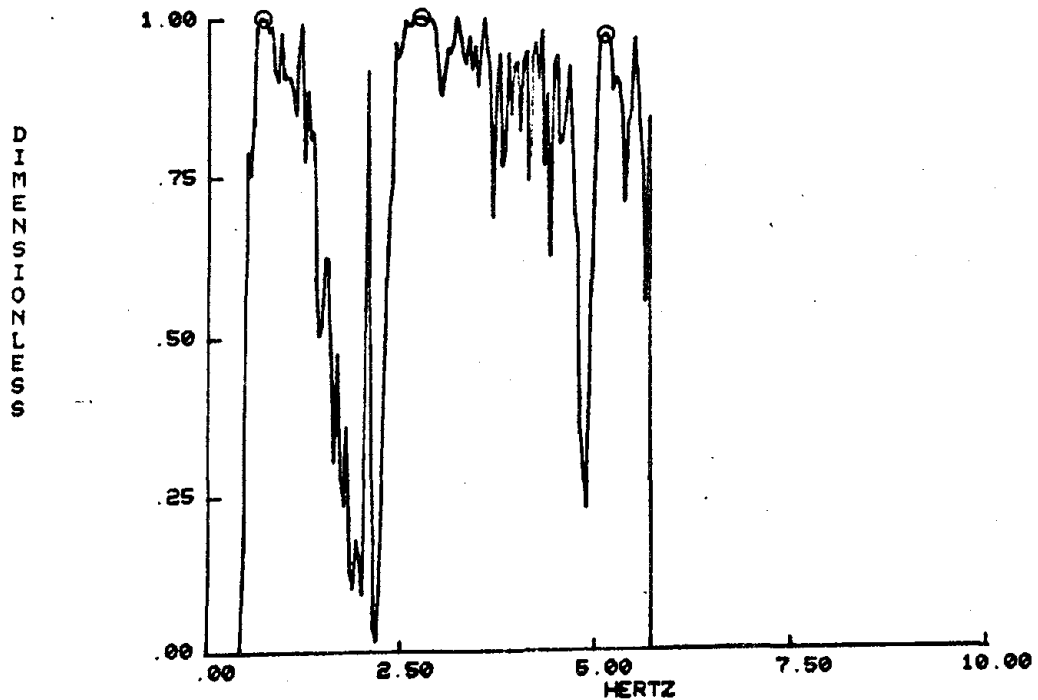


Figure 6.15. COHERENCE FUNCTION, LONGITUDINAL RESPONSE NODE 3
AND LONGITUDINAL RESPONSE NODE 1
A-R-1

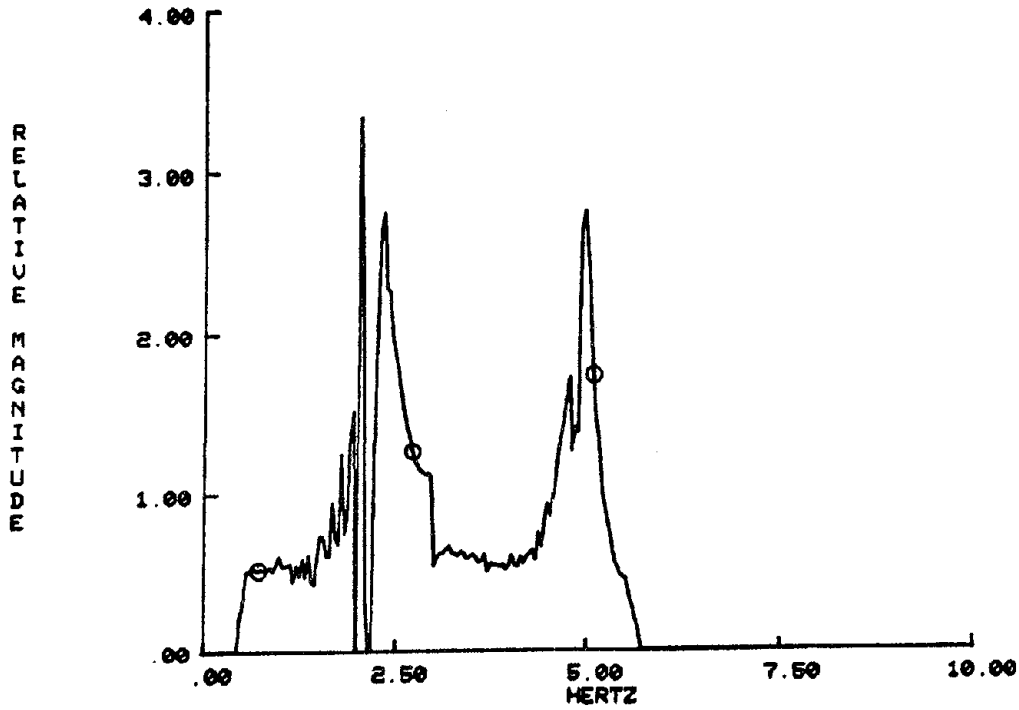


Figure 6.16. TRANSFER FUNCTION MAGNITUDE, LONGITUDINAL RESPONSE
 NODE 3 RELATIVE TO LONGITUDINAL RESPONSE NODE 1
 A-R-1

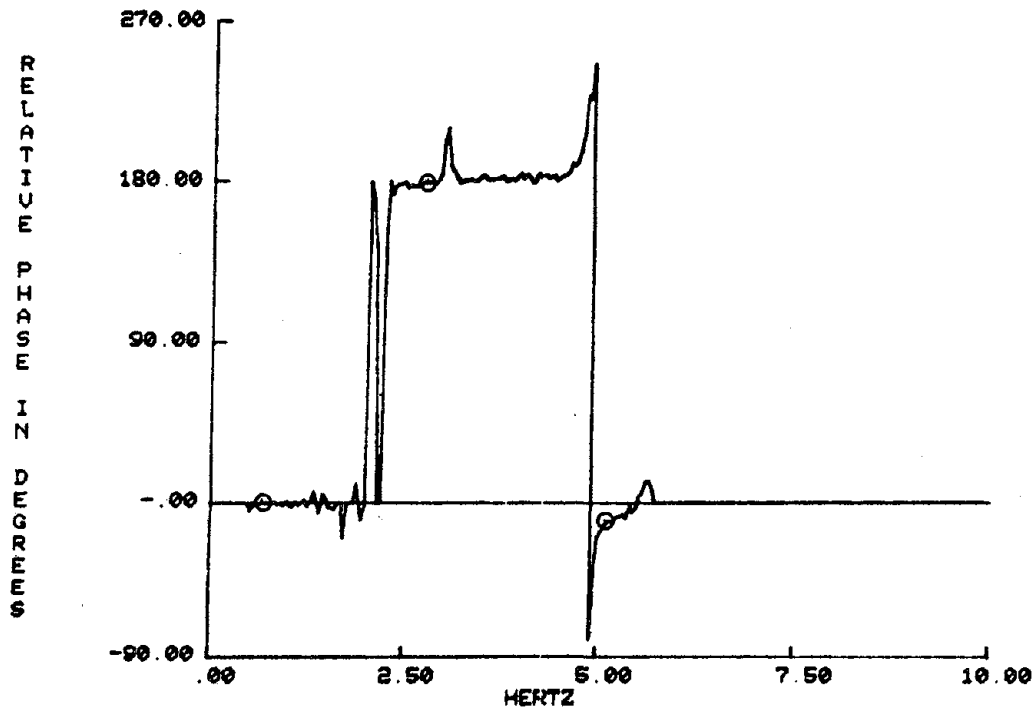


Figure 6.17 TRANSFER FUNCTION PHASE, LONGITUDINAL RESPONSE
 NODE 3 RELATIVE TO LONGITUDINAL RESPONSE NODE 1
 A-R-1

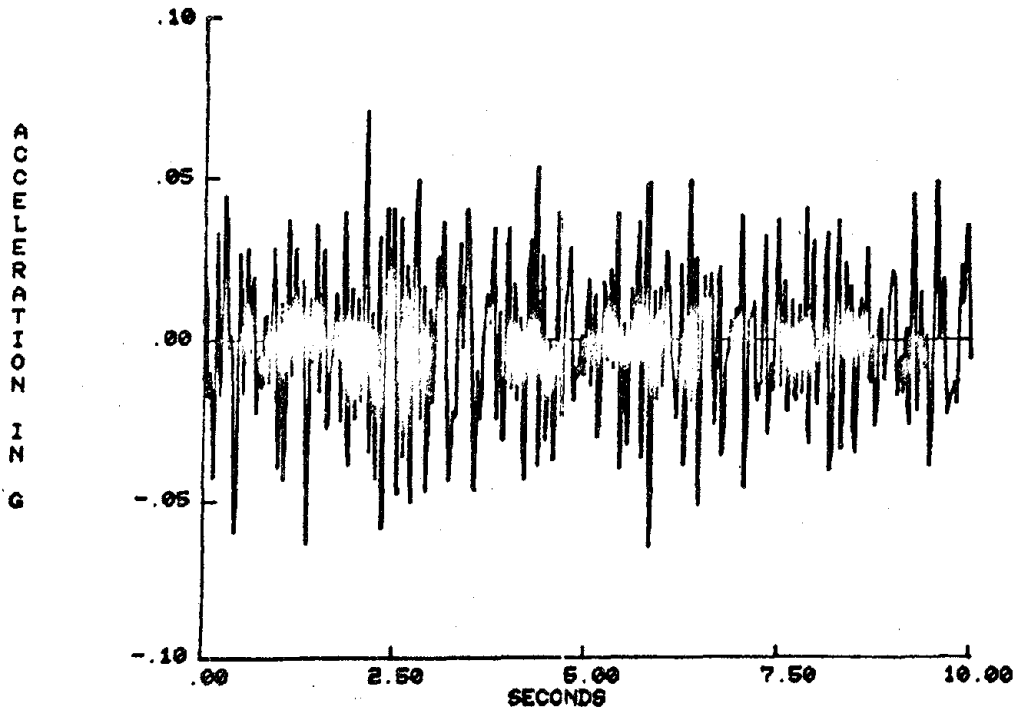


Figure 6.18 ACCELERATION TIME HISTORY, NODE 1, TRANSVERSE RESPONSE
A-R-1

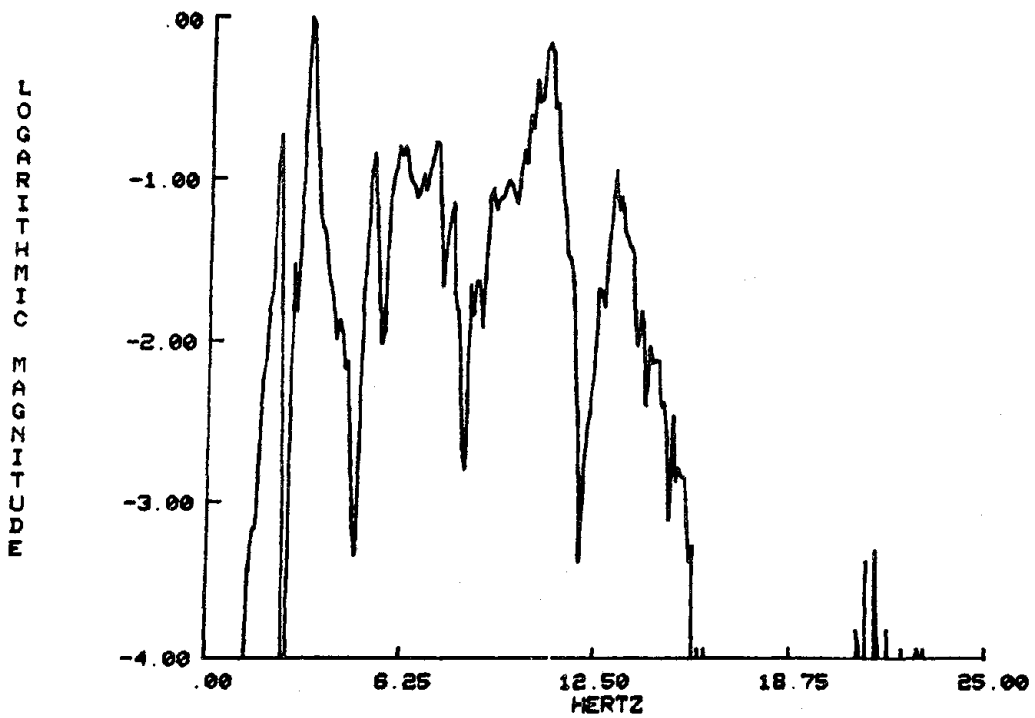


Figure 6.19 AVERAGE AUTOPOWER SPECTRAL DENSITY FUNCTION, 50 SUMS
NODE 1, TRANSVERSE RESPONSE
A-R-1

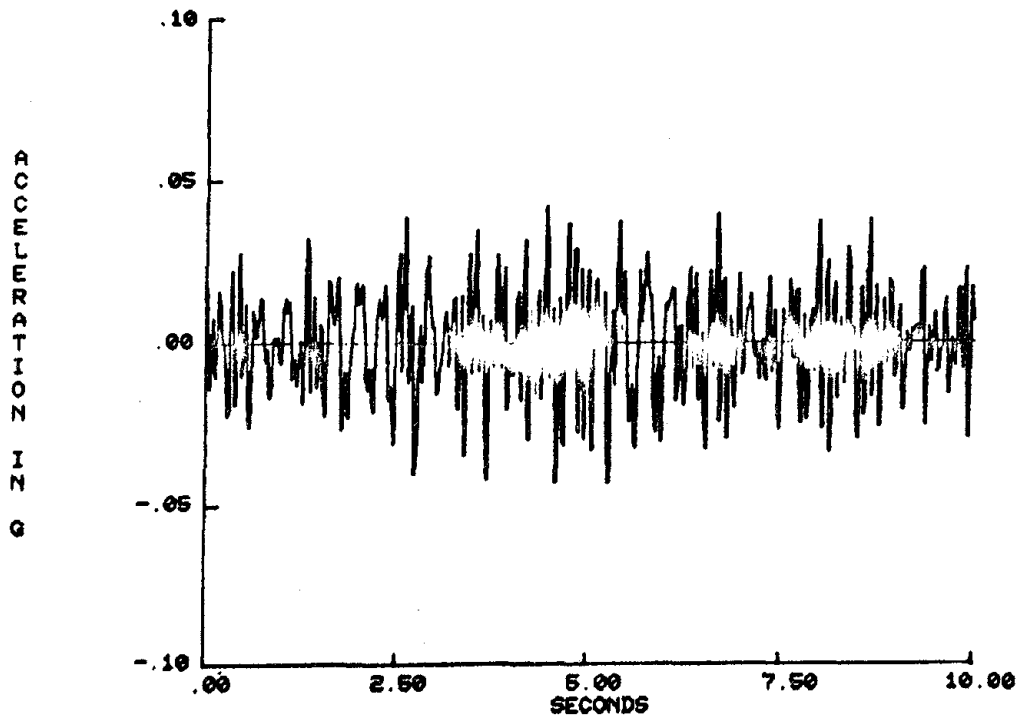


Figure 6.20 ACCELERATION TIME HISTORY, NODE 2, TRANSVERSE RESPONSE
A-R-1

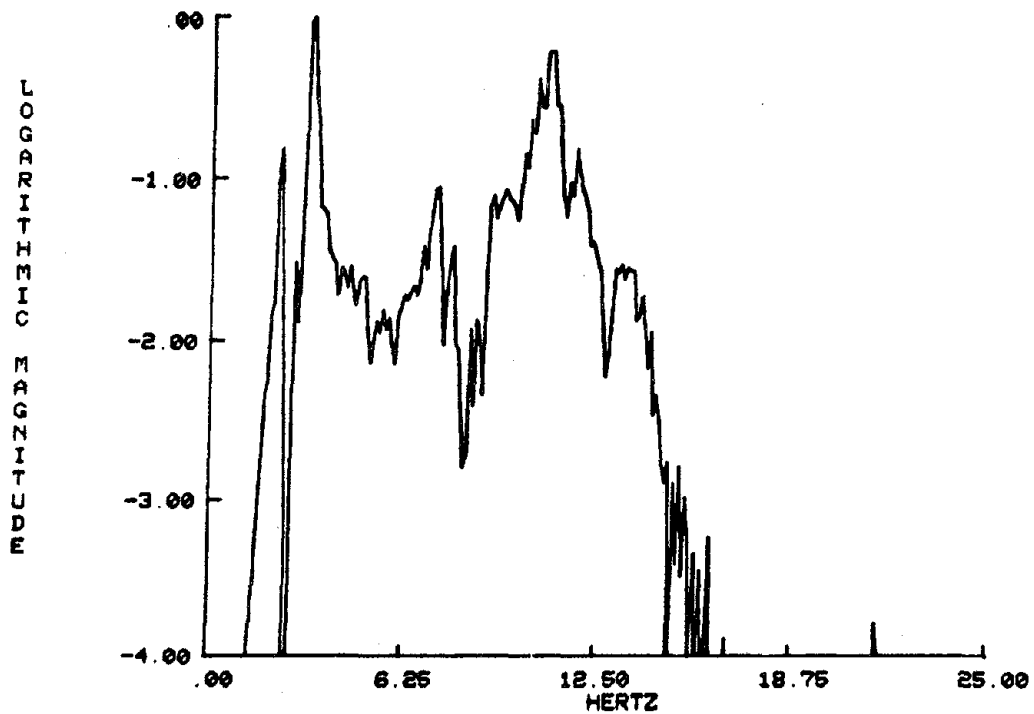


Figure 6.21 AVERAGE AUTOPOWER SPECTRAL DENSITY FUNCTION, 50 SUMS
NODE 2, TRANSVERSE RESPONSE
A-R-1

MODE	FREQUENCY (HERTZ)	RELATIVE MAGNITUDE	RELATIVE PHASE (DEGREES)	COHERENCE
1	2.25	0.69	0	0.999
2	2.83	0.71	1	0.985
3	3.22	0.72	0	0.999
4	5.27	0.20	34	0.998
5	6.25	0.24	9	0.990
6	7.32	0.53	6	0.998
7	8.98	0.70	-7	0.998
8	10.84	0.72	2	0.999
9	12.99	0.35	46	0.991
10	13.87	0.86	18	0.981

SUMMARY OF PRINCIPLE MODES, TRANSVERSE RESPONSE NODE 2
RELATIVE TO TRANSVERSE NODE 1

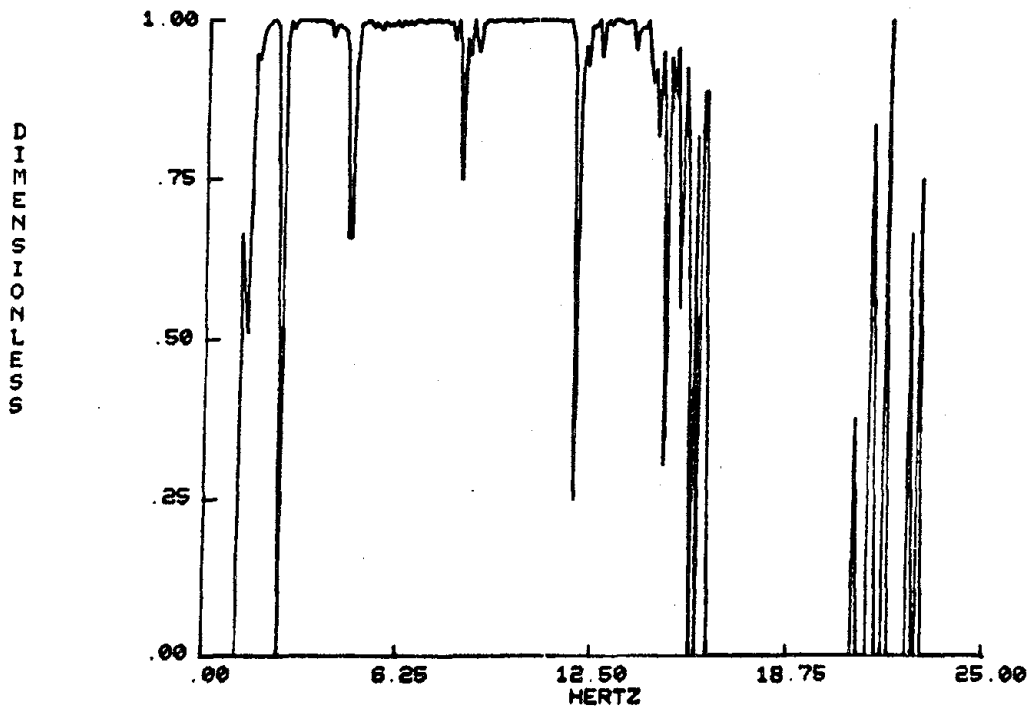


Figure 6.22 COHERENCE FUNCTION, TRANSVERSE RESPONSE NODE 2,
AND TRANSVERSE RESPONSE NODE 1

A-R-1

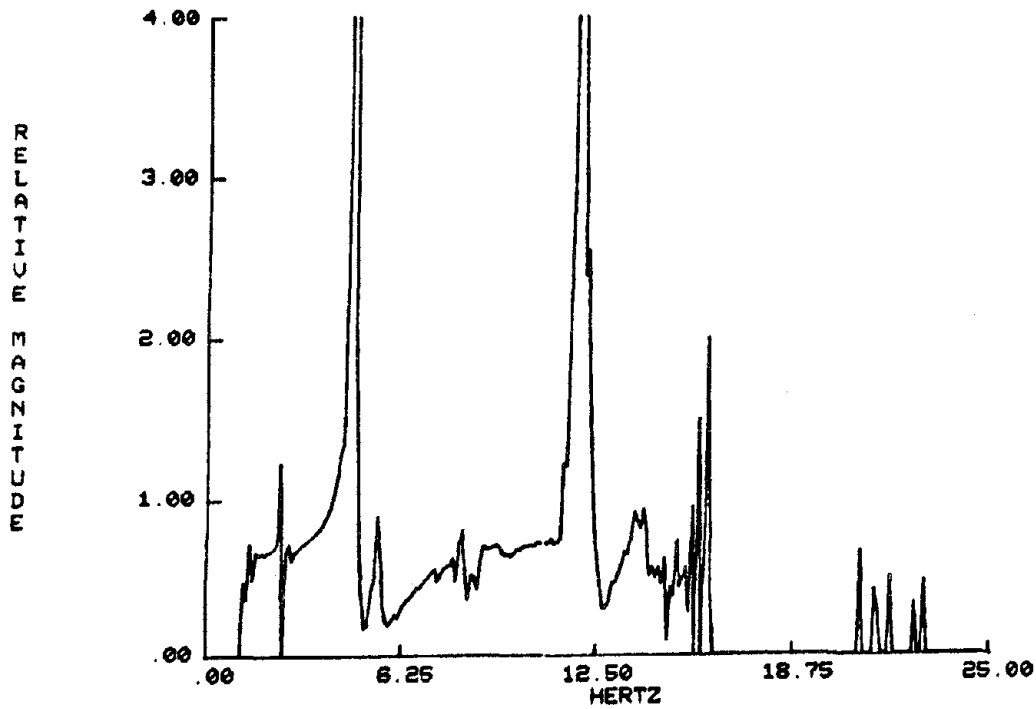


Figure 6.23 TRANSFER FUNCTION MAGNITUDE, TRANSVERSE RESPONSE
 NODE 2 RELATIVE TO TRANSVERSE RESPONSE NODE 1
 A-R-1

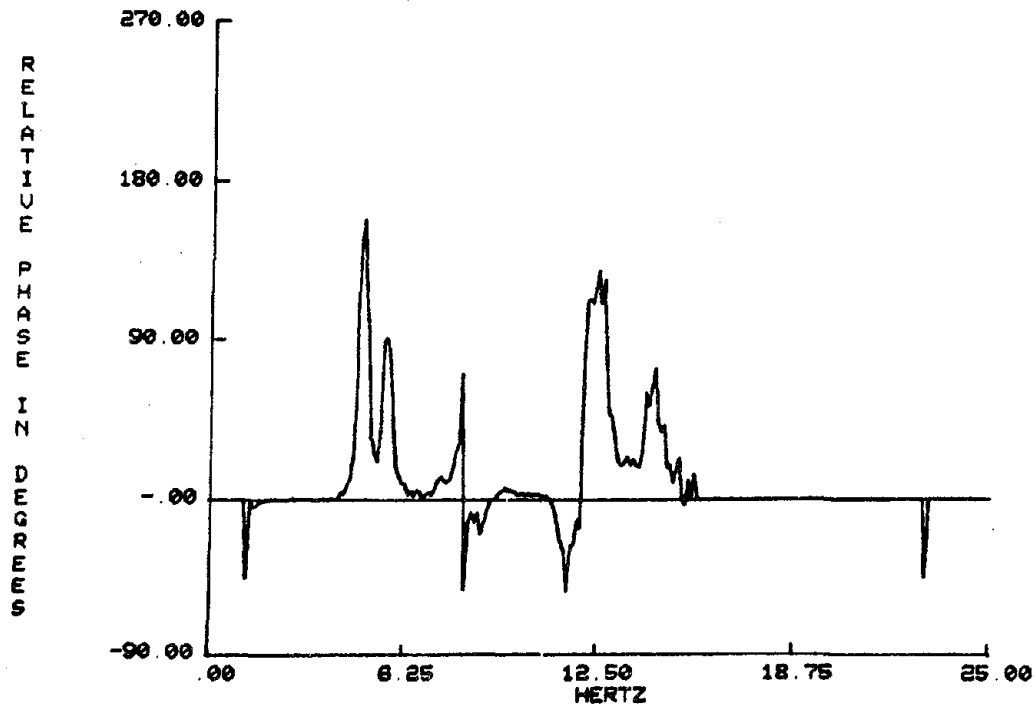


Figure 6.24 TRANSFER FUNCTION PHASE, TRANSVERSE RESPONSE
 NODE 2 RELATIVE TO TRANSVERSE RESPONSE NODE 1
 A-R-1

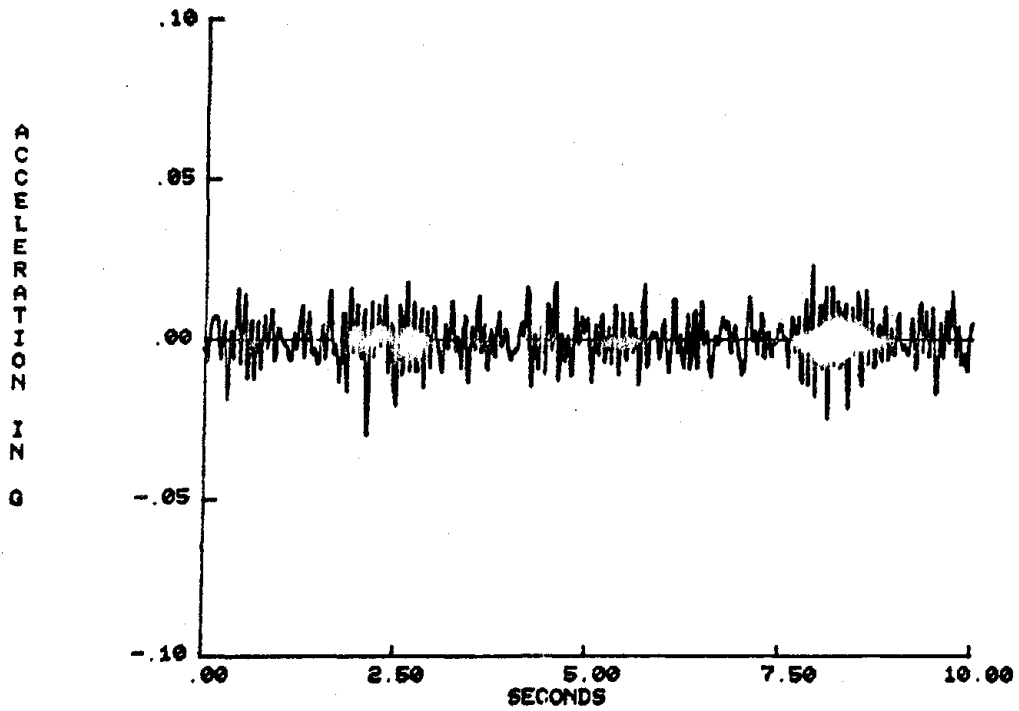


Figure 6.25. ACCELERATION TIME HISTORY, NODE 1, LONGITUDINAL RESPONSE

A-R-1

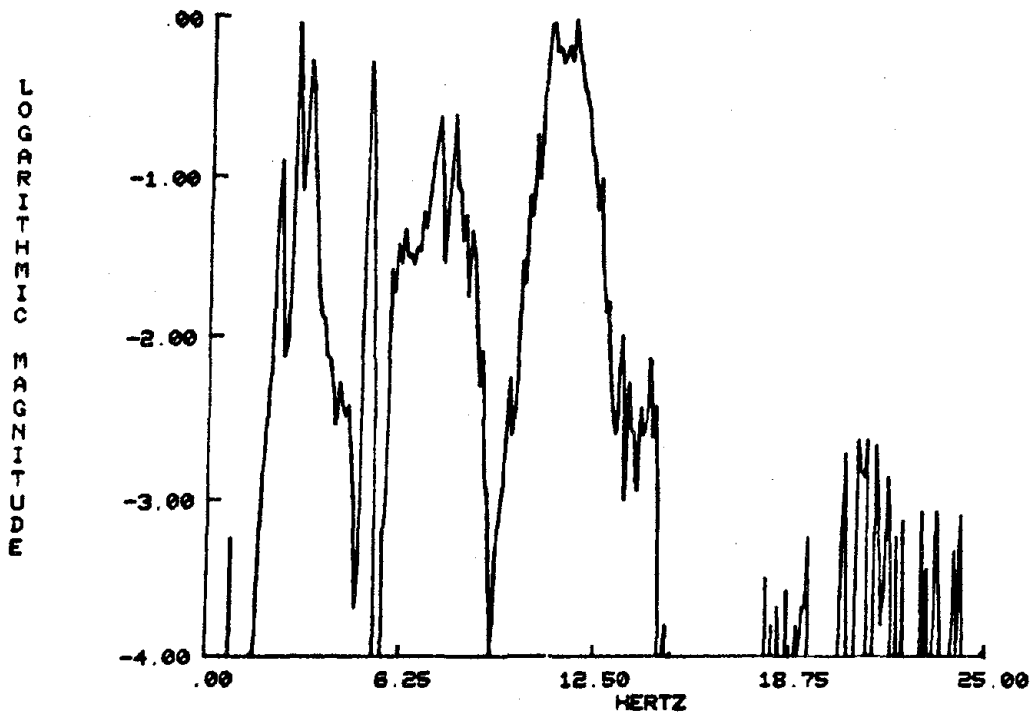


Figure 6.26 AVERAGE AUTOPOWER SPECTRAL DENSITY FUNCTION, 50 SUMS
NODE 1, LONGITUDINAL RESPONSE

A-R-1

MODE	FREQUENCY (HERTZ)	RELATIVE MAGNITUDE	RELATIVE PHASE (DEGREES)	COHERENCE
1	2.25	0.25	182	1.000
2	2.83	1.66	11	0.991
3	3.22	0.22	178	1.000
4	5.27	0.15	-27	0.996
5	6.25	0.16	177	0.998
6	7.32	0.36	196	0.999
7	8.98	0.035	37	0.965
8	10.84	0.34	202	1.000
9	12.99	0.051	78	0.991
10	13.87	0.149	30	0.980

SUMMARY OF PRINCIPLE MODES, LONGITUDINAL RESPONSE NODE 1
RELATIVE TO TRANSVERSE RESPONSE NODE 1

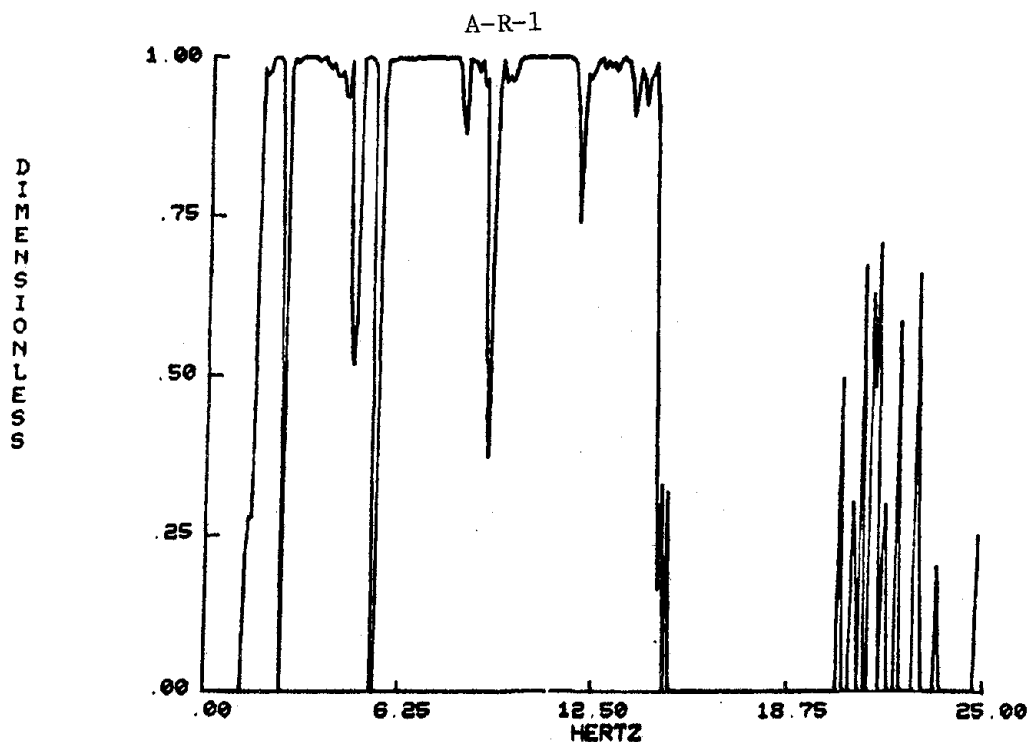


Figure 6.27 COHERENCE FUNCTION, LONGITUDINAL RESPONSE NODE 1
AND TRANSVERSE RESPONSE NODE 1

A-R-1

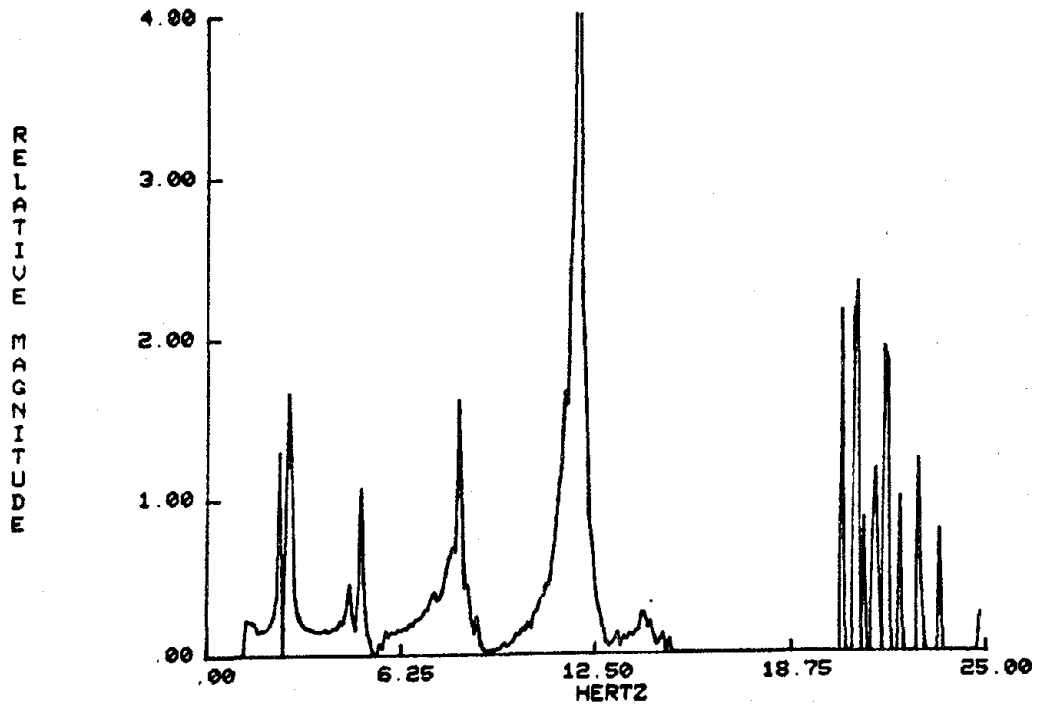


Figure 6.28 TRANSFER FUNCTION MAGNITUDE, LONGITUDINAL RESPONSE
 NODE 1 RELATIVE TO TRANSVERSE RESPONSE NODE 1

A-R-1

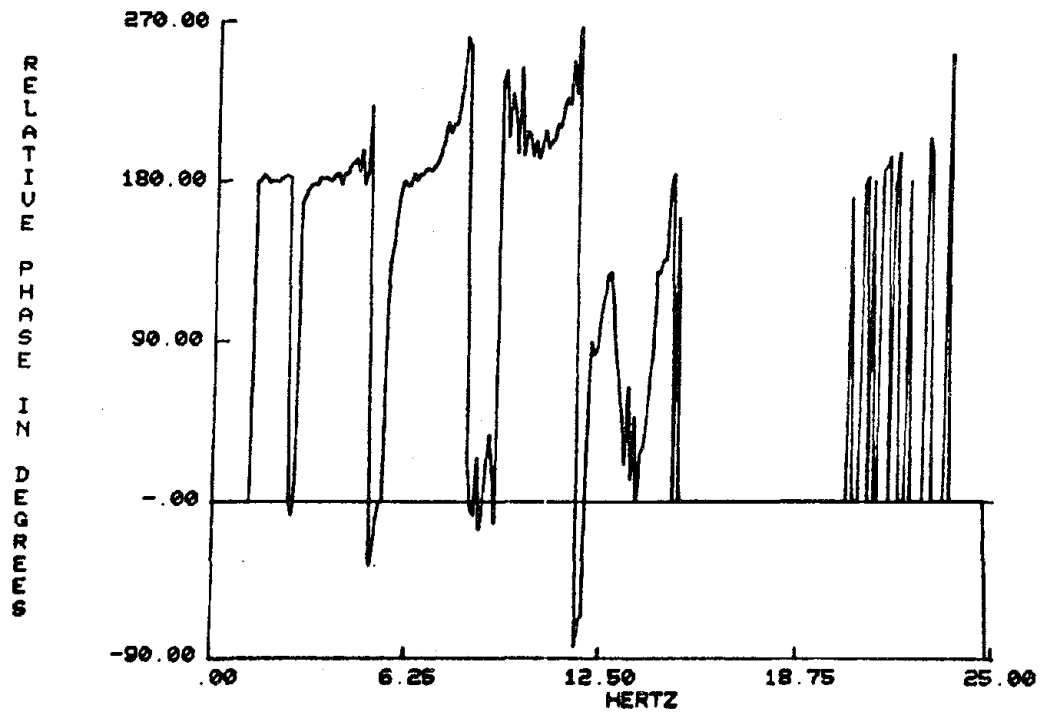


Figure 6.29. TRANSFER FUNCTION PHASE, LONGITUDINAL RESPONSE
 NODE 1 RELATIVE TO TRANSVERSE RESPONSE NODE 1

A-R-1

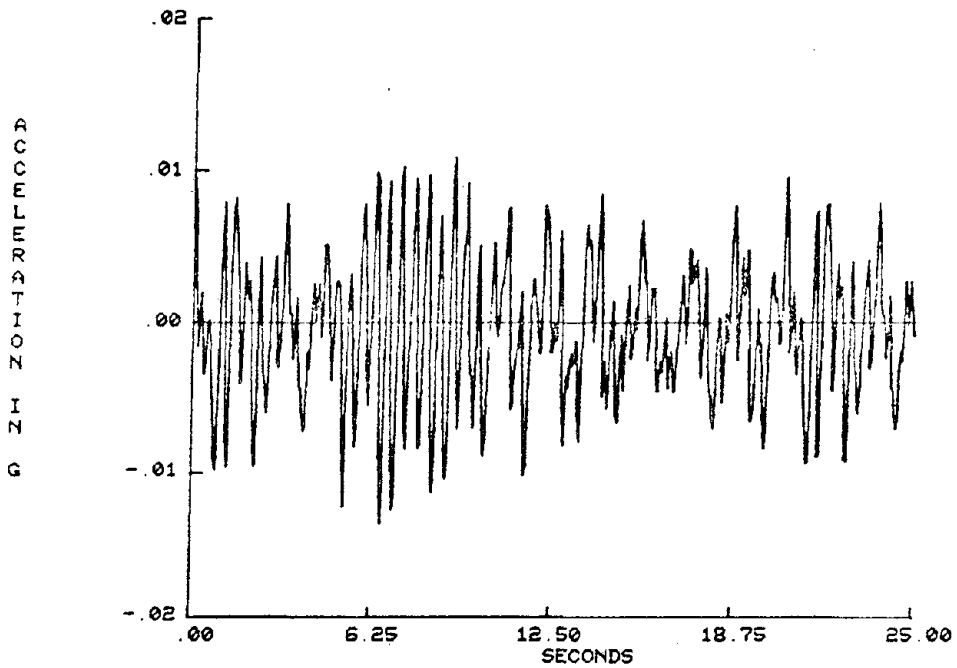


Figure 6.30 ACCELERATION TIME HISTORY, NODE 1, LONGITUDINAL RESPONSE
B-R-1

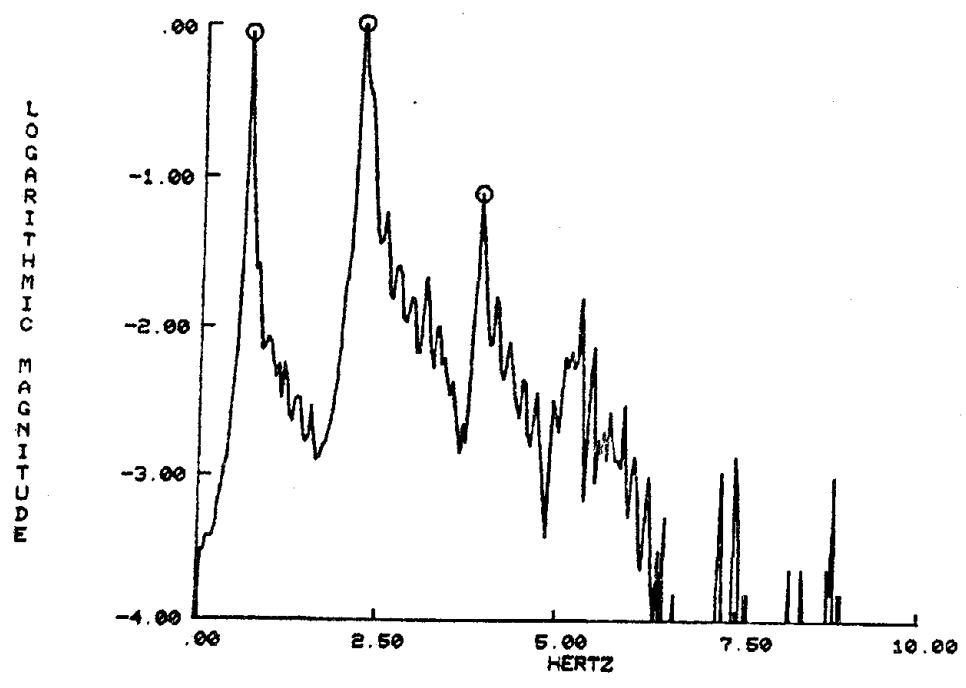


Figure 6.31 AVERAGE AUTOPOWER SPECTRAL DENSITY FUNCTION, 50 SUMS,
NODE 1, LONGITUDINAL RESPONSE
B-R-1

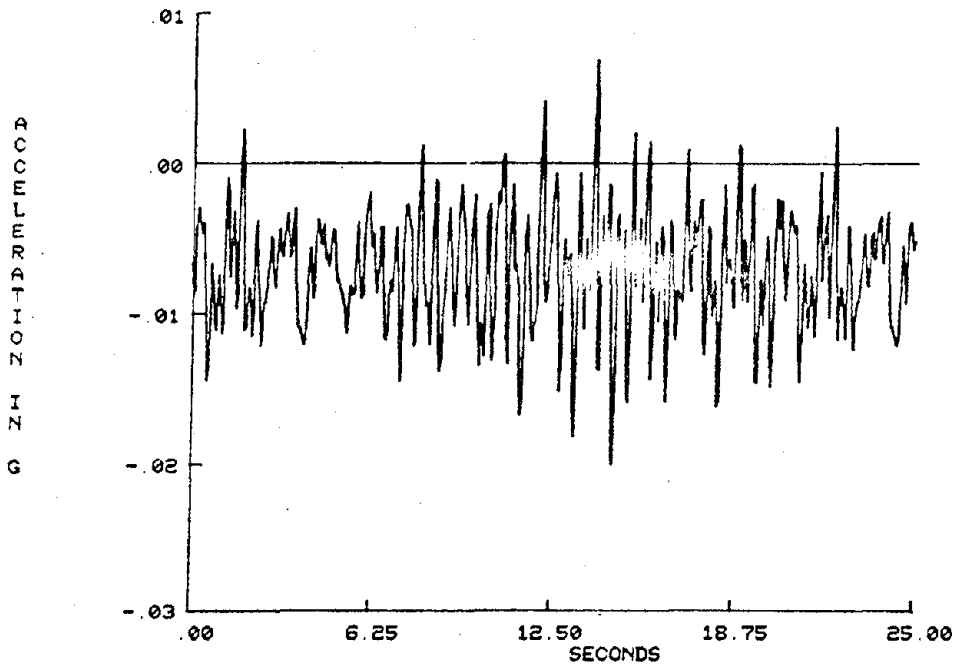


Figure 6.32 ACCELERATION TIME HISTORY, NODE 2, LONGITUDINAL RESPONSE
B-R-1

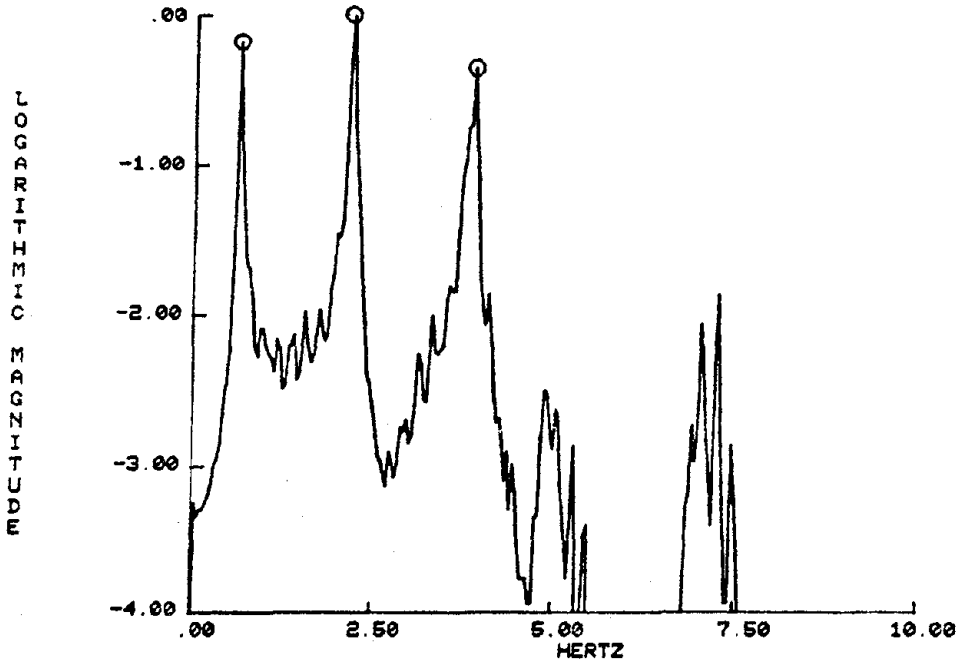


Figure 6.33 AVERAGE AUTOPOWER SPECTRAL DENSITY FUNCTION, 50 SUMS,
NODE 2, LONGITUDINAL RESPONSE
B-R-1

MODE	FREQUENCY (HERTZ)	RELATIVE MAGNITUDE	RELATIVE PHASE (DEGREES)	COHERENCE
1	0.63	0.77	0	0.999
2	2.19	0.85	182	0.951
3	3.87	2.33	168	0.988

SUMMARY OF PRINCIPLE MODES, LONGITUDINAL RESPONSE NODE 2
RELATIVE TO LONGITUDINAL RESPONSE NODE 1

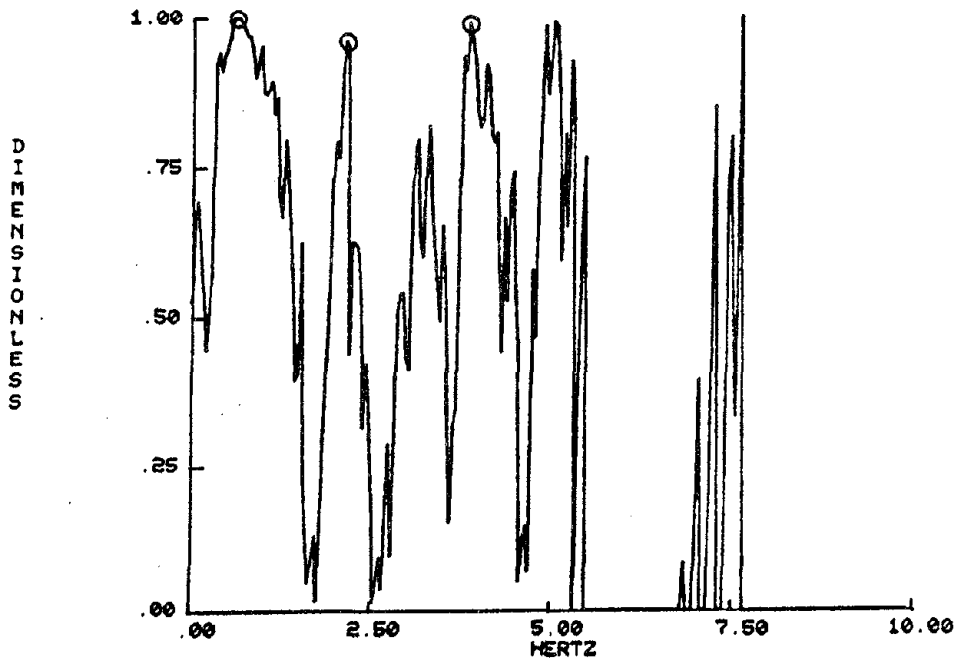


Figure 6.34 COHERENCE FUNCTION, LONGITUDINAL RESPONSE NODE 2
AND LONGITUDINAL RESPONSE NODE 1

B-R-1

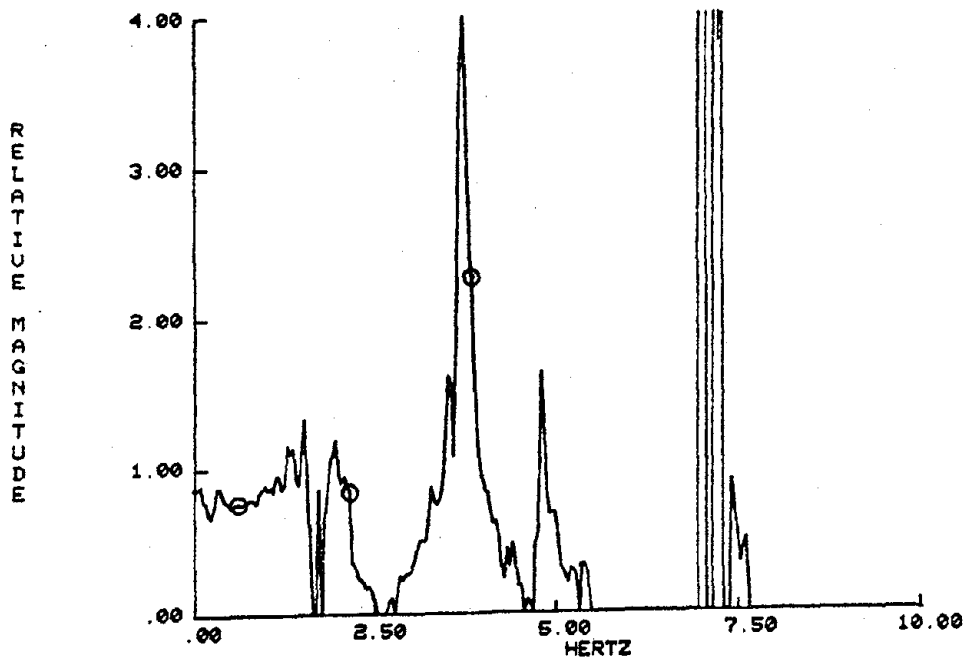


Figure 6.35 TRANSFER FUNCTION MAGNITUDE, LONGITUDINAL RESPONSE
 NODE 2 RELATIVE TO LONGITUDINAL RESPONSE NODE 1
 B-R-1

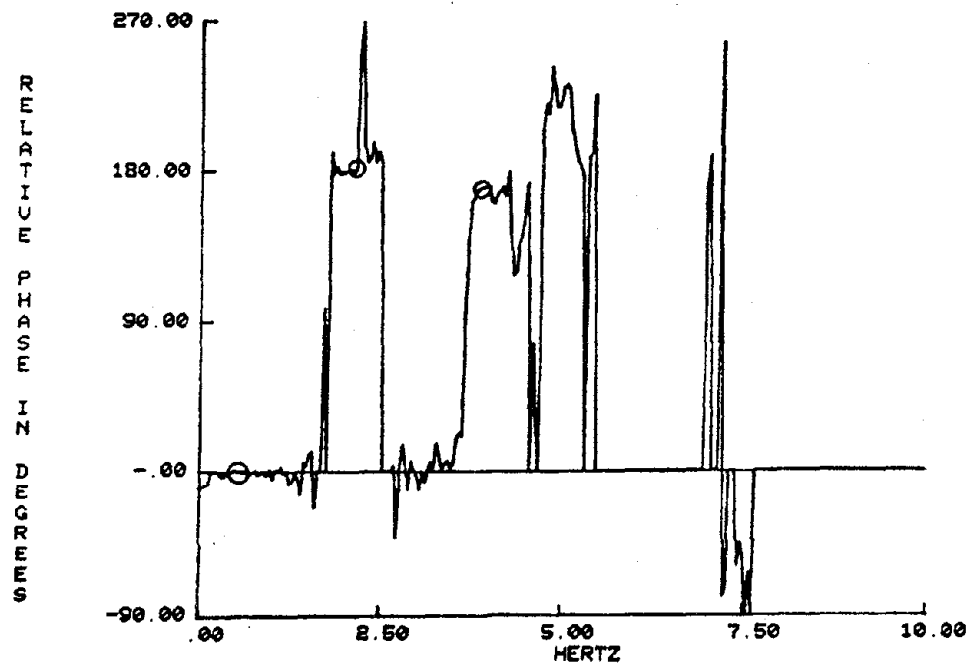


Figure 6.36 TRANSFER FUNCTION PHASE, LONGITUDINAL RESPONSE
 NODE 2 RELATIVE TO LONGITUDINAL RESPONSE NODE 1
 B-R-1

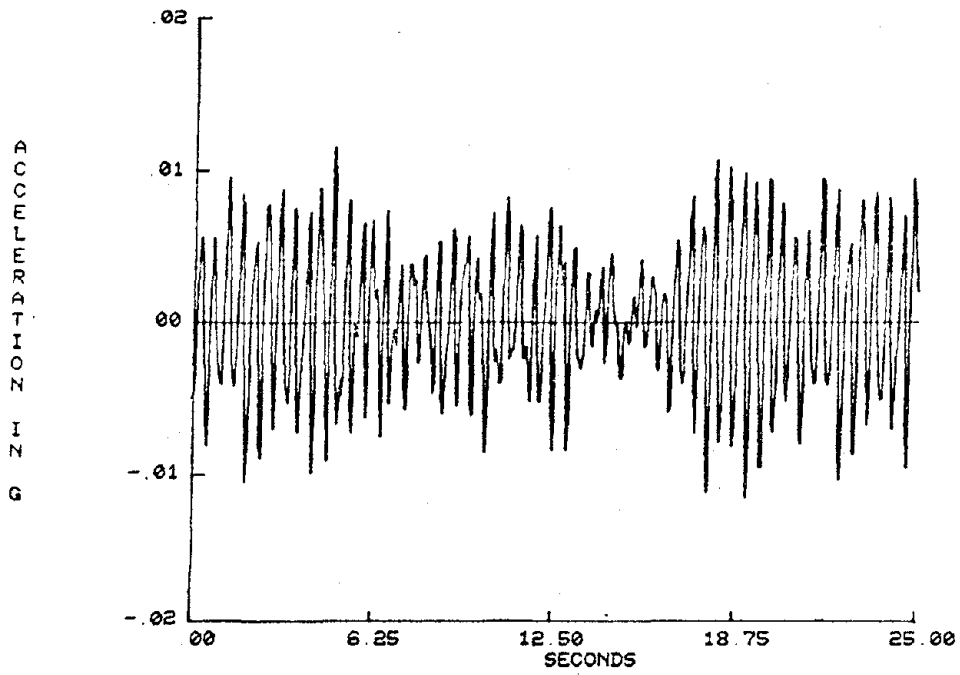


Figure 6.37 ACCELERATION TIME HISTORY, NODE 3, LONGITUDINAL RESPONSE
B-R-1

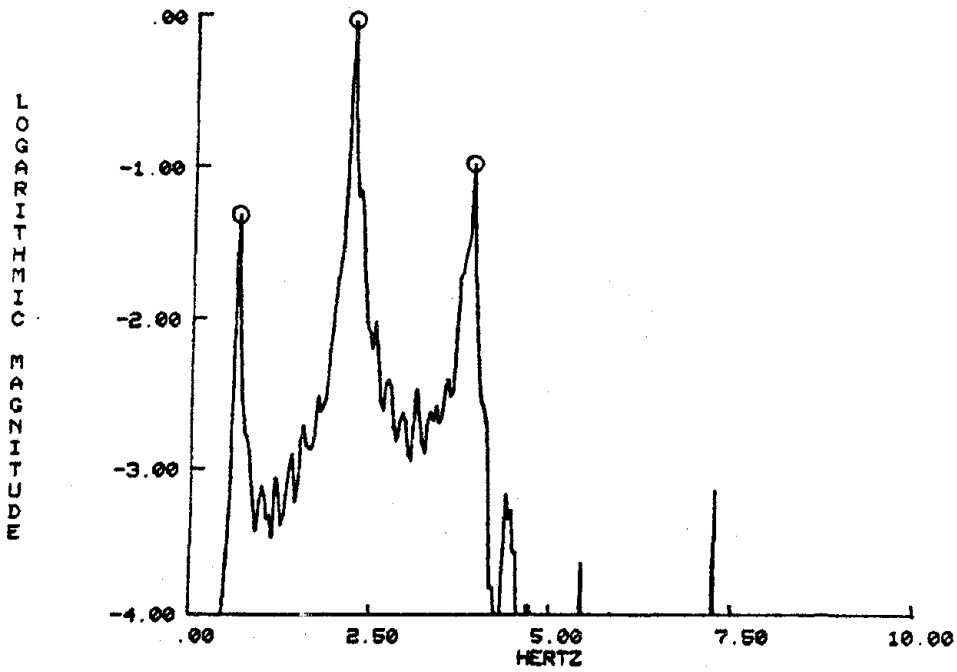


Figure 6.38 AVERAGE AUTOPOWER SPECTRAL DENSITY FUNCTION, 50 SUMS,
NODE 3, LONGITUDINAL RESPONSE
B-R-1

MODE	FREQUENCY (HERTZ)	RELATIVE MAGNITUDE	RELATIVE PHASE (DEGREES)	COHERENCE
1	0.63	0.44	0	0.999
2	2.19	1.46	182	0.984
3	3.87	2.01	-12	0.990

SUMMARY OF PRINCIPLE MODES, LONGTUDINAL RESPONSE NODE 3
RELATIVE TO LONGITUDINAL RESPONSE NODE 1

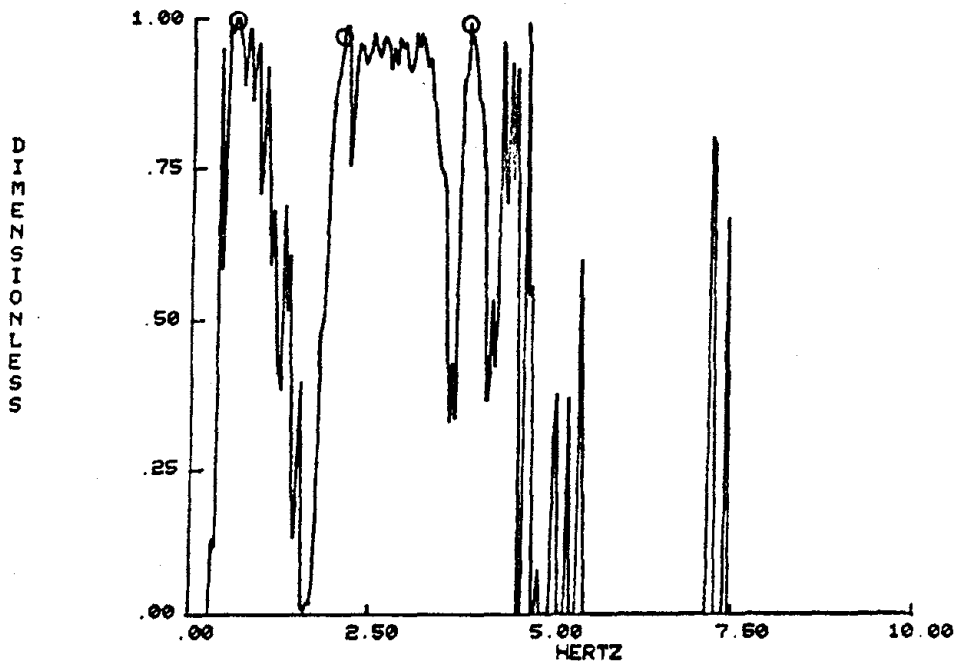


Figure 6.39 COHERENCE FUNCTION, LONGITUDINAL RESPONSE NODE 3
AND LONGITUDINAL RESPONSE NODE 1
B-R-1

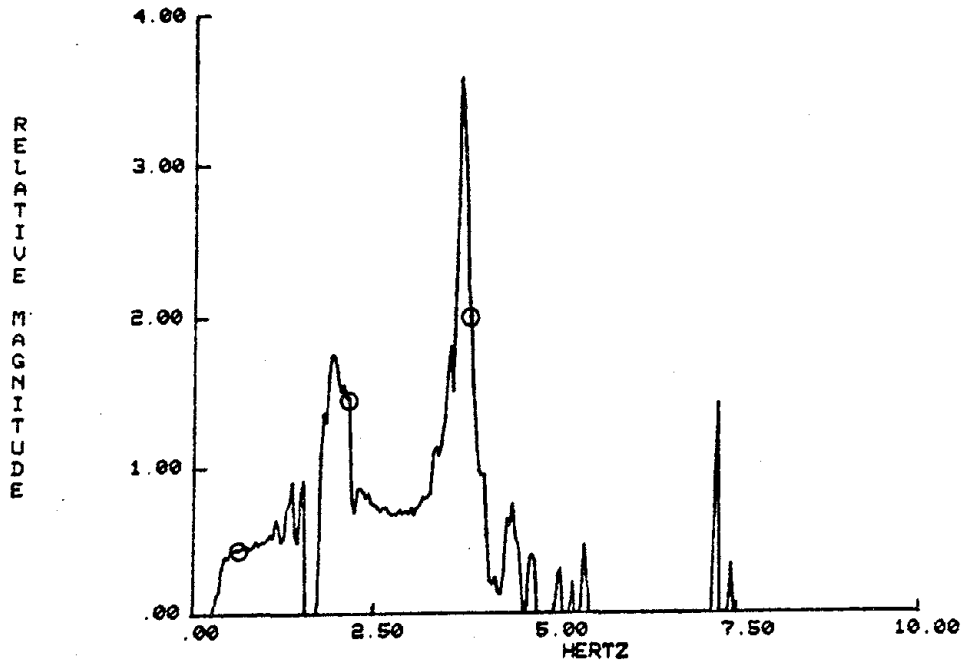


Figure 6.40 TRANSFER FUNCTION MAGNITUDE, LONGITUDINAL RESPONSE
 NODE 3 RELATIVE TO LONGITUDINAL RESPONSE NODE 1
 B-R-1

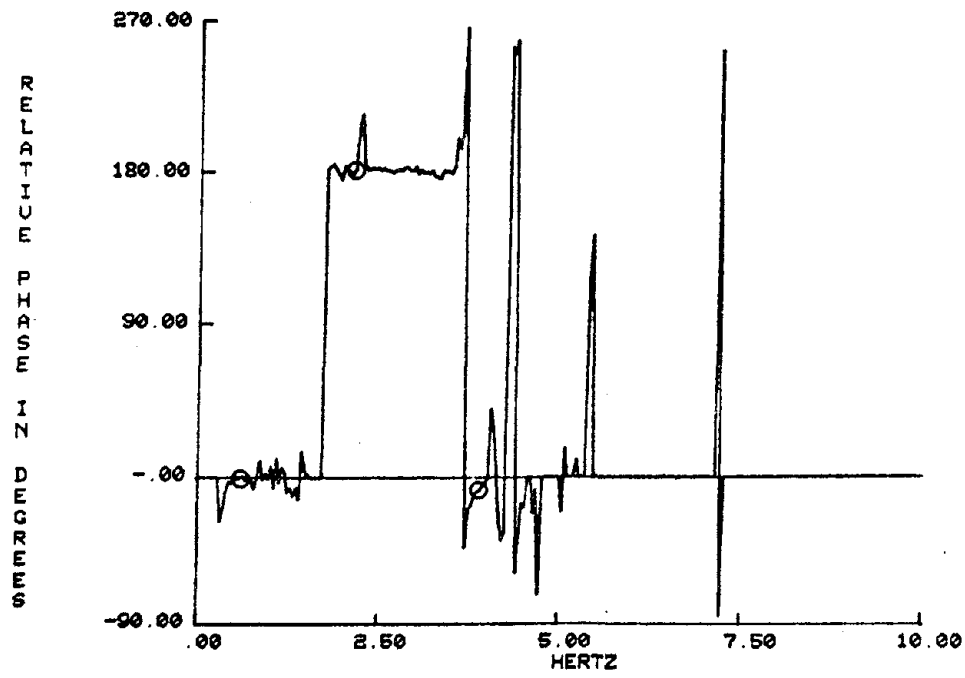


Figure 6.41 TRANSFER FUNCTION PHASE, LONGITUDINAL RESPONSE
 NODE 3 RELATIVE TO LONGITUDINAL RESPONSE NODE 1
 B-R-1

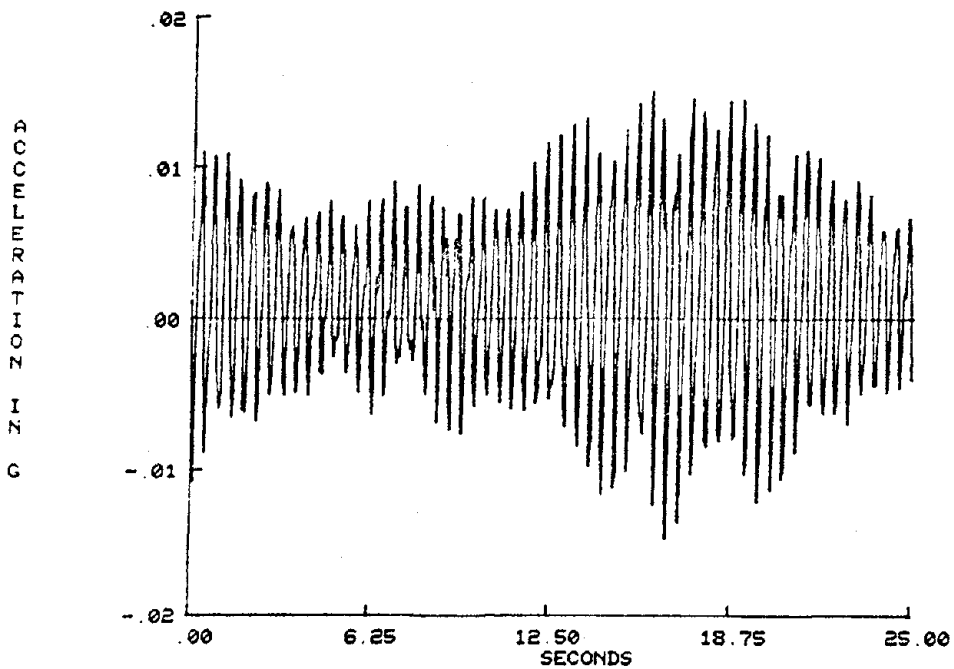


Figure 6.42 ACCELERATION TIME HISTORY, NODE 1, TRANSVERSE RESPONSE
B-R-1

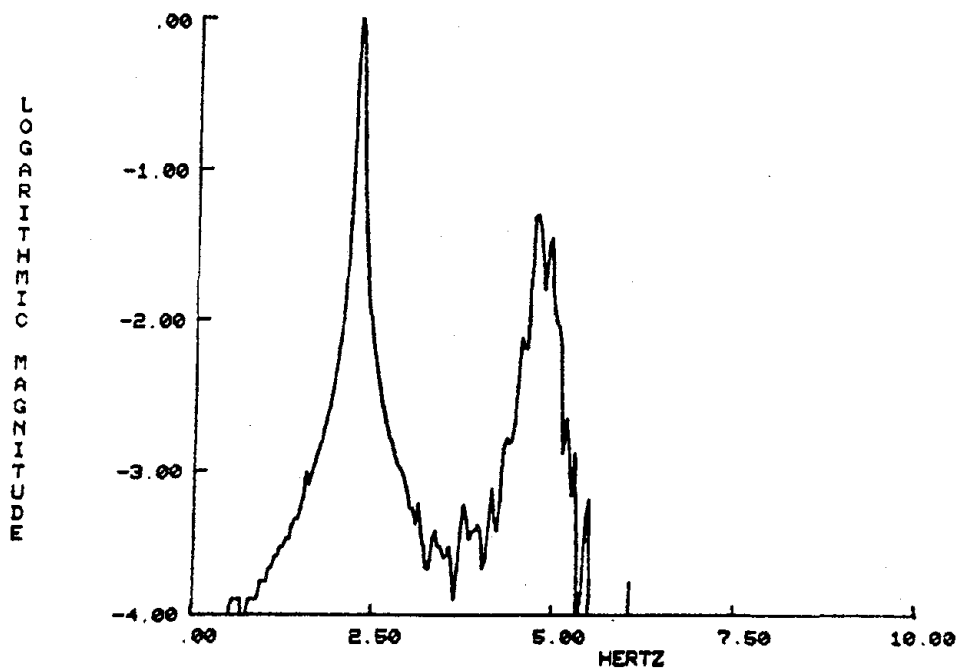


Figure 6.43 AVERAGE AUTOPOWER SPECTRAL DENSITY FUNCTION, 50 SUMS,
NODE 1, TRANSVERSE RESPONSE
B-R-1

MODE	FREQUENCY (HERTZ)	RELATIVE MAGNITUDE	RELATIVE PHASE (DEGREES)	COHERENCE
1	0.63	0.01	173	0.239
2	2.19	0.92	14	0.664
	2.25	2.25	139	0.683
	3.71	0.65	209	0.518
3	3.87	0.09	-77	0.419
	4.10	0.29	198	0.831
	5.47	0.534	163	0.911

SUMMARY OF PRINCIPLE MODES, TRANSVERSE RESPONSE NODE 1
RELATIVE TO LONGITUDINAL RESPONSE NODE 1

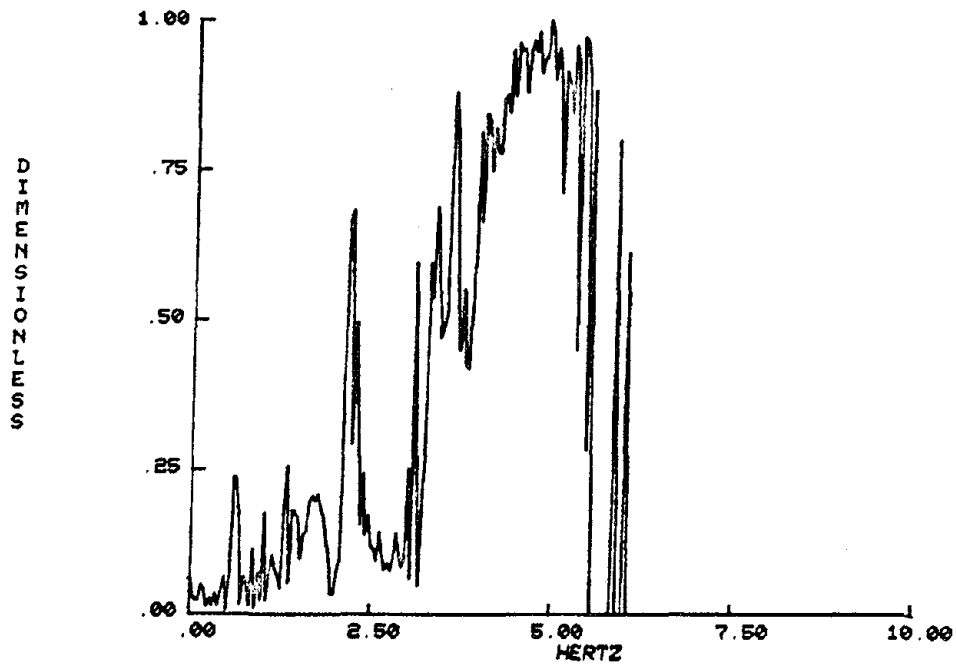


Figure 6.44 COHERENCE FUNCTION, TRANSVERSE RESPONSE NODE 1 AND
LONGITUDINAL RESPONSE NODE 1
B-R-1

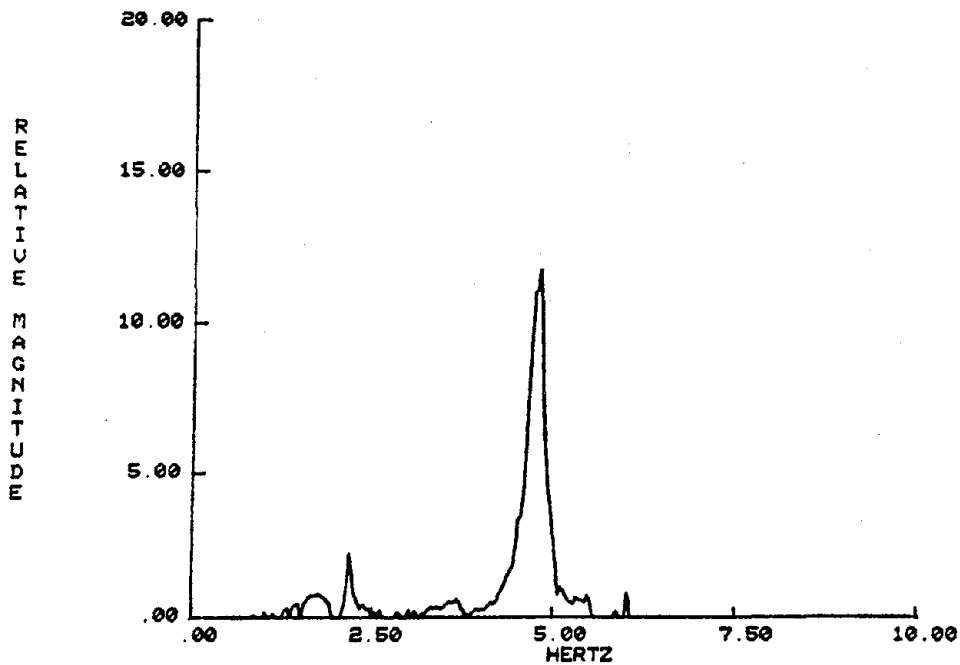


Figure 6.45 TRANSFER FUNCTION MAGNITUDE, TRANSVERSE RESPONSE
 NODE 1 RELATIVE TO LONGITUDINAL RESPONSE NODE 1
 B-R-1

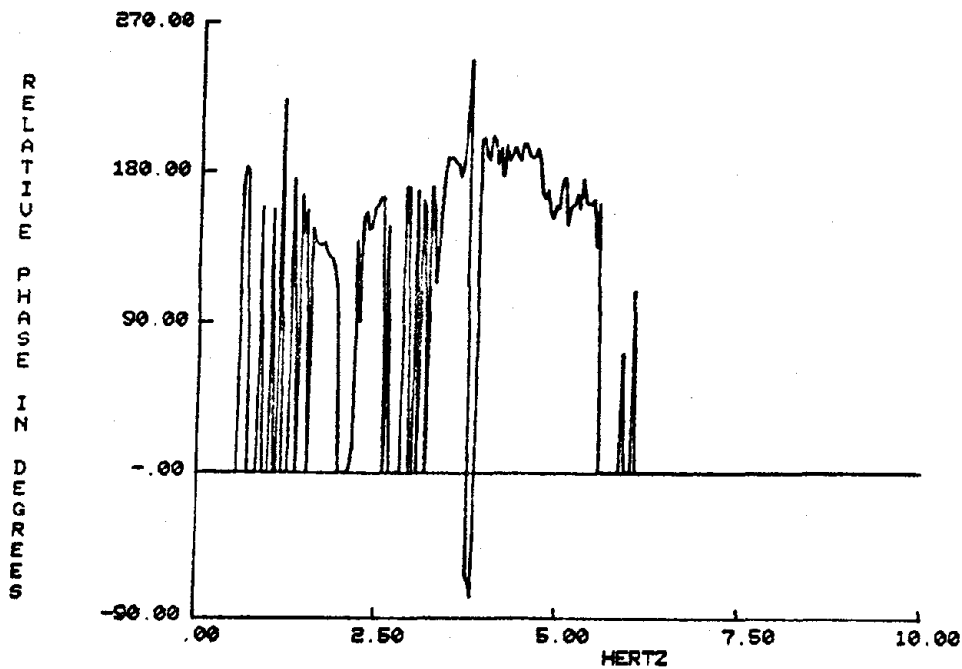


Figure 6.46 TRANSFER FUNCTION PHASE, TRANSVERSE RESPONSE
 NODE 1 RELATIVE TO LONGITUDINAL RESPONSE NODE 1
 B-R-1

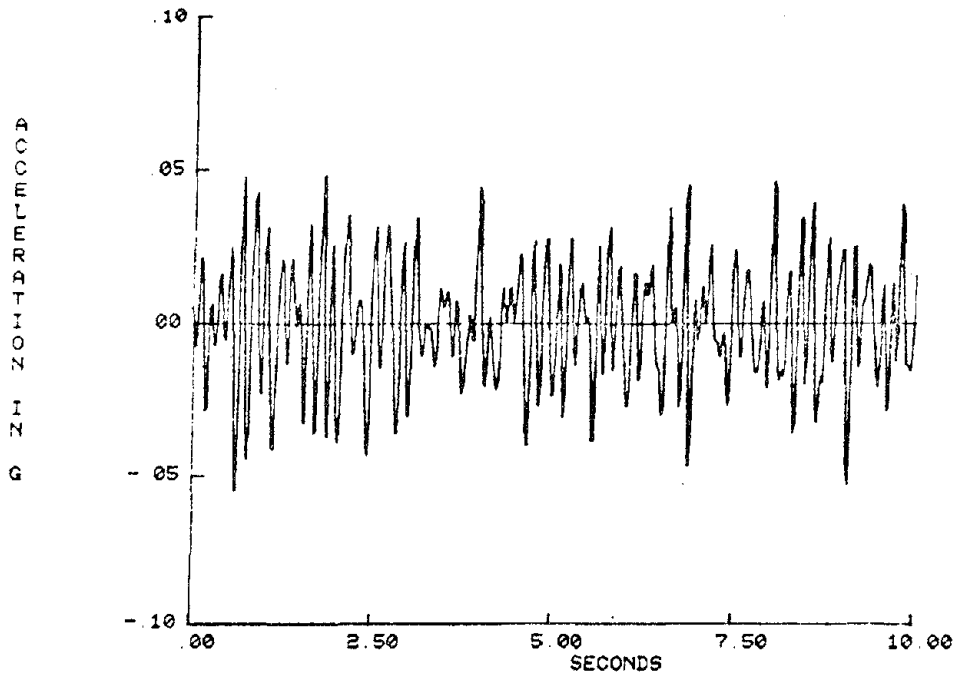


Figure 6.47 ACCELERATION TIME HISTORY, NODE 1, TRANSVERSE RESPONSE
B-R-1

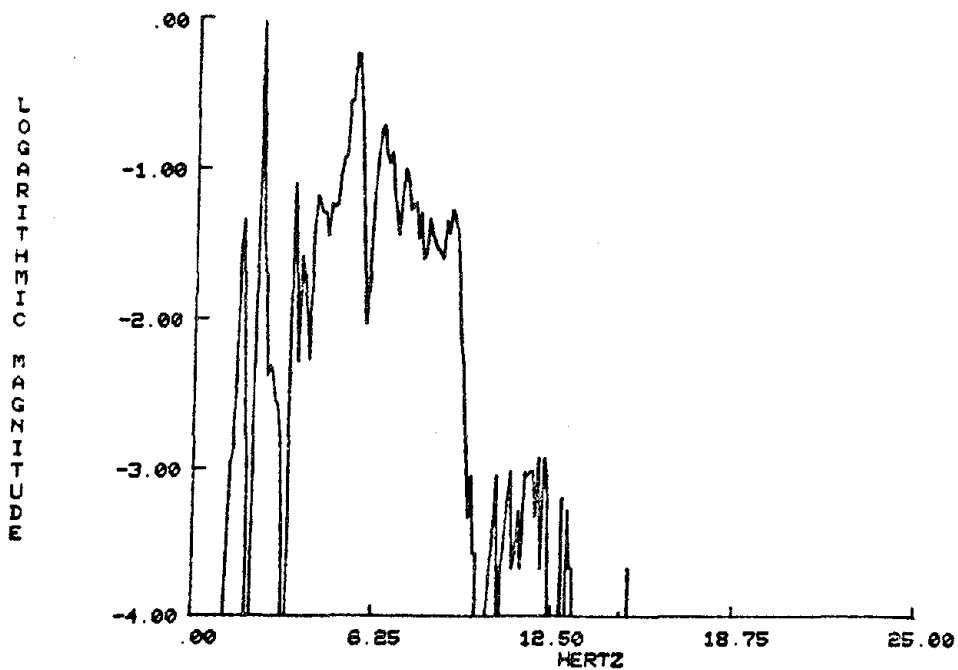


Figure 6.48 AVERAGE AUTOPOWER SPECTRAL DENSITY FUNCTION, 50 SUMS
NODE 1, TRANSVERSE RESPONSE
B-R-1

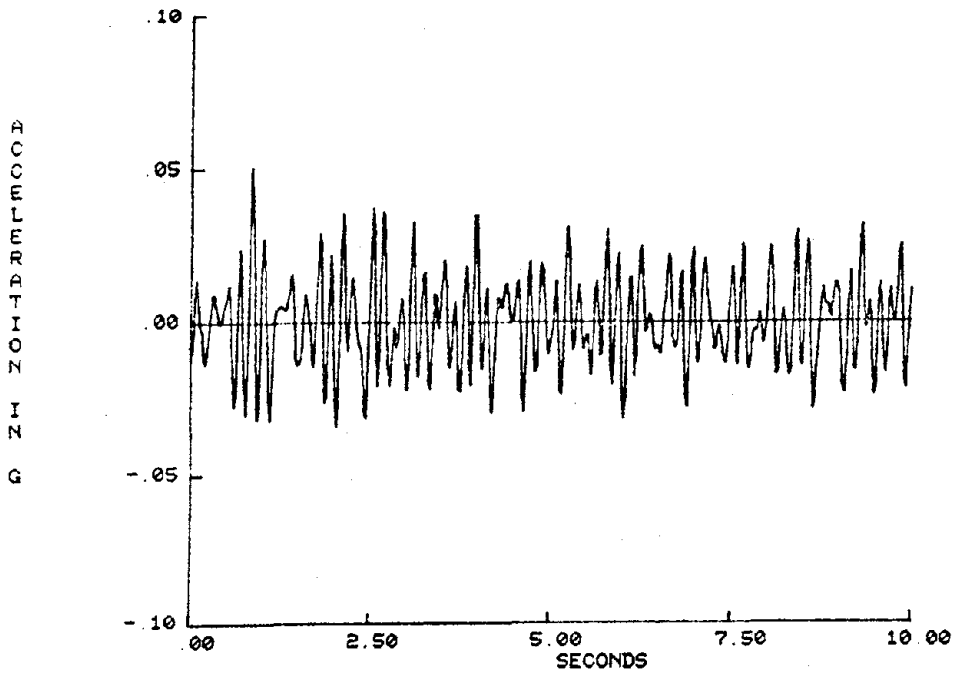


Figure 6.49 ACCELERATION TIME HISTORY, NODE 2, TRANSVERSE RESPONSE
B-R-1

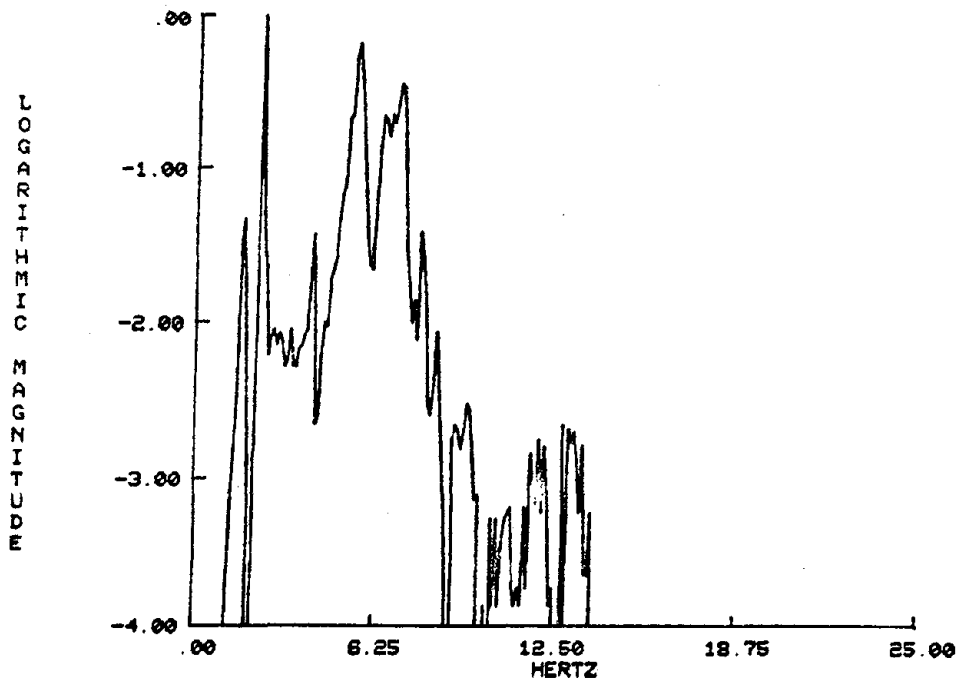


Figure 6.50 AVERAGE AUTOPOWER SPECTRAL DENSITY FUNCTION, 50 SUMS
NODE 2, TRANSVERSE RESPONSE
B-R-1

MODE	FREQUENCY (HERTZ)	RELATIVE MAGNITUDE	RELATIVE PHASE (DEGREES)	COHERENCE
1	1.66	0.77	-0	0.998
2	2.25	0.80	-0	0.999
3	3.42	0.20	116	0.982
4	3.71	0.40	58	0.997
5	4.10	0.73	126	0.999
6	5.47	0.73	2	0.999
7	6.45	0.68	15	0.998

SUMMARY OF PRINCIPLE MODES, TRANSVERSE RESPONSE NODE 2
RELATIVE TO TRANSVERSE RESPONSE NODE 1

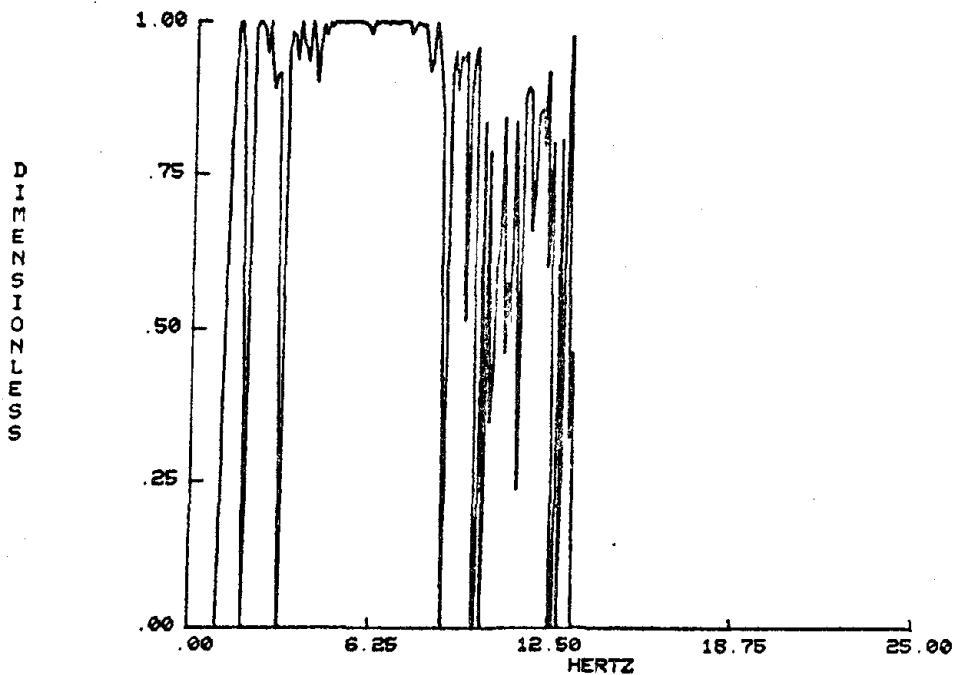


Figure 6.51 COHERENCE FUNCTION, TRANSVERSE RESPONSE NODE 2
AND TRANSVERSE RESPONSE NODE 1

B-R-1

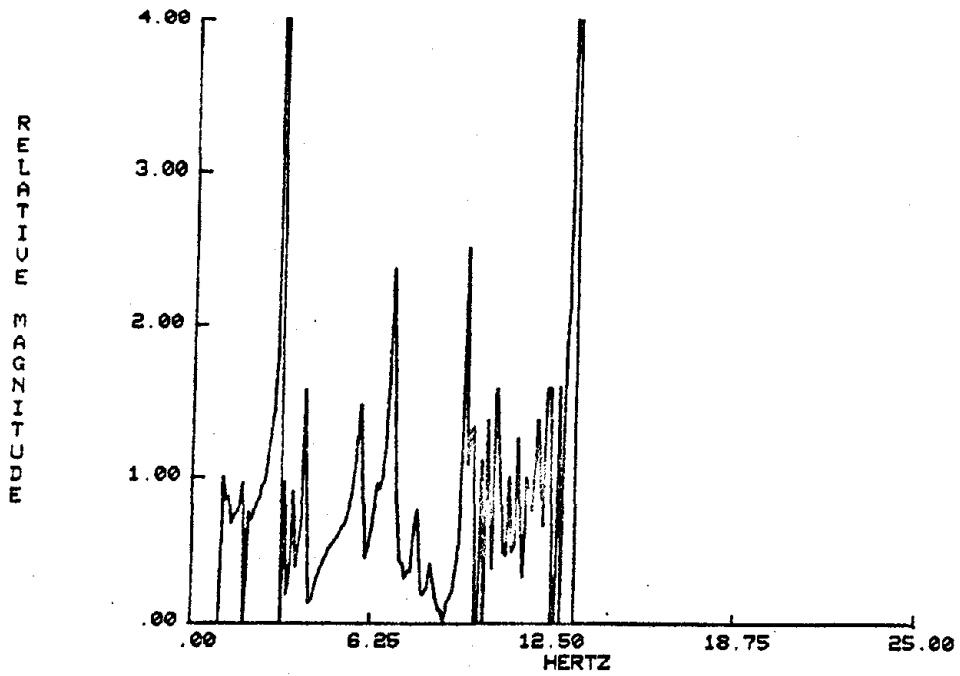


Figure 6.52 TRANSFER FUNCTION MAGNITUDE, TRANSVERSE RESPONSE
 NODE 2 RELATIVE TO TRANSVERSE RESPONSE NODE 1
 B-R-1

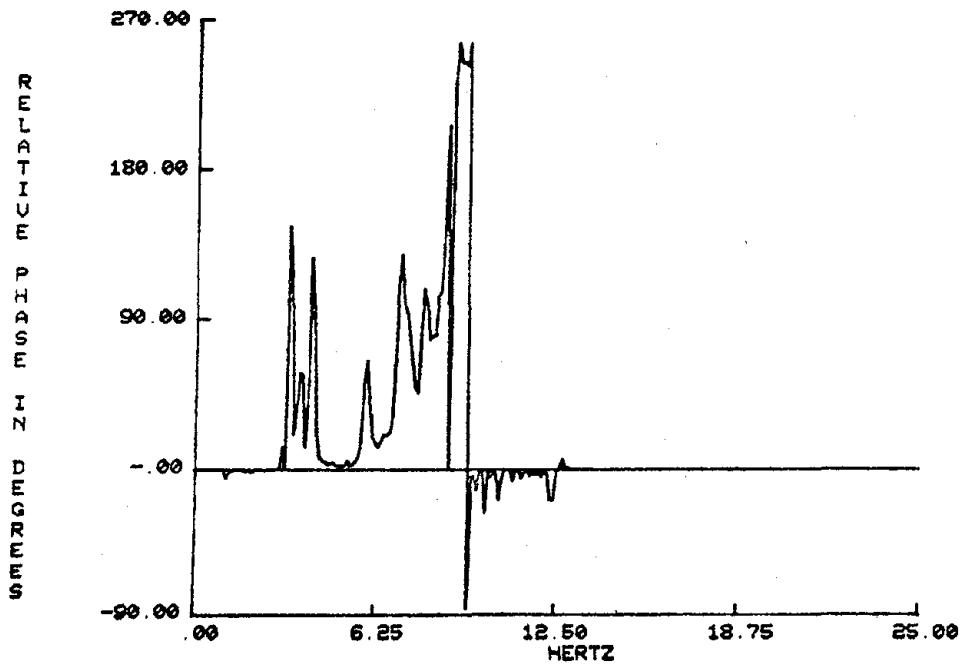


Figure 6.53 TRANSFER FUNCTION PHASE, TRANSVERSE RESPONSE
 NODE 2 RELATIVE TO TRANSVERSE RESPONSE NODE 1
 B-R-1

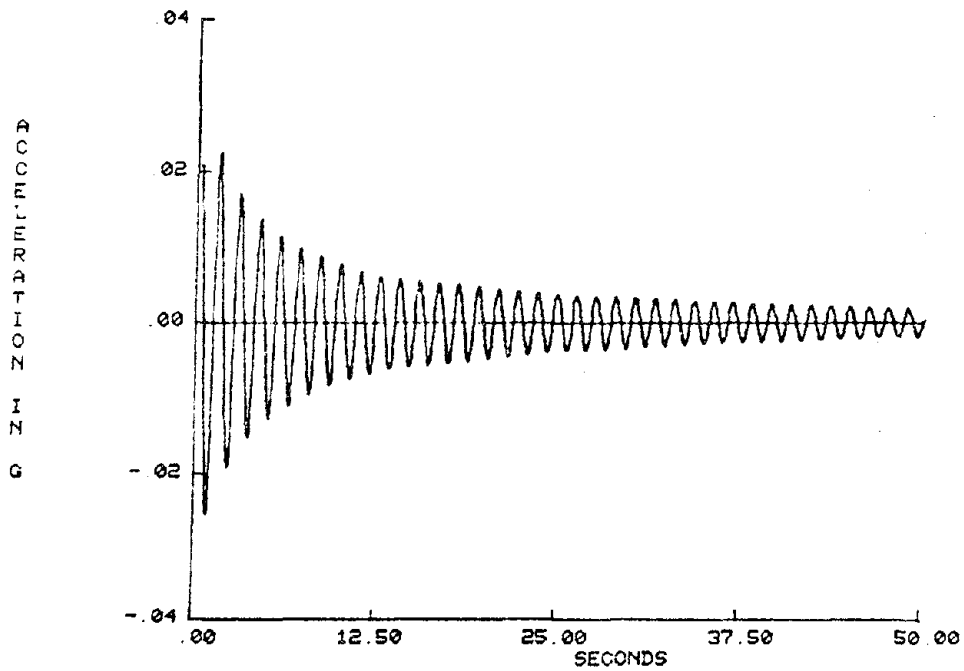


Figure 6.54 ACCELERATION TIME HISTORY, NODE 1, LONGITUDINAL
 FREE VIBRATION, MODE 1.
 A-R-1

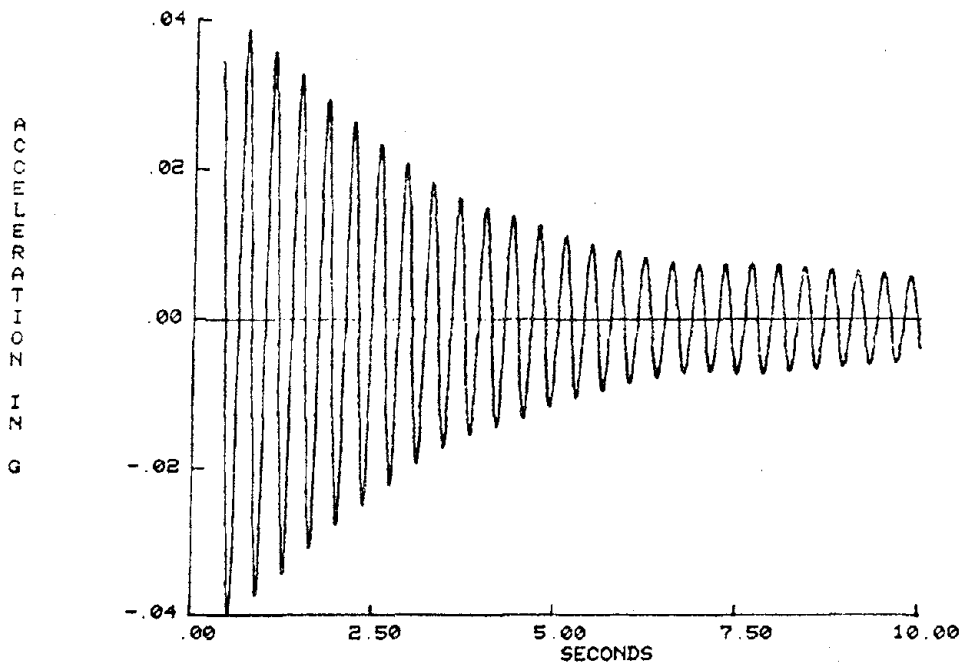


Figure 6.55 ACCELERATION TIME HISTORY, NODE 1, LONGITUDINAL
 FREE VIBRATION, MODE 2
 A-R-1

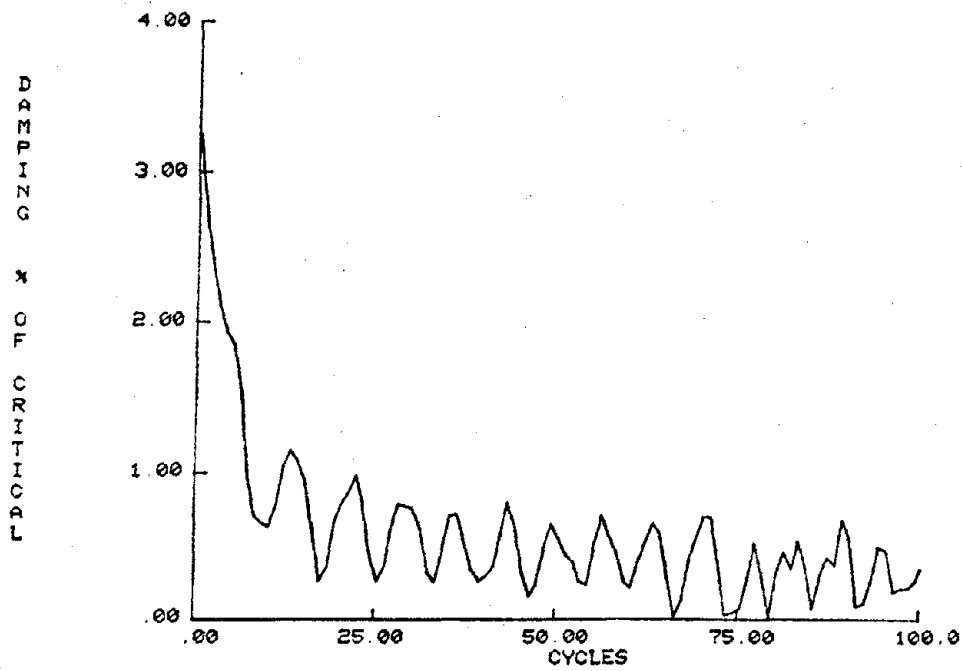


Figure 6.56 ENERGY DISSIPATED PER CYCLE OF LONGITUDINAL FREE VIBRATION, MODE 1
A-R-1

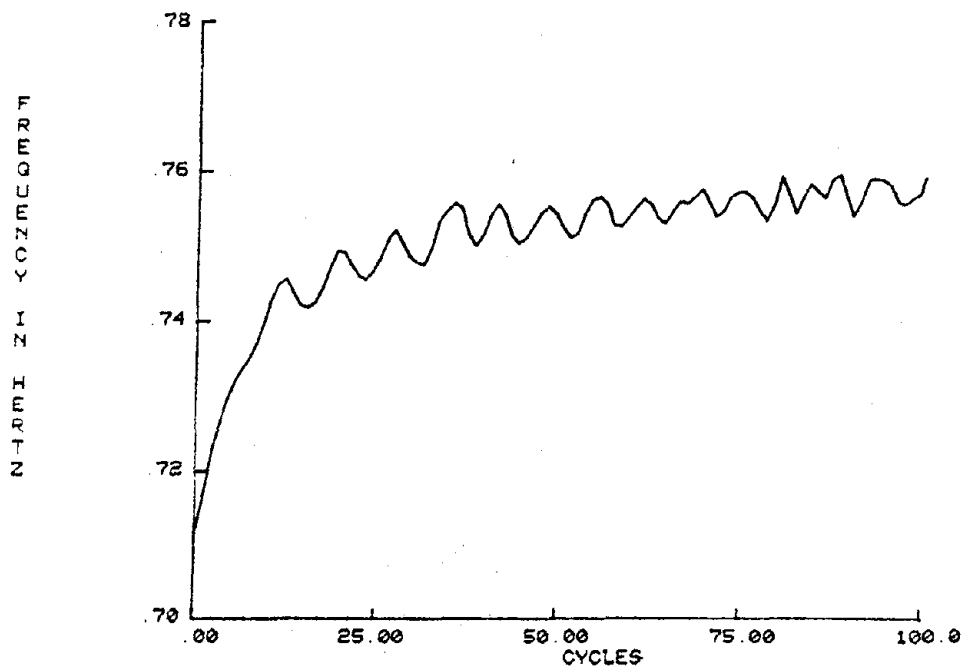


Figure 6.57 FREQUENCY PER CYCLE OF LONGITUDINAL FREE VIBRATION, MODE 1
A-R-1

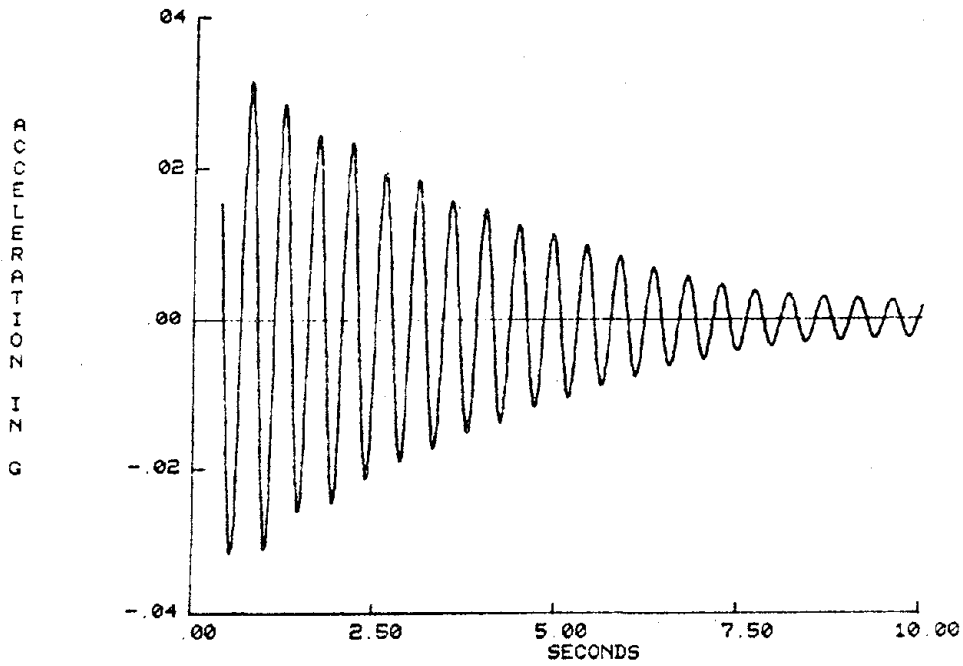


Figure 6.58 ACCELERATION TIME HISTORY, NODE 1, TRANSVERSE
 FREE VIBRATION, MODE 1
 A-R-1

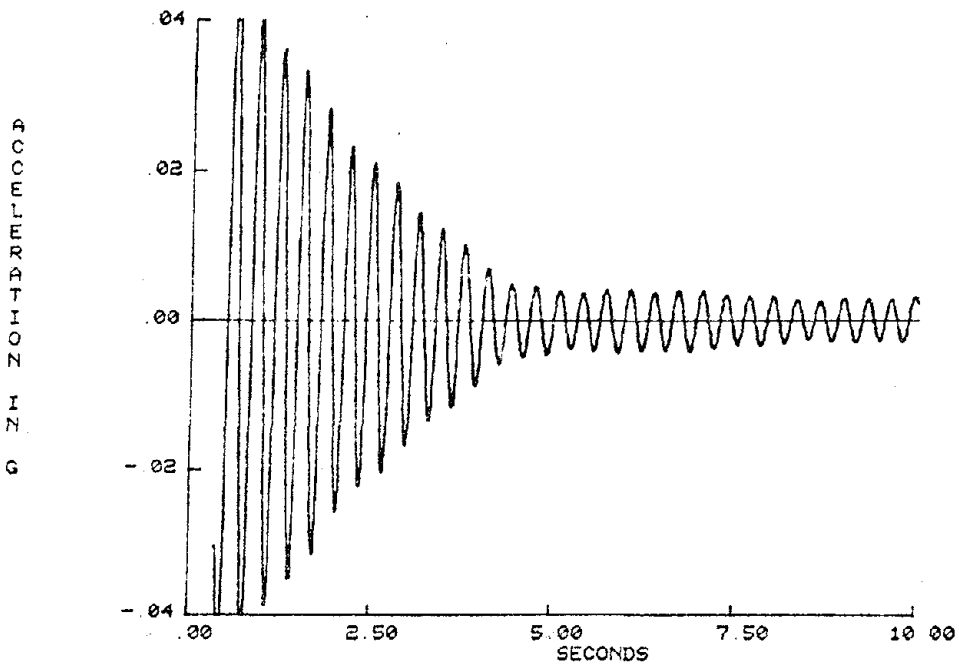


Figure 6.59 ACCELERATION TIME HISTORY, NODE 1, TRANSVERSE
 FREE VIBRATION, MODE 3
 A-R-1

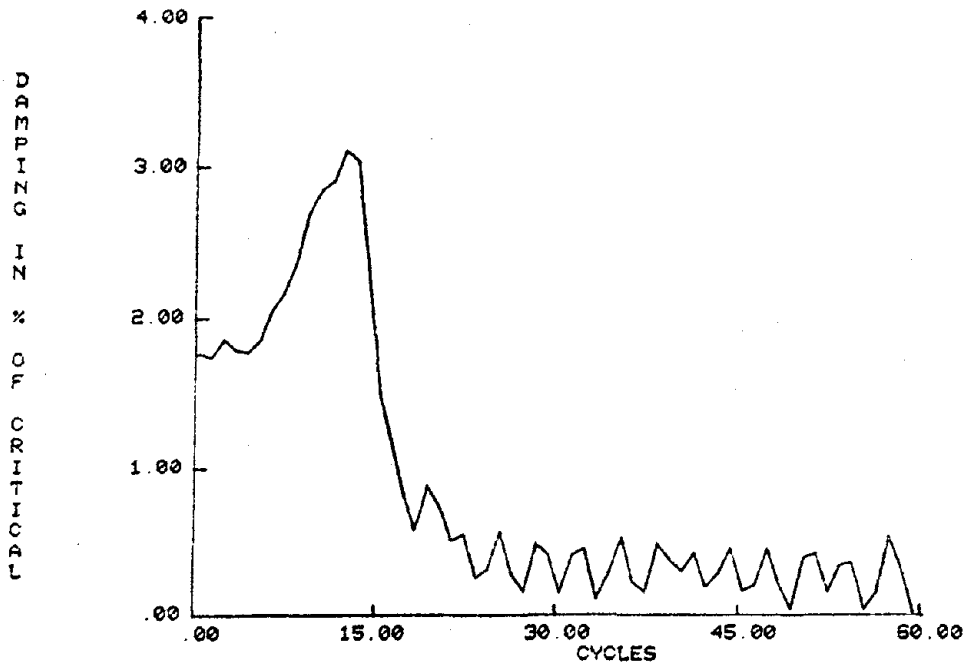


Figure 6.60 ENERGY DISSIPATED PER CYCLE OF TRANSVERSE FREE VIBRATION, MODE 1
A-R-1

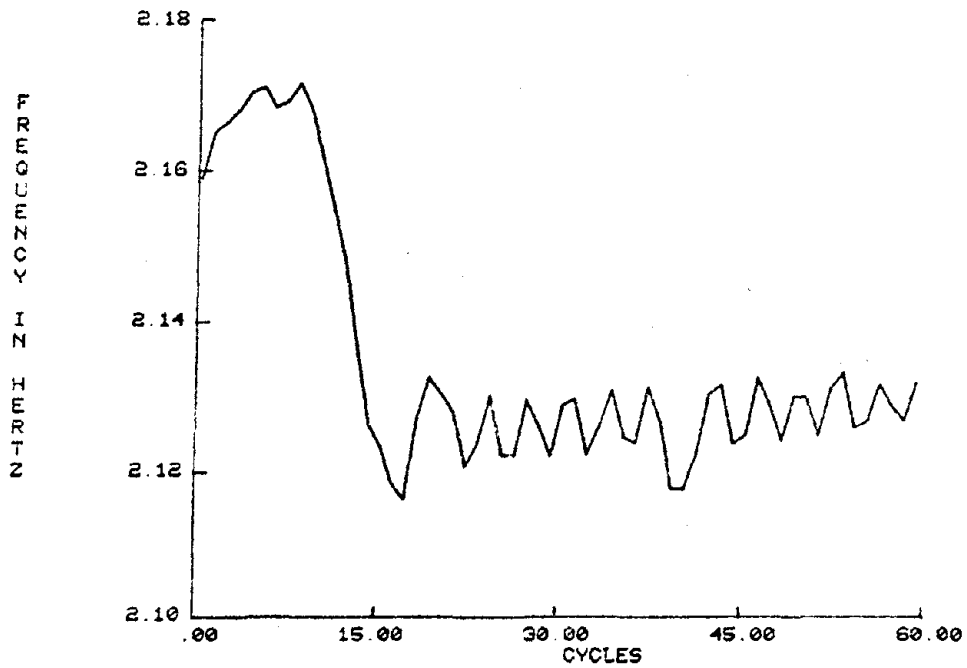


Figure 6.61 FREQUENCY PER CYCLE OF TRANSVERSE FREE VIBRATION, MODE 1
A-R-1

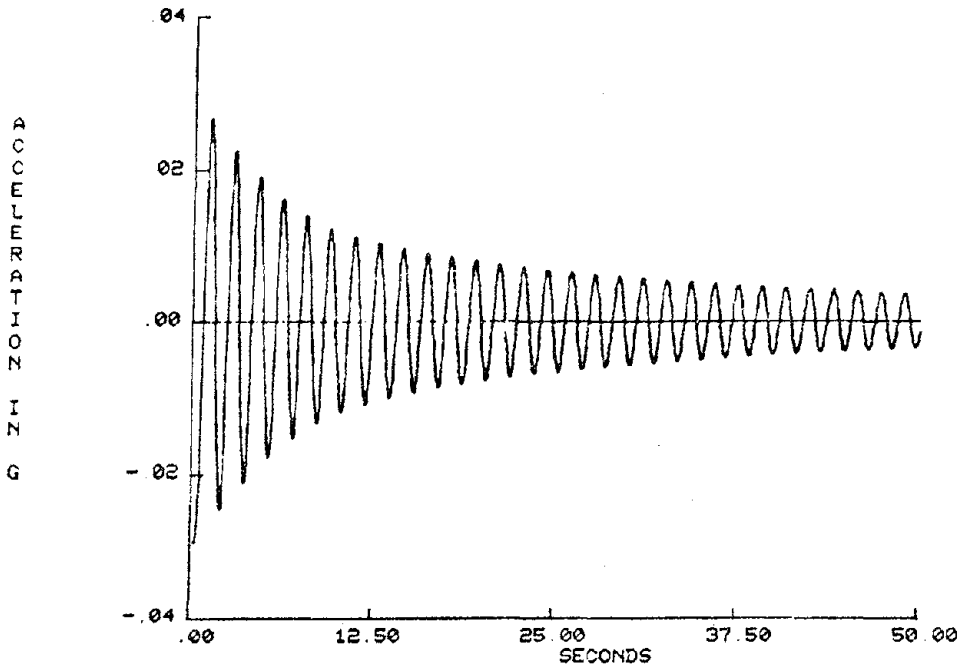


Figure 6.62 ACCELERATION TIME HISTORY, NODE 1,
LONGITUDINAL FREE VIBRATION, MODE 1
B-R-1

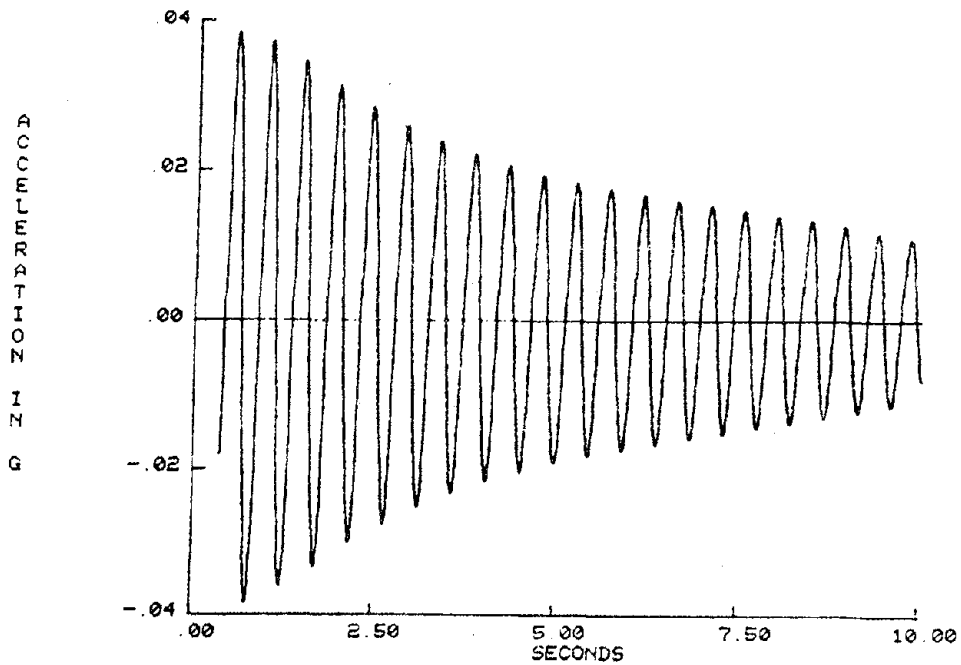


Figure 6.63 ACCELERATION TIME HISTORY, NODE 1,
LONGITUDINAL FREE VIBRATION, MODE 2
B-R-1

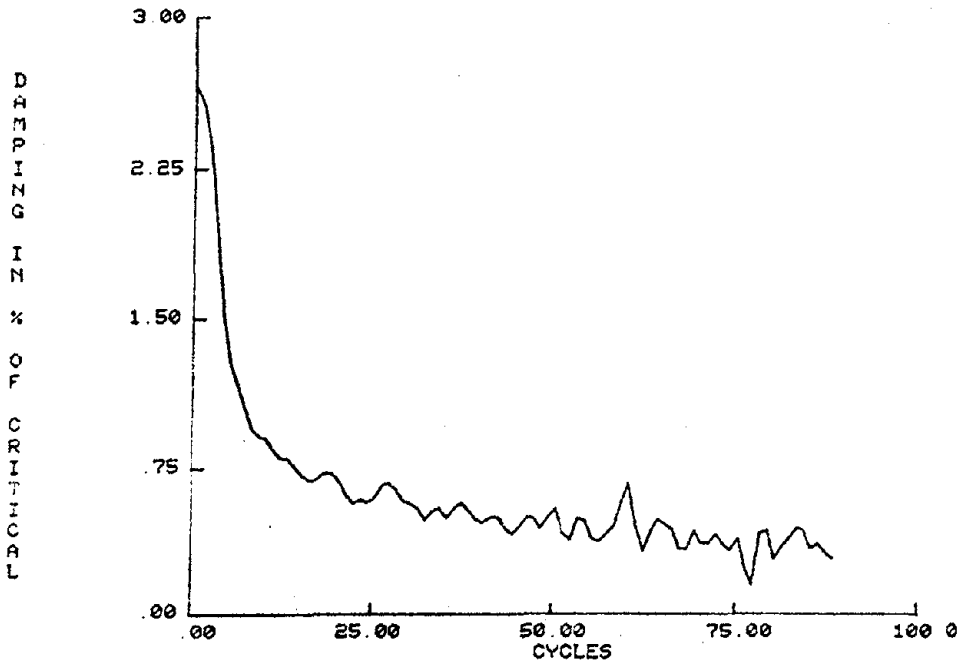


Figure 6.64 ENERGY DISSIPATED PER CYCLE OF LONGITUDINAL FREE VIBRATION, MODE 1
B-R-1

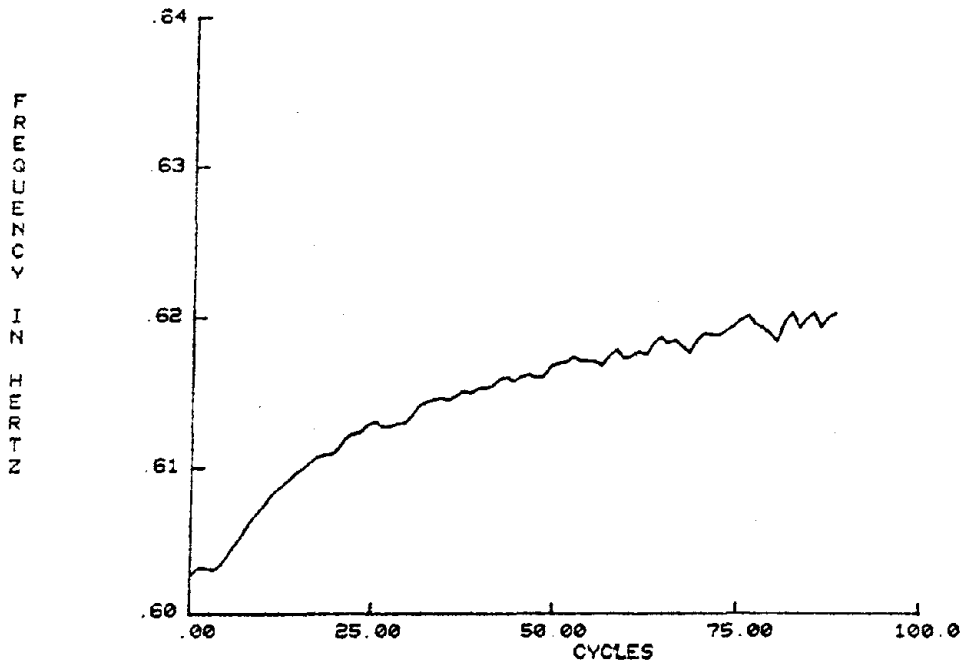


Figure 6.65 FREQUENCY PER CYCLE OF LONGITUDINAL FREE VIBRATION, MODE 1
B-R-1

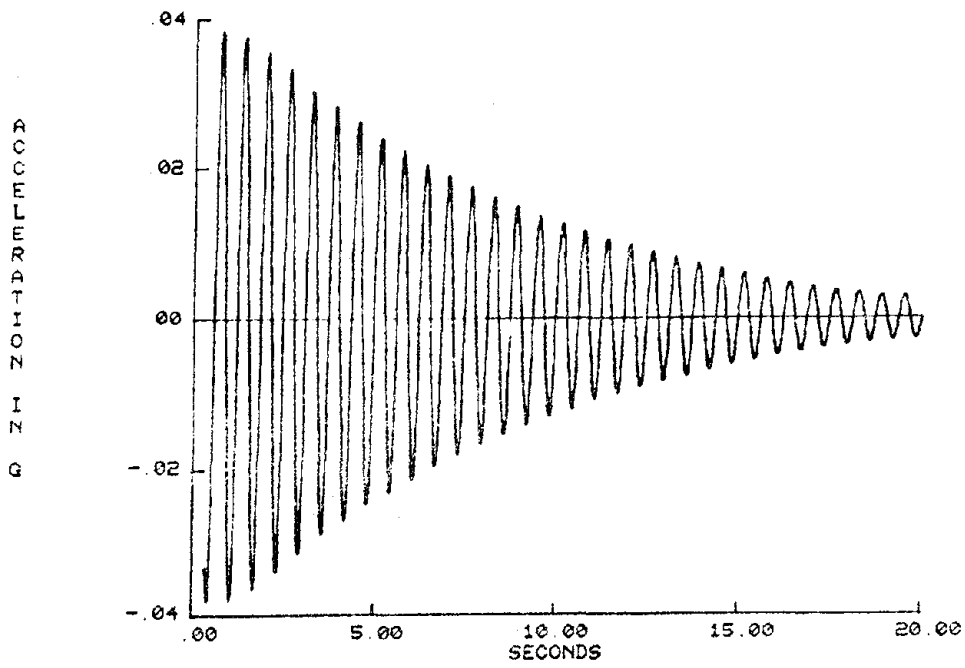


Figure 6.66 ACCELERATION TIME HISTORY, NODE 1, TRANSVERSE
FREE VIBRATION, MODE 1
B-R-1

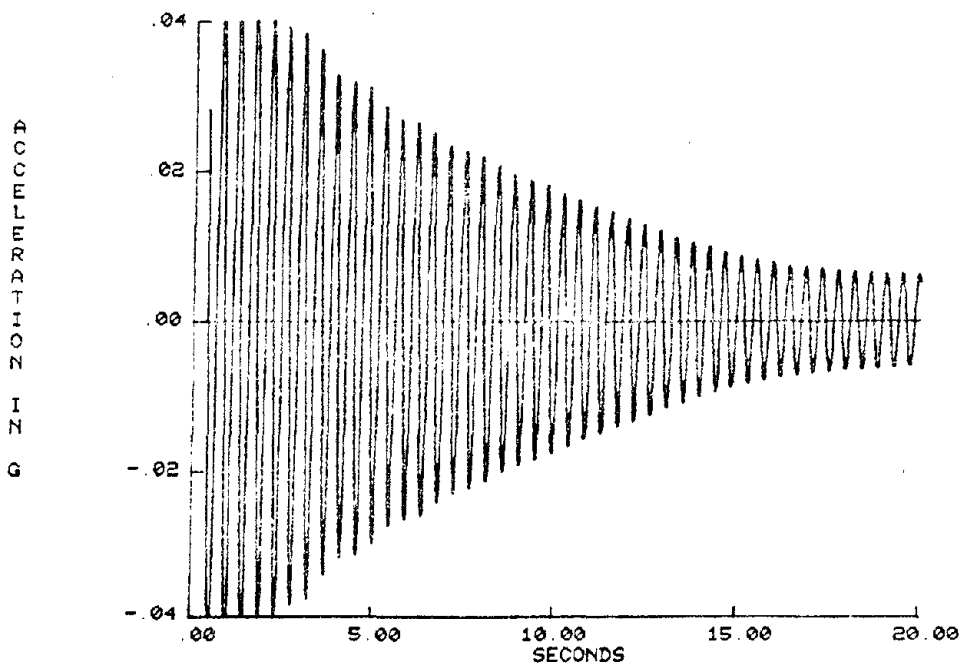


Figure 6.67 ACCELERATION TIME HISTORY, NODE 1, TRANSVERSE
FREE VIBRATION, MODE 2
B-R-1

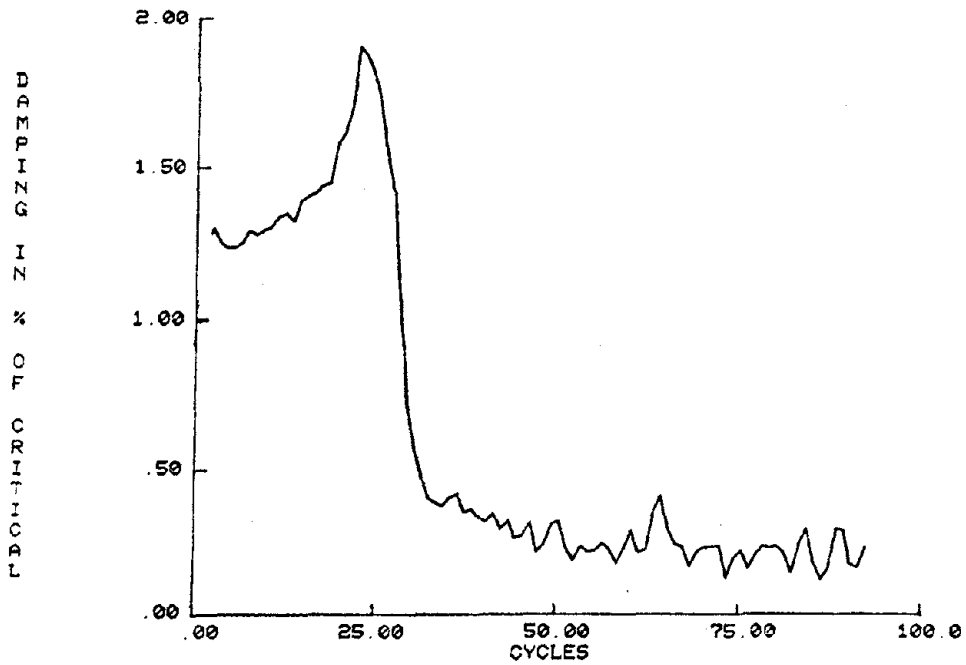


Figure 6.68 ENERGY DISSIPATED PER CYCLE OF TRANSVERSE
FREE VIBRATION, MODE 1

B-R-1

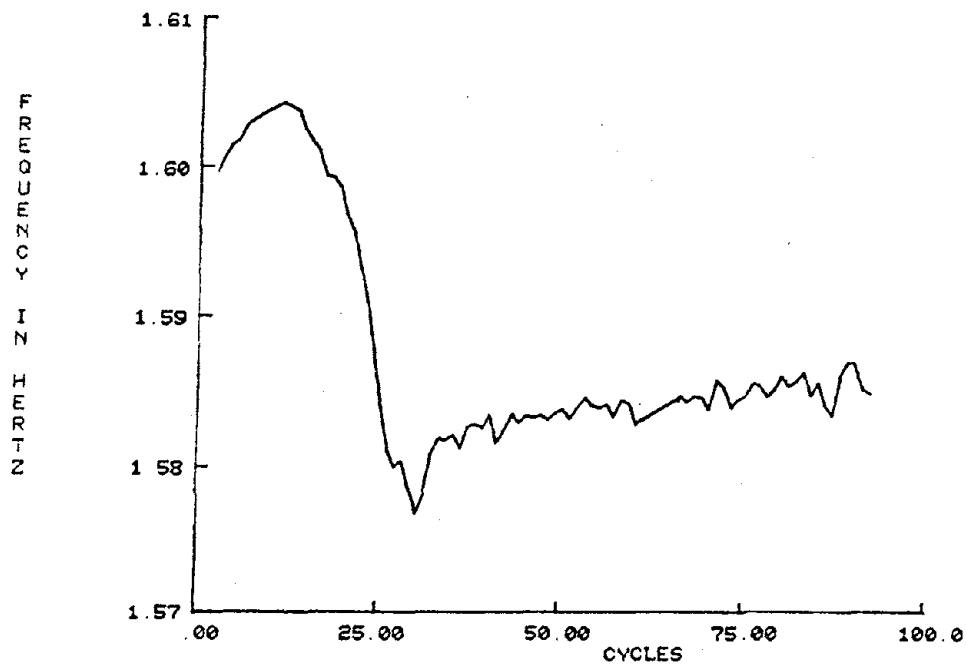


Figure 6.69 FREQUENCY PER CYCLE OF TRANSVERSE
FREE VIBRATION, MODE 1

B-R-1

